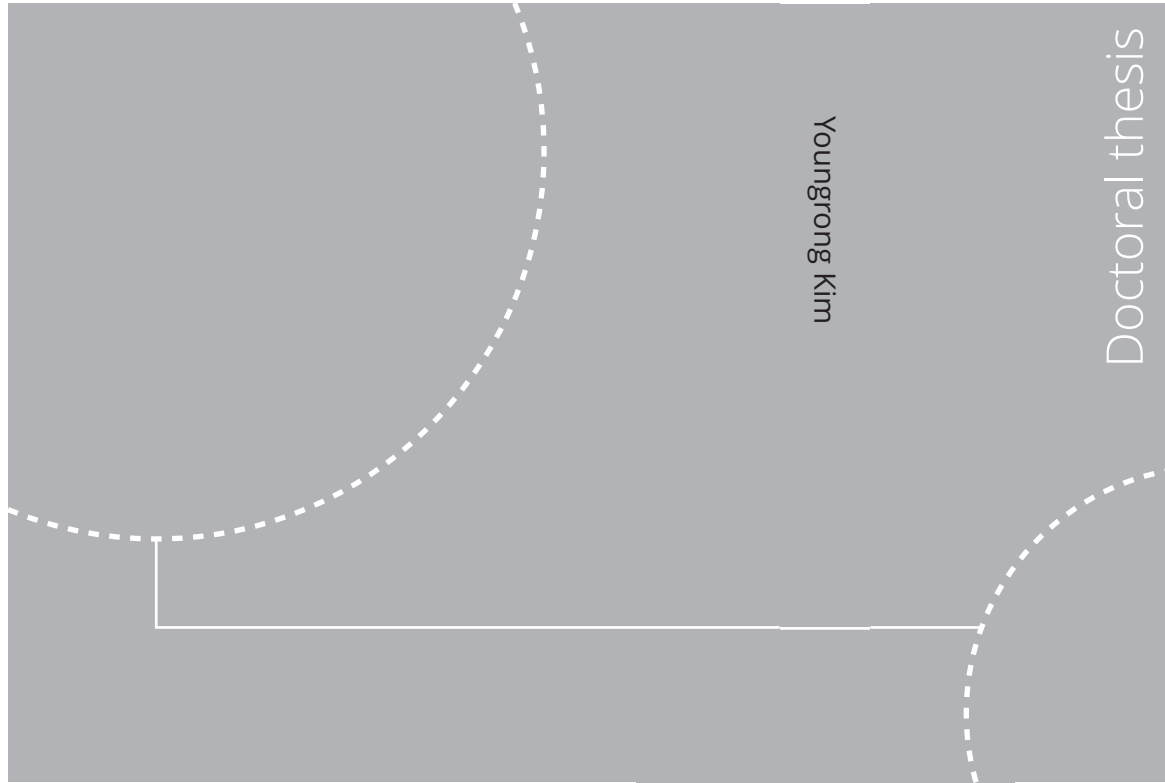


ISBN 978-82-326-6400-9 (printed ver.)  
ISBN 978-82-326-6346-0 (electronic ver.)  
ISSN 1503-8181 (printed ver.)  
ISSN 2703-8084 (electronic ver.)



Doctoral theses at NTNU, 2023:88

Youngrong Kim

# Modeling Operational Performance for the Global Fleet & Application of an Energy Saving Measure

Doctoral theses at NTNU, 2023:88

**NTNU**  
Norwegian University of  
Science and Technology  
Thesis for the degree of  
Philosophiae Doctor  
Faculty of Engineering  
Department of Marine Technology

 **NTNU**  
Norwegian University of  
Science and Technology

 NTNU

 **NTNU**  
Norwegian University of  
Science and Technology

Youngrong Kim

# Modeling Operational Performance for the Global Fleet & Application of an Energy Saving Measure

Thesis for the degree of Philosophiae Doctor

Trondheim, March 2023

Norwegian University of Science and Technology  
Faculty of Engineering  
Department of Marine Technology



Norwegian University of  
Science and Technology

**NTNU**

Norwegian University of Science and Technology

Thesis for the degree of Philosophiae Doctor

Faculty of Engineering  
Department of Marine Technology

© Youngrong Kim

ISBN 978-82-326-6400-9 (printed ver.)  
ISBN 978-82-326-6346-0 (electronic ver.)  
ISSN 1503-8181 (printed ver.)  
ISSN 2703-8084 (electronic ver.)

Doctoral theses at NTNU, 2023:88



Printed by Skipnes Kommunikasjon AS

# Abstract

In order to reduce greenhouse gas emissions (GHG) from ships at sea, various measures have been considered, such as alternative fuels with low carbon intensity, innovative ship technology, and new policies. To successfully achieve GHG reduction in global shipping, it is critical to properly evaluate and understand the impact of the combination of operational scenarios and various mitigation measures, which requires a system that can accurately predict the required power for the global fleet under the actual operating profile and weather conditions.

Global emissions assessments in the maritime sector have relied on relatively simplified calculations and empirical methods to estimate power consumption due to limitations such as a lack of accurate information about ships, uncertainty in the collected data, and computational complexity. This study aims to implement an improved model that can improve the accuracy of power predictions by identifying suitable methods for fleet-wide power estimation or modifying and updating existing methods. Based on the developed model, the application and effectiveness of energy saving measures are also considered.

An overall data processing method for performance analysis of individual ships and entire fleet segments, including a method for processing missing values of ship principal parameters, is presented. In addition, methods for estimating ship resistance components and total propulsive efficiency are reviewed. Here, a new method for estimating added wave resistance of a ship is developed. Moreover, air lubrication technology is combined with the developed power prediction model as a case study for energy saving measures, and its impact on energy savings in global shipping is evaluated.

Based on the comparison results with the full-scale measurements and 2018 EU-MRV (European Union-The Monitoring, Reporting and Verification) data, the developed model seems to well describe the characteristics of the power performance according to the ship's various operational profiles. It can be used to evaluate

fuel consumption, emissions, and energy efficiency for fleet segments, and can be combined with various energy reduction scenarios to be useful in finding suitable pathways to reduce GHG emissions.

# Preface

This thesis is submitted for partial fulfillment of the requirements for the degree of Doctor of Philosophy (Ph.D.) in Marine Technology at the Norwegian University of Science and Technology (NTNU).

This doctoral work has been performed between January 2020 and January 2023 at the Department of Marine Technology at NTNU in Trondheim, with Professor Sverre Steen as the main supervisor. The research project was funded by the Research Council of Norway through the research project CLIMMS - Climate change mitigation in the maritime sector (RCN 294771), and it has been performed by collaborating with SINTEF Ocean and many industrial partners from shipping companies.

The thesis consists of five research papers written as the main author. One research paper is presented at an international conference, and others have been published or submitted in international peer-reviewed scientific journals.



# Acknowledgements

First of all, I would like to express my sincere gratitude to my supervisor, Prof. Sverre Steen, for sufficient guidance, advice, and encouragement throughout my Ph.D. program. Discussion with him was always full of passion and commitment, which aided in my intellectual and mental growth. He also guided me with a lot of trust and respect to grow into an independent researcher. It has been a great honor to study under his guidance for the past three years and I will never forget this valuable time and experience.

I would like to thank all the members involved in CLIMMS project and the industrial partners. Especially, I would appreciate Prof. Anders Hammer Strømman, Senior researcher Helene Muri, and Diogo Kramel, with whom I have worked together for a significant portion of my Ph.D. work. I was able to learn a lot from them, and the valuable opinions and insightful ideas from the discussions were of great help to my research. It was my great pleasure to have been part of the team. I would also like to thank Assoc. Prof. David Kristiansen, who was my co-supervisor during the Ph.D. program.

My good friend Prateek Gupta. From academic research to trivial conversations, the time I spent with him was very precious to me. I am truly grateful to him for being my best collaborator and colleague. I also appreciate my good research partner Ehsan Esmailian, Trondheim trio Yanlin Jin and Sangwoo Kim, and kind office mate Jianxun Zhu. I could not list all the great people here, but I would like to thank all my friends and colleagues in the Department of Marine Technology and NTNU.

Special thanks to my girlfriend, Subeen Lee, who always supported and encouraged my academic journey. I am sincerely grateful to her for overcoming joy and sorrow together. Lastly, I am thankful to my precious family members, parents, brother, and sister. They gave me unending love and care while always motivating and assisting me in reaching my goals and career path.





# List of Publications

The following papers are included as part of this thesis:

1. Kim Y., Steen S., Muri H. A novel method for estimating missing values in ship principal data. *Ocean Engineering*. 2022; 251: 110979.  
DOI: [10.1016/j.oceaneng.2022.110979](https://doi.org/10.1016/j.oceaneng.2022.110979).
2. Kim Y., Esmailian E., Steen S. A meta model for added resistance in waves. *Ocean Engineering*. 2022; 266: 112749.  
DOI: [10.1016/j.oceaneng.2022.112749](https://doi.org/10.1016/j.oceaneng.2022.112749).
3. Kim Y., Steen S. Application of machine learning algorithms for predicting added resistance in arbitrary wave headings of a ship. Proceedings of the ASME 2022 41st International Conference on Ocean, Offshore and Arctic Engineering (OMAE2022), Hamburg, Germany. June 5-10, 2022.  
DOI: [10.1115/OMAE2022-78433](https://doi.org/10.1115/OMAE2022-78433).
4. Kim Y., Steen S., Kramel D., Muri H., Strømman AH. Modeling of ship resistance and power consumption for the global fleet: The MariTEAM model. Submitted to *Ocean Engineering*.
5. Kim Y., Steen S. Potential energy savings of air lubrication technology on merchant ships. Submitted to *International Journal of Naval Architecture and Ocean Engineering*.

The following articles, to which the author made a contribution as a co-author, are not considered to be a part of this Ph.D. thesis. For the first two of these articles, the author mainly made a collaboration regarding the data processing framework and the implementation of the machine learning method for ship performance analysis. For the third article, the author contributed to the ship power prediction module that was utilized in the MariTEAM model for the global emission assessment.

1. Gupta P., Kim Y., Steen S., Rasheed A. Streamlined Semi-automatic Data Processing Framework for Ship Performance Analysis. Submitted to International Journal of Naval Architecture and Ocean Engineering.
2. Esmailian E., Kim Y., Steen S., Koushan K. A new power prediction method towards energy-efficient shipping. Submitted to Ship Technology Research.
3. Kramel D., Muri H., Kim Y., Lonka R., Nielsen JB., Ringvold AL., Bouman EA., Steen S., Strømman AH. Global shipping emissions from a well to wake perspective: The MariTEAM model. Environmental Science & Technology. 2022; 56.9: 5999-6000.  
DOI:[10.1021/acs.est.2c01301](https://doi.org/10.1021/acs.est.2c01301).

# Contents

<b>1</b>	<b>Introduction</b>	<b>1</b>
1.1	Background & Motivation . . . . .	1
1.2	Literature Review . . . . .	3
1.2.1	Power prediction method for the global fleet . . . . .	4
1.2.2	Energy saving measures for ships . . . . .	9
1.3	Thesis Structure . . . . .	10
<b>2</b>	<b>Research Objectives</b>	<b>13</b>
<b>3</b>	<b>Research Design</b>	<b>15</b>
3.1	Overview . . . . .	15
3.2	Research Strategy . . . . .	16
3.2.1	Data Acquisition . . . . .	16
3.2.2	Method & Approach . . . . .	17
3.3	Scope and Limitations . . . . .	19
<b>4</b>	<b>Research Summary</b>	<b>21</b>
4.1	Summary of Publications . . . . .	21
4.1.1	Article 1: Missing Data Imputation for Ship Principal Parameters . . . . .	21

4.1.2	Article 2: Estimation of Added Wave Resistance I (Semi-Empirical method) . . . . .	24
4.1.3	Article 3: Estimation of Added Wave Resistance II (Machine learning method) . . . . .	28
4.1.4	Article 4: Ship Resistance & Power Prediction for the Global fleet . . . . .	31
4.1.5	Article 5: Energy Saving Device: Air Lubrication System	36
<b>5</b>	<b>Conclusion</b>	<b>41</b>
5.1	Original Contributions . . . . .	41
5.2	Conclusion . . . . .	42
5.3	Future Work . . . . .	44
	<b>References</b>	<b>55</b>
	<b>Article 1</b>	<b>59</b>
	<b>Article 2</b>	<b>87</b>
	<b>Article 3</b>	<b>113</b>
	<b>Article 4</b>	<b>127</b>
	<b>Article 5</b>	<b>159</b>
	<b>Previous PhD theses published at the Department of Marine Technology</b>	<b>187</b>

# List of Tables

1.1	Methods used to estimate resistance components and propeller efficiency in previous studies. For successive studies conducted in the same research group, only the methods applied in the most recent study are shown in the table. Details of the abbreviations for each method are listed below the table. . . . .	6
4.1	Comparison of prediction performance for the container ship’s principal data between previous studies and this study. . . . .	22
4.2	The input parameters of ALS model and their estimation methods.	37



# List of Figures

1.1	<i>CO</i> <sub>2</sub> emission reduction potential from individual measures (Bouman et al. 2017). . . . .	12
3.1	An overview of the thesis and the link between the research papers. . . . .	16
4.1	Flowchart of estimating ship principal data considering missing values as proposed in the study. . . . .	23
4.2	The relation between ship length and breadth regarding dimensional constraints (A: Panama Canal, B: New Panama Canal, C: Suez Canal). . . . .	23
4.3	Comparison of several semi-empirical methods for added wave resistance according to wave headings, Froude numbers, and wavelengths. The upper row of the bar graph depicts head waves, the middle, beam waves, and the below, following waves. MSE refers to the mean squared error. . . . .	25
4.4	Comparison of several semi-empirical methods for added wave resistance according to ship type. . . . .	26
4.5	Examples of added wave resistance coefficient predicted by the Combined method: (a) DTC ( $F_n=0.139$ ), (b) HSVA ( $F_n=0.232$ ), (c) S60 ( $F_n=0.283$ ). The figure corresponds to the case of head waves ( $\alpha=180$ ). . . . .	27
4.6	A comparison of errors in different methods against full-scale measurements of two ships. Figure (a) shows RMSE and Figure (b) shows relative RMSE against the Combined method. RMSE refers to the root mean squared error. . . . .	27



4.7	Performance evaluation between machine learning models with test data from nested cross-validation. . . . .	29
4.8	Prediction surface of added wave resistance coefficients of machine learning algorithms (S175 container, $Fn=0.25$ ). . . . .	30
4.9	The relative deviation to the sum of the added resistance in irregular arbitrary waves between the machine learning model (SVR model) and other semi-empirical methods according to the sea state. The number on the bar indicates the added resistance in irregular waves of a ship. . . . .	30
4.10	Schematic diagram of the complete power prediction module for the fleet segment in the MariTEAM model. . . . .	31
4.11	MariTEAM modeling framework for global well-to-wake emission. The blue-shaded part is the ship power prediction module outlined in Figure 4.10. . . . .	32
4.12	Comparison of in-service data and model predictions on main engine power of three ships: (a) Ship A, (b) Ship B, and (c) Ship C. . . . .	34
4.13	Comparison of annual fuel consumption of the fleet segments in 2018 between EU-MRV data and predicted values by the MariTEAM model. . . . .	35
4.14	Geospatial distribution of $CO_2$ emissions from the global shipping in 2018. . . . .	35
4.15	Results of the parametric analysis for the air lubrication systems: (a) ship speed, (b) ratio of the air-covered area to the bottom surface area, (c) draught, and (d) block coefficient. . . . .	39
4.16	Annual net power savings of an ALDR-equipped ship during a laden voyage (NLRTM-USNYC): (a) seasonal variations, (b) weather factors. . . . .	40
4.17	Comparison of the possible net power savings of the global fleet segment by air lubrication type. . . . .	40

# List of Abbreviations

- ABS** American Bureau of Shipping.
- ACES** Air Chamber Energy Saving.
- AHR** Average Hull Roughness.
- AIS** Automatic Identification System.
- ALDR** Air Layer Drag Reduction.
- ALS** Air Lubrication System.
- ANN** Artificial Neural Network.
- BDR** Bubble Drag Reduction.
- CFD** Computational Fluid Dynamics.
- CLIMMS** Climate change Mitigation in the Maritime Sector.
- CO<sub>2</sub>** Carbon Dioxide.
- DTC** Duisburg Test Case.
- DWT** Deadweight Tonnage.
- ECMWF** European Centre for Medium-Range Weather Forecasts.
- EEOI** Energy Efficiency Operating Indicator.
- ERA** ECMWF Re-Analysis.
- EU-MRV** European Union-The Monitoring, Reporting and Verification.

**GH** Guldhammer-Harvald.

**GHG** Greenhouse Gas.

**GPR** Gaussian Process Regression.

**GPS** Global Positioning System.

**HB** Hollenbach.

**HM** Holtrop-Mennen.

**HSVA** Hamburgische Schiffbau Versuchsanstalt.

**ICCT** International Council on Clean Transportation.

**IHS** Information Handling Services.

**IMO** International Maritime Organization.

**ITTC** International Towing Tank Conference.

**KNN** K-Nearest Neighbors.

**L&P** Liu&Papanikolaou.

**MariTEAM** Maritime Transport Environmental Assessment Model.

**MSE** Mean Squared Error.

**NLRTM** Netherlands Rotterdam.

**NTUA-SDL** Ship Design Laboratory of National Technical University of Athens.

**OM** Oortmerssen.

**PCDR** Partial Cavity Drag Reduction.

**RF** Random Forest.

**RMSE** Root Mean Squared Error.

**RPM** Revolutions Per Minute.

**SFI** Senter for Forskningsdrevet Innovasjon.

**SNNM** SHOPERA-NTUA-NTU-MARIC.

**SS** Sea State.

**STA-JIP** Sea Trial Analysis Joint Industry Project.

**STA1** STAWAVE-1.

**STA2** STAWAVE-2.

**STEAM** Ship Traffic Emission Assessment Model.

**SVR** Support Vector Regression.

**USNYC** United States New York.

**XGB** Extreme Gradient Boosting.



# List of Symbols

$\alpha$	Wave heading (0 for following waves; 180 for head waves)
$\dot{m}_g$	Mass flow rate of air necessary to maintain the given volume flow rate of air
$\eta_c$	Air compressor efficiency
$\eta_e$	Electrical motor efficiency
$\eta_H$	Hull efficiency
$\eta_O$	Open water efficiency
$\eta_R$	Relative rotative efficiency
$\eta_S$	Shaft efficiency
$\eta_T$	Total propulsive efficiency
$\lambda$	Wave length
$\rho_1$	Initial density where air is compressed
$\theta$	Trim angle (degree)
$a$	Slope adjustment coefficient of a tangent hyperbolic function (wave frequency)
$A_a$	Air-cover area at bottom surface
$A_w$	Wetted surface area
$B$	Breadth (m)

- $b$  Center position adjustment coefficient of a tangent hyperbolic function (wave frequency)
- $c$  Slope adjustment coefficient of a tangent hyperbolic function (wave heading)
- $C_b$  Block coefficient
- $C_{aw}$  Added wave resistance coefficient
- $C_{beam}$  Added wave resistance coefficients in beam waves
- $C_{CTH}$  Added wave resistance coefficients estimated from [Lang and Mao \(2021\)](#)
- $C_{following}$  Added wave resistance coefficients in following waves
- $C_{head}$  Added wave resistance coefficients in head waves
- $C_{L\&P}$  Added wave resistance coefficients estimated from [Liu and Papanikolaou \(2020\)](#)
- $d$  Center position adjustment coefficient of a tangent hyperbolic function (wave heading)
- $D_R$  Frictional drag reduction due to air lubrication
- $f(\alpha)$  Function that enables combining the various added wave resistance according to the wave headings
- $F_n$  Froude number
- $g(\lambda/L)$  Function that enables combining the various added wave resistance according to the relative wave lengths
- $L$  Length between perpendiculars (m)
- $n$  Polytropic index
- $P_1$  Atmospheric pressure
- $P_2$  Air delivery pressure from the compressor
- $P_B$  Engine brake power
- $P_{comp}$  Power needed to compress a specified quantity of gas
- $P_{cons}$  Power consumed by air compressor

$P_F$	Power required to overcome the frictional drag
$P_{net}$	Net power saving by air lubrication system
$P_N$	Net-percentage power saving
$P_{save}$	Power saved by air lubrication system
$R_T$	Total resistance
$R_{calm}$	Calm water resistance
$R_{wave}$	Added resistance in waves
$R_{wind}$	Added resistance due to wind
$T_d$	Design draught (m)
$T_m$	Mean draught (m)
$V_S$	Ship speed (m/s)

\* Note: The notation of a few symbols in the appended journal papers differs from that of this list. Refer to the symbols included in each paper for the correct representation.





# CHAPTER 1

## Introduction

*This chapter presents the motivation of the study along with the background. Further, the structure of this thesis is outlined.*

### 1.1 Background & Motivation

Global warming has recently emerged as a serious problem due to greenhouse gas (GHG) emissions, and in response, the International Maritime Organization (IMO) announced a strategy to reduce GHG emissions by at least 50% by 2050, compared to the 2008 level (IMO 2018). A number of strategies are being considered by stakeholders in the maritime sector, including the use of low-carbon alternative fuels, the development of energy-efficient ship technologies, and the promotion of new regulations to cut GHG emissions (Bouman et al. 2017). It is important to have a thorough understanding of the combination of the actual climate impact of various mitigation measures and the various measures for the transition of the global fleet. In addition, the estimation of GHG emissions at sea and assessing its impact on the environment and climate will greatly help to establish international rules, identify the most favorable emission mitigation measures, and make future decisions for emissions reduction.

Assessment of GHG emissions from global shipping can be carried out using a top-down or bottom-up approach. The former collects data on total fuel consumption based on bunker sales and models the resulting emissions, while the latter assesses the energy used by individual ships and the resulting emissions. In contrast to the top-down approach, the bottom-up approach has the advantage of enabling a relatively accurate evaluation of emissions based on the ship's automatic identific-

ation system (AIS) data. Another advantage of the bottom-up approach is that the same model can be used to assess the effectiveness of different emission mitigation measures for the global fleet. This approach derives fuel consumption and emissions using the AIS data, which requires a system that can predict required power in a simplified manner with sufficient accuracy according to the actual operational profiles and weather conditions for the global fleet.

Several studies have used AIS data along with ship-specific information to apply a spatial distribution bottom-up approach to the emissions from the marine sector, but they have only used very simple methods to predict the global fleet's power or energy consumption (Jalkanen et al. 2009; Smith et al. 2013, 2014; Rakke 2016; Olmer et al. 2017). For example, the cubic rule<sup>1</sup> or admiralty formula<sup>2</sup> was used to estimate the ship's power in calm water conditions, and a specific percentage of sea margin was applied for weather effect correction. In addition, the increase in resistance due to the biofouling of the ship was considered by applying the same fouling penalty to all ships. For the entire fleet and its subsegments, obtaining more useful estimates requires a relatively simple power prediction approach while accurately capturing trends with respect to various operating profiles. Although more complex methods have recently been used in some studies, it is necessary to develop a comprehensive powering prediction method that could compensate for the shortcomings identified in previous studies and utilize them for the bottom-up approach. For this reason, Bouman et al. (2016) and Muri et al. (2019a,b) presented a Maritime Transport Environmental Assessment Model (MariTEAM), which adopted a resistance-based approach to calculate the instantaneous power demand of a ship.

In Climate change mitigation in the maritime sector (CLIMMS), as an interdisciplinary research project associated with Senter for Forskningsdrevet Innovasjon (SFI) Smart Maritime, life cycle assessment, marine engineering, and climate science approaches are used to improve comprehension of the effects of various GHG mitigation measures and scenarios in the maritime industry. In order to further close the gap with real cases, work package 2 of the project, which the current work has been a central part of, aims to examine the methods used for complete power prediction and develop an improved MariTEAM model. The established power prediction model will be put to use to assess fuel usage, emissions, and energy efficiency for different fleet segments, as well as in combination with other scenarios to determine appropriate GHG reduction strategies.

In order to increase the reliability and accuracy of the MariTEAM model and to

---

<sup>1</sup> $P \propto V^3$  ( $P$ : ship's power,  $V$ : ship's speed)

<sup>2</sup> $C = \frac{\nabla^{2/3} V^3}{P}$  ( $C$ : admiralty coefficient,  $P$ : ship's power,  $V$ : ship's speed,  $\nabla$ : displacement)

show results at the global fleet level based on it, the scientific research conducted here covered several related topics as follows.

The first is the development of appropriate ship data processing methods. In the bottom-up approach for the global fleet, fuel consumption and emissions of ships are obtained through various calculation steps from simple input data. However, proper data preprocessing is essential since inherent errors in raw data may increase the error and uncertainty of the final result. For example, some values in the ship's main parameters are missing in the Sea-web database, which is used in the IMO GHG study. Although methods like median/mean imputation and regression equation were employed to overcome this issue, there is still room for improvement in terms of applicable constraints and result accuracy. As part of this work, an algorithm for handling missing values of the ship's main parameters is proposed.

Secondly, due to the lack of detailed ship information, uncertainties in collected data, and limitations in computational costs, it is necessary to identify applicable methods for predicting the power consumption of the global fleet. For example, there have been various approaches such as numerical methods, experiments, and semi-empirical methods to predict added resistance in waves of a ship, but methods suitable for a such purpose need to be identified. Thus, in this study, the performance of semi-empirical and machine learning methods is reviewed based on experimental data of various ship types and operating environments.

Finally, the application result of an energy-saving measure is demonstrated through the established fleet-wide powering prediction method. Here, among energy-saving measures, the air lubrication system, which has recently received much attention from the stakeholders in the maritime industry, is discussed as a case study. In order to assume the application of technology to the fleet segments in the world, a model that can be easily plugged into the developed model and simulates the basic mechanism of air lubrication under various ship types and operating environments is proposed.

## **1.2 Literature Review**

In relation to the modeling and application of the fleet-wide power performance prediction model, this Section investigates previous studies on major research items of the thesis, such as the estimation of various ship resistance components and energy-saving measures, and explains the overall background.

### 1.2.1 Power prediction method for the global fleet

A large amount of research has already established power prediction methods to evaluate the fuel consumption, emissions, and energy efficiency operating indicator (EEOI) of ships, and different strategies have been adopted depending on the available data and the objectives of the research. The methods used to evaluate ship power performance range from simple empirical methods to conventional model tests and sophisticated numerical analyses like computational fluid dynamics (CFD). However, the analysis of fleet segments relied on relatively simple computations and empirical methodologies due to a lack of precise information about ships, uncertainty in the gathered data, and limitations with respect to time-consuming computations.

Table 1.1 summarizes the details of previous studies of the complete power prediction method. [Jalkanen et al. \(2009\)](#) first presented the Ship Traffic Emission Assessment Model (STEAM) to assess the ship's GHG emissions at sea using AIS data. Here, the ship's power was estimated using a cubic rule, a very rough estimate of the ship's power, and a speed penalty based on the Beaufort scale. Based on the AIS data, the IMO GHG study ([Smith et al. 2014](#); [Faber et al. 2020](#)) and the International Council on Clean Transportation (ICCT) study ([Olmer et al. 2017](#)) examined worldwide shipping emissions, and in their analyses, ship power was determined using the admiralty formula and a sea margin. However, exponent three of the velocity and two-thirds of the displacement commonly used in the admiralty coefficients do not fit well with modern ships, and the gap is larger, especially at higher speeds ([Gupta et al. 2021](#)). On the other hand, more and more studies have recently used an approach to estimate ship resistance in calm water using well-established empirical methods based on ship model tank databases ([Holtrop and Mennen 1982](#); [Hollenbach 1998](#); [Guldhammer and Harvald 1974](#); [Kristensen and Lützen 2012](#)). [Tillig et al. \(2017\)](#) introduced ShipCLEAN, a generic ship energy system model that combines the outputs of numerous existing empirical equations for resistance estimations to compute ship power performance and predict fuel consumption under operating conditions with little input. The VERDE model, developed by [Tvette et al. \(2020\)](#) and [Guo et al. \(2022\)](#), can assess the fuel consumption of ships mainly based on [Holtrop and Mennen \(1982\)](#). In their study, a machine learning algorithm was applied to speed up calculations and obtain added resistance due to the weather effect. However, it is necessary to carefully consider the empirical methods for calm water resistance because the coverage range and input requirements are different, and the accuracy may vary depending on the ship profiles. In addition, the weather effect correction needs to be divided into added resistance due to wind and waves ([Blendermann 1996](#); [Fujiwara 2006](#); [ITTC 2017a](#); [Liu and Papanikolaou 2016, 2020](#)) rather than sea

margin (or Beaufort scale-based speed penalty) for more detailed and accurate consideration. The MariTEAM model of CLIMMS project, which enables the calculation of global fleet emissions using empirical methods, was initially developed by [Bouman et al. \(2016\)](#) and [Muri et al. \(2019a,b\)](#). This study covers the powering prediction method that can be used in the bottom-up approach of the global fleet, including the improvements in conjunction with subsequent studies such as [Dale \(2020\)](#) and [Kramel et al. \(2021\)](#) by complementing the shortcomings identified in previous studies.

### **Calm water resistance and biofouling**

The calm water resistance can be simply calculated through empirical equations such as systematic series and regression-based methods that comprehensively deals with the ship's hydrodynamics. However, methods such as Ayre ([Schneekluth and Bertram 1998](#)), Taylor-Gertler ([Gertler 1954](#)), Series-60 ([Todd 1957](#)), and Lapkeller ([Lap 1954](#); [Auf'm Keller 1973](#)), developed quite a long time ago, are ineffective at predicting resistance for modern hull form and are outdated ([Bertram 2011](#)). Meanwhile, compared to the aforementioned methods, there were other methods such as [Holtrop and Mennen \(1982\)](#), [Hollenbach \(1998\)](#), and [Guldhammer and Harvald \(1974\)](#) that have been developed relatively recently, which have been found to be applicable to various current ships. In some of the later studies, these equations were modified and updated. For example, [Kristensen and Lützen \(2012\)](#) included bulb correction into [Guldhammer and Harvald \(1974\)](#) for application to modern ships, and [Helmore \(2008\)](#) updated the coefficients for precise calculation of [Oortmerssen \(1971\)](#) method applied to small ships. Although many methods have been proposed, their scope of applicability varies according to the ship models used to develop the regression equations, and some of them require more specific input parameters than are typically available at the global fleet level.

The hull roughness of the ship is increased by the degree of biofouling and aging of the hull surface, which can lead to an increase in frictional resistance. [Townsin et al. \(1986\)](#) presented an increase in average hull roughness (AHR) according to ship age based on 86 sample surveys conducted in 1984-1985, and [Stenson \(2015\)](#) analyzed the hull roughness change of 845 ships in dry dock during 2003-2014. Meanwhile, [Uzun et al. \(2019\)](#) proposed a formula for estimating the fouling growth according to water temperature and static time based on extensive field test data, and [Oliveira et al. \(2022\)](#) analyzed the trend of fouling growth according to salinity through experiments on coated panels in the Baltic sea.

Several practical approaches have been proposed to approximate the effect of increase in the resistance resulting from this hull roughness change. Moreover, there are equations from [Bowden and Davison \(1974\)](#) and [Townsin and Mosaad \(1985\)](#)

**Table 1.1:** Methods used to estimate resistance components and propeller efficiency in previous studies. For successive studies conducted in the same research group, only the methods applied in the most recent study are shown in the table. Details of the abbreviations for each method are listed below the table.

Related work	Calm water resistance & Fouling penalty	Weather effect correction	Total propulsive efficiency
STEAM 1, 2, 3; Jalkanen et al. (2009, 2012), Johansson et al. (2017)	HB method	Towrsin-Kwon	Emerson's formula
Smith et al. (2013)	Power scaling based on HM method	Sea margin 10-15%	-
3rd/4th IMO GHG study; Smith et al. (2014), Faber et al. (2020)	Arbitrarily formula + 9% fouling penalty	Sea margin 10-15%	-
Lu et al. (2015)	HM method	Kwon	Sea-trial report
Rakke (2016)	HM method	Sea margin 15%	Values from similar ships
ICCT; Olmer et al. (2017)	Arbitrarily formula + Fouling factor according to ship age	Sea margin 10-15%	-
ShipCLEAN; Tilling et al. (2017), Tilling and Ringsberg (2019), Tilling et al. (2020)	HM method, GH method	Wind: Blendermann; Waves: STA2, NTUA-SDL, NTUA-SDL2	OpenProp, HM method
Kim et al. (2020)	HM method	Wind: Blendermann; Waves: STA1, STA2	Barritsas, HM method
VERDE; Tsvete et al. (2020), Guo et al. (2022)	HM method + 10% fouling penalty	Wind: Blendermann, Fujiwara; Waves: SNNM	Kristensen and Lutzen, HM method
MarITTEAM; Bounan et al. (2016), Muri et al. (2019a,b), Dale (2020), Krannel et al. (2021)	HM method, HB method, GH <sup>1</sup> method, OM <sup>1</sup> method + Fouling factor according to ship age	Wind: Fujiwara, Datasets (STA-JIP, Blendermann); Waves: Combined method	Kristensen and Lutzen, HM/HB/GH method

\* HB: Hollenbach (1998), HM: Holtrop and Mennen (1982), GH: Guldhammer and Harvald (1974), OM: Oortmerssen (1971), GH<sup>1</sup>: Kristensen and Lutzen (2012), OM<sup>1</sup>: Helmore (2008), Towrsin-Kwon: Towrsin and Kwon (1993), Kwon: Kwon (2008), Blendermann: Blendermann (1996), STA-JIP: ITTC (2017b), Fujiwara: Fujiwara (2006), STA/STA2: Boom et al. (2013), NTUA-SDL: Liu and Papanikolaou (2016), NTUA-SDL2: Liu et al. (2016), SNNM: Liu and Papanikolaou (2020), Combined: Kim et al. (2022) Emerson: Watson (1998), Barritsas: Barritsas et al. (1981)

adopted by International Towing Tank Conference (ITTC), which are used for power correction by hull roughness. Additionally, Marintek's formula (Steen and Aarsnes 2014), which assumes only an increase in the frictional resistance due to the effects of hull roughness, is also proposed. Granville's similarity scaling procedure (Granville 1958, 1987), which shifts the friction line based on the roughness function to predict the effect of a given roughness on the frictional drag of a plate of arbitrary length, has been adopted in some studies.

According to Olmer et al. (2017), biofouling on the hull surface may result in an average increase in the total resistance of 2-11% on global fleet segments. Despite these effects, many preceding studies of the bottom-up approach just applied the typical hull roughness of a newly built ship or applied the same percentage of fouling penalty for all the ships.

### **Added resistance due to wind and waves**

To simply take into account the power loss caused by the weather effect, studies analyzing emissions from global shipping have applied around 10-15% sea margin (Smith et al. 2013, 2014; Faber et al. 2020; Rakke 2016; Olmer et al. 2017). However, this approach cannot properly capture the weather effects according to the geographical and seasonal changes of the region that the ship is operating. There was another approach applying the correction for speed loss in accordance with the Beaufort scale (Jalkanen et al. 2009, 2012; Johansson et al. 2017). This method can be more thorough than applying the same sea margin to all ships, but it was pointed out that it cannot differentiate the increase in resistance due to wind and waves and may be somewhat less accurate than the method from recent studies (Lang and Mao 2021).

According to ITTC (2017b), the increase in resistance due to wind load can be calculated using the wind tunnel model test or CFD results of the ship, and if that is not possible, it can be estimated using a regression equation based on the wind tunnel model test data (Fujiwara 2006) or the wind tunnel coefficient data (Boom et al. 2013; Kaiser 2016). The ITTC (2018) also took the results of the Blendermann (1996)'s wind tunnel tests into account when calculating ship speed loss. While these databases offer wind resistance coefficient curves based on apparent wind angle for a particular ship type, in a regression equation, superstructure-related parameters can be employed as inputs. Information about the dimensions of the superstructure can be estimated using either the detailed hull form of the vessel or the regression formula given in Kitamura et al. (2017).

To estimate the added wave resistance, numerous semi-empirical approaches based on theory and experimental data have been suggested. There have been straight-



forward formulas, such as Kreitner's method (ITTC 2005) and Shopera's method (Papanikolaou et al. 2015), which can be used to calculate the added resistance in irregular waves directly. STAWAVE-1 and STAWAVE-2, which were adopted in ITTC (2014), were presented in Boom et al. (2013) as two simple methods of calculating the added resistance in waves for the purpose of correcting ship speed-power trials. The STAWAVE-2 method took into account both reflection and radiation contributions when estimating transfer functions for added wave resistance, while the STAWAVE-1 method was developed on the assumption that wave reflection contributions dominate added wave resistance. However, the application of these methods was only restricted to waves within 45 degrees off the bow, implicitly assuming the added resistance to be zero for other wave headings. The SHOPERA-NTUA-NTU-MARIC (SNNM) method was proposed by Liu and Papanikolaou (2020), and it was validated by Wang et al. (2021). Liu and Papanikolaou (2020) introduced a wave heading based trigonometric function into a statistical method, combining Faltinsen (1980) and Jinkine and Ferdinande (1974), and they extended the applicability range to arbitrary wave headings through regression analysis based on extensive model test data. In another study, Lang and Mao (2020) proposed a method to estimate the added wave resistance for a ship in head sea conditions only. This method was based on the approach suggested by Tsujimoto et al. (2008) and Jinkine and Ferdinande (1974), and it was also influenced by the method developed by Liu and Papanikolaou (2016). The suggested approach was further improved by including encountered wave frequency correction parameters, which enabled the estimation of peak amplitude positions in all wave headings (Lang and Mao 2021).

### **Total propulsive efficiency**

The main engine brake power can be estimated from the ship's total resistance estimate after taking into account the total propulsive efficiency of the ship. In most cases, the total propulsive efficiency is estimated approximately by applying a straightforward empirical formula, or by calculating each efficiency coefficient that makes up the total propulsive efficiency, such as open water efficiency, hull efficiency, relative rotative efficiency, etc., separately. Since it is not easy to gather detailed information about ship propellers generally, relatively simple methodologies have been used in research on the fleet level. In the former case, there exist approaches like Emerson's formula (Watson 1998), the method of Danckwardt (1969), and the method of Auf'm Keller (1973). The Emerson's formula covers contemporary propeller designs but only applies to low propeller RPM (Revolutions Per Minute), and Danckwardt (1969) and Auf'm Keller (1973) are only relevant to specific ship types (Birk 2019). In the latter case, it may be possible to estimate the total propulsive efficiency for a ship by estimating the sub-components

related to the hull and propeller, and engine & shaft connections, and then, multiplying them together.

There are approaches, such as [Gawn \(1957\)](#), [Newton \(1961\)](#), and [Oosterveld \(1970\)](#) to estimate open water efficiency, but they may not be suitable for current propeller designs and have a limited range of ships for which they are applicable. In general, the Wageningen B series, which covers a broad range of conventional open, fixed-pitch propellers, is widely used for the calculation of open water efficiency. In addition, [Kristensen and Lützen \(2012\)](#) extended its scope to a higher thrust loading based on an approximation curve proposed by [Breslin and Andersen \(1996\)](#). The thrust deduction factor and wake fraction, which are estimated by some calm water resistance methods [Holtrop and Mennen \(1982\)](#), [Hollenbach \(1998\)](#), and [Guldhammer and Harvald \(1974\)](#), can be used to determine the hull efficiency. [Alte and Baur \(1986\)](#) suggested an average value of 1.0 for single screw ships for relative rotative efficiency, which often ranges from 0.95 to 1.05.

## 1.2.2 Energy saving measures for ships

According to [Psaraftis and Kontovas \(2009\)](#), there are primarily two sorts of emission reduction strategies for shipping: technical and operational measures. The goal of technical measures is to lower the  $CO_2$  emissions from ships in comparison to conventional ships by utilizing modern technology, while operational measures refer to reducing emissions through operational strategy at the level of the ship or fleet, such as speed optimization, voyage planning, fleet management, and onboard energy management. In [Bouman et al. \(2017\)](#)'s study, the technical measures are further subdivided into four categories: hull design, power and propulsion, alternative fuels, and alternative energy sources. [Bouman et al. \(2017\)](#) also presented the potential reduction of  $CO_2$  emissions collected from a number of previous studies in each category, shown in [Figure 1.1](#).

Improvements to the current ship design, including optimization of hull design, installation of air lubrication systems (ALS) and appropriate hull coatings, can reduce ship resistance. As a different approach, expanding the size of the ship increases the amount of cargo that can be transported per unit distance, which can significantly reduce overall emissions per transport work. Meanwhile, switching from conventional fossil fuels to alternative fuels will result in the greatest emission reduction, and biofuels have the potential to cut  $CO_2$  emissions by up to 80% according to [Figure 1.1](#). Additionally, alternative energy sources like solar power, fuel cells, and wind-assisted propulsion can be taken into account for energy saving measures. Despite the fact that power and propulsion systems have the capacity to cut  $CO_2$  by about 5-20%, the median reduction in value is quite small when compared to other classifications, as shown in [Figure 1.1](#). Despite

these various measures, potential energy savings may vary depending on the type of ship, operational profile, environment, etc., and some technologies require special conditions for installation or operation. This fact illustrates the necessity for transparent modeling and evaluation of these technologies' potential for GHG reduction, applicability, and operating cost.

### **Air lubrication system**

In this work, the air lubrication techniques are discussed as an example case study among the energy saving measures in order to assess the impact on global fleet segments. According to the surveys (ABS 2019; Gebraad et al. 2021), as of 2021, there are about 50 ships with an air lubrication system, and interest in technology is continuously increasing considering the recent orders. There are three different types of air lubrication technology: injecting micro air bubbles into the lower part of the hull to reduce drag (bubble drag reduction); covering the bottom of the hull with a continuous air layer by increasing airflow (air layer drag reduction); and filling a cavity in the bottom of the hull with air (partial cavity drag reduction) (Foeth et al. 2009).

Numerous earlier studies used model tests, sea trials, or CFD to examine the performance and usability of air lubricating systems. The first commercial ALS was installed on a ship by Mitsubishi Heavy Industries, and the module carrier's sea trial demonstrated a net energy savings of up to 12% (Mizokami et al. 2010). In additional research, CFD was used to evaluate the distribution of bubbles on the hull surface and their effect on propeller performance (Kawabuchi et al. 2011). Silberschmidt et al. (2016) has developed a commercially available air carpet technology in which fine bubbles cover the entire bottom of the ship, achieving a net energy savings of about 4% in the actual operation of a 40k DWT tanker. Lee et al. (2017) observed the results of model tests, sea trials, and full-scale measurement data from two operating ships equipped with Samsung Heavy Industries' SAVER system. Meanwhile, Damen Group developed an air chamber energy saving (ACES) system that prevents water from contacting the lower surface of the hull by designing a cavity on the bottom of the hull and injecting air in order to establish an air cushion in the cavity (Pavlov et al. 2020).

## **1.3 Thesis Structure**

Chapter 2 lists the objectives defined for this study.

Chapter 3 presents research strategies that were used to achieve the objectives, and includes the scope and limitations of research.

Chapter 4 provides an overview of the research papers and how they contributed to fulfilling the objectives.

Chapter 5 describes the original contributions of the research papers, conclusions of this study, and ideas for future research.

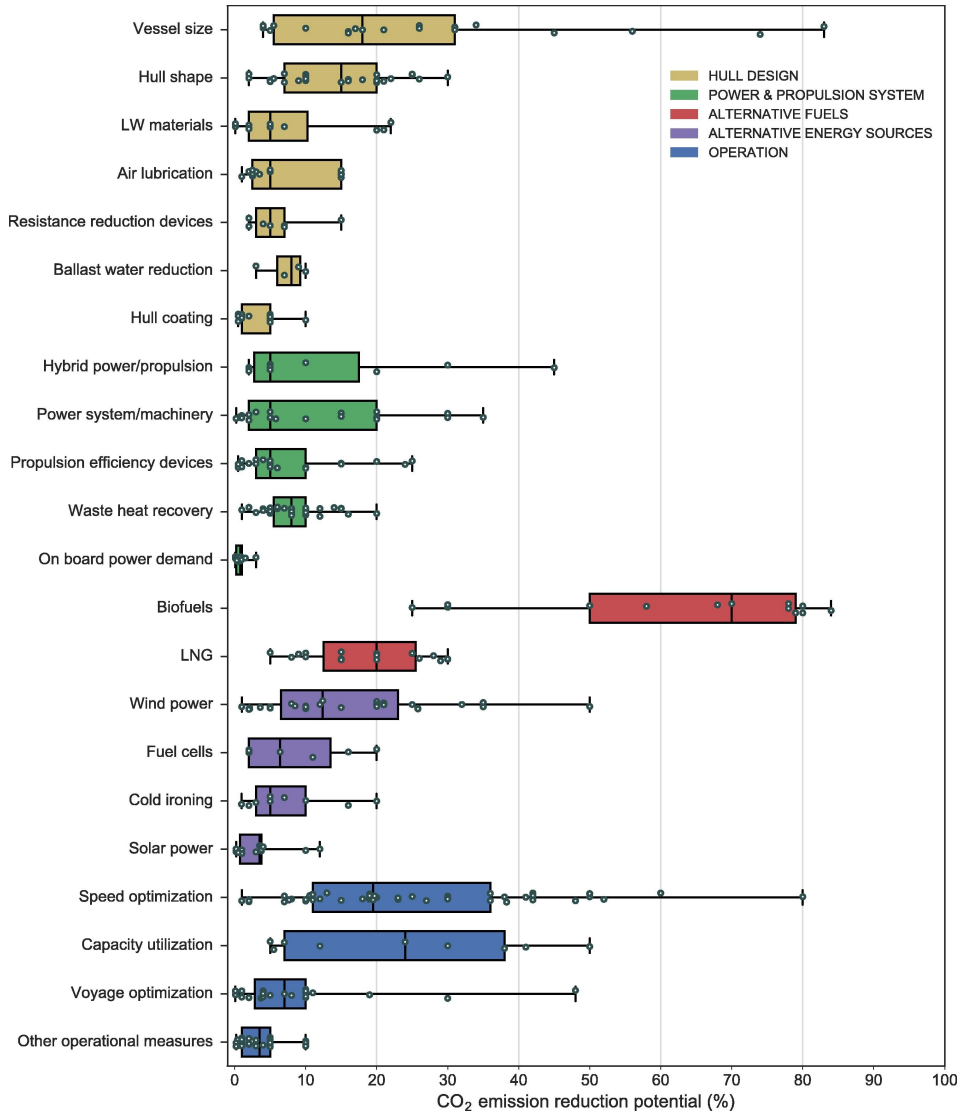


**Figure 1.1:** CO<sub>2</sub> emission reduction potential from individual measures (Bouman et al. 2017).

# Research Objectives

*This chapter lists the objectives formulated to guide this research.*

The purpose of this study is to develop and implement an efficient power prediction model for the global fleet based on fleet composition and trading patterns. Moreover, it is to enable scenario studies of energy-saving and emission-reduction measures using the established model. In order to reach the overall objective as described above, the following sub-objectives are formulated:

1. Development of appropriate data processing methods for different ship data sources
2. Identification and implementation of appropriate methods for estimating ship resistance components
3. Establishment of an improved power prediction method
4. Demonstration of the fleet-wide powering prediction method with application to an energy saving measure

The developed model should be applicable on a variety of ships only with limited ship information and require little computation time, while at the same time still being sufficiently accurate for the purpose of assessment of emissions from global shipping. To achieve this, appropriate data processing methods for ship data sources, which can primarily be used for bottom-up analysis, must first be identified and applied. In addition, a suitable approach should be determined through an

examination of possible methods for estimating each ship's resistance component and propulsion efficiency, which are used to predict the ship's necessary power at sea. To showcase how the developed powering prediction model can be applied in practical work, an example of such a study should also be provided.

# Research Design

*This chapter presents the research strategy. The scope of the work and limitations are also included here.*

## 3.1 Overview

Since it is a paper-based doctoral thesis, it includes five main papers written during the Ph.D. program. Figure 3.1 depicts a collection of studies to achieve the defined research objective, as well as how they are arranged and connected. It also shows co-authored papers as a reference.

An algorithm for handling missing values of ship technical information is presented in [Article 1](#) and the overall data processing work adopted in this thesis is covered in [Article 4](#). Although mentioned in [Article 4](#), some algorithms are referred to in [Co-author Article 1](#).

Methods for estimating ship resistance components and total propulsive efficiency are reviewed in [Article 4](#), and an improved complete power prediction method is developed based on the previous version of the MariTEAM model [Co-author Article 3](#). In this process, methods of estimating the added resistance in waves of a ship are discussed in detail in [Article 2](#) and [Article 3](#). In [Article 2](#), various semi-empirical methods are compared using model test data and a new semi-empirical method is proposed to increase the accuracy of the added wave resistance estimations, and in [Article 3](#) the data-driven models applying machine learning algorithms is demonstrated using the same dataset.

In [Article 5](#), the established model is demonstrated in combination with an energy-



saving measure, where the impact on the global fleet segment of various air lubrication systems is analyzed.

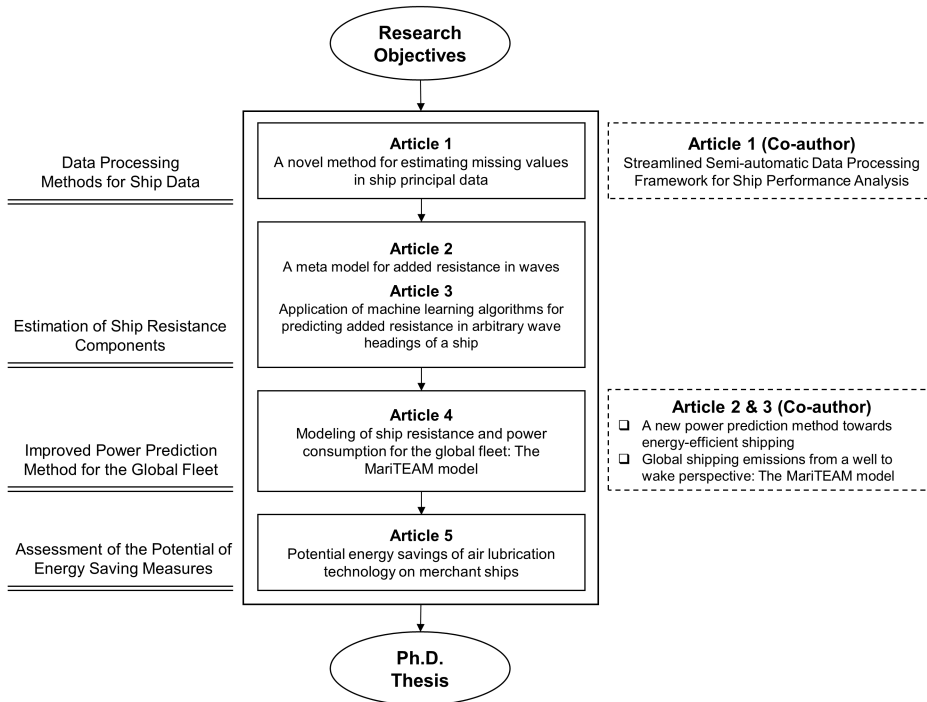


Figure 3.1: An overview of the thesis and the link between the research papers.

## 3.2 Research Strategy

### 3.2.1 Data Acquisition

In the bottom-up type of calculation performed in the CLIMMS project, it is necessary to have information about each ship, both the ship itself and its operation and weather profiles. The CLIMMS project obtains the ship's technical information from the sea-web database of Information Handling Services (IHS) Markit. It consists of the ship design-related parameters such as main dimensions, and engine specifications, of a total of 76,937 ships, including 14 different types with a total tonnage of 100 tons or more. Ship trajectory information such as position, velocity, and ship heading for the global fleet is obtained from a collection of ground-based AIS messages combined with data collected by two satellites (NorSat-1, NorSat-2) from 2017 to 2020. In this project, port call data is collected from the IHS Markit, including data on the date and time of arrival and departure of each vessel. From project-related industrial partners, high frequency in-service data of a

few ships is also provided. Global ocean weather data is obtained from the ERA-Interim (ECMWF reanalysis) dataset provided by the ECMWF (European Center for Mid-Range Weather Forecasting). It contains weather parameters including major environmental loads, i.e., wind, waves, and ocean currents. Apart from the previously mentioned data, in order to compare and evaluate the several semi-empirical methods for added resistance in waves, the measured values for added wave resistance coefficients of model ships were collected from publicly available sources. The data set consists of a total of 2559 samples of approximately 49 ships and 255 different experimental cases.

### 3.2.2 Method & Approach

#### Data Processing

In this study, various types of datasets are used, such as AIS data, Sea-web data, ECMWF data, data from previous model tests, and in-service data. Before the raw data is used for ship resistance and power estimation, various errors in the data should be properly handled and the data converted into the input form required by each module.

The ship's technical information is very important because it is to be used as a basic input for further calculations. However, for some ships some parameter values in the data might be missing. Therefore, an imputation method is developed based on a statistical approach to fill in the missing values as a part of this research ([Article 1](#)). The main process of the method consists of initial calculation (curve fitting), final imputation (multiple regression analysis + variable selection), and minor adjustment (domain knowledge). It will be further described in [Section 4.1.1](#).

There are often missing trajectories in AIS data due to heavy traffic or irregular reception of AIS data. Also, since AIS data is acquired in different ways (satellite, shore-based reception) the AIS data for a single voyage of a single ship might be found in different sources. Some missing trajectories in AIS data are restored using the combined A\* algorithm and Dijkstra's algorithm with reference to the port call data. In addition, draught data in AIS records often contain abnormal values because they are not automatically updated but are entered manually onboard. Therefore, if the acquired draught data of the ship is outside the range between the minimum allowable draught defined by the ship's classification rule and the design draught, it is considered an abnormal value and corrected. The AIS data does not contain information on weather conditions in the ship's navigational area. Thus, weather information corresponding to the time and location of the ship's voyage is interpolated based on the weather information gathered from the hindcast data

repositories ([Article 4](#)).

The high frequency in-service data is used for the validation of the empirical methods developed for the global fleet segments ([Article 2](#), [Article 4](#)). For a more accurate comparison between the predicted value from the model and the ship's in-service data, the steady-state detection algorithm presented in [Co-author Article 1](#), which can be used to filter out the parts of the time series in which the ship's propulsion state changes, is applied here. It may be erroneous to use data in unsteady conditions for analysis because the speed may change somewhat later than the ship's power when the propulsion state of the ship changes, such as during acceleration, deceleration, and maneuvering.

### **Complete power prediction method**

In a bottom-up assessment of energy consumption and emissions of the global fleet (or segments of it), the powering prediction method must work with very limited information about each ship, and it must be computationally very fast. Both requirements indicate that traditional high-fidelity powering prediction methods using model testing or first-principles-based numerical methods like CFD cannot be applied. Therefore, the research initially screened the literature for existing empirical methods, as well as simple numerical methods.

A variety of methods are analyzed, ranging from proven empirical techniques to relatively simple computational techniques. Some of these techniques may not be appropriate for all ship types and require many input parameters. In addition, traditional empirical methods were developed quite a long time ago and may not be appropriate for contemporary hull forms. Therefore, in this study, these approaches are examined thoroughly, and research strategies are adopted either to identify relevant empirical methods and how to estimate specific input parameters ([Article 4](#)) or to revise and further improve existing methods ([Article 2](#), [Article 3](#)). For example, various semi-empirical methods for added wave resistance are compared based on the model test data according to wave heading, ship type, wavelength, and Froude number. Based on the comparison results, a new method is developed by combining two already existing methods to improve the accuracy of the added wave resistance estimates. The newly developed method is further explained in [Section 4.1.2](#).

A thorough ship-to-ship and voyage-to-voyage validation of the power prediction against the global fleet is hardly possible. In this work, appropriate methodologies are identified and reviewed for each ship resistance module as part of the process of developing a complete power prediction model. The predicted values are then compared with full-scale measurements from several ships for which high fre-

quency in-service data is available in order to assess the accuracy of the suggested model. Finally, the improved MariTEAM model's overall accuracy is evaluated by comparing the annual fuel consumption reported by the EU-MRV<sup>3</sup> data for 2018 with that predicted by the model using the AIS data for the corresponding global fleet segment.

### Energy saving measures

As depicted in Figure 1.1, various energy saving measures can potentially help reduce the emissions from global shipping. Among them, switching to alternative fuels like LNG and biofuel instead of conventional fossil fuels appears to have one of the largest potential reductions. The MariTEAM model can, of course, be used to analyze these results, but as the focus of this thesis is mainly on ship technology, such as ship resistance and power prediction, it is not addressed here. In this study, air lubrication technology, one of the measures related to hull design, is explored as a case study for energy saving measures for the global fleet (Article 5). The use of air lubricating technology on actual ships is becoming more common, and it has recently gained greater attention. Since it can be easily installed on ships that are already in service, with the exception of the air cavity type, and has a substantial potential to cut emissions, it is particularly useful for analysis of energy reduction impacts in global shipping.

## 3.3 Scope and Limitations

The study aims to develop and implement an efficient power prediction model for the global fleet, taking into account fleet composition and trading patterns. To make this improvement, several sub-modules, covering the ship's hydrodynamic performance, speed-power analysis, and hull-propeller performance, were implemented as part of this work. Since the power prediction method is developed for application to the global fleet, a simple empirical method that can be applied to various ship types while having low computational time, and can have moderately good accuracy is mainly considered. Data-driven methods (semi-empirical methods and machine learning algorithms) based on the gathered model test data are also employed in this work concerning the prediction of added wave resistance of ships. CFD is not taken into account in the current study since it requires detailed hull form and information about the ship and takes a lot of time for the calculation. The influence of steering and maneuvering on power consumption is neglected. Similarly, as for resistance, propulsive efficiency is only considered using simple

---

<sup>3</sup>EU-MRV (European Union-The Monitoring, Reporting and Verification). The MRV Regulation provides requirements for the monitoring, reporting, and verification of carbon dioxide (<https://mrv.emsa.europa.eu>). The guidance is applicable to all ships over 5,000GT that transport passengers or cargo to, from, or within EU/EEA ports, regardless of Flag (European Union 2015).

empirical methods.

The project primarily collects AIS data, technical information, and weather hind-cast data for the global fleet, and they are used in a variety of ways, from model input to the creation of a new approach. The high-frequency onboard measurements of a few operating ships that can be obtained from the project are considered for verification of the developed model.

Regarding the analysis of energy saving measures for the global fleet, with consideration of the duration of the Ph.D. program, this study considers only air lubrication technologies according to various types as case studies. Although the CLIMMS project analyzes a variety of scenarios, including switching from current fossil fuels to alternative fuels like LNG and biofuels, these are not covered in this thesis because the thesis primarily focuses on ship technology linked to resistance and power prediction. The developed powering prediction method is suitable for studying other energy saving measures as well, such as wind-assisted propulsion or more slender ship designs, but time did not allow for going into these.

# Research Summary

*The summary of publications contributing to this thesis is presented here.*

## 4.1 Summary of Publications

### 4.1.1 Article 1: Missing Data Imputation for Ship Principal Parameters

In order to analyze the powering performance of the global fleet, ships' technical information like main dimensions, engine specifications, etc., is required. The CLIMMS project obtains information including a total of 76,937 principal parameters from the IHS Sea-web database. For some ships in the database, values of some variables are missing or clearly erroneous.

Deleting all the ship cases with missing parameters would make 46.6% of the data set unavailable, reducing the number of ship cases for analysis, degrading the statistical power of the model, and negatively affecting our ability to perform a comprehensive and reliable bottom-up analysis of the global fleet. Meanwhile, a method of simply replacing a missing value with an average or intermediate value of samples may lead to very low accuracy. Many studies have proposed curve-fitting equations or regression equations related to the main parameters of the ship, ensuring fairly high accuracy. However, it is not suitable for all ship cases because it can not be applied if the essential parameters used in the formula are missing. On the other hand, in other research fields, machine learning methods such as random forest have been adopted to replace missing values, but the applicability of such methods to the ship data set is uncertain and it is not easy to interpret the results

from the machine learning model.

Accordingly, a model-based calculation method using regression analysis that estimates the missing value of the ship's main data is developed here as shown in Figure 4.1. It consists of initial calculation, final imputation, and minor adjustment steps. The algorithm replaces missing values with appropriate values through curve fitting, updates the curve-fitted values again through nonlinear regression analysis, and finally corrects them based on domain knowledge.

As shown in Table 4.1, the accuracy of the model has been compared with that of several regression equations proposed in previous studies (Piko 1980; Takahashi et al. 2006; Charchalis and Krefft 2009; Kristensen 2013; Papanikolaou 2014; Charchalis 2014; Radfar et al. 2017; Abramowski et al. 2018; Cepowski 2019), which shows significant improvements by up to 15.6% of the R-squared value over the other methods. It is also compared with the random forest based machine learning model and showed no significant difference in performance. For ships having specific dimensional limitations due to the passage of the Suez Canal or Panama Canal, this model still shows good applicability (ref to Figure 4.2).

The methodology proposed in this paper can be applied not only to the estimation of the principal parameters of the ship but also to the handling of missing values of data sets with similar characteristics and has the advantage of being able to interpret the results. In conclusion, the completed data set from this method is used as the basic data for further work.

**Table 4.1:** Comparison of prediction performance for the container ship's principal data between previous studies and this study.

Ship principal parameters	This study				Best result from previous studies				Random forest model			
	MAE	RMSE	MSE	Adj - R <sup>2</sup>	MAE	RMSE	MSE	Adj - R <sup>2</sup>	MAE	RMSE	MSE	Adj - R <sup>2</sup>
AEP	341	453	2.05E+5	0.8508	-	-	-	-	181	352	1.24E+5	0.9093
B	0.83	1.07	1.16	0.9875	1.49	1.90	3.61	0.9613	0.11	0.35	0.12	0.9987
T	0.32	0.43	0.19	0.9788	0.40	0.54	0.29	0.9672	0.07	0.18	0.03	0.9963
DWT	1,877	3,141	9.87E+6	0.9946	2,906	4,447	1.98E+7	0.9892	355	858	7.36E+5	0.9995
GT	1,616	2,998	8.99E+6	0.9950	2,347	3,762	1.42E+7	0.9921	208	852	3.38E+5	0.9995
LDT	750	2,072	4.29E+6	0.9701	1,259	2,436	5.93E+6	0.9591	1,051	2,855	8.15E+6	0.9430
LOA	1.55	2.08	4.36	0.9993	1.63	2.24	5.00	0.9992	0.47	1.66	2.76	0.9995
LBP	1.49	1.98	3.92	0.9993	8.91	12.21	149	0.9742	0.74	2.96	8.76	0.9984
MEC	0.74	1.04	1.10	0.7062	-	-	-	-	0.12	0.39	0.15	0.9594
MEP	2,760	4,009	1.61E+7	0.9620	4,760	7,056	4.98E+7	0.8824	378	872	7.61E+5	0.9981
MER	17.8	44.7	1,995	0.9227	-	-	-	-	6.53	30.1	903	0.9649
MES	0.01	0.14	0.02	0.9609	-	-	-	-	0.01	0.10	0.01	0.9823
V	0.72	1.09	1.20	0.8989	1.16	1.70	2.87	0.7578	0.30	0.73	0.53	0.9551
TEU	2,211	332	1.10E+5	0.9931	265	456	2.08E+5	0.9872	41.0	152	2.31E+4	0.9985

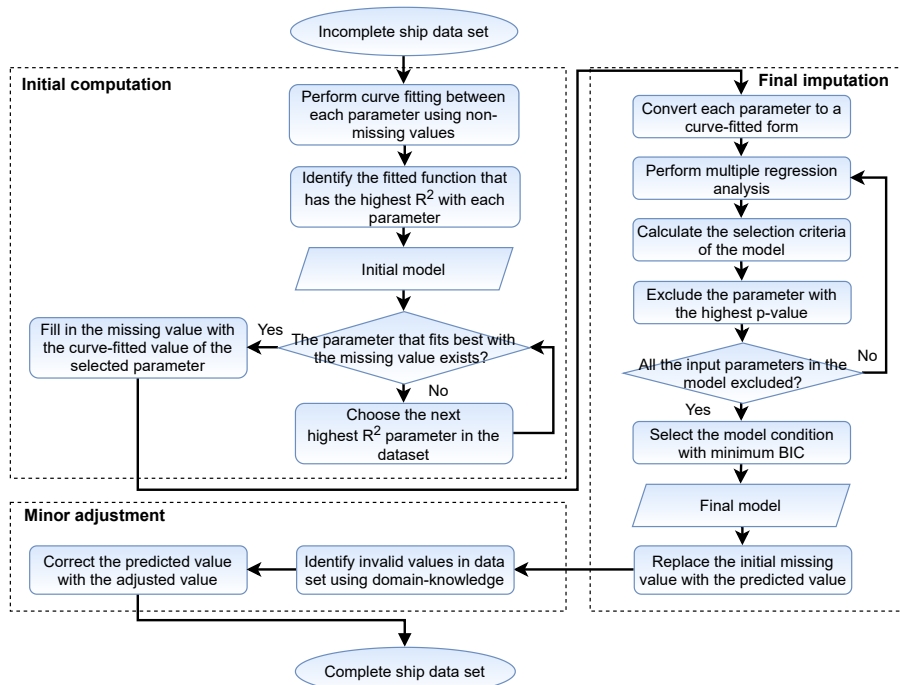


**Figure 4.1:** Flowchart of estimating ship principal data considering missing values as proposed in the study.

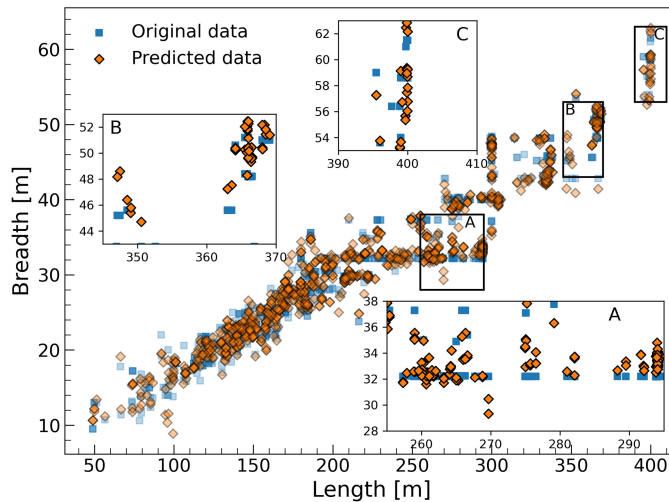


**Figure 4.2:** The relation between ship length and breadth regarding dimensional constraints (A: Panama Canal, B: New Panama Canal, C: Suez Canal).



### 4.1.2 Article 2: Estimation of Added Wave Resistance I (Semi-Empirical method)

To minimize the prediction error of the added resistance in waves and examine the applicability to the fleet segments, various semi-empirical methods are compared using extensive experimental samples under different ship types and operating conditions. The joint-industry project STA-JIP developed the STAWAVE-1 (STA1) and STAWAVE-2 (STA2) methods to correct the added resistance due to the waves for sea trial conditions, and it can provide good results with only a limited number of input variables (Boom et al. 2013). However, STA1 only considered the conditions where the contribution of wave reflection dominates the added resistance, and both STA1 and STA2 methods are limited to the added resistance in head waves within 45 degrees from the bow, implicitly assuming that the added resistance can be neglected in other headings. On the other hand, studies from Lang and Mao (2021) (CTH method) and Liu and Papanikolaou (2020) (L&P method) have broadened the application area to arbitrary waves by employing regression analysis based on substantial experimental data and introducing methods to calculate the added wave resistance including the contribution from both ship reflection and radiation.

As shown in Figures 4.3-4.4, the L&P method shows the smallest error overall among the listed methods, but there seems to be no absolutely perfect method because CTH may perform better depending on experimental conditions such as wavelength, Froude number, wave heading, and ship type. For the purpose of fleet segment application, this study requires a method to estimate added resistance of a ship with overall good accuracy for various ship characteristics and operating profiles.

Therefore, based on the findings, a new method (further referred to as Combined method), that combines two methods used to calculate added resistance in arbitrary waves is suggested. According to the wavelength and wave heading, the results of the two approaches (CTH and L&P) are combined, as in Equations (4.1)-(4.2), where the weighting factor is tuned to minimize the mean squared error between the model test data and the predicted results from the equations. The tangent hyperbolic function is used to determine the weighting factor, which has the advantage of smoothly connecting the two results by just tuning several coefficients (Refer to Equations (4.3)-(4.4)).

$$C_{aw} = \begin{cases} [1 - f(\alpha)]C_{head} + f(\alpha)C_{beam}, & \text{for } 90 \leq \alpha \leq 180 \\ [1 - f(\alpha)]C_{beam} + f(\alpha)C_{following}, & \text{for } 0 \leq \alpha < 90 \end{cases} \quad (4.1)$$

$$C_{head}(C_{beam} \text{ or } C_{following}) = [1 - g(\lambda/L)]C_{CTH} + g(\lambda/L)C_{L\&P} \quad (4.2)$$

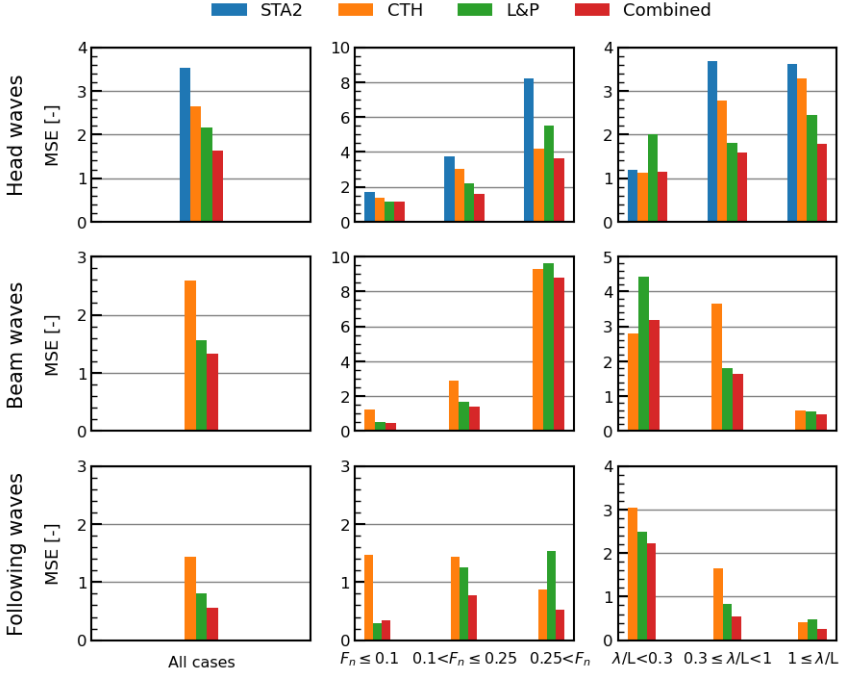


**Figure 4.3:** Comparison of several semi-empirical methods for added wave resistance according to wave headings, Froude numbers, and wavelengths. The upper row of the bar graph depicts head waves, the middle, beam waves, and the below, following waves. MSE refers to the mean squared error.

where  $C_{head}$ ,  $C_{beam}$ , and  $C_{following}$  represent the added wave resistance coefficients in head waves, beam waves, and following waves, respectively.  $C_{CTH}$  and  $C_{L\&P}$  represent added wave resistance coefficients estimated from CTH and L&P.  $f(\alpha)$  and  $g(\lambda/L)$  are functions that enable combining the various added wave resistance according to the wave headings and wavelengths, respectively. By multiplying  $1 - g(\lambda/L)$  and  $g(\lambda/L)$ , which are outputs of tangent hyperbolic function, by  $C_{CTH}$  and  $C_{L\&P}$ , respectively, the two results according to  $\lambda/L$  are smoothly connected. The same applies to  $1 - f(\alpha)$  and  $f(\alpha)$ .

$$f(\alpha) = \frac{1}{2}[1 + \tanh(c(d - \alpha))] \quad (4.3)$$

$$g(\lambda/L) = \frac{1}{2}[1 + \tanh(a(b - \lambda/L))] \quad (4.4)$$

where  $a$  and  $c$  are coefficients to determine the slope of the weighting function, and  $b$  and  $d$  are coefficients to adjust the center position of the function. All of the

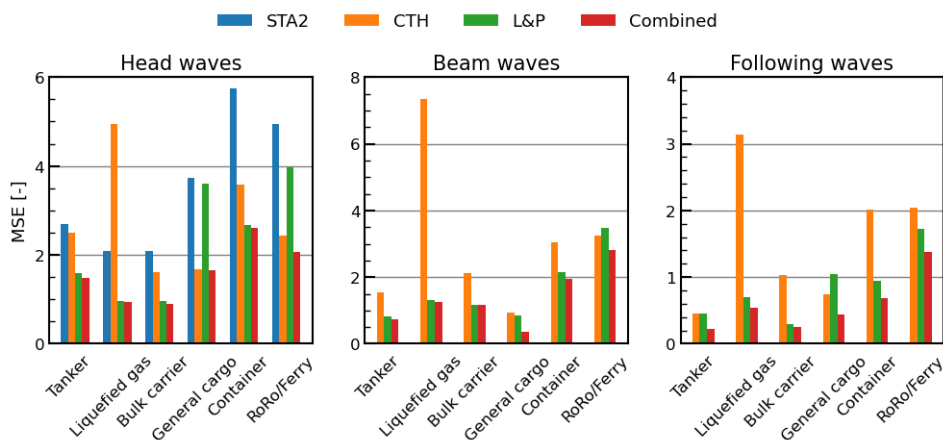


**Figure 4.4:** Comparison of several semi-empirical methods for added wave resistance according to ship type.

coefficients ( $a$ ,  $b$ ,  $c$ ,  $d$ ) are tuned to reduce the discrepancy between the estimated value from Equation (4.1) and the model test data.

The Combined method, as seen in Figure 4.5, obtained improved outcomes for experimental data while minimizing total error without considerably departing from the original methods' prediction range. As a result of validating the Combined method using the high frequency in-service data from two ships (a general cargo and a container ship), it performed the best among the other methods (ref to Figure 4.6). The relative RMSEs of Kreitner, Shopera, and STA2 were quite substantial, ranging from 14% to 45%, and CTH and L&P provided errors ranging from 1% to 9%. It also performed well when estimating added wave resistance under different conditions of wave heights, wave headings, and ship speeds.

The robustness and applicability for various ship types and operating conditions are the main strengths of the new method. It can be widely applied to early design stages where detailed hull design is not decided and advanced tools are not available, speed correction at sea trials, and overall performance evaluation of the fleet segment.

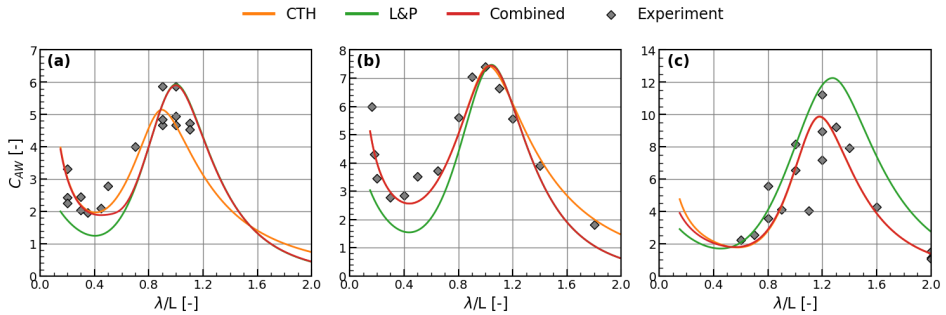


**Figure 4.5:** Examples of added wave resistance coefficient predicted by the Combined method: (a) DTC ( $F_n=0.139$ ), (b) HSVA ( $F_n=0.232$ ), (c) S60 ( $F_n=0.283$ ). The figure corresponds to the case of head waves ( $\alpha=180$ ).

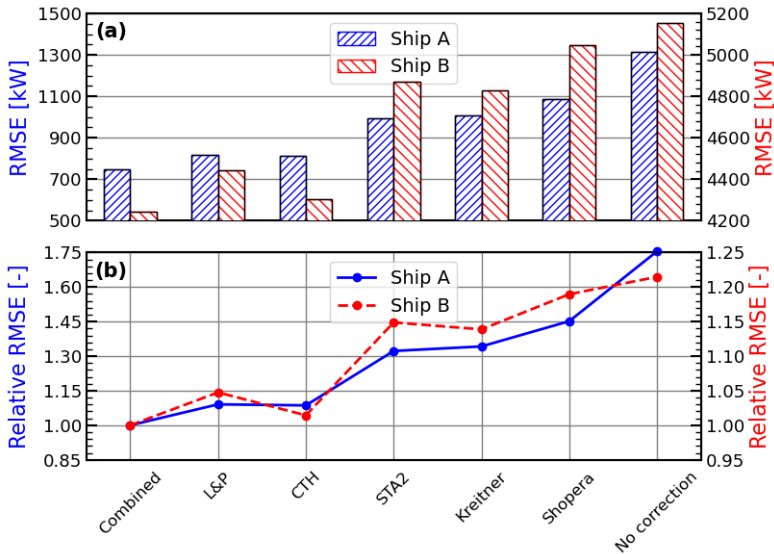


**Figure 4.6:** A comparison of errors in different methods against full-scale measurements of two ships. Figure (a) shows RMSE and Figure (b) shows relative RMSE against the Combined method. RMSE refers to the root mean squared error.

### 4.1.3 Article 3: Estimation of Added Wave Resistance II (Machine learning method)

In contrast to the semi-empirical approach shown in [Article 2](#), this study aimed to investigate the applicability of machine learning algorithms, a purely data-driven approach, to predict added resistance in arbitrary waves. According to literature surveys, there have not been many studies that applied machine learning algorithms to predict added wave resistance. Based on the model test results of 14 ships, [Cepowski \(2020\)](#) used an artificial neural network (ANN) to predict added resistance in head waves, and in [Martić et al. \(2021\)](#), results from the 3D panel method of a container ship were used to train an ANN model. However, there is room for improvement as their application was limited to head waves and only the ANN was used as a machine learning algorithm.

In order to develop models that predict added wave resistance coefficients ( $C_{aw}$ ) in this study, various algorithms are taken into consideration. Dimensionless parameters related to hull dimensions and operating conditions are employed as inputs to the model and the same model test dataset as in [Article 2](#) is used. The input variables are indicated in Equation (4.5).

$$C_{aw} = f(L/B, B/T_m, T_m/T_d, \theta, C_b, F_n, \alpha, \lambda/L) \quad (4.5)$$

where  $f(\mathbf{x})$  represents machine learning algorithms such as extreme gradient boosting (XGB), random forest (RF), k-nearest neighbors (KNN), artificial neural network (ANN), gaussian process regression (GPR), and support vector regression (SVR).  $L$  is length between perpendiculars,  $B$  is breadth,  $T_m$  is mean draught,  $T_d$  is design draught,  $\theta$  is trim angle,  $C_b$  is block coefficient,  $F_n$  is Froude number,  $\alpha$  is wave heading, and  $\lambda$  is wave length. The input variables in Equation (4.5) are selected to cover what is believed to be important for added resistance, and being available information in the MariTEAM model.

Here, nested cross-validation (CV) is employed to maximize data usage by evaluating machine learning algorithms and simultaneously tuning hyperparameters when using limited amounts of data samples. The test results of nested cross-validation as well as the response surface of the predicted values are shown in [Figures 4.7-4.8](#). Overall, SVR has demonstrated good predictive performance for all metrics employed, is robust to outliers due to its smoothly connected response surface and equally dispersed sample colors, and seems to adequately represent the ship's added resistance in arbitrary waves.

Assuming that the ship encounters waves in all directions randomly, and calculat-

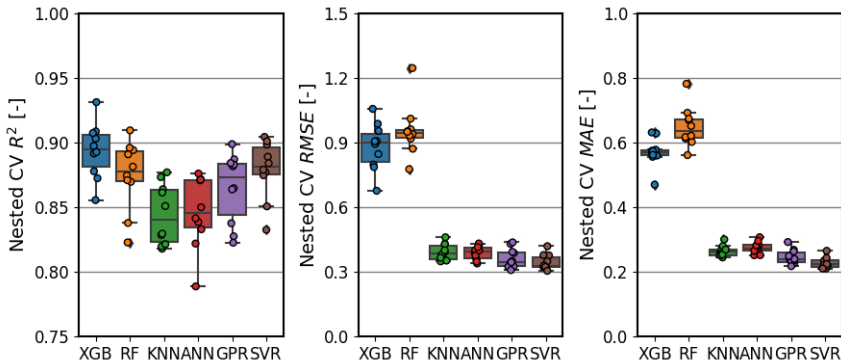


**Figure 4.7:** Performance evaluation between machine learning models with test data from nested cross-validation.

ing the added wave resistance in irregular waves, the relative deviations between the SVR model and other methods are shown in Figure 4.9. Here, a 280m-bulk carrier is used for a case study, and a modified Pierson-Moskowitz wave spectrum is applied. While STA2 and Cepowski (2020) show a difference of 50–80% for sea states (SS) varying from 3 to 7, CTH and SNNM show a difference of less than 10% on average. These differences in results highlight the need for methods in arbitrary waves, given the realistic environment experienced by ships at sea. Moreover, the relative deviation of the SVR model with SNNM and CTH, which provides the most accurate prediction in regular as well as irregular waves (as shown in Article 2), is not significant, showing the reliability of the SVR model in irregular waves.

This study has proven the applicability of a data-driven machine learning model with only using a few input parameters, in order to predict the added wave resistance for various ships. However, the results of the current study have not observed better performance of the machine learning models than the existing semi-empirical methods. Therefore, based on the results of Article 2 and Article 3, the Combined method is adhered to as an added wave resistance estimation method of the MariTEAM model.

Nevertheless, there is ample room for improvement in accuracy and coverage if more data is available for the training of machine learning models. In this case, potential benefits may be expected because retraining the currently proposed machine learning methods would be relatively easier than, for example, SNNM methods or other semi-empirical methods.

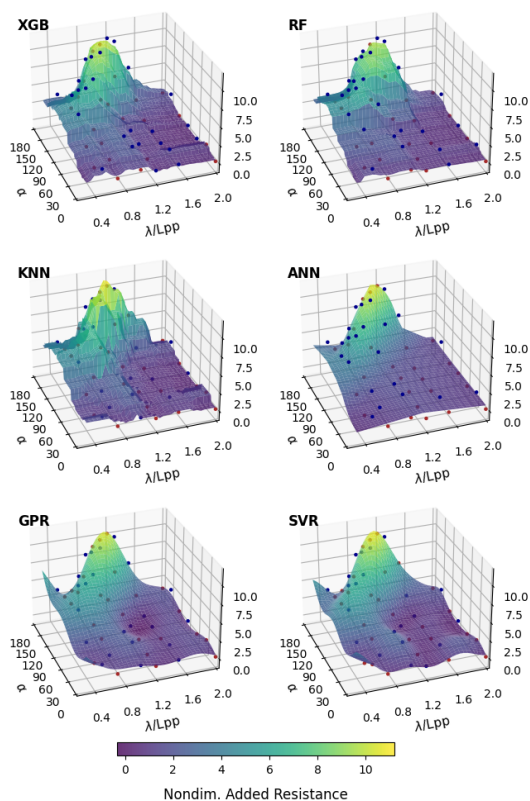


**Figure 4.8:** Prediction surface of added wave resistance coefficients of machine learning algorithms (S175 container,  $F_n=0.25$ ).

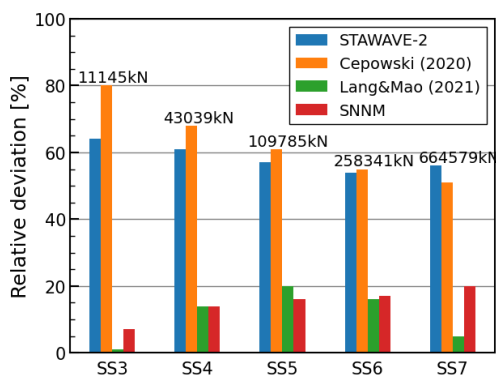


**Figure 4.9:** The relative deviation to the sum of the added resistance in irregular arbitrary waves between the machine learning model (SVR model) and other semi-empirical methods according to the sea state. The number on the bar indicates the added resistance in irregular waves of a ship.

#### 4.1.4 Article 4: Ship Resistance & Power Prediction for the Global fleet

Due to the lack of detailed ship information, the uncertainty of the collected data, and the limitations in computational cost, the power prediction of the fleet segment mostly relied on relatively simple calculations and empirical methodologies. In this study, an approach is taken to identify the most suitable method or combination of methods among the methods used in previous studies or to modify and improve existing methods. The suggested method, which is based on the MariTEAM model, uses AIS data, the ship's technical information, and meteorological data to estimate the amount of power that an operational ship needs at any given time in the operation, taking into account the effects of ship loading condition, wind, waves, current and hull fouling. The overall flowcharts of the MariTEAM model and the power prediction method are shown in Figures 4.10 and 4.11.

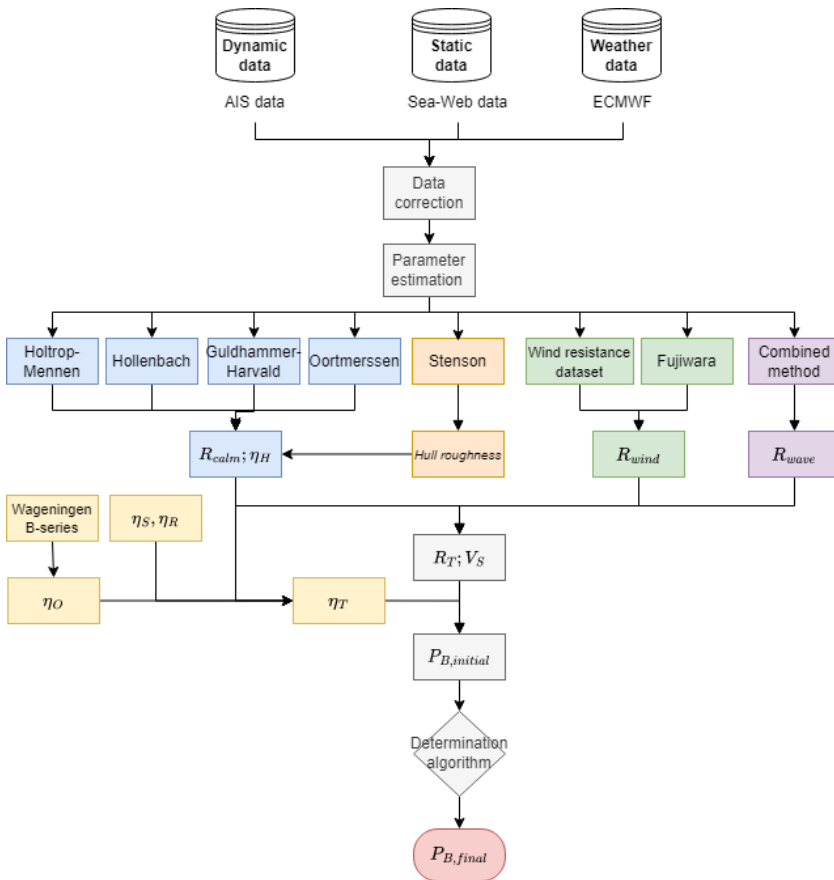


**Figure 4.10:** Schematic diagram of the complete power prediction module for the fleet segment in the MariTEAM model.



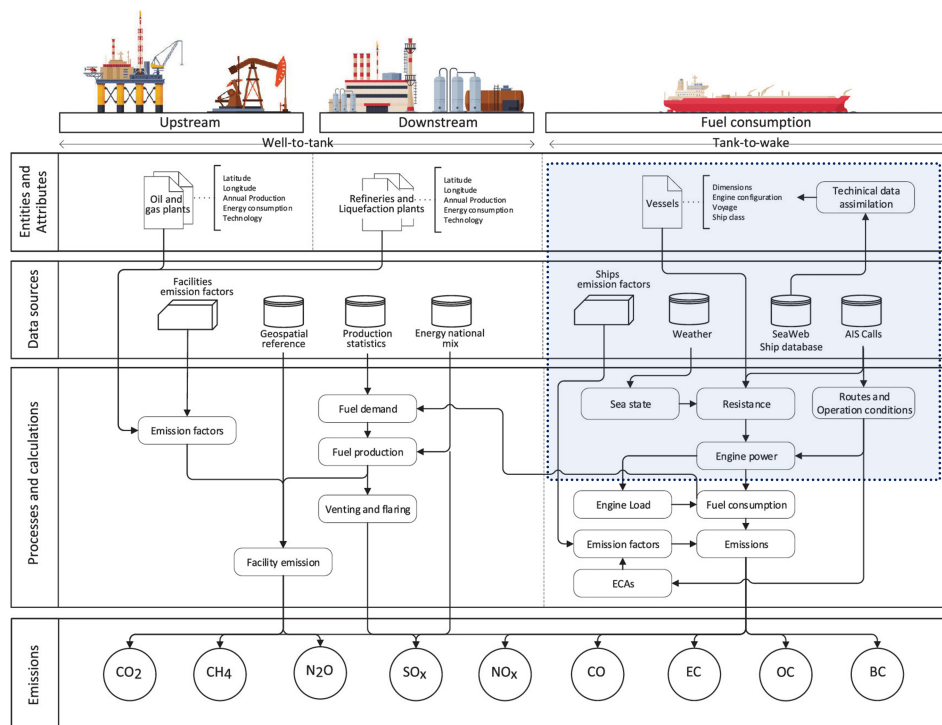


**Figure 4.11:** MariTEAM modeling framework for global well-to-wake emission. The blue-shaded part is the ship power prediction module outlined in Figure 4.10.

Here, HM (Holtrop and Mennen 1982), HB (Hollenbach 1998), GH (Guldhammer and Harvald 1974; Kristensen and Lützen 2012), and OM (Oortmerssen 1971; Helmore 2008) methods are taken into consideration as candidate approaches to estimate the ship’s calm water resistance in order to broaden the application to different ships. According to the determination algorithm, a suitable method is selected among the candidate methods for each ship case, and when multiple methods are selected, the average of their prediction is calculated. The determination algorithm is based on two main criteria for selecting a suitable method: one for determining whether the power prediction under the ship’s design conditions falls within the 80-95% range of the MCR and the other for determining whether the ship falls within the applicable range of the different methods. Additionally, using data on hull roughness obtained from the dry dock provided by Stenson (2015), this study extends it to the global fleet and calculates the average hull roughness change in accordance with ship age and average coating performance. In order to determine the added resistance caused by the hull roughness, Marintek’s equation (Minsaas 1982; Steen and Aarsnes 2014) is used.

For weather effect correction, added resistance due to wind and waves is estimated according to the surrounding weather conditions and characteristics of the ship. It is necessary to consider as many wind tunnel test results as possible to more accurately estimate the added resistance due to wind of the global fleet, which includes various ship types and a wide range of sizes. Therefore, in this study, the wind tunnel test results of ITTC (2017b) and Blendermann (1996) and the regression equation of Fujiwara (2006) are mainly used. If there is a wind tunnel test result of the ship type and size consistent with the target ship, the average value between the wind tunnel tests and the estimated value by Fujiwara (2006) is used, otherwise, only Fujiwara (2006) is used. The parameters related to the superstructure of the ship used as the input of the regression equation are estimated using Kitamura et al. (2017). To calculate a ship's added resistance in arbitrary waves, the Combined method introduced in Article 2 is used.

The main engine brake power is estimated from the ship's total resistance estimate after taking into account the total propulsive efficiency of the ship. Here, Kristensen and Lützen (2012) is applied to estimate the total propulsive efficiency, which contains methods for simply calculating each efficiency term with limited information. In their study, open water efficiency is estimated from the approximation of Wageningen B-series (Oosterveld and van Oossanen 1975), hull efficiency is determined from wake fraction and thrust deduction factor (HM/HB/GH), and relative rotational efficiency and shaft efficiency are replaced by approximate values.

As shown in Figure 4.12, the developed model is validated using in-service data from three ships; LNG carrier, general cargo, and container, each consisting of different data collection periods and sampling intervals. It demonstrates that the prediction of changes in power in different operational profiles is consistent. In addition, the performance of the developed model for the actual fleet segments is compared by benchmarking the EU-MRV (European Union-The Monitoring, Reporting and Verification) data for 2018 (Figure 4.13). The EU-MRV data contains information on the annual fuel consumption and emissions of approximately 12,000 ships with European origin or destination. The annual fuel consumption of individual vessels is estimated using AIS data matching with EU-MRV data, and it is compared with the reported information. At the aggregation level, the distribution of fuel consumption across all segments appears to be fairly accurately reproduced by the model, complementing the validation of the in-service data in a good manner. Since EU-MRV data is a type of top-down approach, it is particularly reassuring to observe that our bottom-up calculation is in such good agreement. Figure 4.14 shows the geographical distribution of energy consumption of the global fleet, calculated by MariTEAM.

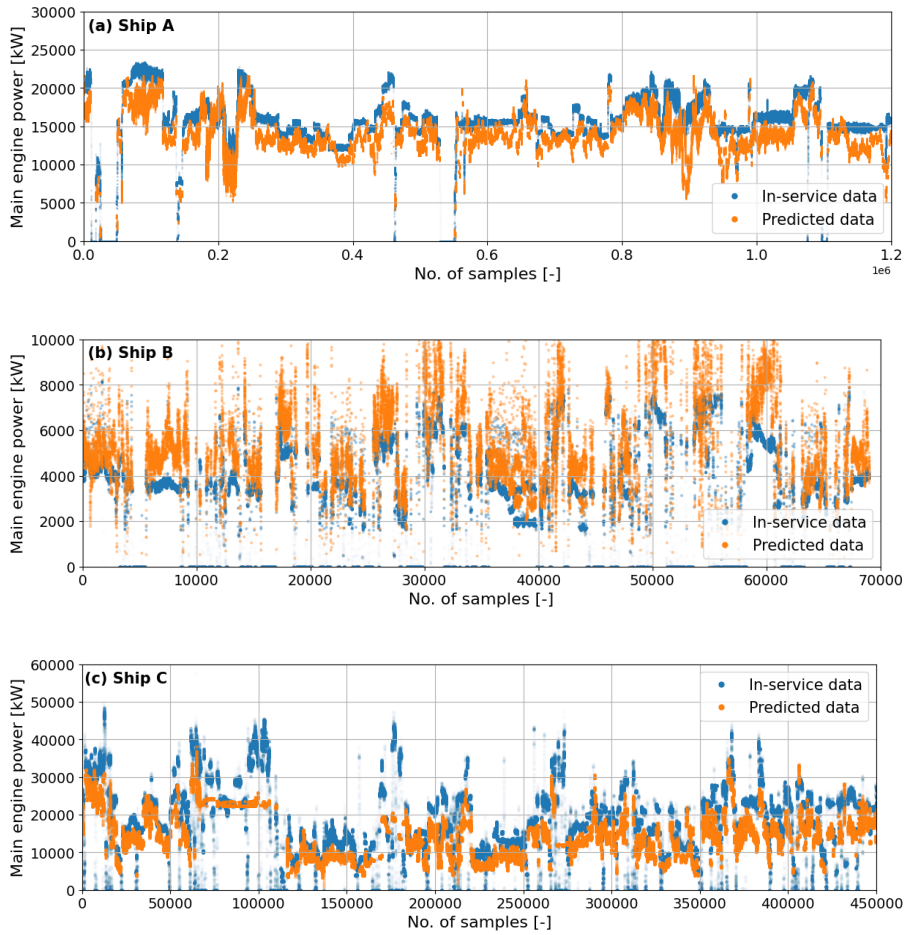


**Figure 4.12:** Comparison of in-service data and model predictions on main engine power of three ships: (a) Ship A, (b) Ship B, and (c) Ship C.

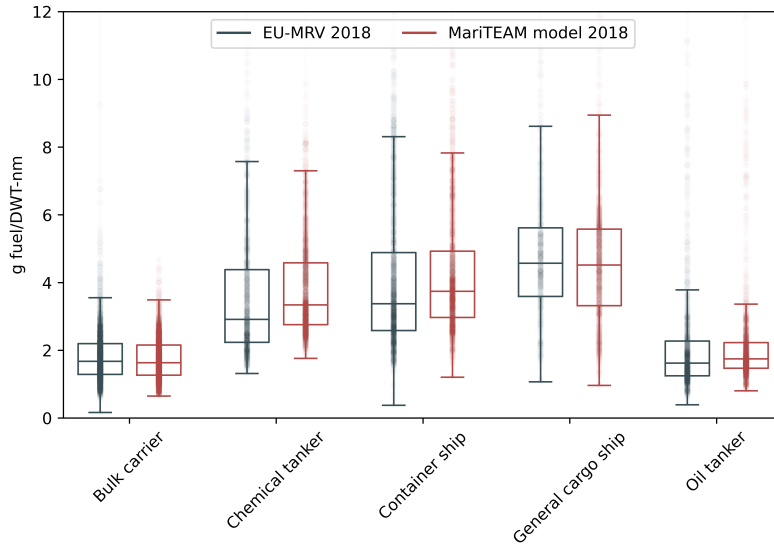


**Figure 4.13:** Comparison of annual fuel consumption of the fleet segments in 2018 between EU-MRV data and predicted values by the MariTEAM model.

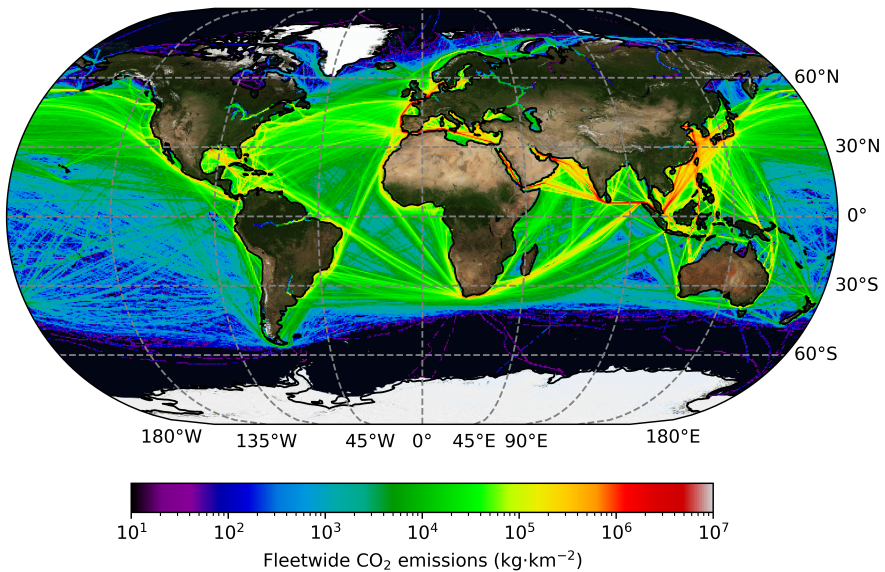


**Figure 4.14:** Geospatial distribution of CO<sub>2</sub> emissions from the global shipping in 2018.

#### 4.1.5 Article 5: Energy Saving Device: Air Lubrication System

Based on the power prediction model developed in [Article 4](#), the effect of energy saving measures on global fleet segments can be evaluated. Here, the air lubrication system (ALS) is modeled as an example of the potential energy saving measures. The theoretical background, estimation methods, and assumptions supporting the model are addressed.

For most commercial cargo ships, frictional resistance is the largest component of resistance, often more than 50% of the total. Therefore, a reduction of frictional resistance is relevant for energy efficiency improvement. Keeping the hull smooth and clean is of course important, but additional savings might be obtained by air lubrication. Net savings can be obtained by considering the power consumed in the blower to discharge bubbles to the bottom of the hull and the energy saving from the propulsion system with the help of ALS. Taking into consideration the above underlying ideas and the designed assumptions, a simplified empirical model is proposed as in Equations (4.6)-(4.8), which can evaluate the performance of three air lubrication techniques: bubble drag reduction (BDR), air layer drag reduction (ALDR), and partial cavity drag reduction (PCDR). Experimental results, reports, empirical formulas, and so on that are used to estimate information such as system setup, air flux rate, achievable drag reduction, blower specifications, etc., of which are necessary for modeling air lubrication systems are listed in [Table 4.2](#).

$$P_N[\%] = \frac{P_{save} - P_{cons}}{P_B} \times 100 = \frac{P_{net}}{P_B} \times 100 \quad (4.6)$$

$$P_{save} = P_F D_R \frac{A_a}{A_w} \quad (4.7)$$

$$P_{cons} = \frac{P_{comp}}{\eta_e} = \frac{\dot{m}_g}{\eta_c \rho_1} P_1 \frac{n}{n-1} \left( \left[ \frac{P_2}{P_1} \right]^{\frac{n-1}{n}} - 1 \right) \quad (4.8)$$

where  $P_N$  is net-percentage power saving,  $P_{save}$  is power saved by air lubrication system,  $P_{cons}$  is power consumed by air compressor,  $P_{net}$  is net power saving by air lubrication system,  $P_B$  is total brake power,  $P_F$  is the power required to overcome the frictional drag,  $D_R$  is frictional drag reduction due to air lubrication,  $A_a$  is air-covered area at the bottom surface,  $A_w$  is wetted surface area,  $\eta_e$  is the efficiency of electrical motor,  $\eta_c$  is efficiency of an air compressor,  $\dot{m}_g$  is the mass flow rate of air necessary to maintain the given volume flow rate of air on the bottom surface,  $\rho_1$  is the initial density of the air where it is compressed,  $P_1$  is the atmospheric pressure,  $P_2$  is the air delivery pressure from the compressor, and  $n$  is the polytropic index.

**Table 4.2:** The input parameters of ALS model and their estimation methods.

Parameter	Estimation method
$P_B$ [kW]	Estimated by power prediction method (Kim et al. 2022)
$P_F$ [kW]	Estimated by power prediction method (Kim et al. 2022)
$D_R$ [-]	Assumed 0.20, 0.80, 0.95 for BDR, ALDR, PCDR (Elbing et al. 2008; Lay et al. 2010)
$A_a/A_w$ [-]	$A_b/A_w$ : Estimated by the regression equation (Kim and Steen 2022) $A_a/A_b$ : Assumed 0.84 (Wu and Ou 2019)
$\dot{m}_g$ [kg/s]	$Q$ : Estimated based on the model test results (Mäkiharju et al. 2012) $P_{loss}$ : Conservatively assumed 1.5 bar (Ceccio and Mäkiharju 2012; Jang et al. 2014)
$n$ [-]	Assumed 1.4 (Nag 2013)
$\eta_c$ [-]	Conservatively assumed 0.6 (Mäkiharju et al. 2012; Jang et al. 2014)
$\eta_e$ [-]	Assumed 0.9 (Mäkiharju et al. 2012)

Based on the developed ALS model, parametric analysis on the energy savings of air lubrication technology is carried out for a 50,000 DWT general cargo ship according to variations in ship speed, ratio of air-covered area to the bottom surface area, loading condition, and block coefficient, as illustrated in Figure 4.15. Due to the dominance of frictional resistance at low speeds, it is desirable for ships to operate at low service speeds. Nevertheless, the speed conditions that can produce the greatest savings may slightly vary due to different air flux requirements of blowers depending on the ALS types. It is obvious that the system configuration such as the arrangement of the air release unit, which affects how much air can cover the bottom area, can have a considerable impact on performance in addition to the ship's flat bottom area. Furthermore, as the draught rises, the hydrodynamic drag also rises, increasing the required power.

Assuming that the corresponding vessel navigates between Rotterdam (NLRTM) and New York (USNYC) for one year, a simulation of the energy saving of the ALS is performed. As a result of ALDR for laden voyages, Figure 4.16 (a) shows seasonal changes, and Figure 4.16 (b) shows three different scenarios: calm sea conditions, actual sea conditions, and actual sea conditions with weather adjustment factors. In comparison to the calm water condition, the overall energy saving impact is decreased by around 15% to 35% when taking into account the actual weather condition and the weather correction factor.

The potential net percentage power savings for BDR, ALDR, and PCDR, respectively, would be 2–5, 8–14, and 16–22 %, according to a case study that is conducted under the assumption that the global fleet (see Figure 4.15) is outfitted with ALS and operates in calm sea conditions. From Figure 4.17, as compared to container ships with slender hulls and high service speeds, bulk carriers and tankers with blunt hulls and moderate operating speeds can achieve higher energy savings

from the air lubrication system. The amounts of savings revealed in the fleet-wide analysis match fairly well with numerous studies on individual ships that can be found in the literature.

The methodology used in this study can be used to assess the expected effects on a worldwide fleet with a variety of operating profiles, including variations in ship locations and seasons. From the analysis results of the global fleet and keeping in mind that it can be easily installed on ships already in service except in the case of the air cavity type ALS, it is judged that air lubrication technology has considerable potential to reduce emissions from global shipping. As is also discussed in [Article 5](#), partial cavity drag reduction (PCDR) is immature technology, with known challenges related to stability, loss of air in high waves, and additional drag due to keels and other air cavity-related appendages.

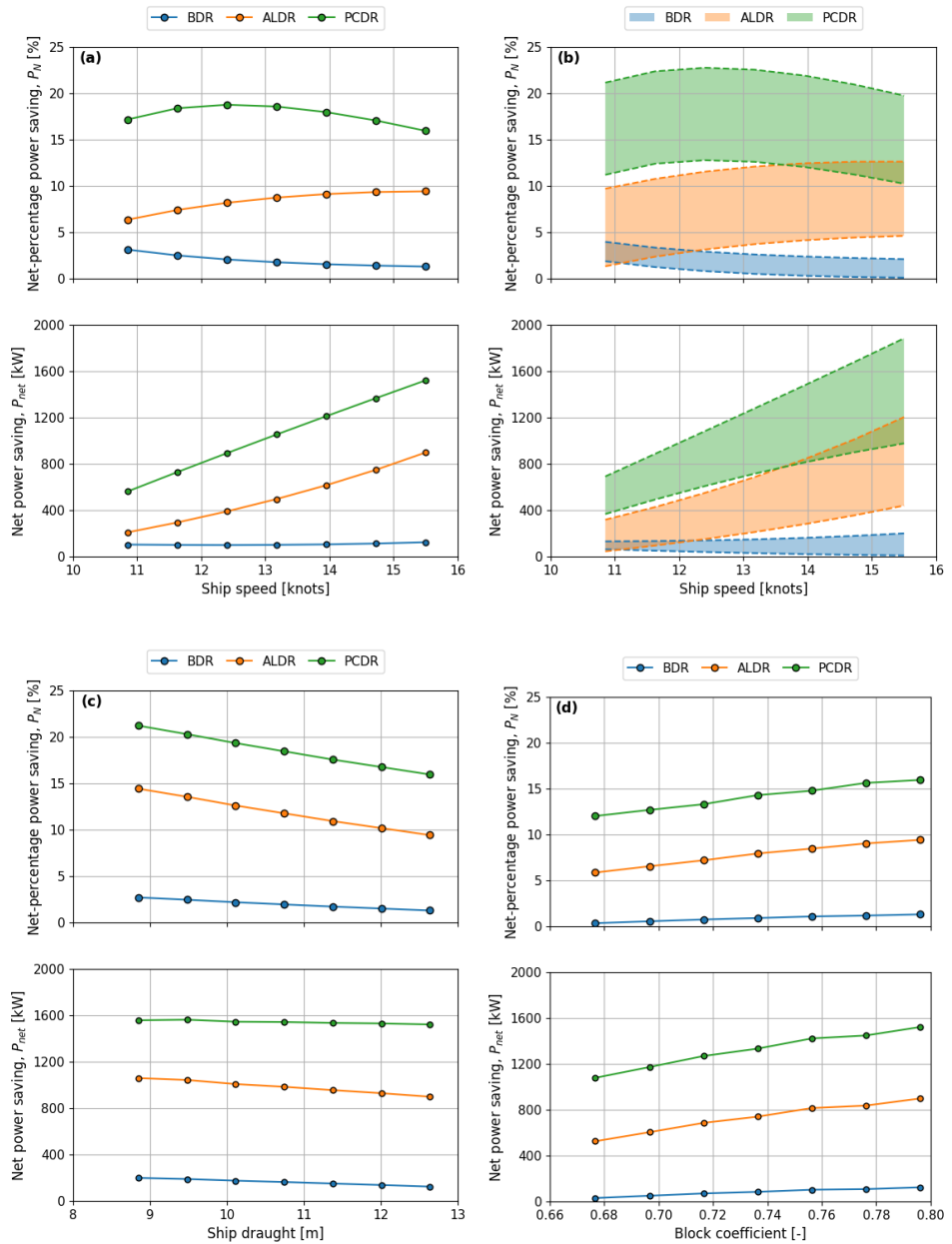


**Figure 4.15:** Results of the parametric analysis for the air lubrication systems: (a) ship speed, (b) ratio of the air-covered area to the bottom surface area, (c) draught, and (d) block coefficient.



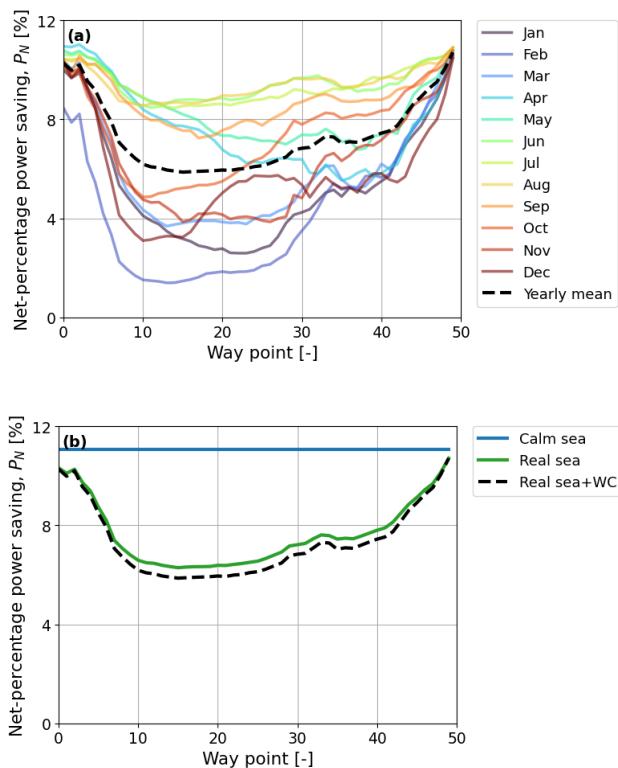


**Figure 4.16:** Annual net power savings of an ALDR-equipped ship during a laden voyage (NLRTM-USNYC): (a) seasonal variations, (b) weather factors.

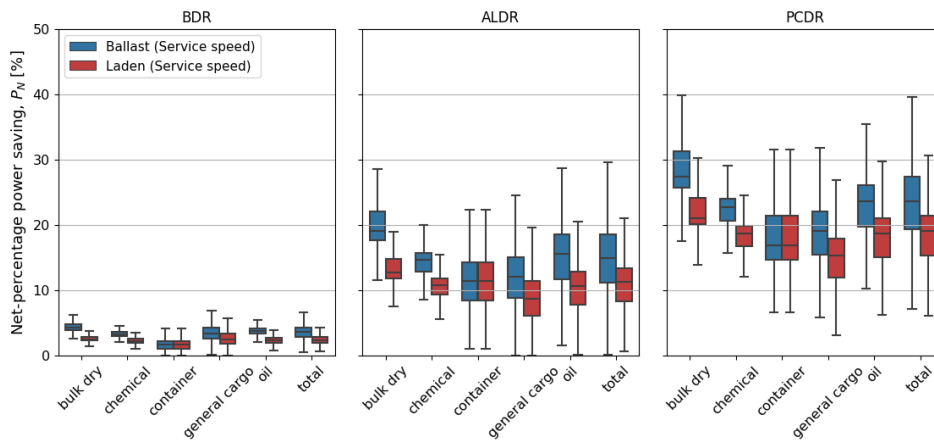


**Figure 4.17:** Comparison of the possible net power savings of the global fleet segment by air lubrication type.

# CHAPTER 5

## Conclusion

*This chapter presents the original contribution of this research to the corresponding field, the conclusion of this research, and ideas for future work.*

### 5.1 Original Contributions

The papers summarized earlier are related to the prediction of power consumption in global shipping and contribute directly or indirectly towards narrowing the gap between the reality and the estimate. It is also helping to find solutions to reduce emissions in various ways. The main contributions in detail for each research item are as follows:

- Different issues that could occur when using data like AIS data, ship's technical information, and weather hindcast data for estimating the power performance of a global fleet segment are described. As part of this work, an algorithm for handling missing values like ship's principal parameters has been developed. Due to the nature of the fleet-level analysis, detailed ship information such as hull form cannot be obtained, so the method of parameter estimation is discussed based on reasonable assumptions. Additionally, data correction and processing methods are presented.
- Numerous semi-empirical approaches and machine learning algorithms for estimating the added wave resistances have been compared and reviewed using extensive experimental data under various conditions. As a result, a meta-model has been developed by combining two existing methods to in-

crease the accuracy of added wave resistance estimates, and a data-driven model based on support vector regression (SVR) also has been presented to predict the added wave resistance coefficients for ships. While the data-driven model provides almost the same level of accuracy as the meta-model, the meta-model is still selected for use in the MariTEAM model in this project. When more model test results become available, the data-driven model might be easily updated and might become the preferred model in the future.

- The applicability and accuracy of methods for estimating resistance components and total propulsive efficiency are reviewed through previous studies presented with the complete power prediction method. As a result, an improved method for powering prediction of ships, suitable for bottom-up analysis of the global fleet, has been developed for implementation in the MariTEAM model.
- A straightforward model developed based on published results of previous studies has been presented to evaluate the potential energy savings according to the operational profiles of various ships and configurations of air lubrication systems (ALS). Based on this model, parametric analysis and sensitivity analysis have been performed, and the achievable energy saving trend assuming the ALS installation for the global fleet has been evaluated.

## **5.2 Conclusion**

This thesis develops a model that can evaluate power consumption in fleet segments based on ship operational data, and deals with applications of energy saving techniques and scenario simulations. An improved powering prediction method, suitable for bottom-up studies of the global fleet (or large fleet segments), has been successfully developed and implemented, and successfully validated against full-scale measurements and EU-MRV fuel consumption data together with the entire MariTeam model. In this regard, five papers have been written, and findings obtained from the research are presented as follows:

- It is necessary to thoroughly check and verify raw data, and proper data handling process is essential. Ship-related datasets such as AIS data, ship's technical information, weather data, and in-service data inevitably may include errors and missing values, which could cause errors and increased uncertainty in the results. In particular, data processing is important when results can be obtained through various processes, from basic parameters to appropriate forms of inputs, resistance components, required power, fuel consumption, and emission, as in this study.

- The approach capable of estimating the added wave resistance in all wave headings can greatly reduce the error compared to that of only taking into account head waves when estimating the increase in resistance of a ship due to waves in actual seaways. As a result of comparing the Combined method with the semi-empirical methods only available for head waves using onboard measurement data from two ships, the Combined method reduces NRMSE (RMSE in power prediction normalized by MCR) by about 2.4–3.3% on Ship A and about 0.9–1.2% on Ship B.
- The Combined method presented in Section 4.1.2 developed in the study demonstrates good overall performance in estimating added wave resistance for different wave heights, arbitrary wave headings, and ship speeds. It is relatively robust compared to other semi-empirical methods in estimating the added wave resistance of the global fleet including various operating conditions and ship types.
- It is possible to use machine learning methods to predict the added wave resistance coefficients for different ship types. The support vector regression (SVR) method is found to be most effective here due to its smooth prediction surface and good accuracy across all evaluation metrics. The results from machine learning models indicate that relative wavelength is the most important parameter for predicting the added wave resistance coefficients, followed by wave heading and Froude number.
- Thorough ship-to-ship and voyage-to-voyage validation of power prediction for the global fleet is practically difficult. A comparison of estimated value with three ships' in-service data demonstrates that the model can consistently predict the power changes in different operational profiles and weather conditions. Moreover, validation with the 2018 EU-MRV data also shows that the model is capable of predicting the annual fuel consumption in fleet segments reasonably.
- The benefits of using an air lubrication system (ALS) are substantially dependent on the ship type and operating conditions. It is best suited for blunt hull forms operating at moderate speeds, as in the case of bulk carriers and oil tankers. Moreover, the net power-saving from ALS can be reduced by up to 15-35% in realistic environmental conditions as compared to the calm-water condition.
- Given the analysis results, and simple installation on ships in service the bubble drag reduction (BDR) and air layer drag reduction (ALDR) types of air lubrication technology have considerable potential to reduce emissions in

global shipping. The net power-saving from air lubrication systems (ALS) is highly dependent on the type of ALS system adopted for a ship. According to a case study conducted under the assumption that an air lubrication system is equipped across the entire global fleet, the possible net percentage power savings would be bubble drag reduction (BDR) 2-5%, air layer drag reduction (ALDR) 8-14%, and partial cavity drag reduction (PCDR) 16-22%.

Although the results of these studies are applicable for various purposes, it should be noticed that they were mainly developed for the purpose of power calculation for the evaluation of the emissions from the global fleet.

### 5.3 Future Work

This study has been conducted during the three-year Ph.D. program, and the research objectives pursued are considered to have been achieved within the available time, support, and resources. Due to the scope of the study and practical issues of the project, there is still room for development and improvement of current research. In addition, new research items related to this study have been found in the process of conducting this study. The following topics should be considered as future research directions.

- In [Article 2](#), an approach was developed to combine existing methods, focusing on estimating added resistance in arbitrary waves of various ships. Although many model test results were used to develop the Combined method, uncertainty still exists for some experimental conditions. In addition, there was a possibility that the results could still be affected if there were weaknesses in the fundamental methods used for the Combined method. In future studies, it is necessary to identify a methodology that can further improve the Combined method beyond these limitations. If improved versions of the two approaches that we combined become available in which some of the shortcomings are complemented, our method should be updated.
- The machine learning model developed in [Article 3](#) is a purely data-driven approach, which has shown almost a similar level of accuracy as the well-established semi-empirical methods for the arbitrary waves. However, there is still room for further improvement in the accuracy and coverage if more experimental data are available for the model training. Furthermore, it is expected that further advanced models can be implemented by applying physics-guided neural networks that combine the scientific knowledge of physics-based models with machine learning structures in future studies. In

contrast, it is also worth considering using the ship's in-service data as training data for machine learning models for the purpose of predicting the added wave resistance of a specific ship.

- In [Article 4](#), the average hull roughness of ships according to age was estimated based on the data of ships in the dry dock obtained from [Stenson \(2015\)](#). It is worth considering a more specific model that analyzes the degree of contribution to the actual fouling growth and resistance increase according to the coating type, cleaning interval, seawater condition, and ship idle time.
- Due to the nature of the fleet study, parameters related to the propeller could not be obtained, and for convenience of calculation, the open water propeller efficiency was calculated by the simplified Wageningen B series ([Article 4](#)). These results are susceptible to errors due to the estimated propeller diameter. If detailed data is available in future work, further investigation and improvement in these areas are believed to enable a significantly improved accuracy.
- Based on the developed complete power prediction model, follow-up research will be conducted on emissions assessment and strategy derivation according to various trade routes and operating patterns.
- In this thesis, the air lubrication system was modeled and analyzed as an example case study of energy saving measures applicable to the ship ([Article 5](#)). Future research should take into account the effects of other energy saving measures on global shipping, including wind-assisted propulsion systems and hull shape modification, in conjunction with the developed comprehensive power prediction approach. The combination of different energy saving measures for an individual ship can also be studied. Moreover, it may be possible to assess the effectiveness of different measures according to the type of ship, its route, cargo, etc. so that the best measures can be adopted for each individual ship.

In addition to the aforementioned research items, the lack of detailed information, inaccuracy of data, and computational cost served as fundamental problems in the fleet-level analysis ([Article 1](#), [Article 4](#)). If sea-trial and in-service data of ships with various operating profiles are obtained, a close verification of the developed model will be possible. Also, if significant amounts of in-service data are available, using such data to improve (tune or correct) the powering prediction method could be of interest. Future advancements in data collection and processing technology are anticipated to help with these issues.



# References

- Abramowski, T., Cepowski, T., Zvolenský, P., 2018. Determination of regression formulas for key design characteristics of container ships at preliminary design stage. *New Trends in Production Engineering* 1, 247–257.
- ABS, 2019. Air lubrication technology. American Bureau of Shipping: Spring, TX, USA .
- Alte, R., Baur, M., 1986. Propulsion. *handbuch der werften*. Hansa 18, 132.
- Auf'm Keller, W., 1973. Extended diagrams for determining the resistance and required power for single-screw ships. *International Shipbuilding Progress* 20, 133–142.
- Barnitsas, M.M., Ray, D., Kinley, P., 1981. KT, KQ and efficiency curves for the Wageningen B-series propellers. Technical Report. University of Michigan.
- Bertram, V., 2011. *Practical ship hydrodynamics*. Elsevier.
- Birk, L., 2019. *Fundamentals of ship hydrodynamics: Fluid mechanics, ship resistance and propulsion*. John Wiley & Sons.
- Blendermann, W., 1996. Wind loading of ships collected data from wind tests tunnel in uniform flow. Institut für Schiffbau der Universität Hamburg .
- Boom, H., Huisman, H., Mennen, F., 2013. New guidelines for speed/power trials. Level playing field established for IMO EEDI. *SWZ Maritime* , 1–11.
- Bouman, E.A., Lindstad, E., Riialand, A.I., Strømman, A.H., 2017. State-of-the-art technologies, measures, and potential for reducing ghg emissions from shipping—a review. *Transportation Research Part D: Transport and Environment* 52, 408–421.



- Bouman, E.A., Lindstad, H.E., Stromman, A.H., 2016. Life-cycle approaches for bottom-up assessment of environmental impacts of shipping, in: SNAME Maritime Convention, OnePetro.
- Bowden, B., Davison, N., 1974. Resistance increments due to hull roughness associated with form factor extrapolation methods. NPL.
- Breslin, J.P., Andersen, P., 1996. Hydrodynamics of ship propellers. 3, Cambridge university press.
- Ceccio, S.L., Mäkiharju, S., 2012. Air lubrication drag reduction on great lakes ships. Great Lakes Maritime Research Institute .
- Cepowski, T., 2019. Regression formulas for the estimation of engine total power for tankers, container ships and bulk carriers on the basis of cargo capacity and design speed. Polish Maritime Research .
- Cepowski, T., 2020. The prediction of ship added resistance at the preliminary design stage by the use of an artificial neural network. Ocean Engineering 195, 106657.
- Charchalis, A., 2014. Determination of main dimensions and estimation of propulsion power of a ship. Journal of KONES 21, 39–44.
- Charchalis, A., Krefft, J., 2009. Main dimensions selection methodology of the container vessels in the preliminary stage. Journal of KONES 16, 71–78.
- Dale, T., 2020. Development of Simplified Methods for Ship Powering Performance Calculations. Master's thesis. NTNU.
- Danckwardt, E., 1969. Ermittlung des widerstandes von frachtschiffen und hecktrawlern beim entwurf.
- Elbing, B.R., Winkel, E.S., Lay, K.A., Ceccio, S.L., Dowling, D.R., Perlin, M., 2008. Bubble-induced skin-friction drag reduction and the abrupt transition to air-layer drag reduction. Journal of Fluid Mechanics 612, 201–236.
- European Union, 2015. Regulation (eu) 2015/757 of the european parliament and of the council of 29 april 2015 on the monitoring, reporting and verification of carbon dioxide emissions from maritime transport, and amending directive 2009/16/ec. Off J Eur Union 58, 55–76.
- Faber, J., Hanayama, S., Zhang, S., Pereda, P., Comer, B., Hauerhof, E., Schim van der Loeff, W., Smith, T., Zhang, Y., Kosaka, H., et al., 2020. Fourth imo ghg study. London, UK .

- Faltinsen, O.M., 1980. Prediction of resistance and propulsion of a ship in a seaway, in: Proceedings of the 13th symposium on naval hydrodynamics, Tokyo, 1980.
- Foeth, E., Eggers, R., van der Hout, I., Quadvlieg, F., 2009. Reduction of frictional resistance by air bubble lubrication, in: SNAME Maritime Convention, OnePetro.
- Fujiwara, T., 2006. A new estimation method of wind forces and moments acting on ships on the basis of physical components models. *Journal of the Japan society of naval architects and ocean engineers* 2, 243–255.
- Gawn, R., 1957. Effect of cavitation on the performance of a series of 16 in. model propellers, in: Meeting of the Institution of Naval Architects, TINA, London, 1954, Published in: RINA Transactions: 1957-32, Paper 3.
- Gebraad, J., Quispel, M., Karaarslan, S., Lehne, M., Rafael, R., Eppich, M., Janssens, G., Smidt, H., Barcanescu, M., 2021. Structuring towards zero emission waterborne transport, d2.1. state-of-play of decarbonisation of waterborne transport “technology application atlas. <https://www.waterborne.eu/projects/coordination-projects/steerer/results>, Last accessed on, 2022-09-18.
- Gertler, M., 1954. A reanalysis of the original test data for the Taylor Standard Series. Technical Report. DAVID TAYLOR MODEL BASIN WASHINGTON DC.
- Granville, P.S., 1958. The frictional resistance and turbulent boundary layer of rough surfaces. *Journal of ship research* 2, 52–74.
- Granville, P.S., 1987. Three indirect methods for the drag characterization of arbitrarily rough surfaces on flat plates. *Journal of Ship Research* 31.
- Guldhammer, H., Harvald, S.A., 1974. Ship resistance-effect of form and principal dimensions.(revised). Danish Technical Press, Danmark, Danmarks Tekniske Højskole, kademisk Forlag, St. kannikestrade 8, DK 1169 Copenhagen .
- Guo, B., Liang, Q., Tvette, H.A., Brinks, H., Vanem, E., 2022. Combined machine learning and physics-based models for estimating fuel consumption of cargo ships. *Ocean Engineering* 255, 111435.
- Gupta, P., Taskar, B., Steen, S., Rasheed, A., 2021. Statistical modeling of ship’s hydrodynamic performance indicator. *Applied Ocean Research* 111, 102623.

- Helmore, P., 2008. Update on van oortmerssen's resistance prediction, in: Pacific 2008 International Maritime Conference.
- Hollenbach, K.U., 1998. Estimating resistance and propulsion for single-screw and twin-screw ships-ship technology research 45 (1998). Schiffstechnik 45, 72.
- Holtrop, J., Mennen, G., 1982. An approximate power prediction method. International Shipbuilding Progress 29, 166–170.
- IMO, 2018. Initial imo strategy on reduction of ghg emissions from ships. imo resolution mepc.304(72). [https://wwwcdn.imo.org/localresources/en/KnowledgeCentre/IndexofIMOResolutions/MEPCDocuments/MEPC.304\(72\).pdf](https://wwwcdn.imo.org/localresources/en/KnowledgeCentre/IndexofIMOResolutions/MEPCDocuments/MEPC.304(72).pdf), Last accessed on, 2022-09-18.
- ITTC, 2005. Recommended procedures and guidelines: Full scale measurements speed and power trials analysis of speed .
- ITTC, 2014. Recommended procedures and guidelines, preparation, conduct and analysis of speed/power trials.
- ITTC, 2017a. 1978 ittc performance prediction method.
- ITTC, 2017b. Recommended procedures and guidelines, preparation, conduct and analysis of speed/power trials.
- ITTC, 2018. Recommended procedures and guidelines, calculation of the weather factor  $f_w$  for decrease of ship speed in wind and waves.
- Jalkanen, J.P., Brink, A., Kalli, J., Pettersson, H., Kukkonen, J., Stipa, T., 2009. A modelling system for the exhaust emissions of marine traffic and its application in the baltic sea area. Atmospheric Chemistry and Physics 9, 9209–9223.
- Jalkanen, J.P., Johansson, L., Kukkonen, J., Brink, A., Kalli, J., Stipa, T., 2012. Extension of an assessment model of ship traffic exhaust emissions for particulate matter and carbon monoxide. Atmospheric Chemistry and Physics 12, 2641–2659.
- Jang, J., Choi, S.H., Ahn, S.M., Kim, B., Seo, J.S., 2014. Experimental investigation of frictional resistance reduction with air layer on the hull bottom of a ship. International Journal of Naval Architecture and Ocean Engineering 6, 363–379.
- Jinkine, V., Ferdinande, V., 1974. A method for predicting the added resistance of fast cargo ships in head waves. International Shipbuilding Progress 21, 149–167.

- Johansson, L., Jalkanen, J.P., Kukkonen, J., 2017. Global assessment of shipping emissions in 2015 on a high spatial and temporal resolution. *Atmospheric Environment* 167, 403–415.
- Kaiser, M., 2016. Results of aerodynamic model tests for HSBC. Technical Report. Technical Report No. RH-2016/T-104E, CTO S.A., Gdansk, Poland.
- Kawabuchi, M., Kawakita, C., Mizokami, S., Higasa, S., Kodan, Y., Takano, S., 2011. Cfd predictions of bubbly flow around an energy-saving ship with mitsubishi air lubrication system. *Mitsubishi Heavy Industries Technical Review* 48, 53–57.
- Kim, S.H., Roh, M.I., Oh, M.J., Park, S.W., Kim, I.I., 2020. Estimation of ship operational efficiency from ais data using big data technology. *International Journal of Naval Architecture and Ocean Engineering* 12, 440–454.
- Kim, Y., Esmailian, E., Steen, S., 2022. A meta-model for added resistance in waves. *Ocean Engineering* 266, 112749.
- Kim, Y., Steen, S., 2022. Potential energy savings of air lubrication technology on merchant ships. Available at SSRN 4230155 .
- Kitamura, F., Ueno, M., Fujiwara, T., Sogihara, N., 2017. Estimation of above water structural parameters and wind loads on ships. *Ships and Offshore Structures* 12, 1100–1108.
- Kramel, D., Muri, H., Kim, Y., Lonka, R., Nielsen, J.B., Ringvold, A.L., Bouman, E.A., Steen, S., Strømman, A.H., 2021. Global shipping emissions from a well-to-wake perspective: the mariteam model. *Environmental science & technology* 55, 15040–15050.
- Kristensen, H.O., 2013. Statistical analysis and determination of regression formulas for main dimensions of container ships based on ihs fairplay data. University of Southern Denmark: Odense, Denmark .
- Kristensen, H.O., Lützen, M., 2012. Prediction of resistance and propulsion power of ships. *Clean Shipping Currents* 1, 1–52.
- Kwon, Y., 2008. Speed loss due to added resistance in wind and waves. *Nav Archit* 3, 14–16.
- Lang, X., Mao, W., 2020. A semi-empirical model for ship speed loss prediction at head sea and its validation by full-scale measurements. *Ocean Engineering* 209, 107494.

- Lang, X., Mao, W., 2021. A practical speed loss prediction model at arbitrary wave heading for ship voyage optimization. *Journal of Marine Science and Application* 20, 410–425.
- Lap, A., 1954. Diagrams for determining the resistance of single-screw ships. *International Shipbuilding Progress* 1, 179–193.
- Lay, K.A., Yakushiji, R., Makiharju, S., Perlin, M., Ceccio, S.L., 2010. Partial cavity drag reduction at high reynolds numbers. *Journal of Ship Research* 54, 109–119.
- Lee, J., Kim, J., Jang, J., McStay, P., Raptakis, G., Fitzpatrick, P., 2017. Full scale applications of air lubrication for reduction of ship frictional resistance, in: SNAME Maritime Convention, OnePetro.
- Liu, S., Papanikolaou, A., 2016. Fast approach to the estimation of the added resistance of ships in head waves. *Ocean Engineering* 112, 211–225.
- Liu, S., Papanikolaou, A., 2020. Regression analysis of experimental data for added resistance in waves of arbitrary heading and development of a semi-empirical formula. *Ocean Engineering* 206, 107357.
- Liu, S., Shang, B., Papanikolaou, A., Bolbot, V., 2016. Improved formula for estimating added resistance of ships in engineering applications. *Journal of Marine Science and Application* 15, 442–451.
- Lu, R., Turan, O., Boulougouris, E., Banks, C., Incecik, A., 2015. A semi-empirical ship operational performance prediction model for voyage optimization towards energy efficient shipping. *Ocean Engineering* 110, 18–28.
- Mäkiharju, S.A., Perlin, M., Ceccio, S.L., 2012. On the energy economics of air lubrication drag reduction. *International Journal of Naval Architecture and Ocean Engineering* 4, 412–422.
- Martić, I., Degiuli, N., Majetić, D., Farkas, A., 2021. Artificial neural network model for the evaluation of added resistance of container ships in head waves. *Journal of Marine Science and Engineering* 9, 826.
- Minsaas, K., 1982. Grunnlag for fartsprognoser. Technical Report. Technical report, Marintek (former: Norges Hydrodynamiske Laboratorier . . . .
- Mizokami, S., Kawakita, C., Kodan, Y., Takano, S., Higasa, S., Shigenaga, R., 2010. Experimental study of air lubrication method and verification of effects on actual hull by means of sea trial. *Mitsubishi Heavy Industries Technical Review* 47, 41–47.

- Muri, H., Strømman, A.H., Ringvold, A.L., Lonka, R., Bouman, E., 2019a. Influence of weather on emissions from the global shipping fleet., in: Geophysical Research Abstracts.
- Muri, H., Strømman, A.H., Ringvold, A.L., Lonka, R., Lindstad, E., Bouman, E.A., 2019b. A new emission inventory of the global maritime fleet; the effect of weather, in: AGU Fall Meeting Abstracts, pp. A21W–2637.
- Nag, P., 2013. Engineering thermodynamics. Tata McGraw-Hill Education.
- Newton, R., 1961. Performance data of propellers for high speed craft. Admiralty Experiment Works, Haslar, UK, Published by: The Royal Institution of Naval Architects, RINA Transactions 1961-07, Volume 103, No. 2, Quarterly Transactions, pp. 93-129 .
- Oliveira, D.R., Lagerström, M., Granhag, L., Werner, S., Larsson, A.I., Ytreberg, E., 2022. A novel tool for cost and emission reduction related to ship underwater hull maintenance. *Journal of Cleaner Production* 356, 131882.
- Olmer, N., Comer, B., Roy, B., Mao, X., Rutherford, D., 2017. Greenhouse gas emissions from global shipping, 2013–2015 detailed methodology. *International Council on Clean Transportation: Washington, DC, USA* , 1–38.
- Oortmerssen, G.v., 1971. A power prediction method and its application to small ships. *ISP* 18.
- Oosterveld, M.W.C., 1970. Wake adapted ducted propellers. Technical Report.
- Oosterveld, M.W.C., van Oossanen, P., 1975. Further computer-analyzed data of the wageningen b-screw series. *International shipbuilding progress* 22, 251–262.
- Papanikolaou, A., 2014. Ship design: methodologies of preliminary design. Springer.
- Papanikolaou, A., Zaraphonitis, G., Bitner-Gregersen, E., Shigunov, V., El Moctar, O., Soares, C.G., Reddy, D.N., Sprenger, F., 2015. Energy efficient safe ship operation (shopera), in: SNAME 5th World Maritime Technology Conference, OnePetro.
- Pavlov, G.A., Yun, L., Bliault, A., He, S.L., 2020. Air lubricated and air cavity ships. Springer.
- Piko, G., 1980. Regression analysis of ship characteristics. Australian Government Publishing Service.

- Psaraftis, H.N., Kontovas, C.A., 2009. Co2 emission statistics for the world commercial fleet. *WMU Journal of Maritime Affairs* 8, 1–25.
- Radfar, S., Taherkhani, A., Panahi, R., 2017. Standardization of the main dimensions of design container ships in ports—a case study. *World Journal of Engineering and Technology* 5, 51–61.
- Rakke, S., 2016. Ship emissions calculation from AIS-annotated. Ph.D. thesis. M. Sc. Thesis. Norwegian University of Science and Technology, Norway.
- Schneekluth, H., Bertram, V., 1998. Ship design for efficiency and economy. volume 218. Butterworth-Heinemann Oxford.
- Silberschmidt, N., Tasker, D., Pappas, T., Johannesson, J., 2016. Silverstream system-air lubrication performance verification and design development, in: Conference of Shipping in Changing Climate, Newcastle, UK, pp. 10–11.
- Smith, T., O’Keeffe, E., Aldous, L., Agnolucci, P., 2013. Assessment of shipping’s efficiency using satellite ais data .
- Smith, T.W., Jalkanen, J.P., Anderson, B., Corbett, J.J., Faber, J., Hanayama, S., O’Keeffe, E., Parker, S., Johansson, L., Aldous, L., et al., 2014. Third imo ghg study 2014. International maritime organization (IMO), London, UK , 2014.
- Steen, S., Aarsnes, J.V., 2014. Experimental methods in marine hydrodynamics. Lecture notes .
- Stenson, P., 2015. Predicting the rough and the smooth. *The Naval Architect* February, 36–38.
- Takahashi, H., Goto, A., Abe, M., Kannami, Y., Esaki, T., Mizukami, J., 2006. Study on ship dimensions by statistical analysis: Standard of main dimensions of design ship (Draft). National Inst. for Land and Infrastructure Management, Ministry of Land . . . .
- Tillig, F., Ringsberg, J., Mao, W., Ramne, B., 2017. A generic energy systems model for efficient ship design and operation. *Proceedings of the Institution of Mechanical Engineers, Part M: Journal of Engineering for the Maritime Environment* 231, 649–666.
- Tillig, F., Ringsberg, J.W., 2019. A 4 dof simulation model developed for fuel consumption prediction of ships at sea. *Ships and Offshore Structures* 14, 112–120.

- Tillig, F., Ringsberg, J.W., Psaraftis, H.N., Zis, T., 2020. Reduced environmental impact of marine transport through speed reduction and wind assisted propulsion. *Transportation Research Part D: Transport and Environment* 83, 102380.
- Todd, F., 1957. Series 60-the effect upon resistance and power of variation in ship proportions. *Trans. SNAME* 65, 445–589.
- Townsin, R., Byrne, D., Svensen, T., Milne, A., 1986. Fuel economy due to improvements in ship hull surface condition 1976–1986. *International shipbuilding progress* 33, 127–130.
- Townsin, R., Kwon, Y., 1993. Estimating the influence of weather on ship performance .
- Townsin, R., Mosaad, M., 1985. The ittc line-its genesis and correlation allowance .
- Tsujimoto, M., Shibata, K., Kuroda, M., Takagi, K., 2008. A practical correction method for added resistance in waves. *Journal of the Japan Society of Naval Architects and Ocean Engineers* 8, 177–184.
- Tvete, H.A., Guo, B., Liang, Q., Brinks, H., 2020. A modelling system for power consumption of marine traffic, in: *International Conference on Offshore Mechanics and Arctic Engineering*, American Society of Mechanical Engineers. p. V06AT06A029.
- Uzun, D., Demirel, Y.K., Coraddu, A., Turan, O., 2019. Time-dependent biofouling growth model for predicting the effects of biofouling on ship resistance and powering. *Ocean Engineering* 191, 106432.
- Wang, J., Bielicki, S., Kluwe, F., Orihara, H., Xin, G., Kume, K., Oh, S., Liu, S., Feng, P., 2021. Validation study on a new semi-empirical method for the prediction of added resistance in waves of arbitrary heading in analyzing ship speed trial results. *Ocean Engineering* 240, 109959.
- Watson, D.G., 1998. *Practical ship design*. volume 1. Elsevier.
- Wu, H., Ou, Y.p., 2019. Experimental study of air layer drag reduction with bottom cavity for a bulk carrier ship model. *China Ocean Engineering* 33, 554–562.





# Research Articles



# Article 1

## A novel method for estimating missing values in ship principal data

Youngrong Kim, Sverre Steen, Helene Muri

*Ocean Engineering* 251 (2022) 110979  
DOI: [10.1016/j.oceaneng.2022.110979](https://doi.org/10.1016/j.oceaneng.2022.110979)





## A novel method for estimating missing values in ship principal data

Youngrong Kim <sup>a,\*</sup>, Sverre Steen <sup>a</sup>, Helene Muri <sup>b</sup>

<sup>a</sup> Department of Marine Technology, Norwegian University of Science and Technology, Trondheim, Norway

<sup>b</sup> Industrial Ecology Programme, Department of Energy and Process Engineering, Norwegian University of Science and Technology, Trondheim, Norway

### ARTICLE INFO

#### Keywords:

Missing data  
Ship principal data  
Model-based computation  
Regression analysis

### ABSTRACT

Missing values in the fleet data set acquired in the marine sector reduce the data available for analysis, which can decrease the statistical power of the model and negatively affects the energy-efficient operation and decision-making. This article presents a method to estimate ship principal data. A model-based computation method using regression analysis was used to handle missing values, and a case study was conducted on principal data from 6,278 container ships in the IHS Sea-Web database. To implement a model for predicting missing values, the entire data set was randomly divided into 80% to 20%, which were used as a training data set and test data set. The prediction performance of models was compared with several regression equations proposed in prior studies, which shows that there is a significant improvement with our method. The goodness of fit of the current method has increased by up to 15.6% over the previous methods. It also showed good applicability for ships with restrictions on certain dimensions, such as the standards for Suez and Panama Canal. The findings presented here may be helpful from the estimation for key parameters of the ship to the computation of missing values in the marine sector.

### 1. Introduction

Data sets acquired from industry are often incomplete, which may be due to various reasons, including sensor failures, measurements outside the range of sensors, malfunctions in data collection systems, power cuts, interruption of transmission lines, and errors in data recording (Imtiaz and Shah, 2008; Khatibisepehr et al., 2013). For instance, in the maritime industry, there may be missing values of 4.4% to 26.0% of the data collected from the machinery system due to various circumstances (Tsitsilonis and Theotokatos, 2018; Lazakis et al., 2019). AIS (Automatic Identification System) mounted on a ship may cause loss of signals registered by the satellite if the time slot is overlapped due to interference with other ships when the ship navigates in congested waters, and in bad weather, such as lightning, the transmission may be lost due to shut off of the receiver (Lloyd's list intelligence, 2017). In addition, entire fleet data, which is widely used for ship operational efficiency, emission prediction from maritime transport, and hull design, is comprehensively collected from various organizations such as ships, owners, shipbuilders, and port authorities (Wang et al., 2016; IHS, 2019). Due to the nature of such data, missing values inevitably exist. If a large fraction of the data is missing, it may lead to inaccurate analysis and prediction, which can negatively affect the

energy-efficient operation and decision-making of the fleet (Gutierrez-Torre et al., 2020). Therefore, it is important to process and complete the missing values appropriately before analyzing the acquired data.

Despite the increasing utilization of big data and the use of such in machine learning in the maritime industry, combined with the growing importance of appropriately handling missing values, there are few published studies on missing data. Most of them were to recover missing route information or identify ship behavior patterns through incomplete AIS data analysis (Liu and Chen, 2013; Mao et al., 2018; Dobrkovic et al., 2018; Gutierrez-Torre et al., 2020). There have also been attempts to handle missing data obtained from the machinery system of an operating ship. In Cheliotis et al. (2019)'s study, a hybrid imputation method combining K-nearest neighbor (KNN) and multiple imputation by chained equations algorithms (MICE) has been developed for efficient operation and performance improvement of the main engine systems of ships in operation. Imputation is defined as a method of filling in values of missing data (Little and Rubin, 2019). This method was applied to time-series data collected from a total of eight sensors combined with the main engine. In the process of developing a decision support framework for optimal ship routes based

\* Corresponding author.

E-mail address: [youngrong.kim@ntnu.no](mailto:youngrong.kim@ntnu.no) (Y. Kim).

<https://doi.org/10.1016/j.oceaneng.2022.110979>

Received 30 October 2020; Received in revised form 14 January 2022; Accepted 26 February 2022

Available online 17 March 2022

0029-8018/© 2022 The Authors. Published by Elsevier Ltd. This is an open access article under the CC BY license (<http://creativecommons.org/licenses/by/4.0/>).

on weather and fuel consumption, Gkerekos and Lazakis (2020) used MICE algorithm applied in Cheliotis et al. (2019) to impute the missing points of weather forecast data. Velasco-Gallego and Lazakis (2020) conducted a comparative study investigating a total of 20 machine learning and time-series prediction algorithms to support a real-time decision-making strategy. In their subsequent study (Velasco-Gallego and Lazakis, 2021), they proposed a new framework by implementing the first-order Markov chain with some multiple imputation methods. In addition to the maritime field, various methods based on machine learning such as multiple regression, random forest, KNN, and support vector regression have been tested and applied to process missing data across the industry (Kim et al., 2017; Andiojaya and Demirhan, 2019; Afrifa-Yamoah et al., 2020; Lin and Tsai, 2020; Jung et al., 2020; Wang et al., 2021). It appears that most research related to missing data handling in the maritime industry is limited to continuous time-series data on a specific ship data, such as the state of the machinery system or the location of the ship. Studies related to stationary data such as ship principal data are rare.

Many studies have been conducted to predict the principal dimensions and particulars. Most of these were intended to be used in the initial design or to optimize design variables for specific vessels, and proposed regression formulas using statistical data of ships. Piko (1980) performed a regression analysis on deadweight tonnage and service speed using the length, breadth, draught, gross tonnage, and power based on Lloyd's shipping database, which became a cornerstone for many subsequent studies. Charchalis and Krefft (2009), Charchalis (2014) attempted to design equations for estimating efficient and optimal main parameters during the initial ship design stage. Parameters were predicted using container capacity and deadweight tonnage, but the range and number of ships used in the research was limited. Kristensen (2012, 2013, 2016) performed extensive statistical analysis on bulk carriers, container ships, and tankers and proposed regression equations for a number of parameters. In particular, they were established by dividing groups according to the size of the vessel, which enabled considering the detailed characteristics of each range. Abramowski et al. (2018) presented regression formulas to estimate key characteristics of container ship based on various combinations of deadweight tonnage, container capacity, in addition to some other variables and proved to be a practical application at the preliminary design stage. Such studies using regression formulas showed generally good accuracy based on several key input variables selected in combination with using domain-knowledge. Conversely, recent work has suggested models based on ANN, which showed better prediction performance than previous ones. Abramowski (2013) applied ANN techniques to optimize the design parameters of cargo ships. In this study, seven parameters were used to implement a model for effective power determination. Moreover, optimization for a single objective of the minimum thrust and multi-objective of the minimum propulsion power and maximum deadweight was performed, while implementing the model. Gurgen et al. (2018) presented a design tool for estimating key details of chemical tankers during the preliminary design phase. In that study, an ANN was used for model implementation and key dimensions such as overall length, length between perpendicular, breadth, draught, and freeboard were predicted using the dead weight and service speed of the vessel as the default input. However, there were concerns about the complexity of the model and the possibility of overfitting to the data set when applying ANN. In this regard, the preceding models implemented based on specific vessel data set were somewhat less applicable in other studies. In addition, all such work including regression analysis and ANN to predict the principal components of vessels always assumed a complete data set and did not address the processing of missing values within the data set. In fact, if some data are missing in the data set, or the composition of the data set is different from the previous studies, the estimation methods mentioned above are difficult to apply.

In fleet-wide studies, such as analysis of ship operational energy efficiency and global greenhouse gas emissions at sea, the principal details of ships are used as important basic data along with time-series data such as AIS and in-service data. Sea-Web is used as the source for ship principle data, and it is found that some parameters are missing for a number of ships. If sufficient amounts of data are obtained or there are few missing values, the problem may be solved by simply removing the missing values, otherwise, it can result in an inappropriate analysis result. Although prior studies using machine learning-based missing data imputation methods (Cheliotis et al., 2019; Velasco-Gallego and Lazakis, 2020) have shown high accuracy, they basically focused on time-series data from specific ships. Furthermore, the interpretation of machine learning-based models itself was difficult, and it was not straightforward to obtain ship principal parameters by applying the same settings to other studies.

In this study, we propose a new method that is designed for estimating missing values in ship principal data. To deal with such values, a model-based computation method using regression analysis is used in this study, which is widely applicable to various data compositions and characteristics. Through the method, the relationship between ship principal data is first identified using correlation analysis and regression curve fitting functions. Then the missing data is replaced based on regression analysis accompanied by variable selection. This approach complements previous research for estimating ship principal data with respect to handling the missing data. The estimated models and results can be interpreted and, regression expressions for each ship parameter are provided at last, making it easier to apply in other studies. It is believed that the method can be applied also under other circumstances when it is needed to replace erroneous values.

In Section 2, the new method to estimate the missing values for ship principal data is described, and Section 3 shows the results of the model through a case study of container ships. Section 4 compares the performance of the developed model to the regression models of the previous studies and the random forest model. It also verifies the ability of the method to respect particular dimensional restrictions, such as being able to pass through the Suez Canal and Panama Canal. Finally, in Section 5, the conclusions drawn.

## 2. A new method to estimate missing values for ship main particulars

### 2.1. Missing data types

Missing data can cause problems since robust statistical analysis requires values for each variable. Therefore, in situations where missing values are expected, one needs to decide how to handle them. The missing data can be divided into three different types: missing completely at random (MCAR), missing at random (MAR), and missing not at random (MNAR) by the cause of missing (Rubin, 1976). MCAR means that the values are lost randomly throughout the data range, regardless of the type and value of the variables. Whilst MAR refers to a case in which the loss of the data is not random across all observations, but only within a subset of the data. If the characteristics of MCAR or MAR are not satisfied, data belongs to the MNAR. MNAR refers to a case in which the values of the missing variables and the reasons for the missing are related.

Missing values can be handled in mainly two ways, either by elimination or imputation of them. Deleting the parameter or variable set that includes missing values from the entire data sets is the easiest and simplest way to handle them. However, it can substantially lower the sample size, leading to a severe lack of statistical power. In particular, it is possible when there are many variables associated in the analysis, and each variable has missing data for several cases, which can lead to biased results, depending on the cause of data missing (Little and Rubin, 2019). If only missing values are removed by applying a pair-wise deletion, the change of subset may lead to distort the analysis results and

make it difficult to interpret. In contrast, imputation can preserve all cases by estimating missing data based on other available information, enabling subsequent statistical analysis of the entire data (Hair et al., 2018).

According to Hair et al. (2018), the method of handling missing values varies depends on the ratio of missing in the data set and its characteristics. If the missing values are less than 10%, they can be removed from the data set or any of the completion methods can be applied. If the missing ratio is between 10 and 20%, hot deck replacement and regression analysis methods are appropriate for MCAR data, and the model-based method is recommended for MAR data. In the case of more than 20%, a regression method is recommended to use for MCAR data, and a model-based method for MAR data.

2.2. Missing data handling process

As mentioned in the previous section, there are various methods of processing the missing data depending on the characteristics of the data or the types of missing, and the corresponding results will vary. We propose a model-based computation method using regression analysis that is widely applicable against the ratio and characteristics of missing data, which is able to handle it properly. The main challenge of model-based computation is to establish a model for predicting each target variable that contains missing values in the data set. In fact, many studies have applied regression analysis of statistical data to estimate ship principal parameters and they assumed a complete data set. However, this study aims to complement previous methods from the perspective of missing data handling. In other words, the method proposed in this study is applicable even when the input parameters used in the equations proposed in the previous studies are not in the data set. However, since this algorithm includes several statistical analysis methods, it should be noted that it may not work properly if the size of the data set for filling the missing values is too small. Fig. 1 illustrates the method for completing the ship principal data proposed in this study, and the main steps are composed of the following three steps:

- (i) Initial computation: The objective of the first step is to obtain a complete data set by filling in the empty values with plausible values. Multiple regression analysis used in this study requires a complete matrix of variables. However, with the incomplete data set, since the values of some variables are empty, multiple regression analysis cannot be performed directly. Therefore, this step provides a platform for performing a multiple regression analysis in the next step. First, curve fitting is performed between each ship design parameter using a variety of function forms, including linear, quadratic, cube, power, and logarithmic based on the least-squares method. At this point, the overall data sets of each variable are used. Afterward, a single variable and function type that provides the highest  $R^2$  value (Coefficient of determination) with the variable to be fitted is identified (Refer to Algorithm 1). Finally, missing values in each ship's case are filled by the curve fitting of the other variable with the highest  $R^2$  value (Refer to Algorithm 2). If the corresponding variable is missing in a specific ship case, the next best variable is selected. That is, among the variables that exist in the ship case, the curve fitted value of the variable with the next higher  $R^2$  value is used to fill in the missing value. This process repeats until all missing values within the entire data set are filled.

Let the ship data set ( $X$ ) has  $N \times M$  matrix containing some missing values:

$$X = (X_1, X_2, \dots, X_M) = \left[ \begin{array}{cccc} x_{11} & x_{12} & \dots & x_{1j} \\ x_{21} & x_{22} & \dots & x_{2j} \\ \vdots & \vdots & \ddots & \vdots \\ x_{i1} & x_{i2} & \dots & x_{ij} \end{array} \right] \left. \vphantom{\begin{array}{cccc} x_{11} & x_{12} & \dots & x_{1j} \\ x_{21} & x_{22} & \dots & x_{2j} \\ \vdots & \vdots & \ddots & \vdots \\ x_{i1} & x_{i2} & \dots & x_{ij} \end{array}} \right\} N$$

$M$

where  $x_{ij}$  is  $j$ th parameter in  $i$ th ship case,  $N$  is the number of ship cases, and  $M$  is the number of ship principal parameters.

**Algorithm 1:** Identify the fitted function for each parameter using curve fitting

```

for j ∈ {1, 2, ..., M} do
    for f ∈ [Curve fitting functions] do
        Calculate R2 value between Xj and f(X-j) using the non-missing values.
    end
    Save function f(·) and input parameter X* among X-j that fit best with Xj as fCV(X*).
end
    
```

where  $f(\cdot)$  is curve fitting function (Refer to Eqs. (1)–(5)),  $X_j$  is the  $j$ th parameter vector in all ship cases,  $X_{-j}$  is parameter vector except  $j$ th parameter in all ship cases,  $X^*$  is the selected parameter vector among  $X_{-j}$  in all ship cases, and  $f^{CV}(X^*)$  is the fitted function that has  $X^*$  as an input vector, which shows the highest  $R^2$  value between the target parameter vector  $X_j$ .

**Algorithm 2:** Make an initial guess for all missing values using fitted function

```

for i ∈ {1, 2, ..., N} do
    for j ∈ {1, 2, ..., M} do
        Estimate x̂ij using the fitted function fCV(·) and parameter xi*, i.e., x̂ij = fCV(xi*).
    end
    Fill in xij using the estimated value x̂ij if xij is missing, i.e., xij = x̂ij.
end
    
```

where  $x_i^*$  is the selected parameter that shows the highest  $R^2$  value with the target parameter  $x_j$  in  $i$ th ship case, and  $\hat{x}_{ij}$  is the estimated value of the  $j$ th parameter in  $i$ th ship case from Algorithm 1 and 2.

- (ii) Final imputation: This step is to update the originally missing values with predicted values by performing regression analysis based on the completed data sets obtained from step 1. Before implementing a predictive model for each variable, remaining variables except for a target variable, are converted into the function type with the highest  $R^2$  to the target variable, which is to consider the non-linear physical relations between each variable. That is, the curve-fitted values are entered in the terms of the independent variables in subsequent multiple linear regression expressions. The main process in this step is performing multiple regression analysis with the backward elimination method to make a predictive model for each variable. The  $p$ -value for each variable that makes up the model and the  $BIC$  (Bayesian Information Criterion) of the model are evaluated. It starts with all candidate variables and sequentially removes one of which is the least statistically significant for the model, i.e. the variable with the maximum  $p$ -value. When all models are evaluated according to the number of input variables, the model with the minimum  $BIC$  is selected as a final model (Refer to Algorithm 3). Once the predictive model of each variable is set up, the values filled in the previous step are replaced with the newly predicted values from the model (Refer to Algorithm 4).



**Algorithm 3:** Perform multiple regression analysis with backward elimination to make a prediction model for each parameter

```

for  $j \in [1, 2, \dots, M]$  do
  Convert parameters  $X_{-j}$  to the curve fitted form  $X_{-j}^{CV}$ ,
  i.e.,  $X_{-j}^{CV} = f^{CV}(X_{-j})$ .
  repeat
    Fit a multiple regression model  $f^{MR}(X_{-j}^{CV})$  for the
    target parameter  $X_j$ .
    Calculate BIC of the model and p-value of each input
    parameter.
    Remove the input parameter that has the highest
    p-value.
  until All input parameters in the model have been removed.
  Save the multiple regression model that shows the
  minimum BIC as  $f^{MR}(X^{CV*})$ .
end

```

where  $X_{-j}^{CV}$  are converted parameters using the curve fitted form  $f^{CV}(\cdot)$  that have  $X_{-j}$  as inputs,  $X^{CV*}$  are the selected parameters, and  $f^{MR}(\cdot)$  is the multiple regression model that has  $X^{CV*}$  as inputs, which shows the minimum *BIC*.

**Algorithm 4:** Update the originally missing values using multiple regression model

```

for  $i \in [1, 2, \dots, N]$  do
  for  $j \in [1, 2, \dots, M]$  do
    Estimate  $\hat{x}_{ij}$  using the multiple regression model
     $f^{MR}(X_i^{CV*})$ , i.e.,  $\hat{x}_{ij} = f^{MR}(X_i^{CV*})$ .
  end
  Replace  $x_{ij}$  using the estimated value  $\hat{x}_{ij}$  if  $x_{ij}$  has been
  filled in Algorithm 2, i.e.,  $x_{ij} = \hat{x}_{ij}$ .
end

```

where  $f^{MR}(X_i^{CV*})$  is the multiple regression model that has  $X_i^{CV*}$  as inputs in *i*th ship case, and  $\hat{x}_{ij}$  is the estimated value of the *j*th parameter in *i*th ship case from Algorithm 3 and 4.

- (iii) Minor adjustment: This step is the process of identifying and correcting implausible values, taking into account the normal range of imputed values. Additional information, known as domain or background knowledge, can be integrated into the modeling process from data processing to model development (Rudin and Wagstaff, 2014; Niknafs and Berry, 2017). If one has domain knowledge about a specific variable, one can consider the practical scope of the obtained data. Some values identified as invalid can be newly estimated based on domain knowledge or replaced with the values estimated from previous steps (Refer to Algorithm 5).

**Algorithm 5:** Correct the originally missing values using domain-knowledge

```

for  $i \in [1, 2, \dots, N]$  do
  for  $j \in [1, 2, \dots, M]$  do
    Estimate  $\hat{x}_{ij}$  using the domain-knowledge  $f^{DM}(\cdot)$ , i.e.,
     $\hat{x}_{ij} = f^{DM}(x_{ij})$ .
  end
  Replace  $x_{ij}$  using the estimated value  $\hat{x}_{ij}$  if necessary, i.e.,
   $x_{ij} = \hat{x}_{ij}$ .
end

```

where  $f^{DM}(\cdot)$  is the estimated function based on domain-knowledge, and  $\hat{x}_{ij}$  is the estimated value of the *j*th parameter in *i*th ship case from Algorithm 5.

### 2.3. Regression curve fitting functions

To perform a curve fitting between each parameter, linear, quadratic, cube, power, and logarithmic functions, which are commonly used for data smoothing, have been applied, and they are fitted on the observed data based on the least-squares method. The intercept term of the expression is excluded from those functions so that the predicted value can start at (0, 0) (Eqs. (1)–(5)). Among the curve fitting functions, the most suitable function for the measured values was applied, which was determined based on the  $R^2$  value.

$$\text{Linear function : } y = a \cdot x \quad (1)$$

$$\text{Quadratic function : } y = a \cdot x^2 \quad (2)$$

$$\text{Cubic function : } y = a \cdot x^3 \quad (3)$$

$$\text{Power function : } y = a \cdot x^b \quad (4)$$

$$\text{Logarithmic function : } y = a \cdot \log x \quad (5)$$

where  $a$ ,  $b$  are curvilinear coefficients to be estimated for the model.  $y$  is the design parameter, and  $x$  is the independent variable.

### 2.4. Multiple regression using backward elimination

According to the number of independent variables, using one independent variable is classified as simple regression analysis, and two or more variables are classified as multiple regression analysis. The basic model of multiple linear regression analysis with  $M$  independent variables can be expressed as Eq. (6). The method of minimizing residuals by regression formula is to find a regression coefficient that minimizes the sum of the least-squares errors of the data points, such as Eq. (7). The significance of the estimated regression coefficients in a multiple regression model can be analyzed by performing a *t*-test, which determines whether to reject the null hypothesis that each independent variable has nothing to do with the dependent variable (Mark and Goldberg, 2001).

$$y_i = \beta_0 + \beta_1 x_{i1} + \beta_2 x_{i2} + \dots + \beta_j x_{ij} + \epsilon_i \quad (6)$$

$$\hat{\beta} = \text{argmin}_{\beta} \sum_{i=1}^N \left( y_i - \beta_0 - \sum_{j=1}^L \beta_j x_{ij} \right)^2 \quad (7)$$

where  $y_i$  denotes *i*th observed value of dependent variable,  $\beta_j$  signifies regression coefficient,  $\beta_0$  is intercept term,  $\epsilon_i$  is error term,  $x_{ij}$  is *i*th observed value of *j*th independent variable,  $N$  is the sample size (ship cases), and  $L$  is the total number of independent variables in the regression model.

The multiple regression model has the advantage of being able to include all the candidate variables that can affect the dependent variable. However, if the number of independent variables increases in the model, the complexity of the model increases, which may cause more computational cost and errors. If a statistical model fits too close to a particular data set by including more parameters than can be justified by the data, it may fail to predict additional observations reliably (Anderson and Burnham, 2004). To exclude the redundant explanatory variables, algorithms that add or delete variables based on selected criteria can be introduced (Pituch and Stevens, 2015). They are called variable selection methods, and among them the backward elimination method refers to the process of starting with all candidate variables, sequentially removing a variable of which the most statistically insignificant for the model fit. The criterion for determining the significance of each variable is based on a *p*-value and the variable selection process is repeated until all remaining independent variables satisfy a certain threshold such as *AIC* (Akaike's Information Criterion), *BIC*, or maximum *p*-value (Konishi and Kitagawa, 2008;

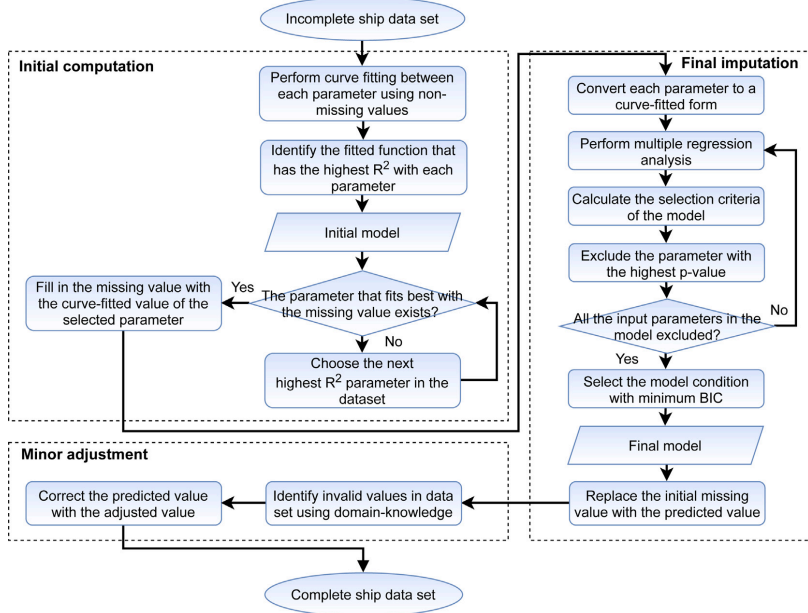


Fig. 1. Flowchart of estimating ship principal data considering missing values as proposed in the study.

Montgomery and Runger, 2014). The backward elimination method is most complicated for the initial phase because it contains all candidate variables, but it has the advantage of testing information for all variables. Since the study uses a given data set, backward elimination was applied to be able to test all candidates sequentially as described in the final imputation step.

### 2.5. Experimental evaluation of prediction accuracy

To verify the performance of models for ship principal data, we used error indices such as mean square error ( $MSE$ ), mean absolute error ( $MAE$ ), root mean square error ( $RMSE$ ), coefficient of determination ( $R^2$ ), adjusted coefficient of determination ( $Adjusted R^2$ ), Akaike's Information Criterion ( $AIC$ ), and Bayesian Information Criterion ( $BIC$ ) as follows:

$$MSE = \frac{1}{N} \sum_{i=1}^N (y_i - \hat{y}_i)^2 \quad (8)$$

$$MAE = \frac{1}{N} \sum_{i=1}^N |y_i - \hat{y}_i| \quad (9)$$

$$RMSE = \sqrt{\frac{1}{N} \sum_{i=1}^N (y_i - \hat{y}_i)^2} \quad (10)$$

$$R^2 = 1 - \frac{\sum_{i=1}^N (y_i - \hat{y}_i)^2}{\sum_{i=1}^N (y_i - \bar{y})^2} \quad (11)$$

$$Adjusted R^2 = 1 - \frac{(1 - R^2) \cdot (N - 1)}{N - L - 1} \quad (12)$$

$$AIC = N \cdot \log(RSS/N) + 2L \quad (13)$$

$$BIC = N \cdot \log(RSS/N) + L \cdot \log(N) \quad (14)$$

where  $y_i$  denotes  $i$ th observed value of dependent variable,  $\hat{y}_i$  represents  $i$ th predicted value of dependent variable,  $\bar{y}$  signifies the mean of the observed data, and  $RSS$  is the residual sum of squares.

$MSE$  and  $MAE$  measure the variance and the average of the residuals, respectively.  $RMSE$  is the standard deviation of the prediction errors, which shows a measure of how spread out the residuals are, and the  $R^2$  value is based on the proportion of total variation of outcomes explained by the model. In the regression model, as the number of independent variables increases, the  $R^2$  value will increase, and as a result, there is a concern that it will be considered the best model (Hair et al., 2018). To compensate for this shortcoming, the  $adjusted R^2$  value is designed to impose penalties as the number of independent variables increases. Similarly,  $AIC$  and  $BIC$  serve to select a parsimonious and explainable model by using penalty term for the number of variables and the fitness term of the model. In this study, the  $R^2$  value is used as the error index for the curve fitting, and  $adjusted R^2$  value is used to compare the prediction performance of models in which two or more variables are used. Both  $AIC$  and  $BIC$  are compared in Section 3.4 for selecting the number of variables when fitting the model.

## 3. Case study

### 3.1. Ship database

IHS Sea-Web database, which contains the following 14 design parameters: auxiliary engine power (AEP), breadth (B), draught (T), deadweight tonnage (DWT), gross tonnage (GT), light displacement

**Table 1**  
Descriptive statistics for the principal data of 6,278 container ships from the Sea-Web database.

Ship principal parameters	Valid data	Missing data	Mean	Median	Std.Dev	Minimum	Maximum	Skewness
Auxiliary engine power, AEP [kW]	3892	2386	1929.6	1720.0	1177.8	50.0	5829.0	0.66
Breadth, B [m]	6277	1	31.6	30.2	9.8	9.5	61.5	0.63
Draught, T [m]	6268	10	11.2	11.5	3.0	1.1	16.5	-0.34
Deadweight tonnage, DWT [t]	6278	0	49299.3	34577.5	44030.0	500.0	228149.0	1.40
Gross tonnage, GT [t]	6278	0	43895.2	27779.0	43506.6	355.0	232618.0	1.68
Light displacement tonnage, LDT [t]	4559	1719	15957.6	11926.0	12202.4	358.0	66939.0	1.30
Length over all, LOA [m]	6277	1	221.9	208.9	80.1	48.9	400.0	0.31
Length between perpendiculars, LBP [m]	6229	49	210.8	196.6	77.0	47.5	388.1	0.34
Main engine cylinder, MEC [-]	6247	31	8.1	8.0	2.0	3.0	16.0	0.85
Main engine power, MEP [kW]	6273	5	27620.0	21560.0	20994.5	352.0	80905.0	0.68
Main engine RPM, MER [-]	6120	158	167.9	104.0	158.0	65.0	1200.0	2.42
Main engine stroke, MES [-]	6254	24	2.3	2.0	0.7	2.0	4.0	1.88
Service speed, V [knot]	6203	75	20.7	21.0	3.5	7.5	29.2	-0.60
TEU capacity, TEU [-]	6254	24	4073.0	2553.5	4131.1	24.0	23756.0	1.84

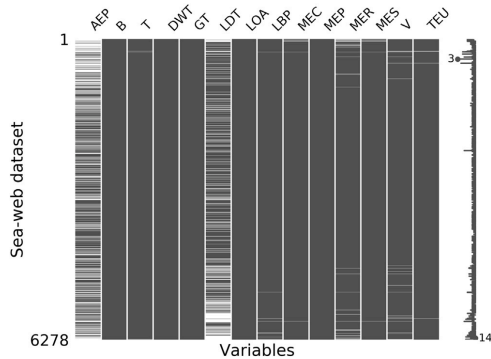


**Fig. 2.** Missing pattern of principal data of container ships collected from the Sea-Web database.

tonnage (LDT), length over all (LOA), length between perpendicular (LBP), main engine cylinder (MEC), main engine power (MEP), main engine RPM (MER), main engine stroke (MES), service speed (V), and container capacity (TEU), was used in this study (IHS, 2019). Here, data analysis and missing data imputation algorithm were mainly performed based on Python programming language. For the case study, the container ship data sets were extracted, consisting of 6,278 vessels from 24 to 23,756 TEU capacity, up until the build year of 2019. The other ship types are not covered in the text, but the results are included in Appendices B and C. Table 1 presents the descriptive statistics of each design parameter, and Fig. 2 visualizes the overall status of missing data. The row of the figure stands for each ship case and the column denotes each parameter. The white cell represents the missing value and the black cell is a non-empty value. The ship data sets are displayed in random order. Among all ship parameters, 38.0%, 27.4%, and 2.5% of the data are missing for the AEP, LDT, and MER. There are also missing data for other parameters, as can be seen from Fig. 2. It should be noted that even if one's data set is different from the data set used in the case study, missing data imputation in ship principal data can be performed according to Algorithms 1–5.

Little's MCAR test is a common method for determining MCAR patterns for missing data in a data set and tests for significant differences between the observed and estimated means for each missing data pattern (Garson, 2015). If the  $p$ -value of the null hypothesis that the missing data is MCAR is not significant, then the data may be assumed to be MCAR (Little, 1988). Table 2 displays the result of Little's MCAR

**Table 2**  
Little's MCAR test for the ship principal data used in the study. Test statistic follows  $\chi^2$  distribution asymptotically with degrees of freedom ( $df = \sum_{k=1}^K M_k - M$ ) under the null hypothesis that there are no differences between the means of different missing-value patterns.  $K$  is the number of missing value patterns among all ship cases,  $M_k$  is the number of observed components in pattern  $k$ ,  $M$  is the number of ship parameter.  $p$ -value means the probability that statistics equal to or more extreme than those actually observed in the sample under the assumption that the null hypothesis is correct.

	$\chi^2$ -value	$df$	$p$ -value
Sea-Web database (Container ship)	4127.053	373	0.00

\* Significant at level  $p < 0.05$ .



**Fig. 3.** Correlation matrix of missing values.

test against current data sets. It showed that the  $p$ -value of the null hypothesis is less than 0.05, which means that our data is not missing at random and there may be some sort of a systematic bias included.

To achieve additional information about missing characteristics, a correlation analysis between missing and non-missing values for ship variables is performed as depicted in Fig. 3. The notable correlations of missing data are highly correlated variables, such as LOA, B, MES, and MEC. This trend seems to be because the number of missing values is so small that just a few missing values can exaggerate the correlation between the two variables. AEP, LDT, V, and MER, which include relatively higher rate of missing values than other variables, have correlation coefficients in the range of 0.1 to 0.2 with most other variables, indicating that there is almost no correlation between missing values.

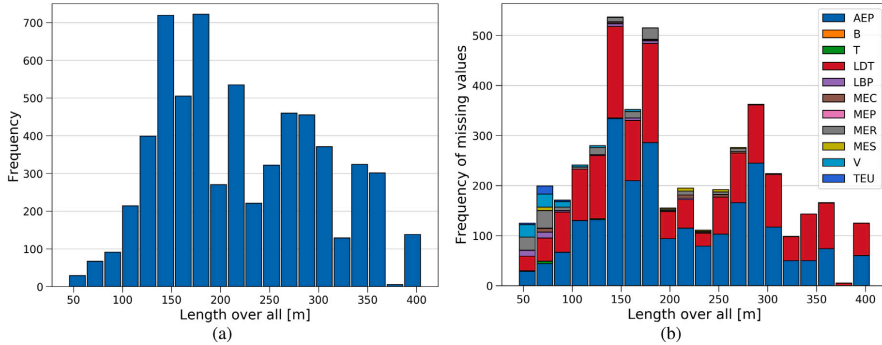


Fig. 4. (a)Histogram of the collected ship data by length, (b)Histogram of the cumulative missing values of variables distributed over length.

Fig. 4(a) shows the histogram of container ships by LOA, and Fig. 4(b) reveals the cumulative missing values of variables. Both histograms have similar distributions, which show the shape of the normal distribution centered on 160 meters and 280 m. Fig. 5 denotes the average ratio of missing values against observed data by LOA. While the average missing rates for the most ranges are almost constant at less than 10%, the missing rates for ranges of less than 100 meters are relatively high at 14%–33%. It seems likely that these results are due to the nature of the maritime data, which is generally collected and integrated from various organizations such as ship, owners, shipbuilders, and port authorities.

If a list-wise deletion method that removes missing values in any of the data sets is applied in this case, 46.6% of the total data should be removed, resulting in the inability to use such information and a decrease in statistical power, and one can estimate the biased regression slope. Judging by the nature of the ship principal data, it is inappropriate to apply list-wise deletion or single imputation for the missing values, since the data are not missing completely at random. A model-based computation method using regression analysis intended to be applied in this study does not eliminate missing values but replaces them with plausible values. It also has the advantage of being relatively easy to apply to the ratios and characteristics of various missing data. As discussed above, for ships with length less than 100 meters have a relatively high rate of missing data, the performance of imputation will be checked in a later section.

3.2. Correlation between ship principal data

The ship main dimensions and related particulars are determined by various factors such as the cargo volume and weight, and the operational routes required by the ship owner or operator, the strength and stability specified by the rules and regulations of the Classification society, the minimum resistance and friction forces for economic purposes (Papanikolaou, 2014). Moreover, the ship principal parameters such as length, breadth, draught, and height, as well as various other characteristics, are correlated with each other. For instance, for container ships, breadth depends on the row numbers on the deck, thus it is directly related to the number of container capacity on board. An increase in breadth is linked to an increase in cargo capacity and hull resistance, which requires more propulsion power for a ship (Charchalıs, 2013). Furthermore, it is important to maintain an appropriate relation between hull length, breadth, draught, and freeboard in terms of securing the ship’s stability and integrity (Charchalıs and Krefft, 2009). Considering the hull resistance, the wave-making resistance

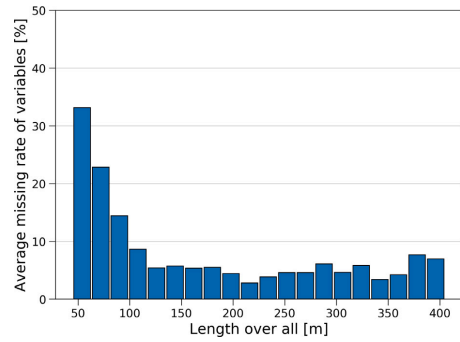


Fig. 5. Average missing rate of each variable according to the length over all.

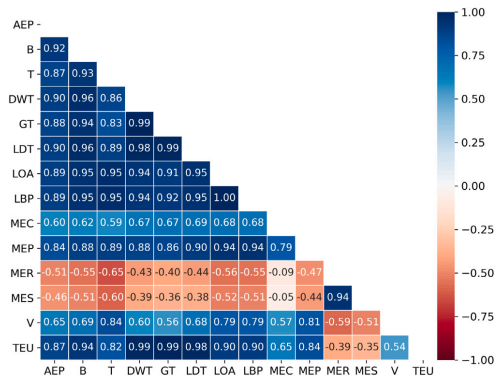


Fig. 6. Correlation matrix of non-missing principal particulars of the container ships of the case study.

of the vessel is closely related to the sailing speed and waterline length (Gertler, 1954; Graff, 1964; Tuck, 1987).

Prior to following the procedure of handling the missing data, we have conducted a Pearson correlation analysis between ship main dimensions and related particulars as defined in Eq. (15), and detailed it on the correlation matrix in Fig. 6. The correlation coefficient has been calculated using all data except missing values. As mentioned above, significant correlations are identified between each variable. It can be seen that there is a strong correlation of 0.7 or higher between the volume, weight, cargo quantity, which are composed of L, B, T, and its combination. Variables related to the engine property of the ship such as MEP, MEC, MER, MES, and AEP also have correlation coefficients of 0.3–0.7. Some correlations between other ship principal variables exist.

$$\rho_{X,Y} = \frac{E[(X - \mu_X)(Y - \mu_Y)]}{\sigma_X \sigma_Y} \quad (15)$$

where  $\rho_{X,Y}$  is correlation coefficient between two variables  $X$  and  $Y$ ,  $E$  is the expected value operator, and  $\sigma_X$  and  $\sigma_Y$  are standard deviations.

### 3.3. Initial computation

A curve fitting between each variable is performed at the initial computation stage, which is intended to fill in the missing values of the ship data sets and make it possible to implement multiple regression models for variables later. To be specific, it is to take a single variable and function form with the highest goodness of fit for each variable and estimate the missing value using it. Here, it is necessary to define a function that returns the result values of the form shown in Eqs. (1)–(5) for input data and find appropriate unknown coefficients such as ‘a’ and ‘b’ for the established function. That is, in order to perform curve fitting on a given data set, optimize.curve\_fit of scipy, an open-source Python library, was used in this study (Virtanen et al., 2020). In Fig. 7, the most fitted function among the curve fittings is marked and the degree of fitness ( $R^2$  value) is expressed as a heat map. Among the results in Fig. 7, the highest-fitting relationship was extracted for each variable and the final curve fitting results of this step is plotted in Figs. 8(a)–8(n). As can be seen in Fig. 7, the relationship between most parameters is best fitted when applying the power function. This is because the defined power function provides more flexibility than that of the relatively simple functions such as linear, quadratic, cubic, and logarithmic so that the non-linear curves between features can be fitted well. In the given data sets, the relationships of DWT-AEP, GT-B, DWT-T, GT-DWT, TEU-GT, LBP-LDT, LBP-LOA, LOA-LBP, MEP-MEC, LOA-MEP, MES-MER, MER-MES, MEP-V, and GT-TEU showed the highest curve fitting results for each other. For GT-DWT, GT-LDT, TEU-GT, and LOA-LBP, the power function was used as the fitted function form, and the exponents of power function were between 0.8 and 1.2, which implies an almost linear relationship.

Regarding the engine factors, it was possible to identify some physical relationships of variables from Figs. 8(a), 8(i), 8(k), 8(l). As the output of the main engine increased, the number of cylinders increased, and as the strokes become from two to four, the rotational speed increased. According to MAN B&W (B&W, 2019), large vessels put a priority on power over speed, so they tend to mount two-stroke engines that have low-speed but good thermal efficiency, low fuel consumption, and high durability. Conversely, the four-stroke engines are mainly installed as a propulsion system for small and medium-sized ships with less than 5,000 kW, or as an auxiliary engine for large ships. It is common to set the rotational speed high to obtain enough power from the auxiliary engine, since the engine is compact and the stroke length can be shortened.

In Fig. 8(m), as the power of the main engine installed on the ship increased, the service speed generally increased logarithmically. In general, main engine power is directly related to maximum speed rather than service speed, but even in the case of the service speed used in this study, it can be seen that  $R^2$  value has a prediction accuracy of 0.8387 when it is fitted with a power function. It is noteworthy that some

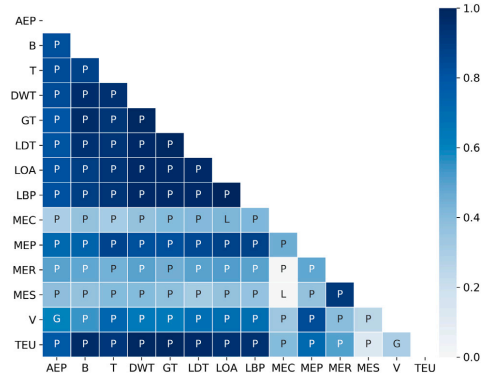


Fig. 7. Heat map for curve fitting results of ship principal particulars (L: Linear, Q: Quadratic, C: Cubic, P: Power, G: Logarithmic).

ships with a power of more than 50,000 kW had service speed ranges from 18 to 22 knots, significantly lower than the general trend, and these were found for the case of recently built mega-container ships. Due to rising oil prices in the early 2010s and the adoption of EEDI to new ships to reduce emissions, many shipping companies adopted a slower and more economical voyage speed than previously for their container fleets (Wiesmann, 2010; Meyer et al., 2012). Subsequently, some of the newly built mega container ships were equipped with smaller engines than previous ships of similar size to design slower service speeds (Congress, 2016).

Through this curve fitting process, missing values in the data sets were filled in initially. As explained earlier, the  $R^2$  values of most curve fittings were high, but some relationships, such as the main engine cylinder and main engine power showed lower correlations. In addition, there have been instances where the average prediction accuracy of the entire data was good, such as the relationship between the main engine power and service speed, but includes data groups that are out of the general trend. If the  $R^2$  value of the resultant model is low or many predicted values deviate from the regression line, it means that a curve-fitted form of a specific single variable is not sufficient to explain the proportion of variance in the dependent variable (Warner, 2020). Therefore, the next section will address the multivariate analysis for explaining more variance.

### 3.4. Final imputation

In this step, multiple regression analysis with backward elimination was performed on the complete data sets obtained from the previous step. According to Mark and Goldberg (2001), the method for testing errors in models produced by stepwise regression is to evaluate the model for data set that are not used to create the model. This method is particularly useful for the case that collects data from different settings or generalizes the model with preventing overfitting. As such, stepwise regression through evaluation criteria such as AIC, BIC, and  $p$ -value was implemented through statsmodels, a statistical package (Seabold and Perktold, 2010). Therefore, in the entire process of initial computation, final imputation, and minor adjustment, only 80% of the total data set which are randomly selected were used for model implementation and the remaining 20% were only used for the performance evaluation of the final model.

An independent variable with the maximum  $p$ -value (i.e., the most insignificant variable) was sequentially removed from the model in the backward elimination process, and Fig. 9 shows the maximum  $p$ -value

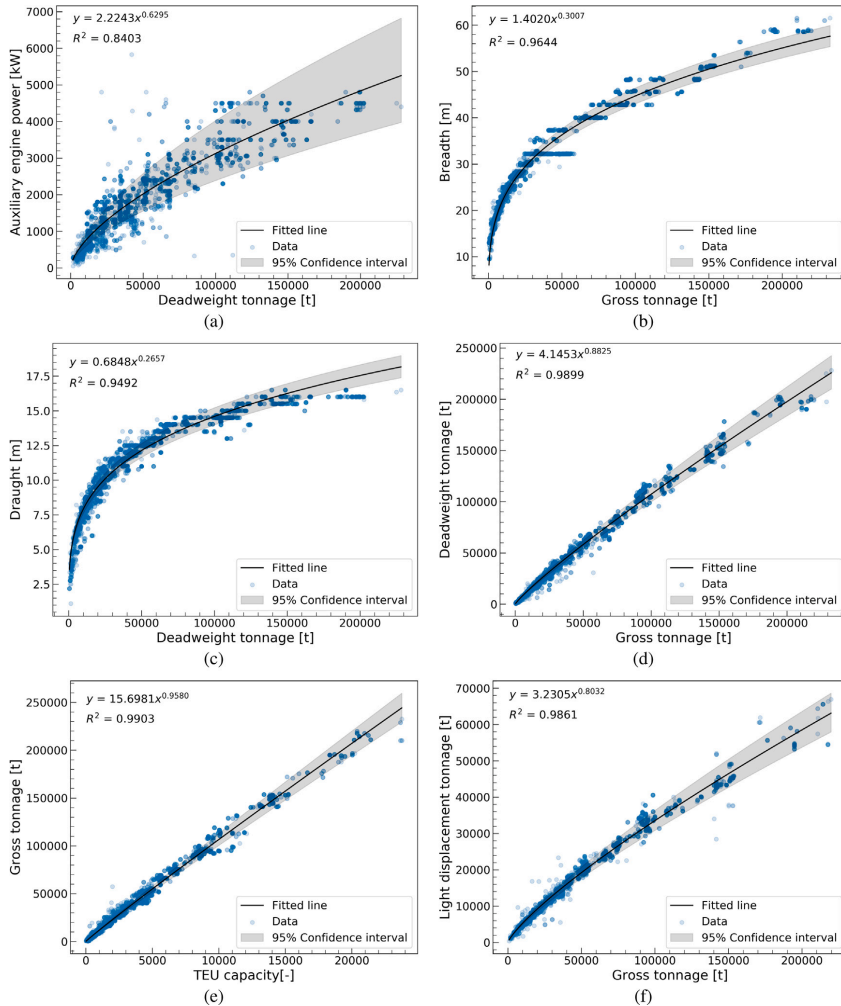


Fig. 8. Results of curve fitting for ship main particulars: (a) Auxiliary engine power, (b) Breadth, (c) Draught, (d) Deadweight tonnage, (e) Gross tonnage, (f) Light displacement tonnage, (g) Length over all, (h) Length between perpendicular, (i) Main engine cylinder, (j) Main engine power, (k) Main engine RPM, (l) Main engine stroke, (m) Service speed, (n) TEU capacity.

of independent variables, *AIC* value, and *BIC* value of the model according to the number of variables. The minimum values for *AIC* and *BIC* are represented by the black edges of the markers. The *AIC* and *BIC* include penalty terms for the number of parameters to avoid the possible overfitting problem of the model. Since the *BIC* puts more penalties for the number of parameters than the *AIC*, fewer variables are selected in the *BIC* based on the minimum values of *AIC* and *BIC*, as shown in the figure. Comparing the maximum *p*-values at the minimum points of *AIC* and *BIC*, some *p*-values for *AIC* are greater than 0.05, but all *p*-values for *BIC* are less than 0.05. In general, the significance of independent variables to the dependent variable is based

on a *p*-value of 0.05 (Montgomery and Runger, 2014). Thus, the final model was chosen based on a minimum *BIC* value considering such criterion.

The following Table 3 outlines the results of multiple regression analysis using the backward elimination procedure. Before performing the variable selection process, there is a total of 13 independent variables, and the maximum *p*-value in each regression model is more than 0.05. Through the variable selection process, the *p*-values of all independent variables in the regression model decreased to less than 0.05 by removing the relatively less statistically significant variables. Finally, 7–13 independent variables were selected. The significance of

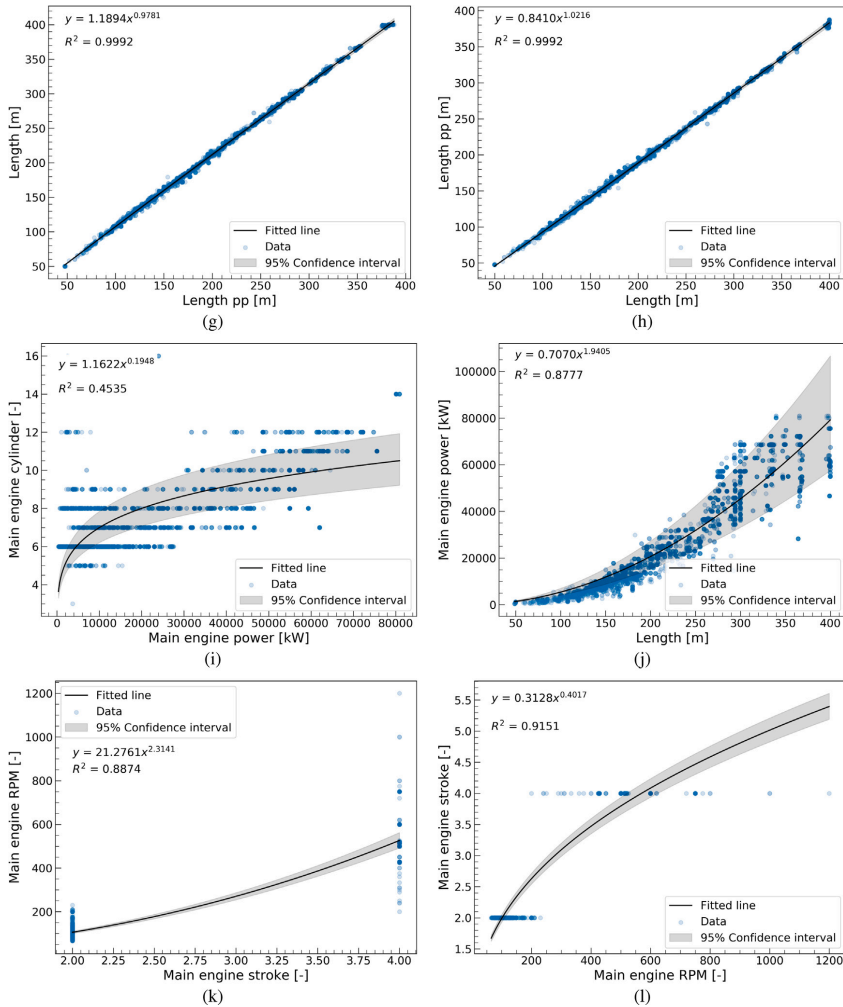


Fig. 8. (continued).

the final models was evaluated statistically through the *f*-test, and it can be seen that all models were significant at a confidence level of 0.05 as shown in Table 3. Comparing the *adjusted R*<sup>2</sup> values of the model for the training data, the *adjusted R*<sup>2</sup> was almost maintained even if some variables were removed. This means that the effect of the removed independent variable on the dependent variable is insignificant. Moreover, in the case of independent variables having a similar effect on the dependent variable, unnecessary variables were removed during the backward elimination process, or redundant effects were reduced by adjusting the regression coefficient. For instance, most of the final formulas that require length factor, include only one of LOA or LBP since LOA and LBP have a strong correlation. However, when both LOA and LBP are included in the equations, such as DWT, TEU, V, and T, the

redundant effect caused by adding two-length variables at the once is reduced by adjusting the sign and size of the regression coefficients. Another example is LDT, DWT, TEU, and GT related to the overall volume and weight of the ship. The final regression equation of each variable obtained through this process can be found in Appendix C.

### 3.5. Minor adjustment

If one has any prior knowledge of a given variables, we can consider the realistic values based on it. This step corrects the predicted values that are considered inappropriate based on expert judgment. For instance, the main engine stroke is classified into two or four strokes, and the main engine cylinder has to be a positive integer. However,

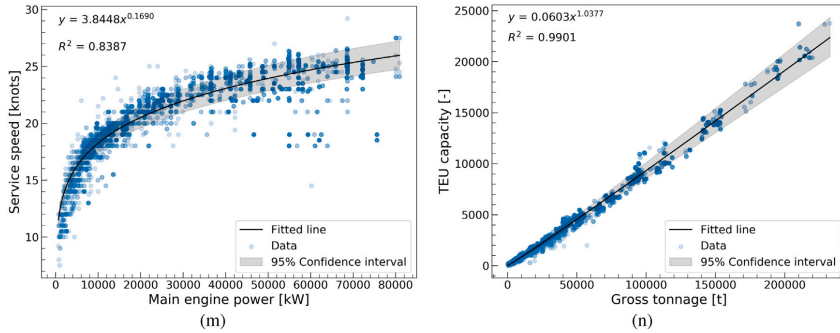


Fig. 8. (continued).

Table 3

The results of multiple regression analysis with backward elimination for training data set of ship principal data. Max  $p$ -value in the table represents the maximum  $p$ -value of all independent variables used in the model, and  $f$ -statistic ( $p$ -value) means the  $f$ -test results of the selected model and its  $p$ -value.

Ship principal parameters	Full model			Selected model			$f$ -statistic ( $p$ -value)
	Adjusted $R^2$	Max. $p$ -value	No. of inputs	Adjusted $R^2$	Max. $p$ -value	No. of inputs	
Auxiliary engine power, AEP [kW]	0.901	0.471		0.901	0.000	9	5064.7 (<0.001)
Breadth, B [m]	0.988	0.106		0.988	0.002	11	37,255.1 (<0.001)
Draught, T [m]	0.977	0.054		0.977	0.000	11	18,972.8 (<0.001)
Deadweight tonnage, DWT [t]	0.995	0.755		0.995	0.000	12	82,946.5 (<0.001)
Gross tonnage, GT [t]	0.996	0.236		0.996	0.000	10	153,187.9 (<0.001)
Light displacement tonnage, LDT [t]	0.993	0.132		0.993	0.000	10	72,405.7 (<0.001)
Length over all, LOA [m]	0.999	0.552		0.999	0.001	7	963,254.6 (<0.001)
Length between perpendiculars, LBP [m]	0.999	0.836	13	0.999	0.000	8	901,284.3 (<0.001)
Main engine cylinder, MEC [-]	0.718	0.911		0.718	0.000	10	1,280.3 (<0.001)
Main engine power, MEP [kW]	0.966	0.767		0.966	0.000	11	13,099.8 (<0.001)
Main engine RPM, MER [-]	0.921	0.728		0.921	0.001	11	5,339.1 (<0.001)
Main engine stroke, MES [-]	0.938	0.646		0.938	0.000	11	6,933.3 (<0.001)
Service speed, V [knot]	0.916	0.800		0.916	0.002	11	4,984.0 (<0.001)
TEU capacity, TEU [-]	0.993	0.001		0.993	0.001	13	63,352.4 (<0.001)

due to the nature of the regression model, predicted values rarely exist as an integer. Therefore, predicted values of the main engine stroke are adjusted to either 2 or 4 depending on what is closer, and those of the main engine cylinder are rounded off to the nearest positive integer (see Figs. 10(a), 10(b)). In another case, some predicted values may be less than zero due to the intercept term in the predictive model even though the model has outstanding performance generally. Such values are replaced with the curve-fitted value of the initial computation step. The formulas listed in Appendix C are the final imputation results of each variable, and it should be noted that if domain knowledge is applicable (e.g., MEC and MES), the minor adjustment step should be processed for the corresponding result values.

#### 4. Results and discussion

##### 4.1. Comparison with previous studies

Here, we compare the model proposed in this study with the model developed in the earlier studies and also with the random forest model, which is widely used in the imputation of missing data in machine learning methods. Table 4 summarizes previous studies that established regression equations of main dimensions and related particulars for a container ship. 20% of the total data not used to implement the model was defined as a test data set and the prediction performance of the models listed in Table 3 was evaluated using it. Table 5 shows the results of comparing the prediction performance of the model in this study, the model with the best result among previous studies, and the

random forest model against test data set. As an error metrics, MAE, RMSE, MSE, and adjusted  $R^2$  values defined in Eqs. (8)–(12) were used.

Random forest is an ensemble method that trains a number of decision trees, outperforming in a variety of fields, such as classification and regression of high-dimensional data (Breiman, 2001). Regarding hyperparameters for the random forest model, this study used Grid-searchCV of Scikit-Learn library (Kramer, 2016; Bisong, 2019) on the following ranges and took the best subset model among them. (The number of trees = [16-512]; the number of variables in attach split = [3-5]; the other parameters = default of Scikit-Learn library. According to Oshiro et al. (2012), the number of trees at a range between 64 and 128 has shown balanced performance between accuracy, processing time, and memory. In James et al. (2013), the number of variables in each split has been recommended as 1/3 of the number of features. Thus, parameter optimizations have been performed for the range that such values can be included.)

Engine factors such as AEP, MEC, MER, and MES were not covered in the comparison studies. In the case of MEP and V, the adjusted  $R^2$  has been increased largely from 0.8824 and 0.7578 to 0.9620 and 0.8989, respectively, while RMSE decreased from 7055.58 and 1.70 to 4008.59 and 1.09, respectively. Additionally, since all the adjusted  $R^2$  and RMSE of other variables have also improved over the previous models, the models proposed in this study are considered to have higher prediction accuracy overall. Since the Sea-Web database used in this study contains a wider range and the number of ships compared to the data sets used in other studies as can be seen from Table 4, the



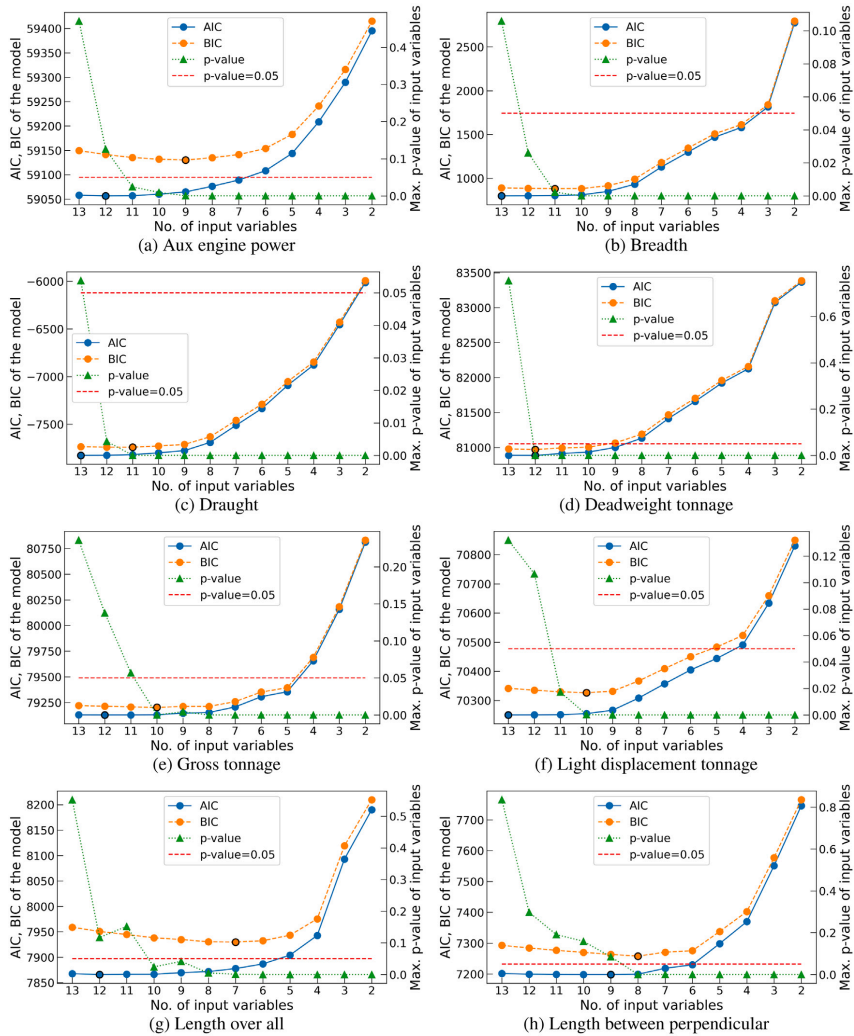


Fig. 9. *AIC*, *BIC*, and max. *p*-value according to the decreasing number of independent variables for the model: (a) Auxiliary engine power, (b) Breadth, (c) Draught, (d) Deadweight tonnage, (e) Gross tonnage, (f) Light displacement tonnage, (g) Length over all, (h) Length between perpendicular, (i) Main engine cylinder, (j) Main engine power, (k) Main engine RPM, (l) Main engine stroke, (m) Service speed, (n) TEU capacity.

**Table 4**  
Summary of previous studies estimating the main particulars of the container ship using regression analysis.

Study	Range (TEU)	Build year	No. of ships
Piko (1980)	Abt. 100–3,000	–1977	289
Takahashi et al. (2006)	Abt. 48–8,468	1979–2005	2,358
Charchalis and Krefft (2009)	Abt. 50–11,000	–	–
Charchalis (2014)	Abt. 1,174–1,388	–	17
Kristensen (2016)	Abt. 50–19,500	1988–2016	2,397
Radfar et al. (2017)	–	1999–2016	985
Abramowski et al. (2018)	Abt. 20–20,000	2005–2015	–
Cepowski (2019)	Abt. 90–19,224	2000–2018	442
This study	Abt. 24–23,756	1957–2019	6,278

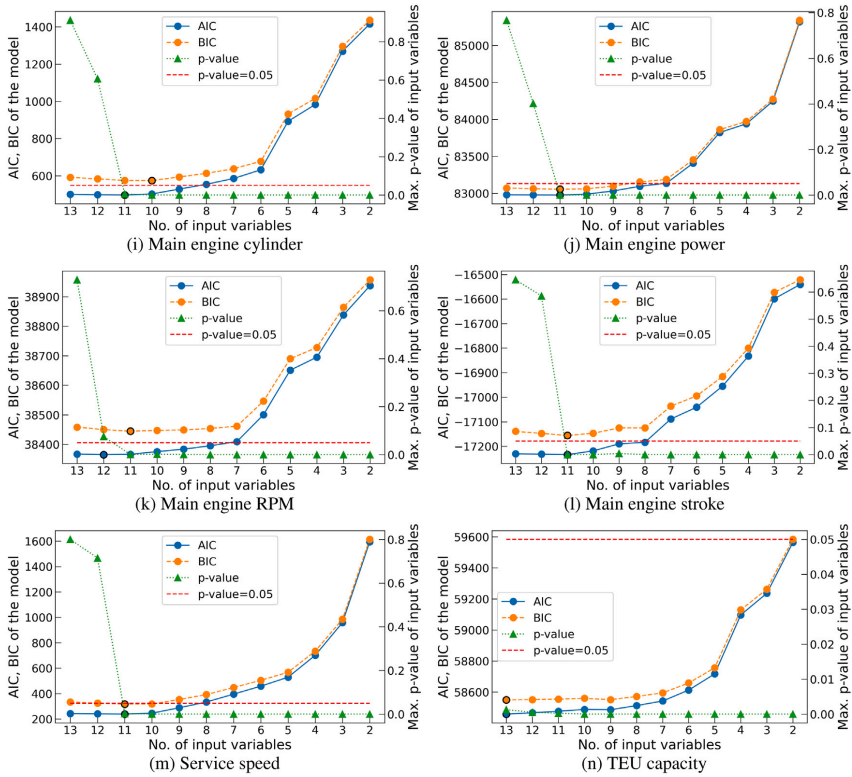


Fig. 9. (continued).

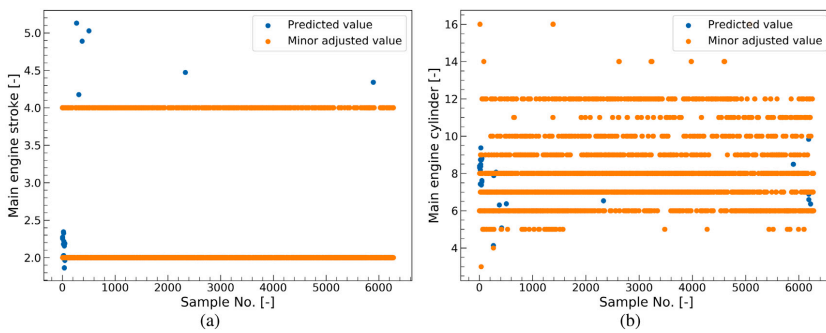


Fig. 10. Corrected values through minor adjustment step: (a)Main engine stroke, (b)Main engine cylinder.

scalability of the estimated regression formula is expected to be higher. Some ships in data sets were built before the 1990s, but the influence on the final model is not much because they account for less than 5 percent of the total number of ships. Referring to some examples of the book

“Ship design: methodologies of preliminary design” (Papanikolaou, 2014), the predicted results of the proposed algorithm are compared with the method showing the highest accuracy in Table 4 and the simple regression equation from the book in Appendix A. The final

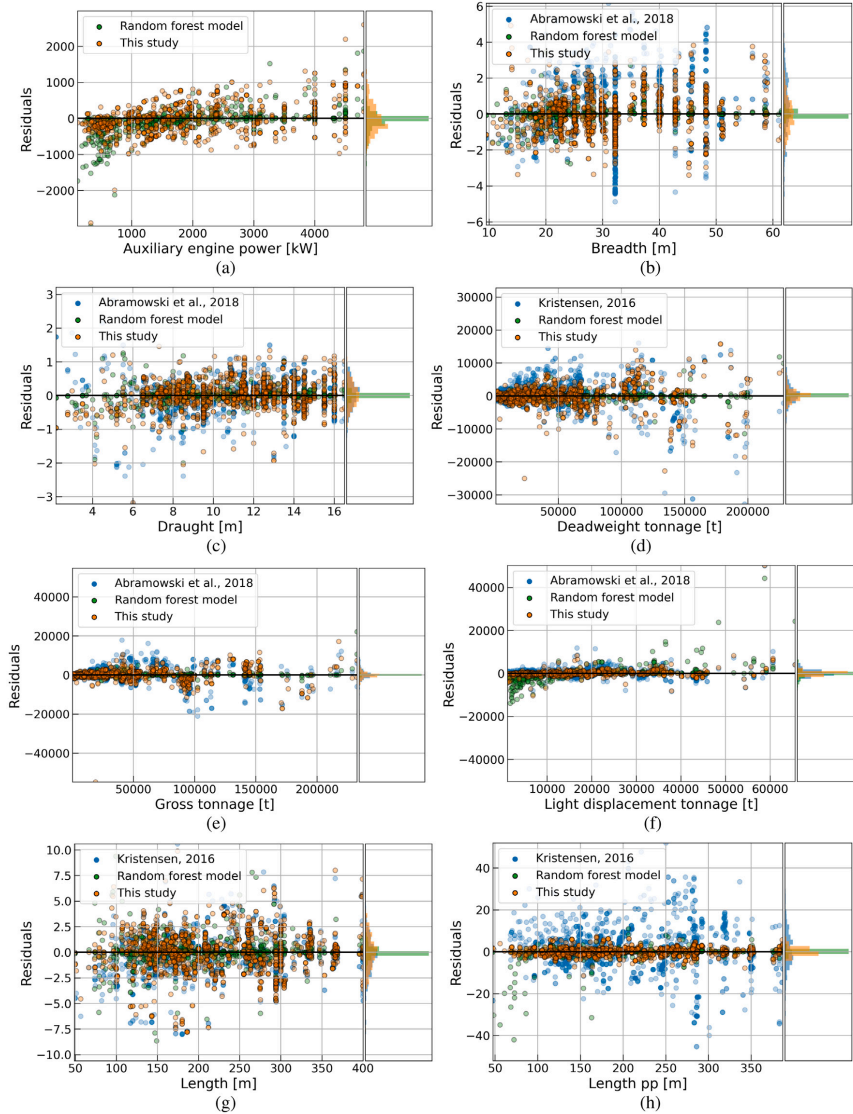


Fig. 11. Distribution of residuals for the predicted values between previous studies, random forest model, and this study: (a) Auxiliary engine power, (b) Breadth, (c) Draught, (d) Deadweight tonnage, (e) Gross tonnage, (f) Light displacement tonnage, (g) Length over all, (h) Length between perpendicular, (i) Main engine cylinder, (j) Main engine power, (k) Main engine RPM, (l) Main engine stroke, (m) Service speed, (n) TEU capacity.

equations for different types of ships and their performance are detailed in Appendix C, showing that the model does not only perform well for container ships.

To examine whether the assumptions about the regression model are satisfied, residual analyses were performed (Hair et al., 2018). As

can be seen from Figs. 11(a)–11(j), residuals for predicted values are plotted across the range of the variable, and a histogram of residuals is expressed on the right axis. Analyzing the histograms of the current model, they represent a shape close to normal distribution, with no bias to any side around zero, but rather spreading evenly on both sides.

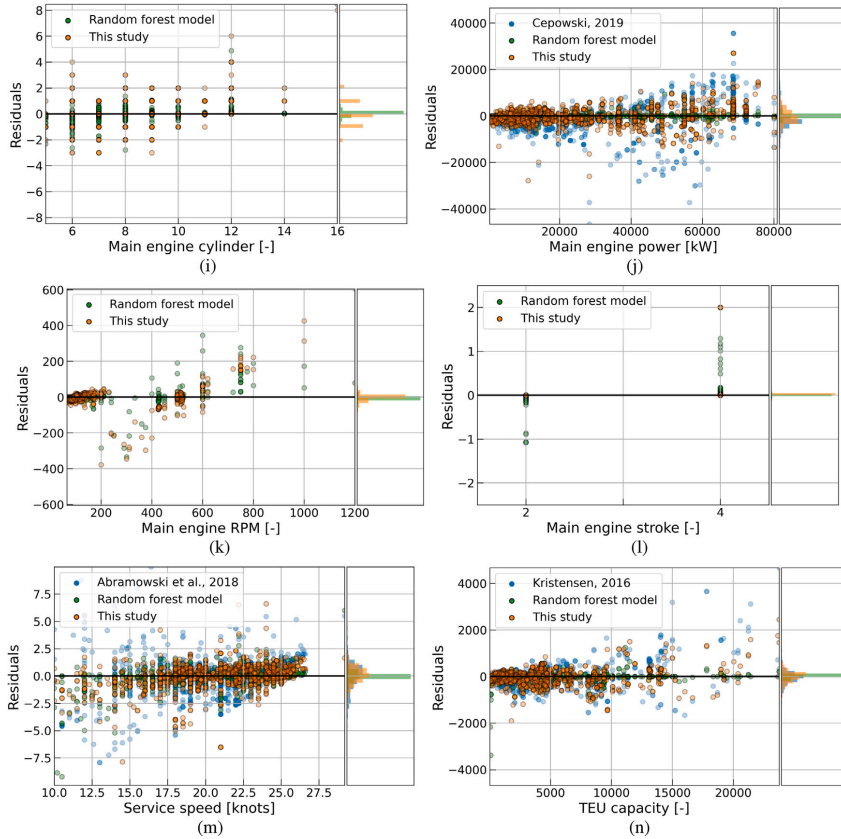


Fig. 11. (continued).

Moreover, the residuals in the figures do not show a particular pattern and are randomly distributed evenly over the entire range of variables. In particular, the residuals in the range of the ship's length less than 100 m, where the missing points of the collected data was relatively high in this study, are similar to those of other studies. These results provide support for the assumption that the regression models satisfy normality, linearity, and equal variance. Since models of the preceding studies and this study satisfy these assumptions overall and show good accuracy for the test data set, it is expected they will be useful in estimating ship principal data. However, for LBP, B, and V predicted from the previous studies, there are relatively large residuals in some ranges, which one should taken care if using in any analysis.

In the case of LBP, there was a slight discrepancy in the range of 250 to 300 m, according to the residual plot. This is considered to be due to the implementation of the regression equation by dividing the Panamax and Post-Panamax groups by the breadth of 32.2 m. The largest ship that can pass through the Panama Canal is called a Panamax, and is usually designed with 32.2 meters in breadth and 12 meters in loaded draught. However, the maximum width of the old Panama Canal was 32.31 m, and there were some ships having breadth between 32.2 meters and 32.31 meters wide, and 445 vessels were in that range in the current study. Therefore, the ships in the corresponding

range were recognized as a Post-Panamax, causing larger residuals. The *adjusted R*<sup>2</sup> value of B was 0.9613, with good predictability for the most, while there were relatively large errors at around 32 meters in breadth. This is because the size of the ship was not classified in the previous study and the characteristics of the dimensional constraints were not sufficiently addressed. Moreover, in the range between 10 and 15 knots of service speed, large residuals were observed. This is mainly judged to be a lack of data fitting on feeders of less than 1,000 TEU.

Comparing the random forest model with the developed model from this study, the random forest model shows slightly higher prediction accuracy for most parameters than the current model, as can be seen from Table 5. The random forest model creates as many trees on the subset of the data and combines the output of all the trees, which makes it possible to handle high dimensional data. From these results, a random forest model is also a good method to handle missing data. However, according to the residual distribution of AEP, LDT, LBP, MER, V, and TEU (Figs. 11(a), 11(f), 11(h), 11(k), 11(m), 11(n)), there are some values that have been deviated from the constant residual trends, while the variance of residual distribution is small overall. In this regard, tuning of hyperparameters plays an important role in the performance of random forest models, and sometimes there is a possibility that such problems might occur. Furthermore, the model

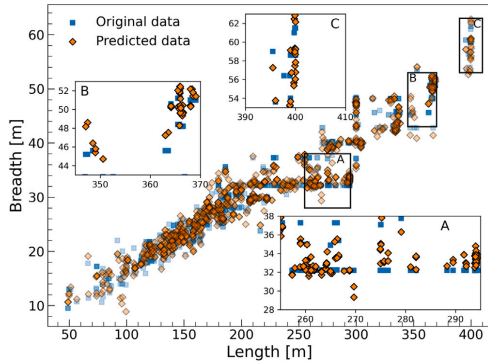


Fig. 12. The relation between ship length and breadth regarding dimensional constraints (A: Panama Canal, B: New Panama Canal, C: Suez Canal).

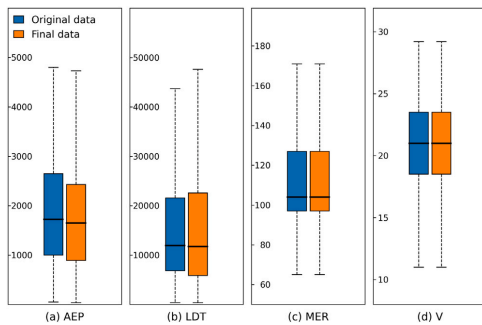


Fig. 13. Box plots for descriptive statistics of original data (white boxes) and final data (gray boxes): (a) Auxiliary engine power, (b) Light displacement tonnage, (c) Main engine RPM, (d) Service speed.

training process can be complex and require significant memory storage, as many independent trees are created and different settings of hyperparameters are tuned depending on the characteristics of the data. On the other hand, the model from this study showed consistent residuals across the entire range of data while showing more improved predictive performance over the regression models of previous studies. In addition, the resulting model is intuitive, interpretable, and can be applied easily in other studies. In particular, we believe that this method has sufficient advantages, such as fleet-wide research covered in this paper, that require not only high accuracy of the model but also an overall performance across data ranges.

#### 4.2. Validation against dimensional constraints due to operation

Apart from the physical characteristics between ship variables, there are some dimensional restrictions that should be satisfied by the ship not only for navigating certain water areas safely, but entering the terminal and using port facilities (Park and Suh, 2019; Garrido et al., 2020). Table 6 represents the representative dimensions of a container ship for navigating Panama Canal and Suez Canal, which also act as

constraints for determining the main dimensions of a ship. If one has domain knowledge for the data set and it is possible to subdivide the samples by clear criteria (e.g., Panamax, Post Panamax vessel) from the initial stage, the implemented model using such a data set may predict the characteristics of corresponding ships more accurately. However, it should be noted that the subdivision of the data set reduces the training sample, which may lead to implementing a model vulnerable to overfitting and outliers.

To confirm the performance of the model against the dimensional constraints for the ship, the breadth and length of container ships are displayed in Fig. 12. According to the 'zoomed in' clusters in boxes A, B, and C in Fig. 12, some clusters are formed around B=32 m, L=366 m, and L=400 m respectively. These clusters seem to represent previous Panamax ships, new Panamax ships, and Suezmax ships. The enlarged plots show that the predicted values of the model satisfy not only the general physical characteristics well, but also the dimensional limitations of canals. Some studies (Takahashi et al., 2006; Kristensen, 2016; Cepowski, 2019) presented in the previous section considered the dimensional constraints by dividing the groups according to the ship size when implementing their models, and it showed higher accuracy than other studies. While this grouping of ships based on domain-knowledge helps improve model accuracy, the detailed grouping reduces the number of data available to implement the model and increases the possibility of overfitting, which may again partly lead to poor performance and low efficiency. In particular, from a missing data processing perspective, the sample size plays an important role in the performance of the resulting model (Heckmann et al., 2014; Hair et al., 2018). Therefore, the estimation method for ship principal data suggested in this study seems to have a novelty in that it shows considerable accuracy without performing grouping and has the benefit of being based on a larger data set than previous studies.

#### 4.3. Validation of statistics for the final data

The performance of the missing data imputation was diagnosed by the statistical characteristics of the values superseded. The most missing variables in the database, such as AEP, LDT, MER, and V are shown in Fig. 13 as a box plot. It outlines descriptive statistics of original data and final data to show the statistical characteristics of values filled by this method. In the case of AEP and LDT, the lower quantile (25%) and upper quantile (75%) values vary slightly, but the variation is not large and the mean value is almost maintained. It can be seen that overall statistical values have not changed significantly, even though 38.0% and 27.4% of the data has been replaced. For MER and V, which had relatively fewer missing values than AEP and LDT, the min, max, mean, lower quantile, and upper quantile values are almost maintained.

Fig. 14 compares their imputed values with original values and shows a relationship with the variable having had the highest  $R^2$  in the curve fitting to ease the identification of initially missing data. The predicted data are aligned with the trend of the original data in general but it does not exactly lie on the curve fitting line of the initial computation step (Figs. 8(g), 8(k), 8(m), 8(n)). Such variance of replaced values can be interpreted as the effect of the several independent variables affecting the dependent variable is reflected in the model. From these results, it can be seen that the imputed values represent the physical relationship without significantly deviating from the statistical characteristics of the original data.

## 5. Conclusions

This study presented a method of estimating missing values in ship principal data. Data sets of 6,278 container ships from the Sea-Web database were used in a case study, and models for estimating missing values of 14 variables were implemented, including main dimensions such as vessel length, breadth, and draught. In this process, the models were created through curve fitting and variable selection. The selected

**Table 5**  
Comparison of prediction performance for the container ship's principal data between previous studies and this study.

Ship principal parameters	This study				Best result from previous studies				Random forest model			
	MAE	RMSE	MSE	Adj - R <sup>2</sup>	MAE	RMSE	MSE	Adj - R <sup>2</sup>	MAE	RMSE	MSE	Adj - R <sup>2</sup>
AEP	341	453	2.05E+5	0.8508	-	-	-	-	181	352	1.24E+5	0.9093
B	0.83	1.07	1.16	0.9875	1.49	1.90	3.61	0.9613	0.11	0.35	0.12	0.9987
T	0.32	0.43	0.19	0.9788	0.40	0.54	0.29	0.9672	0.07	0.18	0.03	0.9963
DWT	1,877	3,141	9.87E+6	0.9946	2,906	4,447	1.98E+7	0.9892	355	858	7.36E+5	0.9995
GT	1,616	2,998	8.99E+6	0.9950	2,347	3,762	1.42E+7	0.9921	208	852	3.38E+5	0.9995
LDT	750	2,072	4.29E+6	0.9701	1,259	2,436	5.93E+6	0.9591	1,051	2,855	8.15E+6	0.9430
LOA	1.55	2.08	4.36	0.9993	1.63	2.24	5.00	0.9992	0.47	1.66	2.76	0.9995
LBP	1.49	1.98	3.92	0.9993	8.91	12.21	149	0.9742	0.74	2.96	8.76	0.9984
MEC	0.74	1.04	1.10	0.7062	-	-	-	-	0.12	0.39	0.15	0.9594
MEP	2,760	4,009	1.61E+7	0.9620	4,760	7,056	4.98E+7	0.8824	378	872	7.61E+5	0.9981
MER	17.8	44.7	1,995	0.9227	-	-	-	-	6.53	30.1	903	0.9649
MES	0.01	0.14	0.02	0.9609	-	-	-	-	0.01	0.10	0.01	0.9823
V	0.72	1.09	1.20	0.8989	1.16	1.70	2.87	0.7578	0.30	0.73	0.53	0.9551
TEU	2,211	332	1.10E+5	0.9931	265	456	2.08E+5	0.9872	41.0	152	2.31E+4	0.9985

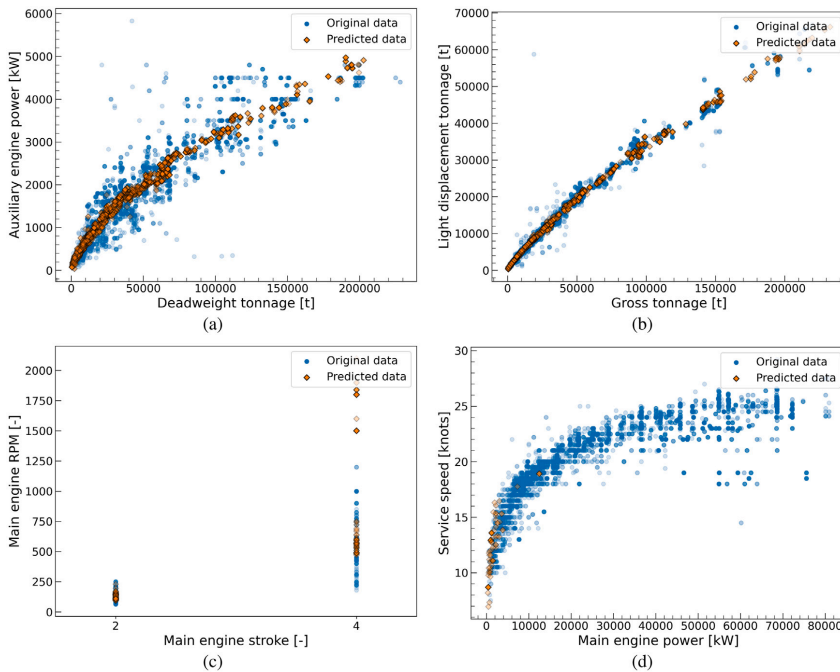


**Fig. 14.** Scatter plots of original data and predicted data: (a)Deadweight tonnage and Auxiliary engine power, (b)Gross tonnage and Light displacement tonnage, (c)Main engine stroke and Main engine RPM, (d)Main engine power and Service speed.

**Table 6**  
Dimensional constraints of Panama Canal and Suez Canal for the container ship.

Region	B [m]	L [m]	T [m]	DWT [t]	TEU
A Panama Canal	32.31	294.13	12.04	52,500	5,000
B Panama Canal (New)	51.25	366.00	15.2	120,000	13,000
C Suez Canal	50.00	400.00	20.1		
	77.50	400.00	12.2		

variables and the final model were proved to be statistically significant at level 0.05 through *f*-test and *t*-test, respectively. The prediction performance of each model was compared with several regression equations proposed in prior research, and the applicability to the canal

passage criteria is verified. Finally, the statistics of complete data were investigated to show consistency with the original data. The main findings of the research are as follows:

- Through correlation analysis and curve fitting, it was found that there are close correlations between many ship principal dimensions and related particulars. Among the fitted results of the variables, pairwise relationships of deadweight tonnage-auxiliary engine power, gross tonnage-breadth, deadweight tonnage-draught, gross tonnage-deadweight tonnage, and cargo quantity-gross tonnage, showed the highest correlations and predictive power with each other.

- As a result of verifying the performance of the model with the test data set, *adjusted R*<sup>2</sup> values of the regression equations from earlier works are in the range of 0.7578–0.9992, whilst the ones of this study are 0.8989–0.9993, which shows that there is a significant improvement in the goodness of fit by up to 15.6%. Compared to an ordinary regression model, the presented model illustrates smaller residuals with a constant trend, proving better generality and practicality for estimating ship principal data.
- Comparison of this model with a random forest model, one of the machine learning techniques that is commonly applied for missing data imputation, has been performed. Comparison of this model with a random forest model, one of the machine learning techniques that is commonly applied for missing data imputation, has been performed. The models developed in this study showed slightly lower accuracy than the random forest model but had the advantage of being interpretable, intuitive, and easily applied in other studies.
- Some clusters of ship data were formed around 32 meters in breadth, 366 meters in length, and 400 meters in length, which are the maximum allowable standards of passage through the Suez Canal and Panama Canal. The prediction shows good performance for such dimensional constraints of the ship, even if a detailed classification of data sets is not performed through the model implementation process.
- The statistics for the final values of the auxiliary engine power, light displacement tonnage, main engine RPM, and service speed, which had the most missing values, were identified. The descriptive statistics of completed data sets in this process are almost identical to those of the original data sets and predicted values are aligned with the trend of original values.

Although it is assumed that the proposed algorithm works in different data configurations, in order for this algorithm to function properly, it should be noted that the minimum number of samples is required for statistical analysis methods used in this paper. If there are not enough samples, using the regression equations of previous studies listed in Table 4 or the results of the curve fitting presented in Fig. 8 will probably provide better predictions.

Using the proposed procedure, we were able to properly replace missing values within the ship data sets. The derived regression for-

mulas not only had good predictive power, but reflected physical characteristics and dimensional limitations of ship variables. Therefore, we believe that the methodology suggested in this paper would be applicable from the estimation for the key variables of the ship to the imputation of missing values for data with similar characteristics. In addition, the same principle can be used to replace the erroneous values in the data set with plausible values.

Future research will be to examine the effectiveness of applying data sets of key variables of ships processed in such a manner to the actual marine industry, and it is expected to be able to further improve our current approach. In terms of the accuracy of the model, it is judged that there is still a possibility of improvement as seen through comparison with the random forest model. It will be necessary to further consider advanced machine learning models including the explainable artificial intelligence method from this point of view.

#### CRediT authorship contribution statement

**Youngrong Kim:** Investigation, Methodology, Software, Visualization, Writing – original draft. **Sverre Steen:** Methodology, Validation, Writing – review & editing, Supervision. **Helene Muri:** Conceptualization, Resources, Data curation, Writing – review & editing, Supervision.

#### Declaration of competing interest

The authors declare that they have no known competing financial interests or personal relationships that could have appeared to influence the work reported in this paper.

#### Acknowledgments

This document is the results of the research project “Climate change mitigation in the maritime sector (CLIMMS)”, funded by the Research Council of Norway (grant number 294771), SFI Smart Maritime (RCN grant number 237917), and Norwegian maritime industry. We would like to acknowledge contributions from Anna Ljønes Ringvold, Mario Amin Salgado Delgado and Anders Hammer Strømman on facilitating the work on the database.

Appendix A. Comparison results of the proposed algorithm and previous studies.

See Fig. A.1.

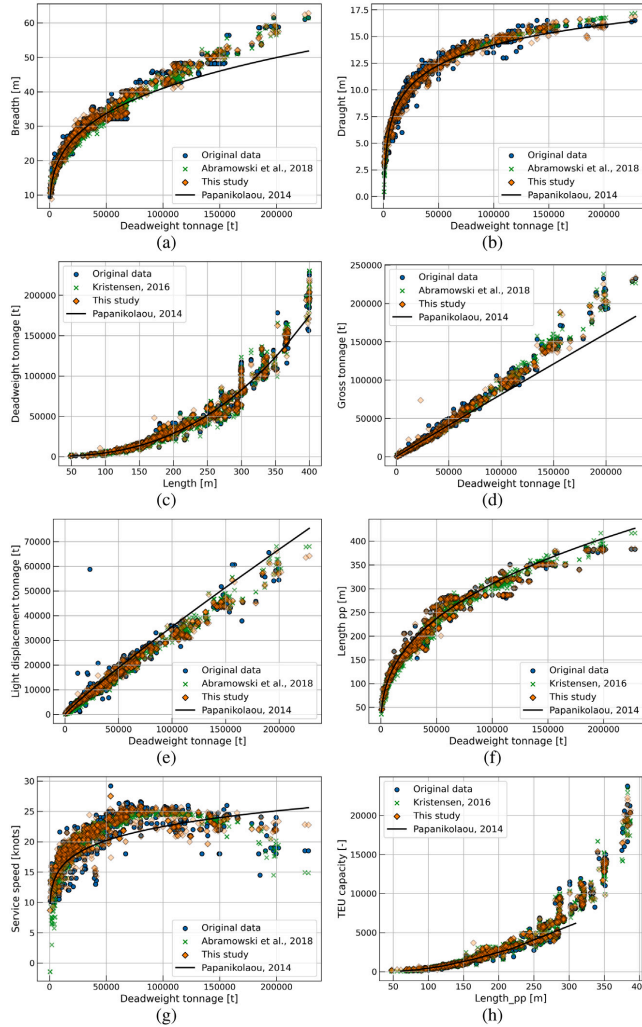


Fig. A.1. Comparison plots of the predicted values from the proposed algorithm and previous studies: (a) Breadth, (b) Draught, (c) Deadweight tonnage, (d) Gross tonnage, (e) Light displacement tonnage, (f) Length between perpendicular, (g) Service speed, (h) TEU capacity.



Appendix B. Prediction of principal data for ship types other than container ships

See Tables B.1–B.3.

**Table B.1**  
Sea-Web database used in this study to estimate the principal parameters according to ship type.

Study	Range	Build year	No. of ships
Bulk carrier	500–403,880 (DWT)	1952–2019	12,649
Oil tanker	80–441,585 (DWT)	1952–2019	9,069
Liquefied gas carrier	140–155,159 (DWT)	1961–2019	2,279
General cargo ship	20–73,296 (DWT)	1881–2019	16,551

**Table B.2**  
Comparison of prediction performance for ship principal data of bulk carrier and oil tanker.

Independent variables	Bulk carrier				Oil tanker			
	MAE	RMSE	MSE	Adj - R <sup>2</sup>	MAE	RMSE	MSE	Adj - R <sup>2</sup>
Auxiliary engine power, AEP [kW]	80.2	113	1.27E+4	0.6154	165	263	6.90E+4	0.6755
Breadth, B [m]	0.63	0.96	0.92	0.9844	0.83	1.15	1.31	0.9954
Draught, T [m]	0.17	0.29	0.08	0.9909	0.32	0.44	0.19	0.9948
Deadweight tonnage, DWT [t]	1266	2057	4.2E+6	0.9986	1301	2266	5.13E+6	0.9994
Gross tonnage, GT [t]	604	1002	1.0E+6	0.9987	814	1407	1.98E+6	0.9991
Light displacement tonnage, LDT [t]	704	1047	1.1E+6	0.9764	750	1143	1.31E+6	0.9929
Length over all, LOA [m]	1.59	2.07	4.28	0.9980	1.31	1.87	3.49	0.9996
Length between perpendiculars, LBP [m]	1.24	1.71	2.91	0.9986	1.25	1.80	3.26	0.9996
Main engine cylinder, MEC [-]	0.25	0.54	0.29	0.2375	0.64	1.15	1.33	0.1633
Main engine power, MEP [kW]	672	994	9.89E+5	0.9436	686	1075	1.15E+6	0.9832
Main engine RPM, MER [-]	10.9	18.4	339	0.9111	162	271	7.32E+4	0.6997
Main engine stroke, MES [-]	0	0.06	0	0.9766	0.07	0.36	0.13	0.8684
Service speed, V [knot]	0.31	0.46	0.22	0.3896	0.62	0.87	0.76	0.8388

**Table B.3**  
Comparison of prediction performance for ship principal data liquefied gas carrier and general cargo ship.

Independent variables	Liquefied gas carrier				General cargo ship			
	MAE	RMSE	MSE	Adj - R <sup>2</sup>	MAE	RMSE	MSE	Adj - R <sup>2</sup>
Auxiliary engine power, AEP [kW]	361	496	2.46E+5	0.8207	94.6	156	2.43E+4	0.7335
Breadth, B [m]	0.67	0.88	0.78	0.9954	0.89	1.24	1.54	0.9426
Draught, T [m]	0.31	0.42	0.17	0.9840	0.33	0.47	0.22	0.9560
Deadweight tonnage, DWT [t]	1640	2485	6.17E+6	0.9949	462	738	5.44E+5	0.9892
Gross tonnage, GT [t]	1683	2950	8.70E+6	0.9955	261	451	2.03E+5	0.9917
Light displacement tonnage, LDT [t]	647	1171	1.37E+6	0.9920	314	555	3.08E+5	0.9641
Length over all, LOA [m]	1.50	2.05	4.18	0.9994	1.25	1.78	3.18	0.9976
Length between perpendiculars, LBP [m]	1.46	1.99	3.97	0.9994	1.24	1.77	3.14	0.9973
Main engine cylinder, MEC [-]	0.64	1.03	1.06	0.6026	0.79	1.26	1.60	0.1723
Main engine power, MEP [kW]	1902	2814	7.92E+6	0.9466	341	532	2.83E+5	0.9387
Main engine RPM, MER [-]	83.3	150	2.25E+4	0.6694	202	292	8.51E+4	0.4715
Main engine stroke, MES [-]	0.07	0.37	0.14	0.8550	0.11	0.47	0.22	0.6054
Service speed, V [knot]	0.76	1.09	1.19	0.8337	0.81	1.09	1.18	0.7356

Appendix C. Estimated regression formulas for ship principal parameters

See Tables C.1–C.5

**Table C.1**  
Regression coefficients and function forms for ship principal parameters of container ship.

Type	Input													Intercept		
	AEP	B	T	DWT	GT	LDT	LOA	LBP	MEC	MEP	MER	MES	V	TEU		
AEP	Form	P														7.89E+1
	a	8.32E-1			1.76E+0	-1.57E+0	9.59E-1	-7.00E-2		-5.69E+0	5.11E-1	2.38E+6	-6.84E+2			
	b	1.77E+0			6.30E-1	5.65E-1	6.98E-1	1.62E+0		1.52E+0	6.81E-1	-2.02E+0	-1.69E+0			
B	Form		P													2.73E+0
	a		-4.79E-1		4.43E-1	1.48E+0	1.15E-1		-4.11E-1	2.56E-1	1.31E-1	6.86E+1	-9.88E+0	-1.34E-2	1.04E+0	
	b		1.16E+0		3.24E-1	3.01E-1	3.58E-1		7.99E-1	8.03E-1	3.19E-1	-5.23E-1	-7.43E-1	1.30E+0	2.98E-1	
T	Form			P												-7.34E-2
	a			-4.10E-1												
	b			7.80E-1		9.81E-1	3.76E-1	8.49E-2	2.18E-1	-4.68E-1	1.38E-1	2.04E+1	-3.39E+0	2.95E-2	-2.05E-1	
DWT	Form	P			P											6.89E+2
	a	6.20E-2			1.43E+0	-2.33E-1	-4.36E-3	1.24E-2		-1.65E+1		-7.48E+8	7.13E+3	-3.23E-2	1.10E+1	
	b	1.30E+0	2.62E+0	4.61E+0	8.83E-1	1.09E+0	2.73E+0	2.68E+0	2.16E+0		-2.91E+0	-2.63E+0	3.66E+0	8.53E-1		

(continued on next page)

**Table C.1** (continued).

Type	Input														Intercept
	AEP	B	T	DWT	GT	LDT	LOA	LBP	MEC	MEP	MER	MES	V	TEU	
GT	Form	P	P	P	P	P	P	P	P	P	P	P	P	P	-1.01E+3
	a	-6.03E-3	2.81E-1		5.20E-2		7.53E-2	1.53E-4		6.59E+0	-7.06E-3	-1.17E+0	5.26E+3		2.60E+0
	b	1.45E+0	2.91E+0		1.13E+0		1.23E+0	3.16E+0		2.36E+0	1.18E+0	-3.18E+0	-2.76E+0		9.58E-1
LDT	Form	P	P	P	P			P		P			P	P	-1.05E+2
	a	3.18E-2	5.15E-1	2.46E-2	-2.78E-1	2.17E+0		9.11E-3		5.21E-2	4.21E+7			-1.54E-2	2.86E+0
	b	1.16E+0	2.39E+0	4.04E+0	8.93E-1	8.03E-1		2.39E+0		9.72E-1	-2.69E+0			4.03E+0	7.87E-1
LOA	Form	P	P	P	P			P		P			P		1.53E-1
	a	-2.14E-2		1.33E-1	-2.49E-1	3.45E-1		1.16E+0		7.07E-2					-5.15E-3
	b	4.73E-1		1.41E+0	3.75E-1	3.45E-1		9.78E-1		4.04E-1					1.84E+0
LBP	Form	P	P	P		P	P		P	P	P	P	P		1.19E+0
	a	-2.81E-1	-2.40E-1	4.48E-1		1.32E-1	7.80E-1		4.06E+1	-5.26E+0					6.18E-3
	b	1.09E+0	1.45E+0	3.83E-1		4.29E-1	1.02E+0		-6.62E-1	-9.32E-1					1.89E+0
MEC	Form	P	P	P	P	P	P		P		P	P		P	-4.80E+0
	a	-3.74E-1	1.53E+0	-1.06E+0	-1.84E+0	1.50E+0		7.00E-1		1.53E+0	-7.54E+1	5.83E+1			-2.00E+0
	b	1.97E-1	5.00E-1	5.23E-1	1.61E-1	1.56E-1		4.53E-1		1.95E-1	-6.59E-2	-5.64E-2			1.53E-1
MEP	Form	P	P	P	P	P	P		P		P	P	P		-9.27E+3
	a	1.18E+0	1.42E+1	3.08E+0	-1.52E+1	5.40E+0	2.64E-1		3.99E+1		-1.88E+7	4.21E+4	4.53E-3		-2.81E+1
	b	9.13E-1	1.85E+0	3.12E+0	6.25E-1	7.89E-1	1.94E+0		2.20E+0		-1.61E+0	4.78E+0	6.03E-1		6.03E-1
MER	Form	P	P	P	P	P	P	P	P	P	P	P	P	P	8.80E+1
	a	1.44E+4	5.18E+2	-5.12E+3	-7.24E+3	4.72E+3	1.21E+5	-6.62E+4		-2.48E+2		1.79E+1	1.65E+4	5.93E+2	
	b	-1.89E+0	-1.26E+0	-5.58E-1	-4.79E-1	-7.95E-1	-1.69E+0	-1.65E+0		-2.53E-1		2.31E+0	-2.27E+0	-5.28E-1	
MES	Form	P	P	P	P	P	P		P	P	P		P	P	-2.15E+0
	a	-1.13E+1	-1.90E+0	1.02E+1	1.11E+1	-3.81E+0	-1.59E+1		3.12E+0	2.89E+0	3.67E-1			-3.44E+0	-3.44E+0
	b	-6.25E-1	-5.46E-1	-1.91E-1	-1.74E-1	-2.24E-1	-4.92E-1		-4.84E-2	-1.88E-1	4.02E-1			-8.10E-1	-1.70E-1
V	Form	P	P	P	P	P	P		P	P	P	P	P	G	4.21E+0
	a	-1.44E+0	3.02E+0	-5.45E+0	1.54E+0	-1.88E+0	-2.94E+0		5.59E+0	1.36E+1	-5.02E+0				2.71E+0
	b	3.91E-1	5.15E-1	1.36E-1	1.26E-1	1.50E-1	3.74E-1	3.65E-1		1.69E-1	-1.96E-1	-3.80E-1			
TEU	Form	P	P	P	P	P	P	P	P	P	P	P	P		2.40E+2
	a	-2.02E-4	1.92E-2	7.69E-5	2.89E-3	1.76E-2	1.50E-3	-6.55E-6	2.36E-5	-1.30E+0	-1.38E-3	-1.07E+8	-7.32E+2	1.01E-3	
	b	1.49E+0	3.02E+0	5.64E+0	1.17E+0	1.04E+0	1.27E+0	3.31E+0	3.25E+0	2.32E+0	1.18E+0	-3.31E+0	-2.69E+0	3.73E+0	

\* Form: Functional form of each independent variable (L: Linear, Q: Quadratic, C: Cubic, P: Power, G: Logarithmic).  
 a: Regression coefficient of each independent variable.  
 b: Exponent number of each independent variable.  
 Intercept: Intercept term of multiple regression model.

**Table C.2**  
 Regression coefficients and function forms for ship principal parameters of bulk carrier.

Type	Input														Intercept
	AEP	B	T	DWT	GT	LDT	LOA	LBP	MEC	MEP	MER	MES	V		
AEP	Form	P	P	P	P	P	P	P	P	P	P	P	P	P	-9.96E+1
	a	2.69E+1	5.93E+1	-1.29E+2	3.83E+1	2.03E+1	-1.51E+1	2.19E+1	2.54E+2	3.13E+0	1.18E+3	-2.31E+2			
	b	8.18E-1	7.77E-1	2.59E-1	2.90E-1	3.65E-1	8.45E-1	8.28E-1	-1.39E-1	4.36E-1	-5.86E-1	-7.50E-1			
B	Form	P	P	P	P	P	P	P	P	P	P	P	P	P	-1.61E+3
	a	5.41E-3	-3.06E+0	1.40E+0	1.01E+0	3.55E-2	1.46E-1	-3.17E-1	1.61E+3	1.09E-2	4.06E+1	-2.19E+0			-2.01E-3
	b	8.52E-1	9.44E-1	3.17E-1	3.51E-1	4.22E-1	1.02E+0	9.90E-1	9.91E-4	5.18E-1	-7.20E-1	-8.52E-1			2.22E+0
T	Form	P	P	P	P	P	P	P	P	P	P	P	P	P	1.09E+1
	a	1.48E-3	-3.23E-1		7.33E-1		3.60E-2	2.87E-2	-7.13E-2	-1.04E+1	7.52E-3	1.43E+1			-6.25E-1
	b	8.05E-1	9.15E-1		3.18E-1	3.46E-1	4.13E-1	1.02E+0	9.97E-1	-3.46E-2	5.16E-1	-7.46E-1			-8.77E-1
DWT	Form	P	P	P	P	P	P	P	P	P	P	P	P	P	1.96E+3
	a	-8.92E-4	4.07E-1	4.34E+0	5.39E-1	-4.29E-2	-2.51E-4	9.49E-4	-2.98E+3			-1.36E+8	-3.64E+3	2.27E-4	
	b	2.23E+0	2.66E+0	3.14E+0	1.07E+0	1.27E+0	3.23E+0	3.19E+0				-2.71E+0	-2.38E+0	5.65E+0	
GT	Form	P	P	P	P	P	P	P	P	P	P	P	P	P	-3.31E+2
	a	7.54E-1	8.54E-1		8.54E-1		1.02E-1	3.33E-4	-4.70E-4		2.93E-4	4.92E+7			-2.21E-4
	b	2.51E+0	9.29E-1		9.29E-1		1.19E+0	2.99E+0	2.95E+0		1.47E+0	2.54E+0			5.28E+0
LDT	Form	P	P	P	P	P	P	P	P	P	P	P	P	P	4.71E+3
	a	4.73E-3	-6.23E-1	1.96E+0	-3.43E+0	4.12E+0		-8.42E-3	1.66E-2	-3.15E+3	8.94E-3	-4.69E+6			-1.43E+3
	b	1.85E+0	2.11E+0	2.37E+0	7.61E-1	8.26E-1		2.45E+0	2.41E+0	1.94E-1	1.23E+0	-2.08E+0			-1.94E+0
LOA	Form	P	P	P	P	P	P	P	P	P	P	P	P	P	1.90E-2
	a	-2.54E-2	1.31E+0	2.44E+0	-2.18E+0	-3.83E-1	-2.47E-1		1.36E+0		8.15E-2	-9.85E+1	3.87E+0		-7.81E-3
	b	7.83E-1	8.87E-1	9.17E-1	3.02E-1	3.30E-1	3.97E-1		9.74E-1		4.91E-1	-7.02E-1	-8.06E-1		2.18E+0
LBP	Form	P	P	P	P	P	P	P	P	P	P	P	P	P	2.74E+0
	a	1.76E-2	-1.44E+0	-3.15E+0	2.69E+0	4.20E-1	2.53E-1	6.69E-1		-3.12E-2	1.25E+2	-6.25E+0			2.56E-3
	b	8.07E-1	9.08E-1	9.44E-1	3.10E-1	3.39E-1	4.08E-1	1.02E+0		5.03E-1	-7.38E-1	-8.44E-1			2.26E+0
MEC	Form	P	P	P	P	P	P	P	P	P	P	P	P	P	4.08E+1
	a	3.54E+0	-4.83E+1	-5.37E+1	4.73E+1	3.98E+1	1.87E+1	-5.85E+1							-6.89E+0
	b	-8.01E-2	-5.55E-2	-4.88E-2	-1.84E-2	-2.20E-2	-2.99E-2	-5.58E-2				1.34E-1			-5.44E-1
MEP	Form	P	P	P	P	P	P	P	P	P	P	P	P	P	-2.72E+2
	a	5.01E-2	4.18E+0	2.97E+1	2.32E+0	1.70E+0	3.47E-1	-2.73E-1		-1.56E+3		-1.84E+6	8.43E+3	2.34E-2	
	b	1.45E+0	1.64E+0	1.79E+0	6.27E-1	7.51E-1	1.86E+0	1.82E+0		1.99E-1		-1.33E+0	-1.73E+0	4.19E+0	
MER	Form	P	P	P	P	P	P	P	P	P	P	P	P	P	-3.32E+1
	a	1.49E+4	9.21E+3	1.07E+3	-8.08E+3	-5.09E-1	-2.72E+5	3.35E+5	2.46E-2	-1.76E+4					9.92E+7
	b	-1.25E+0	-1.65E+0	-1.28E+0			-1.56E+0	-1.52E+0		3.58E+0	-6.63E-1				-6.33E+0
MES	Form	P	P	P	P	P	P	P	P	P	P	P	P	P	1.06E+0
	a	-1.84E+0	-6.69E+0	-4.98E+0	1.30E+1	-8.08E+0	2.96E+1	-5.25E+1	-2.17E-2	1.65E+1	3.73E-1				7.41E-1
	b	-3.96E-1	-4.53E-1	-3.97E-1	-1.53E-1		-4.46E-1	-4.32E-1		-2.40E-1	3.89E-1				-2.33E+0
V	Form	P	P	P	P	P	P	P	P	P	P	P	P	P	4.71E+0
	a	-1.02E+0	-7.76E+0	-9.98E+0	1.79E+1	-3.55E+0	-2.78E+1	1.90E+1		-4.35E+0	1.28E+1	1.10E+1			5.74E+0
	b	8.33E-2	9.42E-2	9.29E-2	3.07E-2	4.07E-2	9.76E-2	9.56E-2		-7.77E-2	5.55E-2	-7.92E-2			-2.18E-1

\* Form: Functional form of each independent variable (L: Linear, Q: Quadratic, C: Cubic, P: Power, G: Logarithmic).  
 a: Regression coefficient of each independent variable.  
 b: Exponent number of each independent variable.  
 Intercept: Intercept term of multiple regression model.

**Table C.3**  
Regression coefficients and function forms for ship principal parameters of oil tanker.

Type	Input													Intercept			
	AEP	B	T	DWT	GT	LDT	LOA	LBP	MEC	MEP	MER	MES	V				
AEP	Form		P														1.60E+1
	a		1.47E+1	-3.83E+1			2.73E+1	-3.81E+0	4.35E+0		7.04E+0	4.15E+3					-4.74E-3
	b		9.59E-1	3.04E-1			3.86E-1	1.03E+0	1.01E+0		5.01E-1	-7.44E-1					3.71E+0
B	Form		P	P	P	P		P	P	P	P	P	P				2.63E+1
	a		-1.57E+0	1.54E+0	5.68E-1	7.50E-2					2.66E+1	2.66E-2	9.93E+1	-8.19E+0			-3.38E-5
	b		1.00E+0	3.21E-1	3.37E-1	4.01E-1					1.06E+0	-8.47E-2	-2.85E-2	5.14E-1	-7.90E-1	-1.70E+0	3.81E+0
T	Form		P			P	P	P			P	P	P	P			3.02E-1
	a		-2.51E-1		7.43E-1		1.06E-1	1.92E-2	-6.34E-2		1.48E-2	4.82E+1	-3.29E+0	3.37E-6			3.37E-6
	b		9.74E-1		3.16E-1		3.96E-1	1.07E+0	1.04E+0		5.10E-1	-7.69E-1	-1.71E+0	3.84E+0			3.84E+0
DWT	Form	P	P		P	P	P		G								7.56E+2
	a	-8.46E-2	4.37E-1	1.51E+1		2.57E-1	-7.81E-2	4.28E-5	1.40E-4	-1.55E+3							
	b	1.36E+0	2.99E+0	2.82E+0		1.06E+0	1.22E+0	3.49E+0	3.41E+0								
GT	Form		P	P	P		P	P		G		P	P				-1.32E+3
	a		2.60E-1	2.99E+0	4.71E-1		1.07E-1	2.41E-4	-6.35E-5		1.27E+3	-6.40E+7	1.92E+4				-4.91E+0
	b		2.80E+0	2.66E+0	9.37E-1		1.15E+0	3.27E+0	3.20E+0			-2.56E+0	-4.91E+0				
LDT	Form	P	P	P	P			P			P	P	P				-1.97E+2
	a	8.08E-2	6.87E-1	1.35E+1	-1.88E+0	1.40E+0					2.38E-3	2.52E-2	9.05E+6	-4.43E+3			-3.03E-7
	b	1.29E+0	2.37E+0	2.32E+0	7.96E-1	8.52E-1					2.72E+0	1.19E+0	-2.25E+0	-4.13E+0			7.68E+0
LOA	Form	P	P	P	P			P		P	P	P	P				-2.80E-1
	a	-4.36E-3		6.46E-1	-6.01E-1	3.78E-1			1.15E+0		4.07E-2	-3.79E+1					1.03E-4
	b	7.66E-1		9.28E-1	2.96E-1	3.09E-1			9.78E-1		4.76E-1	-7.14E-1					3.59E+0
LBP	Form	P	P	P		P	P				P	P	P				5.31E-1
	a	3.53E-3	-3.10E-1	-1.40E+0	1.26E+0		1.20E-1	7.90E-1			-2.04E-2	8.14E+1	-3.77E+0	-8.11E-5			-8.11E-5
	b	7.78E-1	9.34E-1	9.47E-1	3.02E-1		3.77E-1	1.02E+0			4.86E-1	-7.35E-1	-1.66E+0	3.66E+0			3.66E+0
MEC	Form		P				P	P			P	P	P				7.57E+1
	a		-8.59E+1								-1.46E+2	1.56E+2	-2.25E+1	1.42E+1	5.02E+0		
	b		-1.24E-2								-1.78E-2	-1.73E-2	-8.31E-3	4.43E-2	9.10E-2		
MEP	Form	P	P	P	P	P	P	P	P								2.96E+3
	a	2.77E-1	2.94E+0	2.59E+1	-3.65E+0		4.09E+0	1.25E-1	-1.28E-1	-2.78E+3			-5.13E+6				1.06E-5
	b	1.18E+0	1.82E+0	1.83E+0	6.08E-1		7.72E-1	2.12E+0	2.06E+0	9.64E-2			-1.61E+0				7.01E+0
MER	Form	P	P		P			P	P				P	P			-3.23E+2
	a	9.42E+3	-4.63E+3	2.88E+3	-8.56E+3		7.87E+4	-1.05E+0			6.76E+0	-4.34E+3		6.84E+0	1.91E+4		1.91E+4
	b	-6.57E-1	-1.06E+0	-1.14E+0	-3.27E-1						1.85E+0	-4.80E-1		2.79E+0	-2.06E+0		-2.06E+0
MES	Form		P	P	P	P	P					P	P				-1.21E+0
	a		5.24E+0	-2.97E+0	7.29E+0	1.05E+1	-2.64E+0	-2.40E+1			4.46E-1	3.89E-1		4.98E-1	3.78E+0		3.78E+0
	b		-4.03E-1	-3.73E-1	-1.23E-1	-1.22E-1	-1.43E-1	-3.63E-1						2.40E-1	-1.04E+0		-1.04E+0
V	Form	P		P	P	P		G			G	P	P				-2.35E-1
	a	-3.35E-1		6.30E+0	-1.09E+1	3.88E+0					2.96E+0	4.16E+0	5.13E+0	3.41E+0			3.41E+0
	b	2.10E-1		2.30E-1	7.17E-2	7.33E-2							-1.54E-1	-4.26E-1			-4.26E-1

\* Form: Functional form of each independent variable (L: Linear, Q: Quadratic, C: Cubic, P: Power, G: Logarithmic).  
a: Regression coefficient of each independent variable.  
b: Exponent number of each independent variable.  
Intercept: Intercept term of multiple regression model.

**Table C.4**  
Regression coefficients and function forms for ship principal parameters of liquefied gas carrier.

Type	Input													Intercept	
	AEP	B	T	DWT	GT	LDT	LOA	LBP	MEC	MEP	MER	MES	V		
AEP	Form	P	P	P	P	P	P	P	P	P	P	P	P	P	7.83E+1
	a	-7.44E-1	-4.68E-1		2.23E+0					9.73E-1	2.12E+5	-8.80E+2			
b	1.99E+0	3.05E+0	7.72E-1	6.36E-1	8.38E-1	2.00E+0	1.98E+0	1.26E+0	7.02E-1	-1.17E+0	-7.80E-1	4.23E+0			
B	Form	P	P	P	P	P	P	P	P	P	P	P	P	1.14E+0	
	a	-6.87E-2	-3.91E-1	4.93E-1	1.10E+0	1.01E-1	-6.15E-2		-1.72E-2	1.41E+1	-2.14E+0				
b	4.50E-1	1.34E+0	3.43E-1	3.10E-1	4.10E-1	9.49E-1	8.10E-1	4.08E-1	8.10E-1	-4.27E-1	-5.55E-1	2.47E+0			
T	Form	P	P	P	P	P	P	P	P	P	P	P	P	3.59E-1	
	a	-9.49E-1		1.93E+0	2.61E-1	3.71E-1	-3.89E-1		4.45E+0	4.5E+0	-8.43E-1	3.99E-3			
b	3.17E-1	6.79E-1	2.38E-1	2.11E-1	2.81E-1	6.64E-1	6.49E-1	5.27E-1	2.88E-1	-3.58E-1	-5.82E-1	1.76E+0			
DWT	Form	P	P	P	P	P	P	P	P	P	P	P	P	-3.16E+2	
	a	3.36E+0	1.07E-1		-5.84E+0				1.16E-1	1.21E+0	6.23E+5	-4.61E+3	-2.06E-3		
b	9.48E-1	2.34E+0	4.79E+0	7.49E-1	1.00E+0	2.41E+0	2.38E+0	1.55E+0	8.14E-1	-1.29E+0	-8.24E-1	4.88E+0			
GT	Form	P	P	P	P	P	P	P	P	P	P	P	P	1.76E+3	
	a	4.20E-1	4.76E-1	4.03E-3	-1.51E-2		2.69E-2	-3.90E-4	2.05E-3	1.41E-1		-6.39E+3	1.46E-4		
b	1.11E+0	3.05E+0	5.29E+0	1.24E+0		1.27E+0	3.11E+0	3.07E+0	1.75E+0	9.27E-1	-1.39E+0	-6.37E-1	5.73E+0		
LDT	Form	P	P	P	P	P	P	P	P	P	P	P	P	7.33E+2	
	a	1.23E+0	4.57E-2		2.84E+0				1.39E-2	-4.39E+1	1.38E+0		-9.71E+2	-8.93E-4	
b	9.16E-1	2.31E+0	4.17E+0	9.31E-1	7.37E-1	2.32E+0	2.29E+0	1.52E+0	8.00E-1	-1.03E+0	-7.15E-1	4.77E+0			
LOA	Form	P	P	P	P	P	P	P	P	P	P	P	P	4.73E-1	
	a	-7.16E-2			3.27E-1				1.12E+0	6.00E-2		-1.86E+0	1.94E-3		
b	4.61E-1	1.02E+0	1.39E+0	3.53E-1	3.17E-1	4.20E-1	9.76E-1	8.50E-1	4.19E-1	-4.34E-1	-5.56E-1	2.55E+0			
LBP	Form	P	P	P	P	P	P	P	P	P	P	P	P	3.80E-1	
	a	-1.90E-1	-2.39E-1	5.37E-1	2.95E-1	8.26E-2	7.51E-1			-4.20E-2	7.99E+0		-1.18E-3		
b	4.71E-1	1.04E+0	1.43E+0	3.63E-1	3.25E-1	4.30E-1	1.02E+0	8.57E-1	4.27E-1	-4.51E-1	-5.72E-1	2.59E+0			
MEC	Form	P	P	P	P	P	P	P	P	P	P	P	P	-1.56E+1	
	a	-4.80E+0			6.68E-2	1.64E-1	1.58E-1			6.54E+0	5.61E+0	2.21E+0	5.36E-1		
b	7.69E-2	1.67E-1	1.66E-1	5.00E-2	5.19E-2	6.68E-2	1.64E-1	1.58E-1	9.57E-2	1.13E-1	2.52E-1	5.87E-1			
MEP	Form	P	P	P	P	P	P	P	P	P	P	P	P	-4.91E+3	
	a	2.26E+0	-9.89E-1		9.56E-2		2.94E-1	1.30E-2	-2.25E-2	5.84E+1		-8.51E+4	1.09E+4	6.18E-4	
b	9.37E-1	2.42E+0	4.57E+0	1.04E+0	7.92E-1	1.09E+0	2.54E+0	2.49E+0	2.07E+0		-5.02E-1	-3.93E-1	5.23E+0		
MER	Form	P	P	P	P	P	P	P	P	P	P	P	P	-1.13E+2	
	a	9.01E+3	1.97E+3	-3.78E+3	-8.50E+3		1.54E+4			1.65E+1	2.22E+3		2.22E+1		
b	-3.33E-1	-8.08E-1	-9.00E-1	-2.38E-1	-2.18E-1	-2.99E-1	-7.35E-1	-7.15E-1	1.18E+0	-3.57E-1	1.18E+0	2.04E+0	-1.76E+0		
MES	Form	P	P	P	P	P	P	P	P	P	P	P	P	-1.24E+0	
	a	-1.16E+1	-2.69E+0	1.59E+1	2.61E+1	-8.53E+0	-2.93E+1			4.19E-1	-5.13E+0	3.48E-1			
b	-1.67E-1	-3.58E-1	-4.13E-1	-1.15E-1	-1.06E-1	-1.40E-1	-3.31E-1	-3.24E-1	5.27E-1	-1.44E-1	3.53E-1	-8.24E-1			
V	Form	P	P	P	P	P	P	P	P	P	P	P	P	-5.25E+0	
	a	2.96E+0	-5.64E+0	5.72E+0	-2.85E+0	7.39E+0	-7.06E+0	1.59E+0	3.97E+0	6.33E+0					
b	1.43E-1	3.02E-1	3.66E-1	9.79E-2	9.29E-2	1.22E-1	2.93E-1	2.85E-1	3.55E-1	1.38E-1	-1.12E-1	-1.89E-1			

\* Form: Functional form of each independent variable (L: Linear, Q: Quadratic, C: Cubic, P: Power, G: Logarithmic).  
a: Regression coefficient of each independent variable.  
b: Exponent number of each independent variable.  
Intercept: Intercept term of multiple regression model.

**Table C.5**  
Regression coefficients and function forms for ship principal parameters of general cargo ship.

Type		Input											Intercept		
		AEP	B	T	DWT	GT	LDT	LOA	LBP	MEC	MEP	MER	MES	V	
AEP	Form	P	P	P	P	P	P	P	P	P	P	P	P	P	-1.02E+1
	a	2.27E-1	1.18E+0	6.09E-1	3.96E-1	-6.10E-3	1.91E-2	2.46E-1	2.11E+3	8.28E-1	9.32E-1				
	b	1.94E+0	1.82E+0	6.05E-1	7.05E-1	1.96E+0	1.89E+0								
B	Form	P	P	P	P	P	P	P	P	P	P	P	P	P	-3.79E-1
	a	1.78E-1	-2.08E+0	1.54E+0	5.32E-1	3.07E-1	4.31E-1	8.33E-1	2.61E-1	1.79E+1	3.47E-1	-3.49E-1			-1.19E-2
	b	4.02E-1	7.81E-1	2.88E-1	3.07E-1	3.07E-1	3.07E-1								1.43E+0
T	Form	P	P	P	P	P	P	P	P	P	P	P	P	P	-6.37E-2
	a	1.34E-2	-1.38E-1	5.18E-1	-4.81E-2	1.33E-1	3.83E-2	-1.13E-1	4.71E-2	9.20E+0	4.05E-1	-4.26E-1			8.35E-3
	b	4.57E-1	1.04E+0	3.31E-1	3.15E-1	3.51E-1	9.40E-1	9.08E-1							1.76E+0
DWT	Form	P	P	P	P	P	P	P	P	P	P	P	P	P	7.17E+2
	a	-3.48E-1	2.11E-1	6.61E+0	6.62E-1	-2.57E-1	-1.29E-4	7.50E-4	-1.62E+3	-3.75E-2			-6.95E+2	-1.69E-2	-2.31E+0
	b	1.22E+0	3.09E+0	3.04E+0	1.04E+0	1.12E+0	3.27E+0	3.16E+0	-7.31E-1	1.17E+0			-2.32E+0	3.72E+0	
GT	Form	P	P	P	P	P	P	P	P	P	P	P	P	P	-2.01E+2
	a	9.92E-2	2.94E-2	-1.17E+0	6.15E-1	3.86E-1	4.45E-4	-7.04E-4							1.38E+3
	b	1.23E+0	2.95E+0	2.89E+0	9.45E-1	1.10E+0	3.14E+0	3.02E+0							-2.32E+0
LDT	Form	P	P	P	P	P	P	P	P	P	P	P	P	P	-4.25E+1
	a	1.34E-1	1.30E-1	2.97E+0	-6.96E-1	1.42E+0	1.02E-3	3.54E-2							-2.60E+2
	b	1.16E+0	2.65E+0	2.58E+0	8.41E-1	8.84E-1	2.69E+0	1.11E+0							-2.09E+0
LOA	Form	P	P	P	P	P	P	P	P	P	P	P	P	P	2.99E+1
	a	-5.44E-2	7.05E-1	-2.83E-1	1.72E-1	1.36E-1	1.15E+0	-3.32E+1	8.90E-2	1.10E+1					3.04E-2
	b	4.35E-1	8.31E-1	3.11E-1	3.01E-1	3.34E-1	9.75E-1	-1.28E-2	3.74E-1	-3.63E-1					1.58E+0
LBP	Form	P	P	P	P	P	P	P	P	P	P	P	P	P	-2.00E+1
	a	1.03E-1	-9.74E-2	-1.57E+0	6.94E-1	8.24E-1									-1.93E+0
	b	4.42E-1	1.03E+0	8.44E-1	3.17E-1	1.02E+0									-7.16E-1
MEC	Form	P	P	P	P	P	P	P	P	P	P	P	P	P	-1.26E+2
	a	1.07E+2	-6.24E+1	8.17E+1	8.10E-3										1.27E+0
	b	3.93E-3	4.35E-3												1.97E+1
MEP	Form	P	P	P	P	P	P	P	P	P	P	P	P	P	1.28E+3
	a	2.70E+0	1.16E+0	1.56E+1	-1.98E+0	-9.56E-1	1.99E+0	7.76E-2	-1.14E-1	-1.87E+3			-3.26E+4	4.03E-2	3.86E+0
	b	1.01E+0	2.15E+0	2.07E+0	6.75E-1	7.06E-1	7.99E-1	2.22E+0	2.13E+0	-6.44E-2			-1.08E+0		
MER	Form	P	P	P	P	P	P	P	P	P	P	P	P	P	-3.45E+2
	a	1.06E+3	1.70E+3	-3.86E+3	-4.34E+3	2.15E+3	1.82E+4	-5.04E+3	5.51E+1	-1.24E+3					3.97E+1
	b	-2.96E-1	-6.40E-1	-1.74E-1	-1.46E-1	-1.75E-1	-5.77E-1	-5.52E-1	1.12E+0	-2.55E-1					1.60E+0
MES	Form	P	P	P	P	P	P	P	P	P	P	P	P	P	-2.09E+0
	a	2.73E+0		8.46E+0		-1.23E+1		3.98E-1		1.46E+0					
	b	-2.82E-1		-7.29E-2		-2.04E-1		2.28E-1							
V	Form	P	P	P	P	P	P	P	P	P	P	P	P	P	-8.94E+0
	a	-6.29E-1	3.86E+0	-5.14E+0	-1.38E+0	1.34E+0	3.44E+0	-2.44E+0	8.64E+0	3.88E+0					3.24E+0
	b	3.64E-1	3.27E-1	1.06E-1	1.00E-1	1.16E-1	1.16E-1	3.17E-1	3.05E-1	2.84E-2	1.58E-1	-1.46E-1			

\* Form: Functional form of each independent variable (L: Linear, Q: Quadratic, C: Cubic, P: Power, G: Logarithmic).  
a: Regression coefficient of each independent variable.  
b: Exponent number of each independent variable.  
Intercept: Intercept term of multiple regression model.

## References

- Abramowski, T., 2013. Application of artificial intelligence methods to preliminary design of ships and ship performance optimization. *Nav. Eng. J.* 125 (3), 101–112.
- Abramowski, T., Cepowski, T., Zvolenský, P., 2018. Determination of regression formulas for key design characteristics of container ships at preliminary design stage. *New Trends Prod. Eng.* 1 (1), 247–257.
- Afrifa-Yamoah, E., Mueller, U.A., Taylor, S., Fisher, A., 2020. Missing data imputation of high-resolution temporal climate time series data. *Meteorol. Appl.* 27 (1), e1873.
- Anderson, D., Burnham, K., 2004. *Model Selection and Multi-model Inference*, Vol. 63, Second ed. (2020). Springer-Verlag, NY, p. 10.
- Andiojaya, A., Demirhan, H., 2019. A bagging algorithm for the imputation of missing values in time series. *Expert Syst. Appl.* 129, 10–26.
- Bisong, E., 2019. More supervised machine learning techniques with scikit-learn. In: *Building Machine Learning and Deep Learning Models on Google Cloud Platform*. Springer, pp. 287–308.
- Breiman, L., 2001. Random forests. *Mach. Learn.* 45 (1), 5–32.
- B&W, M., 2019. *Propulsion trends in container vessels*. URL [www.man-es.com](http://www.man-es.com).
- Cepowski, T., 2019. Regression formulas for the estimation of engine total power for tankers, container ships and bulk carriers on the basis of cargo capacity and design speed. *Pol. Marit. Res.*
- Charchalis, A., 2013. Dimensional constraints in ship design. *J. KONES* 20.
- Charchalis, A., 2014. Determination of main dimensions and estimation of propulsion power of a ship. *J. KONES* 21.
- Charchalis, A., Krefit, J., 2009. Main dimensions selection methodology of the container vessels in the preliminary stage. *J. KONES* 16, 71–78.
- Cheliotis, M., Gkerekos, C., Lazakis, I., Theotokatos, G., 2019. A novel data condition and performance hybrid imputation method for energy efficient operations of marine systems. *Ocean Eng.* 188, 106220.
- Congress, G.C., 2016. New morsk triple-e ships world's largest and most efficient; waste heat recovery and ultra long stroke engines contribute to up to 50% reduction in CO<sub>2</sub>/container moved.
- Dobrkovic, A., Jacob, M.-E., van Hillegersberg, J., 2018. Maritime pattern extraction and route reconstruction from incomplete AIS data. *Int. J. Data Sci. Anal.* 5 (2–3), 111–136.
- Garrido, J., Saurf, S., Marrero, A., Gül, U., Rúa, C., 2020. Predicting the future capacity and dimensions of container ships. *Transp. Res. Rec.* 0361198120927395.
- Garson, G.D., 2015. *Missing values analysis and data imputation*. Statistical Associates Publishers, Asheboro, NC.
- Gertler, M., 1954. A reanalysis of the original test data for the Taylor Standard Series. Technical Report, DAVID TAYLOR MODEL BASIN WASHINGTON DC.
- Gkerekos, C., Lazakis, I., 2020. A novel, data-driven heuristic framework for vessel weather routing. *Ocean Eng.* 197, 106887.
- Graff, W., 1964. Some extensions of DW Taylor's standard series. In: *Versuchsanstalt FÜR Binnenschiffbau, Duisburg, Germany, Technische Hochschule Aachen, Forschungsberichte Des Landes Nordrhein Westfalen, Presented At: The Annual Meeting of the Society of Naval Architects and Marine Engineers, SNAME Transactions 1964, New York, USA, Paper: T1964-1 Proceedings*.
- Gurgen, S., Allin, I., Ozkok, M., 2018. Prediction of main particulars of a chemical tanker at preliminary ship design using artificial neural network. *Ships Offshore Struct.* 13 (5), 459–465.
- Gutierrez-Torre, A., Berral, J.L., Buchaca, D., Guevara, M., Soret, A., Carrera, D., 2020. Improving maritime traffic emission estimations on missing data with CRBMs. *Eng. Appl. Artif. Intell.* 94, 103793.
- Hair, J., Babin, B., Anderson, R., Black, W., 2018. *Multivariate data analysis* (8. bs.). Cengage Learning, Harlow.
- Heckmann, T., Gegg, K., Gegg, A., Becht, M., 2014. Sample size matters: investigating the effect of sample size on a logistic regression susceptibility model for debris flows. *Nat. Hazards Earth Syst. Sci.* 14 (2), 259.
- IHS, 2019. *Sea-web ships*. URL <https://maritime.ihs.com>.
- Imtiazi, S., Shah, S., 2008. Treatment of missing values in process data analysis. *Can. J. Chem. Eng.* 86 (5), 838–858.
- James, G., Witten, D., Hastie, T., Tibshirani, R., 2013. *Tree-based methods*. In: *An Introduction to Statistical Learning*. Springer, pp. 303–335.
- Jung, S., Moon, J., Park, S., Rho, S., Baik, S.W., Hwang, E., 2020. Bagging ensemble of multilayer perceptrons for missing electricity consumption data imputation. *Sensors* 20 (6), 1772.
- Khatibisepehr, S., Huang, B., Khare, S., 2013. Design of inferential sensors in the process industry: A review of Bayesian methods. *J. Process Control* 23 (10), 1575–1596.
- Kim, M., Park, S., Lee, J., Joo, Y., Choi, J.K., 2017. Learning-based adaptive imputation method with kNN algorithm for missing power data. *Energies* 10 (10), 1668.
- Konishi, S., Kitagawa, G., 2008. *Information Criteria and Statistical Modeling*. Springer Science & Business Media.
- Kramer, O., 2016. *Scikit-learn*. In: *Machine Learning for Evolution Strategies*. Springer, pp. 45–53.
- Kristensen, H.O., 2012. Determination of regression formulas for main dimensions of tankers and bulk carriers based on IHS fairplay data. *Clean Shipp. Curr.* 1 (6).
- Kristensen, H.O., 2013. Statistical analysis and determination of regression formulas for main dimensions of container ships based on IHS fairplay data. In: *Statistical Analysis and Determination of Regression Formulas for Main Dimensions of Container Ships Based on IHS Fairplay Data*. University of Southern Denmark, Denmark.
- Kristensen, H.O., 2016. Revision of statistical analysis and determination of regression formulas for main dimensions of container ships based on data from clarkson. Technical Report, Technical University of Denmark & HOK Marineconsult ApS.
- Lazakis, I., Gkerekos, C., Theotokatos, G., 2019. Investigating an SVM-driven, one-class approach to estimating ship systems condition. *Ships Offshore Struct.* 14 (5), 432–441.
- Lin, W.-C., Tsai, C.-F., 2020. Missing value imputation: a review and analysis of the literature (2006–2017). *Artif. Intell. Rev.* 53 (2), 1487–1509.
- Little, R.J., 1988. A test of missing completely at random for multivariate data with missing values. *J. Amer. Statist. Assoc.* 83 (404), 1198–1202.
- Little, R.J., Rubin, D.B., 2019. *Statistical Analysis with Missing Data*, Vol. 793. John Wiley and Sons.
- Liu, C., Chen, X., 2013. Inference of single vessel behaviour with incomplete satellite-based AIS data. *J. Navig.* 66 (6), 813.
- Lloyd's list intelligence, 2017. *Understanding AIS (automatic identification system)*. URL <https://maritimeintelligence.informa.com/>.
- Mao, S., Tu, E., Zhang, G., Rachmawati, L., Rajabally, E., Huang, G.-B., 2018. An automatic identification system (AIS) database for maritime trajectory prediction and data mining. In: *Proceedings of ELM-2016*. Springer, pp. 241–257.
- Mark, J., Goldberg, M.A., 2001. Multiple regression analysis and mass assessment: A review of the issues. *Apprais. J.* 56 (1), 89–109.
- Meyer, J., Stahlbock, R., Voß, S., 2012. Slow steaming in container shipping. In: *2012 45th Hawaii International Conference on System Sciences*. IEEE, pp. 1306–1314.
- Montgomery, D.C., Runger, G.C., 2014. *Applied Statistics and Probability for Engineers*. Wiley.
- Niknafs, A., Berry, D., 2017. The impact of domain knowledge on the effectiveness of requirements engineering activities. *Empir. Softw. Eng.* 22 (1), 80–133.
- Oshiro, T.M., Perez, P.S., Baranauskas, J.A., 2012. How many trees in a random forest? In: *International Workshop on Machine Learning and Data Mining in Pattern Recognition*. Springer, pp. 154–168.
- Papanikolaou, A., 2014. *Ship Design: Methodologies of Preliminary Design*. Springer.
- Park, N.K., Suh, S.C., 2019. Tendency toward mega containerhips and the constraints of container terminals. *J. Mar. Sci. Eng.* 7 (5), 131.
- Piko, G., 1980. *Regression Analysis of Ship Characteristics*. Australian Government Publishing Service.
- Pituch, K.A., Stevens, J.P., 2015. *Applied Multivariate Statistics for the Social Sciences: Analyses with SAS and IBM's SPSS*. Routledge.
- Radfar, S., Taherkhani, A., Panahi, R., 2017. Standardization of the main dimensions of design container ships in ports—A case study. *World J. Eng. Technol.* 5 (4), 51–61.
- Rubin, D.B., 1976. Inference and missing data. *Biometrika* 63 (3), 581–592.
- Rudin, C., Wagstaff, K.L., 2014. *Machine Learning for Science and Society*. Springer.
- Seabold, S., Perktold, J., 2010. *Statsmodels: Econometric and statistical modeling with python*. In: *Proceedings of the 9th Python in Science Conference*, Vol. 57. Austin, TX, p. 61.
- Takahashi, H., Goto, A., Abe, M., Kannami, Y., Esaki, T., Mizukami, J., 2006. Study on ship dimensions by statistical analysis: Standard of main dimensions of design ship (Draft). National Inst. for Land and Infrastructure Management, Ministry of Land ...
- Tsitilonis, K.-M., Theotokatos, G., 2018. A novel systematic methodology for ship propulsion engines energy management. *J. Cleaner Prod.* 204, 212–236.
- Tuck, E.O., 1987. Wave resistance of thin ships and catamarans. *Appl. Math. Rep.* T8701.
- Velasco-Gallego, C., Lazakis, I., 2020. Real-time data-driven missing data imputation for short-term sensor data of marine systems. A comparative study. *Ocean Eng.* 218, 108261.
- Velasco-Gallego, C., Lazakis, I., 2021. A novel framework for imputing large gaps of missing values from time series sensor data of marine machinery systems. *Ships Offshore Struct.* 1–10.
- Virtanen, P., Gommers, R., Oliphant, T.E., Haberland, M., Reddy, T., Cournapeau, D., Burovski, E., Peterson, P., Weckesser, W., Bright, J., van der Walt, S.J., Brett, M., Wilson, J., Millman, K.J., Mayorov, N., Nelson, A.R.J., Jones, E., Kern, R., Larson, E., Carey, C.J., Polat, I., Feng, Y., Moore, E.W., VanderPlas, J., Laxalde, D., Perktold, J., Cimrman, R., Henriksen, I., Quintero, E.A., Harris, C.R., Archibald, A.M., Ribeiro, A.H., Pedregosa, F., van Mulbregt, P., SciPy 1.0 Contributors, 2020. *SciPy 1.0: Fundamental algorithms for scientific computing in python*. *Nature Methods* 17, 261–272. <http://dx.doi.org/10.1038/s41592-019-0686-2>.
- Wang, M.-C., Tsai, C.-F., Lin, W.-C., 2021. Towards missing electric power data imputation for energy management systems. *Expert Syst. Appl.* 174, 114743.
- Wang, H., Zhuge, X., Strazdins, G., Wei, Z., Li, G., Zhang, H., 2016. Data integration and visualisation for demanding marine operations. In: *OCEANS 2016-Shanghai*. IEEE, pp. 1–7.
- Warner, R.M., 2020. *Applied Statistics II: Multivariable and Multivariate Techniques*. SAGE Publications, Incorporated.
- Wiesmann, A., 2010. Slow steaming—a viable long-term option? *Wartsila Tech. J.* 2, 49–55.



# Article 2

## A meta model for added resistance in waves

Youngrong Kim, Ehsan Esmailian, Sverre Steen

*Ocean Engineering* 251 (2022) 112749  
DOI: [10.1016/j.oceaneng.2022.112749](https://doi.org/10.1016/j.oceaneng.2022.112749)







## A meta-model for added resistance in waves

Young-Rong Kim<sup>\*</sup>, Ehsan Esmailian, Sverre Steen

Department of Marine Technology, Norwegian University of Science and Technology (NTNU), Trondheim, 7052, Norway

### ARTICLE INFO

#### Keywords:

Semi-empirical method  
Added wave resistance  
Propulsion power  
Arbitrary wave heading

### ABSTRACT

In this paper, we perform a comprehensive study of various semi-empirical methods using publicly accessible experimental data on added resistance in waves with different ship types and conditions. Based on the analysis results, a new method (So-called “Combined method”) is proposed, combining two existing methods, which are available in arbitrary wave headings. The results from the two methods are combined smoothly using a tangent hyperbolic function according to wavelengths and wave headings. The coefficients constituting the function are tuned to minimize mean squared error between predictions and model experiments. Finally, the new Combined method is verified by full-scale measurements of a general cargo ship and a container ship, and it seems to give good agreement with measurements in all analysis areas, compared to existing semi-empirical methods. Especially, it showed better performance in estimating added wave resistance at high waves, resonance frequencies, arbitrary waves, and low speeds.

### 1. Introduction

An operating ship experiences additional resistance due to the surrounding weather conditions, resulting in speed reduction and increased fuel consumption, which can be directly related to greenhouse gas emissions. Traditionally, this fact has been of great interest to ship designers and operators from the perspective of speed/power performance. Moreover, with the increasing interest in atmospheric environmental issues recently, IMO has set the EEDI to limit greenhouse gas emissions. In this regard, it is even more necessary to estimate the added resistance of a ship in an accurate and efficient way for the initial design and the management of operations of a ship.

Many theoretical methods have been developed for calculating the added resistance of ships. Havelock (1942) proposed a method of calculating added resistance by integrating longitudinal pressure on the wetted surface of a ship, and Boese (1970) developed a near-field direct pressure integration method using strip theory. Maruo (1957) first introduced the far-field method based on momentum conservation, and it was expanded in later studies (Joosen, 1966; Maruo, 1960, 1963). Radiated energy approach based on Maruo’s far-field method was introduced by Gerritsma and Beukelman (1972), and Salvesen (1978) achieved satisfactory results by applying it to the motion of the ship obtained from the strip theory. Faltinsen (1980) presented an asymptotic formula, assuming the added resistance of wall-sided hull forms in short waves.

Panel methods based on potential theory for computing added wave resistance has been extensively studied by many authors (Joncquez,

2009; Kim and Kim, 2011; Seo et al., 2013; Söding et al., 2014; Lee et al., 2021). However, since most approaches were limited to linear theory, it was generally difficult to accurately calculate the non-linear effect. There were also non-linear panel methods, but they had problems with stability and robustness, and long computational time. Meanwhile, along with the improvement of computational power, Computational Fluid Dynamics (CFD) method based on Reynolds-Averaged Navier–Stokes (RANS) has been widely applied (Orihara and Miyata, 2003; Guo et al., 2012; Sadat-Hosseini et al., 2013; Simonsen et al., 2014; Sigmund and El Moctar, 2018; Lee et al., 2021; T. Kim et al., 2021). It had the advantage of being able to consider nonlinear effects and showed good results overall. However, the output results from the 3D panel method and the RANS equations solver vary depending on the calculation grid and large computational time is required, which leads to a struggle in terms of practicability (Shigunov et al., 2018). Another problem is that they require detailed hull shapes to predict added resistance, which in some cases could serve as an important constraint.

Alternatively, simplified methods based on theory and experimental results have been developed, which could easily estimate added resistance with only a few ship parameters compared to the methods covered earlier. The semi-empirical formula for the added resistance due to wave reflection was first proposed by Fujii (1975), and later further tuned based on more experimental data by Takahashi (1988) and Tsujimoto et al. (2008). In parallel with these studies, for the ship motion-induced added resistance, Jinkine and Ferdinande (1974)

<sup>\*</sup> Corresponding author.

E-mail address: [youngrong.kim@ntnu.no](mailto:youngrong.kim@ntnu.no) (Y. Kim).

<https://doi.org/10.1016/j.oceaneng.2022.112749>

Received 27 October 2021; Received in revised form 24 September 2022; Accepted 26 September 2022

0029-8018/© 2022 The Author(s). Published by Elsevier Ltd. This is an open access article under the CC BY license (<http://creativecommons.org/licenses/by/4.0/>).

Nomenclature	
<b>Abbreviations</b>	
CFD	Computational Fluid Dynamics
COG	Course Over Ground
ECMWF	European Centre for Medium-Range Weather Forecasts
EEDI	Energy Efficiency Design Index
GPS	Global Positioning System
IMO	International Maritime Organization
ITTC	International Towing Tank Conference
M/E	Main engine
MAE	Mean Absolute Error
MSE	Mean Squared Error
RANS	Reynolds-Averaged Navier–Stokes
RMSE	Root Mean Squared Error
STA-JIP	Sea Trial Analysis Joint Industry Project
<b>Nomenclature</b>	
$\alpha$	Wave heading. The wave angle relative to the ship's heading (180 degrees: head waves)
$\Delta C_F$	Roughness allowance
$\eta_T$	Overall efficiency
$\Gamma$	Gamma function
$\hat{C}_{aw}$	Estimated non-dimensional added wave resistance coefficient
$\lambda$	Wave length
$\omega$	Circular wave frequency
$\rho$	Water density
$\theta$	Primary wave direction
$\zeta_a$	Wave amplitude
$a$	Slope adjustment Coefficient of a tangent hyperbolic function (Wave frequency)
$a_2$	Speed correction factor used in wave motion-induced added resistance
$B$	Breadth
$b$	Center position adjustment Coefficient of a tangent hyperbolic function (Wave frequency)
$c$	Slope adjustment Coefficient of a tangent hyperbolic function (Wave heading)
$C_B$	Block coefficient
$C_{aw}$	Non-dimensional added wave resistance coefficient
$C_{H_s}$	Wave height correction factor
$C_{T,Data}$	Total resistance coefficient in calm condition obtained from in-service data
$C_{T,Emp}$	Total resistance coefficient in calm condition estimated from empirical methods
$C_T$	Total resistance coefficient
$d$	Center position adjustment Coefficient of a tangent hyperbolic function (Wave heading)
$E$	Directional wave spectrum

$F_n$	Froude's number
$G$	Angular distribution function
$g$	Gravity acceleration
$H_s$	Significant wave height
$k_{yy}$	Pitch gyration
$L$	Length between perpendiculars
$L_E$	Length of entrance
$L_R$	Length of run
$P_B$	Engine brake power
$P_{EST}$	Ship propulsion power estimated from the empirical method
$P_{MEAS}$	Ship propulsion power measured on-board
$R$	Pearson's correlation coefficient
$R_{aw}$	Added resistance in regular waves
$R_{beam}$	Added wave resistance in beam waves
$R_{calm}$	Calm water resistance
$R_{following}$	Added wave resistance in following waves
$R_{head}$	Added wave resistance in head waves
$R_{total}$	Total resistance
$R_{wave}$	Mean wave resistance increase in irregular waves
$R_{wind}$	Added resistance due to wind
$S$	Standard wave frequency spectrum
$S_w$	Wetted surface area
$T$	Mean draft
$T_m$	Mean wave period
$V$	Ship's speed
$V_d$	Ship's design speed

developed a formula that simplifies the resistance in long waves based on the experimental data of fast cargo ships. Two simple methods have been developed by STA-JIP to correct the added resistance in

waves for sea trial conditions (Boom et al., 2013). The STAWAVE-1 method assumes that the wave reflection contribution dominates the added resistance. From this approach, a practical equation that simplifies the reflection-induced added resistance in irregular waves by approximating the waterline geometry on the bow section and the beam of the ship was presented. Contrary to this, STAWAVE-2 method considers both reflection and radiation contribution in estimating the transfer function for the added wave resistance. Liu and Papanikolaou (2016) originally proposed a statistical method of combining Faltinsen (1980) and Jinkine and Ferdinande (1974). In subsequent studies (Liu and Papanikolaou, 2019, 2020), they introduced wave heading-based trigonometric functions to their previous equation and expanded it to enable calculation for small draft, ballast conditions, and arbitrary waves by regression analysis based on extensive experimental data. Lang and Mao (2020) proposed an added wave resistance model for head seas based on Tsujimoto et al. (2008) and Jinkine and Ferdinande (1974). It was influenced by the formulas presented in Liu and Papanikolaou's paper (Liu and Papanikolaou, 2016; IMO, 2016), and some of its calculations were modified using their experimental datasets. The proposed method was further updated to allow the calculation of the peak position in arbitrary waves by introducing an encountered frequency correction factor (Lang and Mao, 2021). There are also some simple equations that can directly calculate the added resistance in irregular waves such as Kreitner's method (Kreitner, 1939; ITTC, 2005) and Shopera (Papanikolaou et al., 2015). Most simplified methods have been developed to estimate the resistance of a ship operating in head seas. Although studies for added resistance in arbitrary wave headings have been continuously conducted in recent years, comparative analysis and insight into these methods are still insufficient.

To this regard, we perform a comprehensive study of various semi-empirical methods using publicly accessible experimental data on

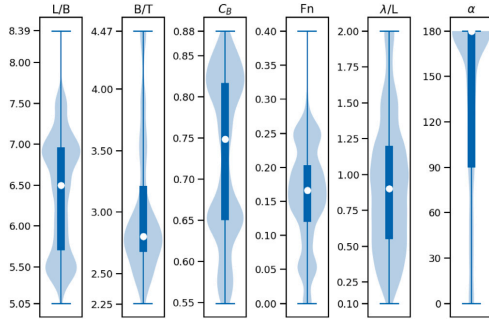


Fig. 1. The composition of the experimental database according to various ship parameters.

added resistance in waves with different ship types and conditions, which is presented in Section 2. Thereafter, in Section 3, a new method is proposed combining two methods available in arbitrary wave headings from the studies of Lang and Mao (2021) and Liu and Papanikolaou (2020), which has been elaborately verified in previous research. The results from these two methods are smoothly connected to wave conditions and wave heading through a combining function. This method is developed for the calculation of added resistance for large fleets of ships, so that robustness, computational efficiency, and applicability to a range of different ship types are priorities. The coefficients of this function are tuned using extensive model test data, and their values are presented according to the ship type. Section 4 verifies the performance of the corresponding method using full-scale measurements of two different ships. Conclusions of the study are addressed in Section 5.

## 2. Comparison of semi-empirical methods with experimental data

### 2.1. Description of the experimental data

The results of various publicly accessible experimental data were obtained to consider the general applicability of added resistance in waves to the fleet level, and the performances of the existing semi-empirical models were compared and analyzed. Fig. 1 shows the distribution of main dimensionless parameters of the ships and experimental conditions used in the study. The whisker in the figure indicates the maximum and the minimum range. The box plot shows 25% and 75% quantiles and the circular marker in it represents the median. The data set consists of a total of 2559 samples of approximately 49 ships and 255 different experimental cases. Most of the experiments were conducted at design loading conditions, without trim. More detailed information on the data set is shown in Tables A.1–A.6 in Appendix A.

### 2.2. Parameter estimation for $L_E$ and $L_R$

Liu and Papanikolaou (2016) introduced the length of entrance ( $L_E$ ) parameter in Falinsen's asymptotic approach to reflect the hull form influence on the component of added resistance due to diffraction effect. Thereafter, corresponding parameters were used in Liu and Papanikolaou (2019, 2020), and Lang and Mao (2020, 2021).  $L_E$  is defined as the horizontal distance from the point where the length of the waterline surface reaches 99% of the breadth to Forepeak (Conversely, Length of run ( $L_R$ ) is the horizontal distance from the point where the length of the waterline surface reaches 99% of the breadth to the endpoint of the waterline), as shown in Fig. 2. These are necessary factors for calculating the entrance angle used in the wave reflection

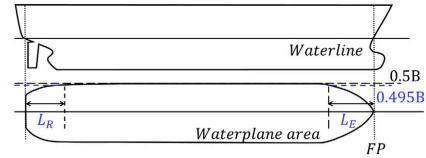


Fig. 2. Definition of length of entrance and run.

contribution to the added resistance. However,  $L_E$  and  $L_R$  cannot be accurately estimated without detailed hull shape information of the ship. Some authors (Liu et al., 2016; Lang and Mao, 2020, 2021) also listed such values of several ships in their papers.

Fig. 3 shows  $L_E$  and  $L_R$  according to the length ( $L_{pp}$ ) of the ships under the design loading conditions we have secured. Overall,  $L_E$  and  $L_R$  increase in proportion to  $L_{pp}$ .  $L_E$  decreases as block coefficient ( $C_B$ ) increases, but in the case of  $L_R$ , the trend according to the  $C_B$  is not clear. In Fig. 4, dimensionless  $L_E$  ( $L_E/L_{pp}$ ) and dimensionless  $L_R$  ( $L_R/L_{pp}$ ) are plotted as a functions of Block coefficient ( $C_B$ ), and a linear regression line for each ship type is also plotted. As  $C_B$  increases, the dimensionless  $L_E$  decreases, and there was a slight difference in the slope and intercept values of the regression line depending on the ship type. On the other hand, the dimensionless  $L_R$  according to  $C_B$  shows a clear difference in trend according to ship type. The dimensionless  $L_R$  values of the tanker, liquefied gas carrier, bulk carrier, and general cargo ship, with relatively high values of  $C_B$ , tend to decrease as  $C_B$  increases, whereas for relatively slender hull types such as ro-ro/ferry and container ship dimensionless  $L_R$  values rather increase. This interpretation is roughly in accordance with what could be expected from knowledge of ship design principles.

Tables 1–2 show the regression equations of dimensionless  $L_E$  and  $L_R$  for each ship type estimated from Fig. 4. If the detailed hull shape or the  $L_E$  and  $L_R$  values of the ship were obtainable from the public source, they were used. Otherwise,  $L_E$  and  $L_R$  values were estimated using the proposed regression equations. It is important to note that one should be careful using regression equations as an alternative to estimating  $L_E$  and  $L_R$  of the ship, in case the input parameters are outside the range listed in Tables 1–2 or if the ship has a specific hull shape such as a bulbous bow or transom stern. In such cases, there may be gaps between the actual value and the estimated value.

### 2.3. Comparison of semi-empirical methods in regular waves

In this section, a comparative analysis of several semi-empirical methods for added resistance in regular waves is presented, where the methods from Boom et al. (2013), Lang and Mao (2021), and Liu and Papanikolaou (2020) are denoted as “STA2”, “CTH”, and “L&P”, respectively. STA2 is also compared as a representation of the method that uses only simple ship dimensions although it is applicable only to head waves. Practically, the greater added wave resistance experienced by ships is of main interest. However, when evaluating the degree of error of the model as a residual, the greater the added resistance of the ship, the greater the residual between the predicted value and the experimental value. Therefore, mean squared error ( $MSE$ ) as defined in Eq. (1), which can give more weight to a larger error by squaring the residual, is used as an evaluation metric. Here, the measurements from model experiments and estimations for the added wave resistance coefficient are compared. As can be found from the figures in the appendices (Fig. B2(a), Fig. B3(c)), there are differences among experimental results for the same ship in the same wave condition, which may be due to the experiment being carried out in different water tank environments. However, the influence of some experimental samples with relative deviations was mitigated by using as many samples as possible.

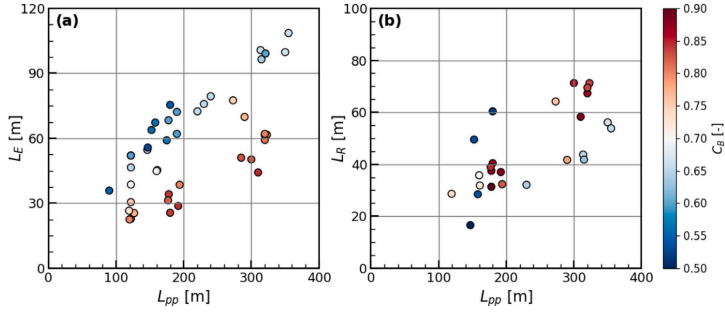


Fig. 3. Scatter plots of (a) length of entrance and (b) length of run against ship length with the color bar showing the block coefficient. (For interpretation of the references to color in this figure legend, the reader is referred to the web version of this article.)

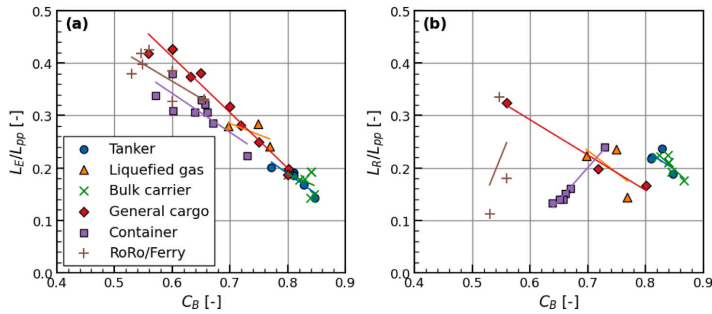


Fig. 4. Scatter plots of dimensionless (a) length of entrance and (b) length of run against block coefficient according to the ship type.

**Table 1**  
Regression equations for the dimensionless  $L_E$  according to the ship type.  $x$  and  $y$  in equation represent  $C_B$  and  $L_E/L_{pp}$ .

Ship type	Range ( $C_B$ )	Linear regression equation ( $y = ax + b$ )	Correlation coefficient ( $r$ )
Tanker	0.772–0.847	$y = -0.7833x + 0.8158$	-0.918
Liquefied gas	0.6973–0.7688	$y = -0.4258x + 0.5828$	-0.658
Bulk carrier	0.8–0.8455	$y = -0.4904x + 0.5814$	-0.384
General cargo	0.559–0.801	$y = -1.061x + 1.049$	-0.983
Container	0.572–0.7296	$y = -0.7414x + 0.787$	-0.814
Ro-Ro/Ferry	0.53–0.656	$y = -0.655x + 0.7583$	-0.787

**Table 2**  
Regression equations for the dimensionless  $L_R$  according to the ship type.  $x$  and  $y$  in equation represent  $C_B$  and  $L_R/L_{pp}$ .

Ship type	Range ( $C_B$ )	Linear regression equation ( $y = ax + b$ )	Correlation coefficient ( $r$ )
Tanker	0.81–0.847	$y = -0.6875x + 0.7821$	-0.587
Liquefied gas	0.6973–0.7688	$y = -0.8447x + 0.8244$	-0.627
Bulk carrier	0.82–0.8665	$y = -1.04x + 1.081$	-0.855
General cargo	0.559–0.801	$y = -0.6722x + 0.6952$	-0.988
Container	0.6393–0.7296	$y = 1.247x - 0.6726$	0.991
Ro-Ro/Ferry	0.53–0.5595	$y = 2.731x - 1.28$	0.353

The mean resistance increase of a ship in waves is influenced by many factors related to hull shape, ship operating conditions, wave characteristics, etc. In relation to the nondimensional transfer function of mean resistance increase in regular waves, it is mainly dependent on wave frequency, wave direction, and ship speed, as shown in Eq. (17). Therefore, as shown in Figs. 5–6, the errors of each method were analyzed by classifying them into Froude number ( $F_n$ ), wavelengths

( $\lambda/L$ ), and ship types according to the wave heading ( $\alpha$ ). For the convenience of analysis, the entire wave heading area in this study is classified into three groups: head seas (180–135 degrees), beam seas (135–45 degrees), and following seas (45–0 degrees). For the detailed formula and application of each method, refer to the original documents (Boom et al., 2013; Lang and Mao, 2020, 2021; Liu and

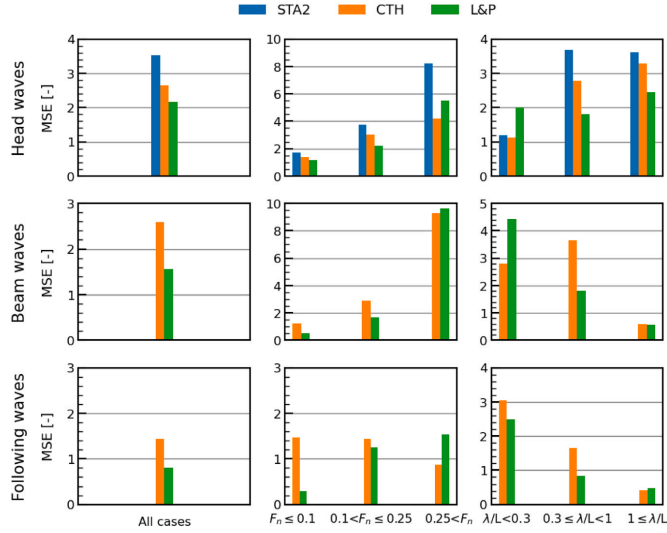


Fig. 5. Comparison of *MSE* results for added wave resistance methods for all ship types, Froude numbers, and wavelengths. The bar graph in the upper row shows head waves, the middle represents beam waves, and the lower is following waves.

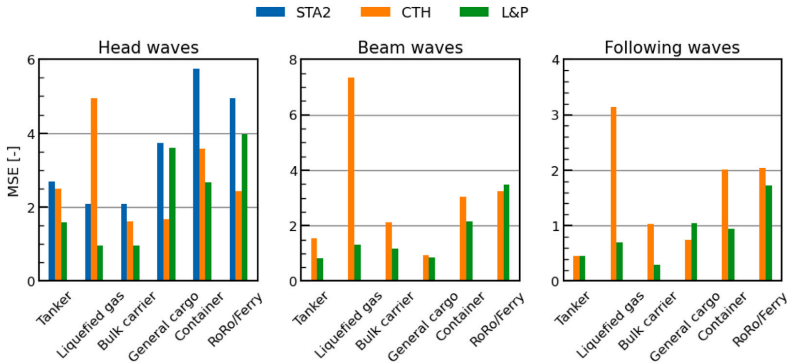


Fig. 6. Comparison of *MSE* results for added wave resistance methods according to the ship type.

Papanikolaou, 2020)

$$MSE = \frac{1}{n} \sum_{i=1}^n (C_{aw_i} - \hat{C}_{aw_i})^2 \quad (1)$$

$$C_{aw} = \frac{R_{aw}}{\rho g \zeta_a^2 B^2 / L} \quad (2)$$

where  $C_{aw}$  represents the nondimensional transfer function of added wave resistance in regular waves from model test,  $\hat{C}_{aw}$  is the estimated value from the semi-empirical method such as STA2, CTH, L&P, and  $n$  is the number of samples for the model test belonging to the corresponding classification.  $R_{aw}$  is the transfer function of added wave resistance,  $\rho$  is the density of water, and  $g$  is the gravity acceleration,  $\zeta_a$  is wave amplitude,  $B$  is breadth of the ship, and  $L$  is the ship length.

Comparing the overall *MSE* for each method in head waves, L&P method had the smallest error. However, CTH was noticeably well estimated in the high-speed region of Froude number more than 0.25

and the short waves of less than 0.3 relative wavelengths. In particular, outstanding performance at short waves appears to be the influence of wavelength correction coefficients used in CTH method, which has been adjusted to capture an increase in resistance in the short wave region. The overall *MSE* of STA2 is about 3.5, which is a relatively larger error than the other two methods, and *MSE* comparisons as functions of  $F_n$  and  $\lambda/L$  also show no better performance than them. This is because, in contrast to the other two approaches, STA2 mainly assumes a general sea trial and does not employ information pertaining to the detailed hull shape when estimating added wave resistance.

In beam seas, overall, L&P had lower *MSE* than CTH, but similarly to the tendency in head waves, CTH had advantages in high Froude number and short wavelength ranges. In following waves, the absolute peak of added resistance was smaller than that of beam or head sea, and accordingly, the *MSE* was relatively small. Likewise, L&P showed better performance than CTH in most classifications, but CTH was better in high-speed region.

In terms of error comparison by ship type, the errors of L&P in tanker, liquefied gas, bulk, and container ships were relatively small, while CTH method prevailed in general cargo, ro-ro/ferry ships under head sea conditions. In beam and following wave conditions, except for some cases, L&P had a slightly smaller error than CTH. The difference in error between these two methods is fundamentally due to the introduction of different factors to implement the shape of added wave resistance of a ship. While CTH method modifies the peak position using an encountered frequency correction factor, and the maximum value is derived by using the amplitude adjustment factor, L&P method uses a wave heading-based trigonometric function to estimate the location of resonance frequency and maximum resistance in arbitrary waves. For a more detailed analysis, added resistance according to the wavelength of several cases are plotted in Figs. B1–B3 in Appendix B.

When the prediction results of STA2 against the experimental data in head waves are used as a benchmark, CTH and L&P methods provide significantly smaller *MSEs*. In addition, since the estimations from the two methods agree fairly well with the experimental data in beam seas and following seas, both are considered to be applicable for estimation of added resistance in the environment of arbitrary waves experienced by ships at sea.

Although L&P method showed a slightly smaller *MSE* overall compared to CTH, it was not clearly a better method because they showed different performances depending on experimental conditions such as wavelength, wave heading, and ship type. In addition, it is clear that there is still much research that has to be done in this field as the experiments in beam and following sea have relatively greater uncertainty and the amount of data is limited compared to that of head sea.

Therefore, through the analysis of these existing methods, this study sought to develop a model that can ensure good overall performance at arbitrary waves without deviating significantly from model experiment data depending on ship type and various conditions. Here, we intend to apply a method that can reduce errors by properly combining the results of CTH and L&P, which is explained in detail in the next section.

### 3. Meta model for added resistance in arbitrary waves

#### 3.1. Procedure for developing a combined method

As seen in the previous results, CTH and L&P methods performed relatively better in almost all comparison cases than STA2, and above all, they had the advantage of estimating results for arbitrary wave headings. Comparing CTH and L&P, the difference in performance according to ship type, wavelength, and wave heading was significant. Therefore, this study attempted to develop a new model capable of improving overall performance based on the CTH and L&P methods. Here, a meta-modeling technique was used, which is to create a new model by combining existing models (It will be denoted as a ‘‘Combined method’’ from here). The combined method basically combines the nondimensional added wave resistance coefficients estimated from CTH and L&P to minimize errors with the experimental data. Due to the lack of available model experiment data under irregular wave conditions, it was difficult to develop the model in accordance with various ship conditions.

As a method of blending the two results, a concept similar to R-function used in several previous papers was introduced. Fujii (1975) proposed a method of estimating added resistance due to wave reflection by applying the reflection coefficient (R-function) derived by Ursell (1947) to Havelock’s formula, where the R-function was initially designed to extend the effect of wave reflection to relatively long waves. Later, this coefficient was further developed and modified by many other researchers to elaborately address the drift force due to the diffraction effect (Kuroda et al., 2008; Liu, 2020; Mourkogiannis and Liu, 2021). On the other hand, Guo and Steen (2011) adopted a method of multiplying R and 1-R by wave reflection term and ship motion term

for the entire wavelength, respectively, to gain the advantage that their contribution to the added wave resistance is smoothly transitioned from short waves to long waves. Recently, Yang et al. (2018) adopted a more simple and practical tangent hyperbolic function as a blending function instead of a R-function composed of Bessel functions.

In this study, R-function is introduced to combine different theoretical calculations as in Guo and Steen (2011) and Yang et al. (2018), and the tangent hyperbolic function is used because of its simplicity which can smoothly connect the results of the two formulas by adjusting a few coefficients. The transition range of the R-function is extended not only to the wave frequency but also to the wave direction to enable the estimation of added resistance in arbitrary waves. Consequently, the added resistance in arbitrary wave headings can be estimated as described in Eq. (3). The output of the tangent hyperbolic function is between 0 and 1, which is used as the weight of the two methods for the final result. In addition, added wave resistance estimation is performed by classifying it for each ship type to reflect different characteristics caused by the hull shape.

$$R_{wave} = \begin{cases} [1 - f(\alpha)]R_{head} + f(\alpha)R_{beam}, & \text{for } 90 \leq \alpha \leq 180 \\ [1 - f(\alpha)]R_{beam} + f(\alpha)R_{following}, & \text{for } 0 \leq \alpha < 90 \end{cases} \quad (3)$$

where  $R_{head}$ ,  $R_{beam}$ , and  $R_{following}$  represent the added wave resistance in head waves, beam waves, and following waves, respectively.  $f(\alpha)$  is a function that enables combining the various added wave resistance according to the wave headings as follows:

$$f(\alpha) = \frac{1}{2}[1 + \tanh(c(d - \alpha))] \quad (4)$$

$$R_{head}(R_{beam} \text{ or } R_{following}) = [1 - g(\lambda/L)]R_{CTH} + g(\lambda/L)R_{L\&P} \quad (5)$$

Here, the coefficient  $c$  adjusts the slope of the tangent hyperbolic function and it is divided into  $c_1$  and  $c_2$  according to  $\alpha$  as shown in Eq. (6). The coefficient  $d$  sets the intermediate position for combining the two results and is divided into 135, 45 degrees according to  $\alpha$  value, as seen in Eq. (7).  $R_{CTH}$  and  $R_{L\&P}$  represent added resistance coefficients estimated from CTH and L&P. By multiplying  $1-g$  and  $g$ , which are outputs of tangent hyperbolic function, by  $R_{CTH}$  and  $R_{L\&P}$ , respectively, the two results according to  $\lambda/L$  are smoothly connected.

$$c = \begin{cases} c_1, & \text{for } 90 \leq \alpha \leq 180 \\ c_2, & \text{for } 0 \leq \alpha < 90 \end{cases} \quad (6)$$

$$d = \begin{cases} 135, & \text{for } 90 \leq \alpha \leq 180 \\ 45, & \text{for } 0 \leq \alpha < 90 \end{cases} \quad (7)$$

The values  $R_{CTH}$  and  $R_{L\&P}$  are combined through the function  $g(\lambda/L)$  given in Eq. (8), from which  $R_{head}$  ( $R_{beam}$  or  $R_{following}$ ) can be estimated.

$$g(\lambda/L) = \frac{1}{2}[1 + \tanh(a(b - \lambda/L))] \quad (8)$$

Here,  $a$  is a slope coefficient such as  $c$ , which is divided into  $a_1$ ,  $a_2$ , and  $a_3$  as shown in Eq. (9). In other words,  $a$  serves to determine the slope of the function when combining the results according to  $\lambda/L$  using the combining function, and  $c$  is used to combine the results according to  $\alpha$ . Coefficient  $b$  represents the center position such as  $d$ , which is divided into  $b_1$ ,  $b_2$ , and  $b_3$  in Eq. (10).

$$a = \begin{cases} a_1, & \text{for } R_{head} \\ a_2, & \text{for } R_{beam} \\ a_3, & \text{for } R_{following} \end{cases} \quad (9)$$

$$b = \begin{cases} b_1, & \text{for } R_{head} \\ b_2, & \text{for } R_{beam} \\ b_3, & \text{for } R_{following} \end{cases} \quad (10)$$

Fig. 7 displays the combining function and its coefficients in this study as examples. Fig. 7(a) presents the combining function value  $f(\alpha)$

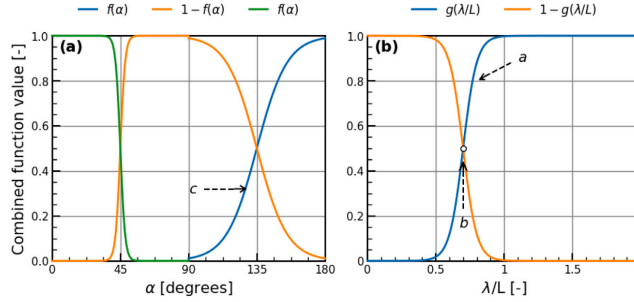


Fig. 7. Coefficients and combining function values according to (a) wave headings, (b) wavelengths proposed in the study.

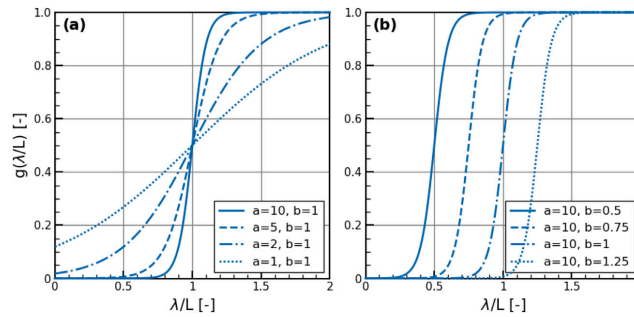


Fig. 8. The results of  $g(\lambda/L)$  according to the (a) slope coefficient and (b) center position coefficient. Coefficient  $c$  also has the same trend as the results shown in Fig. 8(a) as it is a slope coefficient.

Table 3

The coefficients of combining function according to the ship type. The values in parentheses represent the interquartile ranges of 1,000 bootstrap samples for the coefficients.

Ship type	$a_1$	$b_1$	$a_2$	$b_2$	$a_3$	$b_3$	$c_1$	$c_2$
Tanker	-10.00 (1.33)	0.52 (0.13)	7.55 (1.83)	1.08 (0.14)	0.17 (0.34)	1.08 (0.21)	0.04 (0.00)	1.41 (0.53)
Liquefied gas	-9.99 (0.36)	0.26 (0.01)	10.00 (0.01)	2.00 (0.00)	8.16 (1.43)	1.05 (0.10)	-1.2 (0.65)	1.60 (0.54)
Bulk carrier	-1.79 (0.82)	0.59 (0.04)	-0.23 (1.66)	1.84 (0.16)	0.34 (0.10)	1.92 (0.11)	0.00 (0.00)	0.01 (0.02)
General cargo	1.95 (1.01)	0.11 (0.09)	0.92 (0.21)	0.98 (0.07)	0.31 (1.13)	0.74 (0.24)	0.21 (0.39)	0.36 (0.56)
Container	-9.21 (0.77)	0.55 (0.02)	4.52 (1.53)	0.88 (0.13)	2.00 (0.24)	0.95 (0.03)	0.04 (0.00)	-0.08 (0.34)
Ro-Ro/Ferry	-9.35 (0.88)	1.01 (0.03)	-7.91 (1.30)	0.71 (0.15)	6.54 (1.45)	0.84 (0.13)	1.49 (0.50)	0.05 (0.20)

of  $R_{head}$ ,  $R_{beam}$ , and  $R_{following}$  according to wave heading, and Fig. 7(b) shows the combining function value  $g(\lambda/L)$  of  $R_a$  and  $R_b$  according to wavelength. As illustrated in Fig. 8, coefficients  $a$  and  $c$  affect the slope of the combining function value, and coefficient  $b$  adjusts where the combining weight is half. As the absolute value of  $a$  coefficient increases, the slope of the combining function increases ( $c$  has the same trend as  $a$ ), and as the value of  $b$  increases, the center point moves in the direction where  $\lambda/L$  increases.

All the coefficients in Eqs. (6), (9), and (10) were tuned to minimize the error between the model test data and the estimated value from Eq. (3), and in the process, 10 cross-validations with 1000 bootstrap samplings were performed. As a result, the coefficients that provided the smallest errors were obtained through 10 cross-validations per bootstrapping, and 1000 sets of coefficients were finally obtained through 1000 bootstrap sampling. To avoid the influence of some coefficient estimations that deviate extremely from other values, the median value for 1000 bootstrap samples was adopted as the final value of the coefficient in the equation. Table 3 lists the finally obtained coefficient values for each ship type.

### 3.2. Results of a combined method

In this section, we show how the results of the new method calculated by substituting the coefficients of Table 3 into Eq. (3) are actually applied and how they differ from the CTH and L&P methods. Figs. 9–11 represents the  $MSE$  trend of the added wave resistance predictions in head waves, beam waves, and following waves by each method according to the wavelength. As can be seen from the figures, since the coefficients of the combining function are adjusted to minimize the  $MSE$  with model experimental data, the results of the Combined method generally tended to follow the method that provided lower  $MSE$  for each interval section.

In Figs. 12–13, the results of the Combined method have been added to the previously covered ship cases. According to Fig. 12(a) and Fig. 12(b), the Combined method followed CTH in short waves and L&P method in long waves, and these results were well matched with the actual experimental results, and it was opposite in Fig. 12(c). The reason why different blending trends are shown here is that the coefficients of the combined function are applied differently for each ship type. Moreover, since the Combined method was tuned based on two semi-empirical methods, it had the advantage of being smoothly



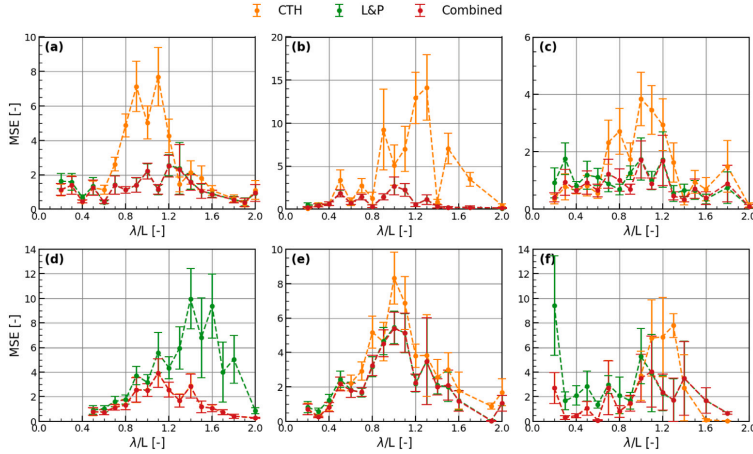


Fig. 9. Comparison of *MSE* according to wavelengths in head waves. (a) Tanker, (b) Liquefied gas, (c) Bulk carrier, (d) General cargo, (e) Container, (f) Ro-Ro/Ferry. The circle marker stands for the mean of the *MSE*s of the samples in the corresponding wavelength interval, and the error bar represents the standard error of *MSE*.

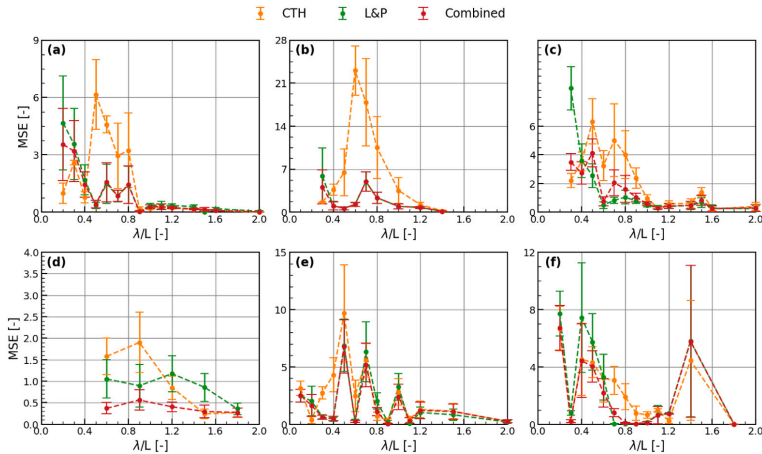


Fig. 10. Comparison of *MSE* according to wavelengths in beam waves. (a) Tanker, (b) Liquefied gas, (c) Bulk carrier, (d) General cargo, (e) Container, (f) Ro-Ro/Ferry.

connected without deviating significantly from the predicted values of the two methods.

### 3.3. Analysis of the combined method by experimental data in regular waves

In addition to *MSE*, several error metrics with correlation coefficient are used to analyze the quality of the predicted value of the Combined method. The Pearson's correlation coefficient (*R*), Mean Absolute Error (*MAE*), and Root Mean Squared Error (*RMSE*) are defined as in Eqs. (11)–(13).

$$R_{y,\hat{y}} = \frac{cov(y,\hat{y})}{\sigma_y\sigma_{\hat{y}}} = \frac{E(y\hat{y}) - E(y)E(\hat{y})}{\sigma_y\sigma_{\hat{y}}} \tag{11}$$

$$MAE = \frac{1}{n} \sum_{i=1}^n |y_i - \hat{y}_i| \tag{12}$$

$$RMSE = \sqrt{MSE} \tag{13}$$

where  $y_i$  is the true value obtained from the experiment,  $\hat{y}$  is the predicted value from the semi-empirical method.

Fig. 14 shows the addition of the results of the Combined method to the *MSE* comparison bar charts in Section 2.3. It can be seen that the Combined method shows a significantly smaller error compared to STA2 in head waves, and overall *MSE* is reduced compared to CTH and L&P for all wave headings. It is confirmed that the error of the Combined method is reduced compared to other methods in each section divided according to the Froude number, wavelength, and ship type.

The scatter plots between all experimental data of added resistance in regular waves and the predicted values of STA2, CTH, L&P, and Combined methods are shown in Fig. 16. The best match line of the predictions and experimental values and 30% deviation line from it

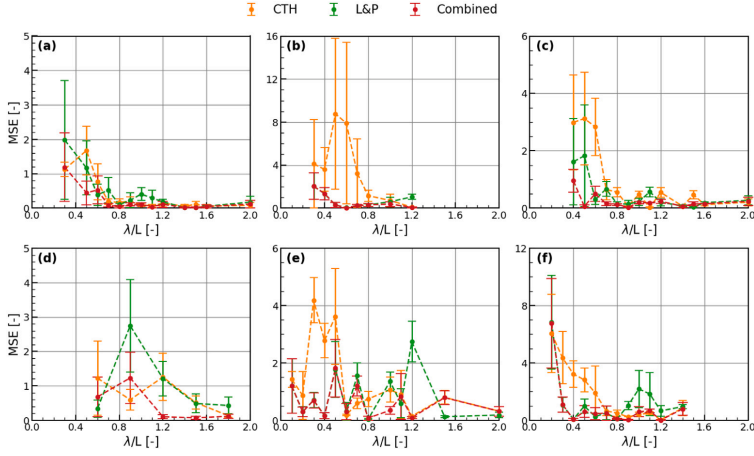


Fig. 11. Comparison of  $MSE$  according to wavelengths in following waves. (a) Tanker, (b) Liquefied gas, (c) Bulk carrier, (d) General cargo, (e) Container, (f) Ro-Ro/Ferry.

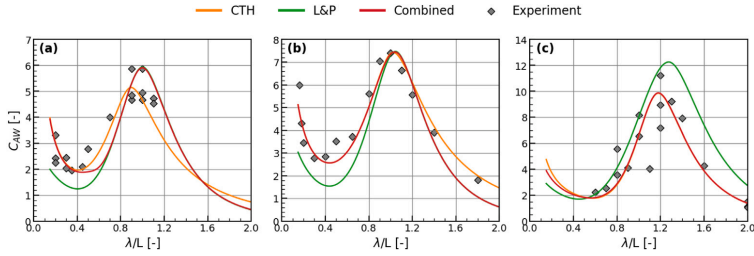


Fig. 12. Examples of Combined method according to the wavelength of (a) DTC,  $F_n = 0.139$ ,  $\alpha = 180$ , (b) HSVA,  $F_n = 0.232$ , (c) S60,  $F_n = 0.283$ . The figure corresponds to the results of head waves.

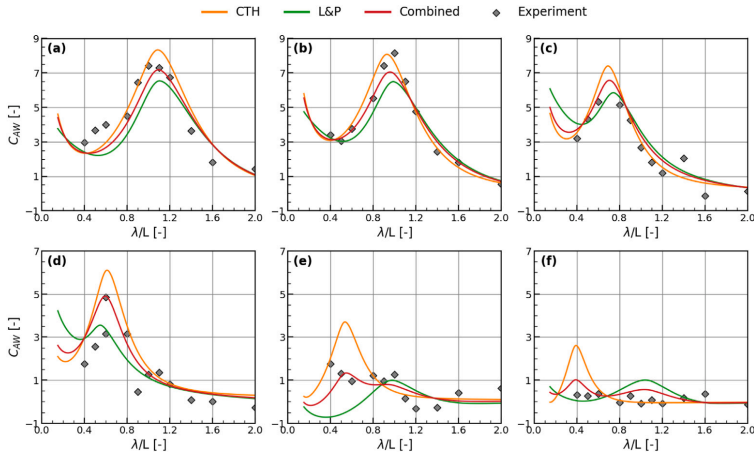


Fig. 13. Examples of Combined method according to the wave heading. 170 k BC,  $F_n = 0.128$  (a)  $\alpha = 180$ , (b)  $\alpha = 150$ , (c)  $\alpha = 120$ , (d)  $\alpha = 90$ , (e)  $\alpha = 30$ , (f)  $\alpha = 0$ .

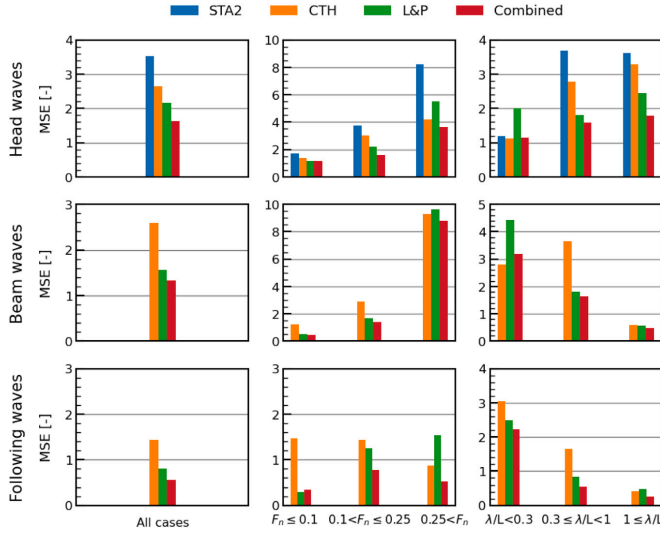


Fig. 14. MSE results of Combined method for added wave resistance according to all cases, Froude numbers, and wavelengths. The bar graph in the upper row shows head waves, the middle represents beam waves, and the lower is following waves.

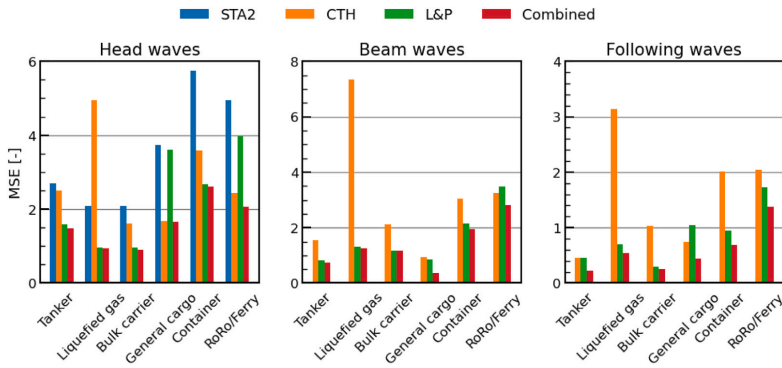


Fig. 15. MSE results of Combined method for added wave resistance according to the ship type.

**Table 4**  
Summary of the components of the correlation coefficients and statistical values for the predicted results in Fig. 16.

Range	Method	R	MAE	RMSE
All area	CTH	0.83	1.18	1.63
	L&P	0.87	1.02	1.43
	Combined	0.90	0.89	1.25
	STA2	0.71	1.44	1.95
Head seas	CTH	0.82	1.21	1.66
	L&P	0.84	1.11	1.51
	Combined	0.88	0.96	1.31
	STA2	0.71	1.44	1.95
Beam seas	CTH	0.68	1.21	1.72
	L&P	0.75	0.94	1.36
	Combined	0.79	0.88	1.27
	STA2	0.71	1.44	1.95
Following seas	CTH	0.33	0.89	1.23
	L&P	0.59	0.67	0.96
	Combined	0.62	0.53	0.80
	STA2	0.71	1.44	1.95

are displayed together in the figure. In addition, various error metrics such as MAE, RMSE with R obtained from the corresponding cases are presented in Table 4. For the comparison using scatterplots and the table, refer to those presented by Wang et al. (2021) in a benchmark study organized by ITTC.

As mentioned earlier, STA2 is less accurate in head waves than CTH, L&P, and Combined methods. In particular, as many of the predicted values from STA2 for experimental measurements are located in the lower right side of the figure beyond the 30% deviation line, it is likely to underestimate when added resistance is large. This trend is also in line with the large error of STA2 at high speed and resonance positions in Fig. 14.

On the other hand, the predicted values of CTH and L&P are evenly distributed on both sides of the best match line, and the correlation coefficients are 0.82, 0.84 at head seas, and 0.68, 0.75 at beam seas, showing good correlation for both methods. In following waves, the correlation coefficients are relatively lower at the 0.33, 0.59, and many predicted values are observed far outside of the 30% deviation line.

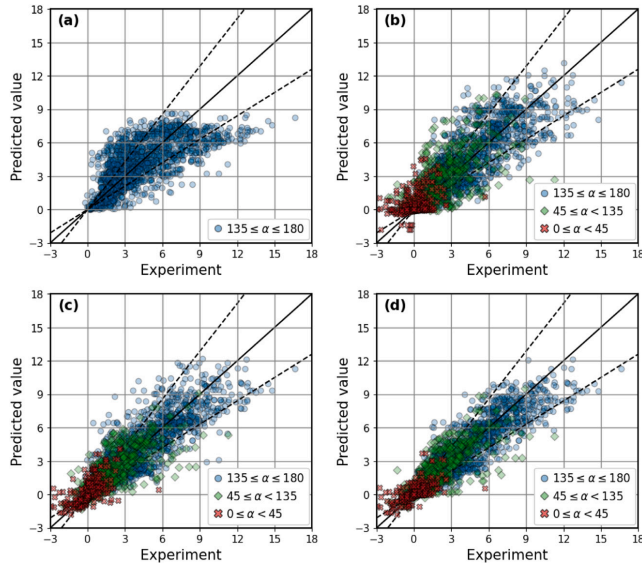


Fig. 16. The scatter plots of the predicted  $C_w$  from (a) STA2, (b) CTH, (c) L&P, (d) Combined method against experimental data. The solid line represents the best match line, and dashed line is 30% deviation line from the best match line.

This might be due to the fact that the experimental data in following sea is limited, highly uncertain, and that many values are close to zero. Most of the predicted samples from the Combined method are evenly distributed around the best match line and remain within the 30% deviation line. Compared to the predictions of CTH and L&P, the correlation coefficients of Combined method in all wave directions are higher by 0.62–0.88, and the MAEs are smaller by 0.53–0.96 (see Fig. 15).

#### 4. Observations from comparison of the combined method with full-scale measurements in irregular waves

##### 4.1. Details of full-scale measurements and weather data

In this section, a comparison between the in-service data collected from the two ships and the wave resistance estimated from the Combined method under the corresponding conditions is performed. To this end, not only waves but also the ship resistance factors in calm water, wind, and fouling and roughness conditions, which mainly account for the total resistance of the ship, are obtained through the empirical methods presented in Sections 4.3–4.5. Moreover, the errors between the estimated values of the added wave resistance and the extracted values from the in-service data are compared in Section 4.6.

Table 5 lists the main characteristics of Ship A and Ship B used in the study, and Fig. 17 shows the trajectories of the two ships for the data recording duration. The data of Ship A and Ship B were recorded continuously for 26 months and 2 months from the various fitted sensors and data acquisition systems, and the average values were stored every 15 min and every 1 min, respectively. The collected in-service data of Ship A includes 26 variables and Ship B includes 392 variables. The composition of the data from the two ships is slightly different, but the following variables were commonly used to estimate the resistance components of the ship. Navigation (GPS position, gyro heading, COG heading); Propulsion system (shaft Power, shaft rpm,

shaft torque, M/E load); Operating condition (draft, trim, GPS speed, Log speed), etc. The information about the measurement methods of the ship parameters used in this study is shown in Table 6. Additionally, it was possible to extract the data of ships in sea passage operation not at berth or maneuvering by obtaining information on the voyage schedule or navigation state.

In order to calculate the added resistance in wind and waves, information on the surrounding environment the ship experiences during its voyage is required. In this study, weather information such as  $u$  and  $v$ -components of wind speed, mean wave direction, wave period, and significant wave height was obtained from the re-analysis dataset ERA5 of European Centre for Medium-Range Weather Forecasts (ECMWF), which is a global prediction model and is widely known as one of the most reliable models simulating actual sea weather conditions, instead of onboard measurement (Haiden et al., 2018). There were wind speed and direction data obtained from anemometers installed on ships, but as a result of comparison with wind data from ECMWF, it was found that some parts of the longitudinal wind speed measured from the corresponding ship are changing signs or directions without any probable cause. In addition, there was no data related to waves that could be obtained from the ship.

The horizontal resolution of the dataset is provided based on a grid of  $0.25^\circ \times 0.25^\circ$  for atmosphere and  $0.5^\circ \times 0.5^\circ$  for ocean waves, respectively, and the temporal resolution of it is hourly. The weather data at the closest position and time grid can be obtained by matching each data sample of the ship with data from the ECMWF. Through the sequential interpolations on weather data according to the location and timestamp of the ship, the actual environment encountered by the ship can be extracted. It is used as an input value for calculating added resistance, and Figs. 18–19 display distributions of wind speed and significant wave height during the data collection periods.

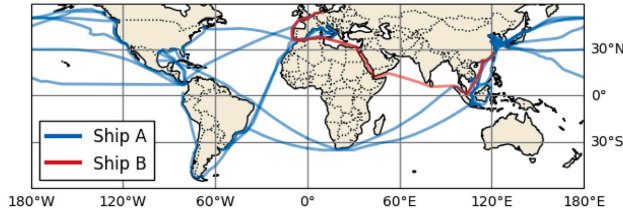


Fig. 17. Operational routes of Ship A and B for the data recording duration.

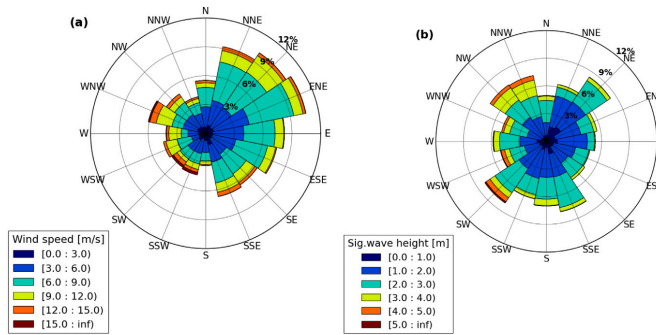


Fig. 18. The distribution plots of (a) wind, (b) waves encountered by Ship A. Figure (a) shows the degree of wind occurrence according to the true wind direction in %. The color sector shows the true wind speed in m/s. Figure (b) represents the degree of waves occurrence according to the wave direction in %. The color sector shows the significant wave height in meters. (For interpretation of the references to color in this figure legend, the reader is referred to the web version of this article.)

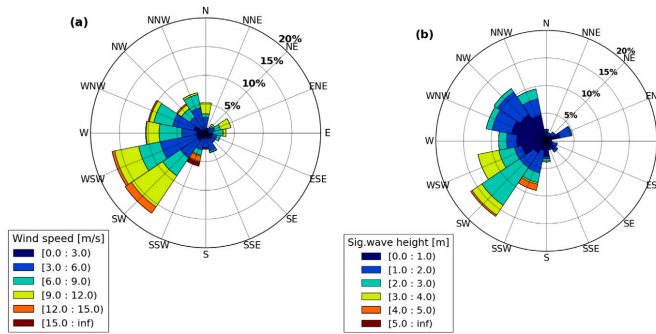


Fig. 19. The distribution plots of (a) wind, (b) waves encountered by Ship B. (For interpretation of the references to color in this figure legend, the reader is referred to the web version of this article.)

4.2. Data pre-processing

Raw measurement data includes all types of navigation status, such as accelerating, decelerating, maneuvering, and even in port. To perform accurate speed-power performance analysis, it is necessary to extract the data sections in which the ship operates steadily. In this study, the steady-state detection algorithm proposed by Dalheim and Steen (2020) was applied. This algorithm identifies a change point among the samples by using a sliding window and its corresponding *r*-value of the local slope. The slope of the fitted regression line from the regression analysis is used to check the unsteady state. In addition, sections with propeller speed below a certain limit were considered to be in the state of maneuvering. The voyage classification of data

samples to which steady-state detection and filtering are applied is shown as an example in Fig. 20. As a result, Figs. 21–22 show the histograms of speed through water, propeller speed, mean draft, and engine power for the pre-processed data of Ship A and Ship B.

4.3. Estimation of ship resistance factor by empirical approaches

In general, the resistance components that account for most of the total resistance of a ship are calm water resistance, added resistance due to wind, and added resistance in waves. The effects of drifting and rudder on added resistance are neglected in this study. To extract the contribution of the added wave resistance to the power demand from in-service data, the resistance in calm water conditions

**Table 5**  
Main dimensions and information of ships used in the study.

	Ship A	Ship B
Ship type	General cargo	Container
Length [m]	194	350
Breadth [m]	32	48
Block coefficient [-]	0.79	0.66
Radius of pitch gyration [-]	0.25	0.25
Deadweight tonnage [ton]	12.6	14.5
Maximum continuous rating [kW]	10780	65640
Design draft [m]	12.6	14.5
Service speed [knots]	15.5	24.7

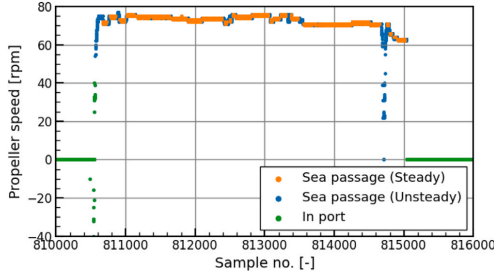


**Fig. 20.** Classification of voyage status according to propeller speed. It shows an example of one short voyage data.

and added resistance due to wind, were considered as expressed in Eqs. (14)–(15).

$$R_{total} = R_{calm} + R_{wind} + R_{wave} \quad (14)$$

$$P_B = \frac{R_{total} \cdot V}{\eta_T} \quad (15)$$

where  $R_{total}$  is the total resistance of a ship,  $R_{calm}$  is calm water resistance,  $R_{wind}$  is the added resistance due to wind,  $\eta_T$  is the overall efficiency, and  $P_B$  is engine brake power.

Here, the frictional coefficient was obtained from ITTC-1957 correlation line, and the residual resistance coefficient was calculated using Hollenbach's method (1998) since it was found that Hollenbach's method fits relatively well for the given ship. It was developed based on regression analysis of 433 relatively modern ship models, requiring basic ship design parameters such as length, breadth, draft, displacement, wetted surface area, block coefficient, and propeller diameter for the calculation. According to the original paper, Hollenbach's method had a relatively lower standard deviation of the error in resistance against its validation test cases compared to Holtrop–Mennen (1984), Guldhammer (1974), Lap-Keller (1973), and Series-60 (1972).

Due to changes in hull roughness caused by marine fouling, differences in powering performance may occur during the operational period, and such differences should be additionally corrected as a roughness allowance. The roughness allowance ( $\Delta C_F$ ) can be calculated as the difference between the total resistance coefficient of in-service data ( $C_{T,Data}$ ) filtered by wind speeds less than 5.5 m/s, where calm water resistance dominates, and the total resistance coefficient in the same conditions obtained from empirical methods ( $C_{T,Emp}$ ) as shown in Eq. (16) (Gupta et al., 2021).  $C_{T,Data}$  represents the total resistance coefficient due to calm water resistance as well as the added resistance due to the wind and waves and fouling, while  $C_{T,Emp}$  denotes the total resistance coefficient due to calm water resistance, added resistances due to wind and waves without taking fouling into account. Therefore, it is assumed that only fouling contribution is left after the subtraction. Furthermore, trends of roughness allowance were observed over

cumulative static time between specific hull cleaning events, and a fitted trend line is used as a corrected roughness allowance ( $\Delta C_F$ ), as shown in Fig. 23(c). The overall operating speed range of the two ships used in this study was about Froude number 0.09 to 0.18, the impact of the speed of the wave-making resistance coefficient or viscous resistance coefficient within this range is not that significant, thus the corresponding resistance coefficients, which are less than Froude number 0.2 is assumed to be constant.

$$\Delta C_F = C_{T,Data} - C_{T,Emp} \quad (16)$$

There were a total of four propeller and hull cleaning events of Ship A in 2.5 years, and the roughness allowance was estimated considering this. In case of the Ship B, there was no specific data related to fouling and roughness such as cleaning event history. Since the berthing time of the container ship was relatively short, and data of one voyage (approximately 2 months) was used, it was assumed that there would have been no significant change in the hull roughness during the period. As a result, the typical average hull roughness of an operating ship, 150  $\mu\text{m}$ , was applied for the estimation of the roughness allowance according to MARINTEK's formula (Minsas, 1982; Steen and Aarnes, 2014).

The wind resistance coefficient was estimated from the regression formula developed by Fujiwara (2006), and the resistance increase due to relative wind was calculated according to the method recommended by ISO 15016 (2015). Wind affected areas of the hull were calculated based on the depth and draft of Ship A and B. Since the wind-affected area above the water surface of Ship A is mainly an accommodation area, the upper structure according to the draft of the ship was estimated using a detailed hull shape. Meanwhile, the container ship has not only accommodation areas but also cargoes on the deck, and since there was no detailed information on cargo volume and arrangement, the parameter estimation method from Kitamura et al. (2017) was used for the above-water structure area for Ship B.

Finally, the relevant resistance components of each ship obtained through the previous estimation process are shown in Figs. 23–24. In the case of Ship B, the figure related to the roughness allowance is not included as it was assumed to be constant. The detailed process to estimate added wave resistance is covered in the next section.

#### 4.4. Wave spectrum and response amplitude operator in regular waves

The mean resistance increase in short-crested irregular waves ( $R_{wave}$ ) can be calculated as a linear superposition of the transfer function of added resistance in regular waves ( $R_{aw}$ ) and directional wave spectrum ( $E$ ), as expressed in Eq. (17). The transfer functions of added resistance in regular waves according to different speeds for the subject ships estimated from the Combined method are shown in the following Figs. 25–26.

$$R_{wave} = 2 \int_0^{\frac{\pi}{2}} \int_0^{\infty} \frac{R_{aw}(\omega, \alpha; V) E(\omega, \alpha)}{\zeta_a^2} d\omega d\alpha \quad (17)$$

The directional spectrum is not measured in this study, standard frequency spectrum ( $S$ ) with the angular distribution function ( $G$ ) is considered as in Eq. (18).

$$E(\omega, \alpha) = S(\omega) \cdot G(\alpha) \quad (18)$$

There are various wave spectra representing different characteristics depending on the location and environment of the ocean. In this study, the modified Pierson–Moscowitz spectrum of ITTC 1978 (2017), commonly used for the open ocean, is applied through the process as shown in Eqs. (19)–(21).

$$S(\omega) = \frac{A}{\omega^5} \exp\left(-\frac{B}{\omega^4}\right) \quad (19)$$

$$A = 173 \frac{H_m^2}{T_m^4} \quad (20)$$

**Table 6**  
Measurement methods of the ship parameters used in the study.

Parameter	Measurement device	Unit
Position	DGPS	latitude, longitude
Heading	Gyro compass	degree
Course over ground	DGPS	degree
Speed over ground	DGPS	knots
Speed through water	Doppler speed log	knots
Shaft power	Shaft horsepower meter	kW
Shaft revolutions	Ship revs counter	rev/min
Draft	Draft gauges	meter
Weather information	ECMWF ERA5 reanalysis	Temporal resolution: hourly Horizontal resolution: 0.25° × 0.25° (atmosphere) Horizontal resolution: 0.5° × 0.5° (Ocean waves)

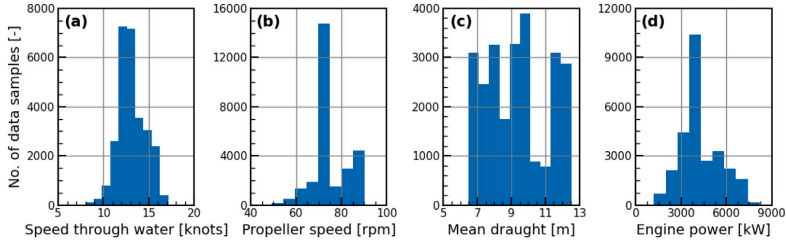


Fig. 21. Histograms of (a) speed, (b) main engine rpm, (c) mean draft, and the (d) engine power of Ship A for the data recording duration.

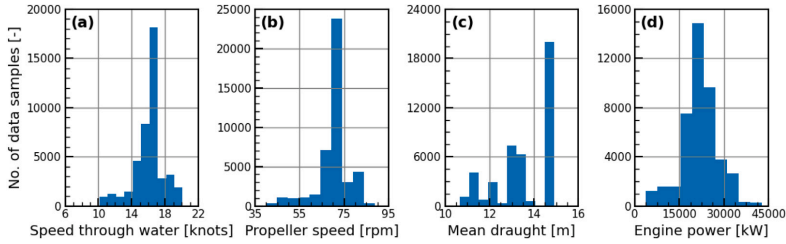


Fig. 22. Histograms of (a) speed, (b) main engine rpm, (c) mean draft, and the (d) engine power of Ship B for the data recording duration.

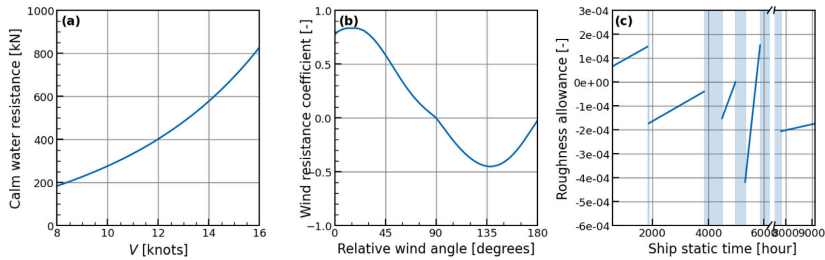


Fig. 23. Ship resistance components for Ship A: (a) calm water resistance, (b) wind resistance coefficient, (c) roughness allowance. The resistance factors in Figures (a) and (b) are calculated based on the design loading condition. The blue shaded part in (c) is propeller cleaning event, and the solid line shows the trend line of mean roughness allowance according to the ship static time. (For interpretation of the references to color in this figure legend, the reader is referred to the web version of this article.)

$$B = \frac{691}{T_m^4} \tag{21}$$

where  $\omega$  is the circular wave frequency,  $H_s$  is the significant wave height, and  $T_m$  is the mean wave period.

For the angular distribution function for the wind waves, the cosine-power type is applied such as in Eq. (22), and the spreading parameter

is set to 1 (ITTC, 2017)

$$G(\alpha) = \begin{cases} \frac{2^{2s}}{\pi} \frac{\Gamma^2(s+1)}{\Gamma(2s+1)} \cos^2(\theta - \alpha), & -\frac{\pi}{2} \leq \theta - \alpha \leq \frac{\pi}{2} \\ 0, & \text{otherwise} \end{cases} \tag{22}$$

where  $\theta$  is the primary wave direction,  $s$  is a directional spreading parameter, and  $\Gamma$  is a Gamma function.

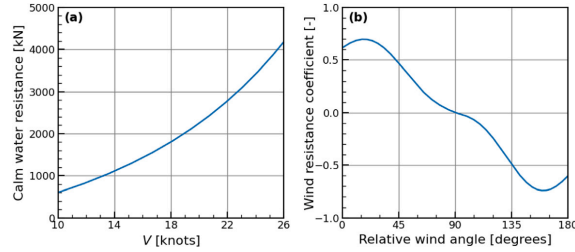


Fig. 24. Ship resistance components for Ship B: (a) calm water resistance, (b) wind resistance coefficient.

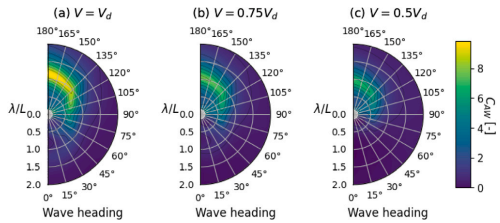


Fig. 25. Comparison of added resistance coefficient in regular waves of Ship A at (a)  $V = V_d$ , (b)  $V = 0.75V_d$ , (c)  $V = 0.5V_d$  computed using Combined method.  $V_d$  represents the design speed, and the results of the figures are based on the design loading condition of the ship.

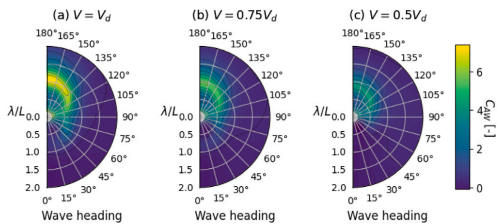


Fig. 26. Comparison of added resistance coefficient in regular waves of Ship B at (a)  $V = V_d$ , (b)  $V = 0.75V_d$ , (c)  $V = 0.5V_d$  computed using Combined method.

#### 4.5. Comparison of semi-empirical methods in irregular waves

Theoretical estimations for added resistance in irregular waves of Ship A and Ship B by various methods are plotted in Fig. 28 and Fig. 29, respectively, in which sensitivity analysis according to significant wave height ( $H_s$ ), mean wave period ( $T_m$ ), wave heading ( $\alpha$ ), and ship speed ( $V$ ) is performed. The reference conditions for the comparative case of Ship A are  $H_s = 1$  m,  $T_m = 10$  s,  $\alpha = 180$ , and  $V = 15.5$  knots, and Ship B are  $H_s = 1$  m,  $T_m = 12$  s,  $\alpha = 180$ , and  $V = 24.7$  knots. It is assumed that the remaining conditions are constant while analyzing variation for each parameter. Basically, the added resistance in irregular waves is calculated through the process of Section 4.4, and the RAOs of the two ships under the reference conditions are shown in Fig. 27. For the comparison in irregular waves, not only STA2, CTH, and L&P but also Shopera and Kreitner's methods that can directly calculate the added resistance in irregular waves are added. The CTH, L&P, and Combined methods take into account the angular distribution function in estimating added resistance in irregular waves as shown in Eq. (17), while for Shopera and Kreitner the angular distribution function is not applied, since these methods work directly with irregular waves, so a

normal directional spreading is presumably included in the methods. Since STA2 is applicable to the mean resistance increase in long crested irregular head waves according to the original intention, the angular distribution function in Eq. (18) was not used.

According to the study of Lang and Mao (2021), it was found that the added resistance rose more drastically as the significant wave height increased compared to the linear superposition. In their work, a wave height correction factor ( $C_{H_s} = \sqrt[3]{H_s}$ ) was established that can be used to account for the effects of higher resistance brought on by a large vessel's motion as well as decreased propulsion efficiency in rough seas. This correction is reflected by multiplying the added resistance due to waves ( $R_{wave}$ ) by the wave height correction factor ( $C_{H_s}$ ), and its effectiveness in minimizing errors between full-scale measurements and estimated values from the semi-empirical method has been shown. In this study, since the Combined method basically implemented the CTH method in its original form, the wave height correction factor was applied to the CTH method also when it was used as part of the Combined method.

#### Wave resistance over the significant wave height

As the significant wave height increased, added resistance due to waves tended to increase very steeply. In particular, the difference in results between methods at a height of 2 m or more was noticeable. For the considered ships A and B, the results of the Combined, CTH methods, and STA2 were the largest. In both cases, the Shopera and L&P methods provided similar results, while the Kreitner provided smaller values compared to the other methods.

#### Wave resistance over the mean wave period

STA2, CTH, L&P, and Combined method formed a peak at around 8–9 s for Ship A and 11–12 s for Ship B, and considering the actual length of the ships, it seemed to match with the resonance frequency positions properly. In addition, weak local crests were formed at around 4–6 s and 5–7 s, respectively, which was interpreted as reflecting the increase in added resistance at a short wavelength. The Combined method seemed to properly reflect the characteristics of CTH and L&P methods according to the mean wave period. Shopera and Kreitner methods showed constant results over the mean wave period, as expected. Since they focus on estimating maximum added wave resistance and do not include the mean wave period in the formula, Shopera provided similar results as the maximum values seen from CTH, L&P, Combined methods, and STA2, while Kreitner had values less than that.

#### Wave resistance over the wave heading

Since Shopera, Kreitner, and STA2 only consider added wave resistance in head waves, it was assumed that STA2 and Kreitner provided the same values at wave headings from 135 to 180 degrees, and from 150 degrees to 180 degrees for Shopera. Moreover, their results in beam and following waves were set to zero. According to the estimated results from CTH, L&P, and Combined method, the maximum added resistance occurred in head waves, and the magnitude became smaller as it went to the stern direction. It can be seen that the added resistance in the range between 180 degrees and 135 degrees decreased slightly, then



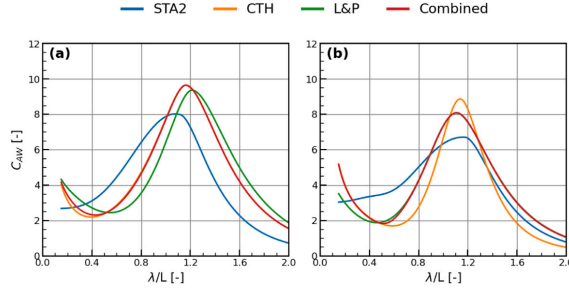


Fig. 27. Added resistance coefficient in regular waves of (a) Ship A ( $\alpha = 180$ ,  $V = 15.5$  knots), (b) Ship B ( $\alpha = 180$ ,  $V = 24.7$  knots).

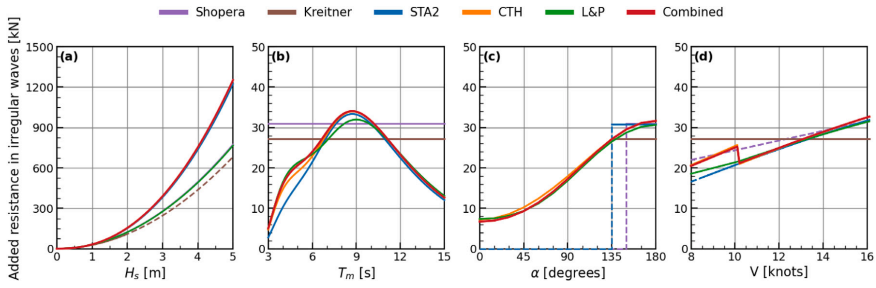


Fig. 28. Added resistance of Ship A in irregular waves against (a) significant wave height, (b) mean wave period, (c) wave heading, (d) vessel speed according to various estimation methods. The y axis represents added resistance in irregular waves, and the section indicated by the hatched line is the range beyond the restriction of the corresponding method (Reference conditions:  $H_s = 1$  m,  $T_m = 10$  s,  $\alpha = 180$ ,  $V = 15.5$  knots).

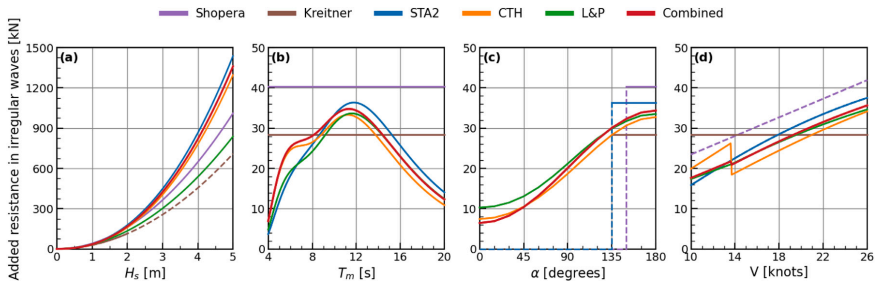


Fig. 29. Added resistance of Ship B in irregular waves against (a) significant wave height, (b) mean wave period, (c) wave heading, (d) vessel speed according to various estimation methods (Reference conditions:  $H_s = 1$  m,  $T_m = 12$  s,  $\alpha = 180$ ,  $V = 24.7$  knots).

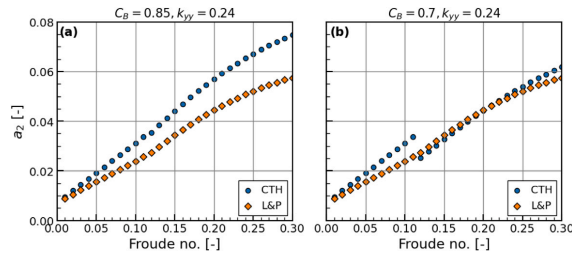


Fig. 30. Speed correction factor ( $a_2$ ) according to Froude no. at (a)  $C_B = 0.85$ ,  $k_{yy} = 0.24$ , (b)  $C_B = 0.7$ ,  $k_{yy} = 0.24$ .

in the range between 135 degrees and 0 degrees dropped sharply. The Combined method seemed to follow the results of the two methods, which were properly weighted for the wave headings. In head waves, STA2, Shopera provided similar resistances to CTH, L&P, and Combined method, and Kreitner tended to underestimate significantly compared to other methods.

**Wave resistance over the speed of the ship**

Most methods showed a trend of almost linearly increasing added resistance in proportion to speed. CTH showed a drop in resistance at a certain speed, which was found to be due to the influence of the  $a_2$  coefficient used in wave motion-induced added resistance. Since the calculation of  $a_2$  in the CTH method is different for Froude number smaller and larger than 0.12, where block coefficient ( $C_B$ ) and pitch gyration ( $k_{yy}$ ) were introduced in the  $a_2$  equation only at  $F_n = 0.12$  or higher, it turned out that some combinations of  $C_B$  and  $k_{yy}$  result in a discontinuous  $a_2$  as a function of  $F_n$ . This trend can be seen from the comparison results of the speed correction factor between the two methods according to Froude number in Fig. 30. Meanwhile, the Kreitner method estimated a constant value according to the ship speed, which was larger or smaller than the other methods depending on the speed. The Combined method mainly followed the CTH method in the case of the general cargo ship and the L&P method for the container ship. As the Combined method integrates the results of the two methods, the discontinuity of added resistance as a function of  $F_n$  occurring in the CTH method may be visible in some cases.

**4.6. Observations from comparison of the combined method with full-scale measurements**

In this section, the results of the combined method were compared with using full-scale measurement data of ships A and B. As shown in Eq. (15), the brake power of the ship is estimated by considering the ship resistance factors, propulsive efficiency, and speed. It is compared with the main engine power measured from the shaft horsepower meter on-board.

Figs. 32 and 33 show the percentage of absolute error between the measured power ( $P_{MEAS}$ ) and the estimated power ( $P_{EST}$ ) for each parameter ( $H_s, T_m, \alpha, V$ ), and it is calculated according to Eq. (23). Fig. 31 shows an example of the confidence interval, mean line, and histogram for the error of the data samples. The shadowed range in the figure is the confidence interval of 95% mean for the samples, which represents the range of values that there is a 95% probability that the mean value of the samples falls within. The collected data of each parameter were divided at regular intervals to obtain the error defined in Eq. (23) for the samples for each section. In addition, the confidence interval and mean line representing each section were estimated, and they were connected. Here, “no correction” means that added resistance due to waves is not included in the total estimated power.

$$\text{Error of power prediction [\%]} = \frac{|P_{MEAS} - P_{EST}|}{P_{MEAS}} \times 100 \tag{23}$$

**Error trend over the significant wave height**

From Fig. 32(a) and Fig. 33(a), it can be seen that for a significant wave height of 1 m or less, there is little difference in error between the methods, including the “no correction”. This is as expected since the added resistance is a small fraction of the total for small waves. At a significant wave height of 1 m or more, the difference between “no correction” and the other correction methods is clearly visible. Since there were not many data samples in the range between 3 m to 4 m, uncertainty was included in the error trend, but the relative performance difference of each method can be distinguished. It can be seen that the Combined method gives the smallest error compared to the other methods over the entire  $H_s$  range, with values in the range 7%–20%, while CTH and L&P show an error of about 10%–25%. The

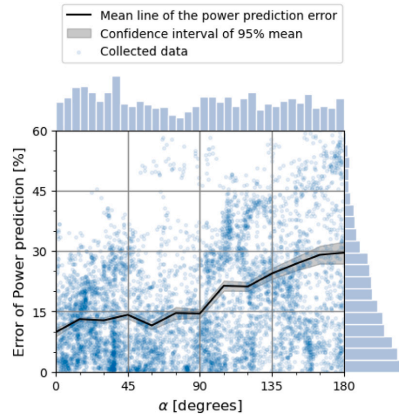


Fig. 31. An example showing the power prediction errors of collected samples with the histogram and confidence interval. It corresponds to the case of the “no correction” according to wave headings of Ship A (Refer to Fig. 32(c)). The solid line indicates the mean line of the power prediction error, shadowed area represents its confidence interval of 95% mean, and marker is the collected data.

errors of Kreitner, Shopera, and STA2 methods show much larger errors than these.

**Error trend over the mean wave period**

The error plotted as a function of the mean wave period in Fig. 32(b) and Fig. 33(b) ranges from 8 to 26% over the entire range, which is somewhat smaller than for the other parameters. Compared with “no correction”, the effect of wave correction can be identified for periods larger than 5 s for Ship A and 7 s for Ship B. It can also be seen that the errors of CTH, L&P, and Combined methods are significantly smaller in the vicinity of the peak compared to other methods.

**Error trend over the wave heading**

Since Shopera, Kreitner, and STA2 are applicable only to head waves, they have the same error as “no correction” in following and beam waves. The errors of CTH, L&P, and Combined methods differ significantly in the range between 60 to 135 degrees compared to other methods. The Combined method gives the smallest error over most of the heading range. However, the increase of propulsion power due to waves of Ship A and Ship B in the range of 0–30 degrees and 0–45 degrees, respectively, seems to be almost insignificant.

**Error trend over the speed of the ship**

Looking at the error trends over the speed in Fig. 32(d) and Fig. 33(d), the relative effect of wave correction on the propulsion power generally decreases as the speed of the ship increases, which indicates that added resistance increase less rapidly with speed than the calm water resistance. The Combined method shows a similar error trend as CTH for the general cargo ship and as L&P for the container ship and provides generally good performance for all speeds.

Fig. 34(a) shows  $RMSE$  of power prediction by each method for the entire in-service data, and Fig. 34(b) represents the relative  $RMSE$ , of which all the  $RMSE$  results are normalized based on the  $RMSE$  of Combined method to identify the relative error degree of each method. The error metrics used in Fig. 34 are defined in Eqs. (24)–(25). Since Fig. 28 and Fig. 29 show theoretical results of added resistances assuming specific conditions, and Figs. 32 and 33 represent the error of the predicted value for the actual data in all operating conditions, the results of those figures might give slightly different levels of agreement

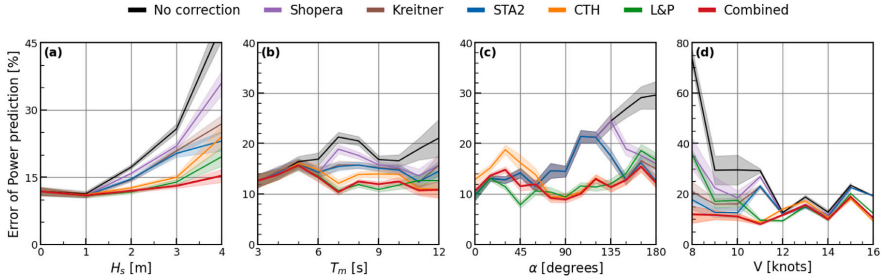


Fig. 32. Power prediction error of Ship A against (a) significant wave height, (b) mean wave period, (c) wave heading, (d) vessel speed according to various estimation methods. The y axis represents the absolute errors between the measurements and the estimation as a percentage.

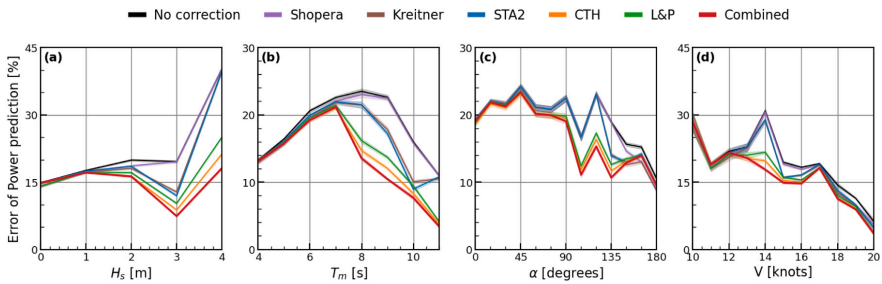


Fig. 33. Power prediction error of Ship B against (a) significant wave height, (b) mean wave period, (c) wave heading, (d) vessel speed according to various estimation methods.

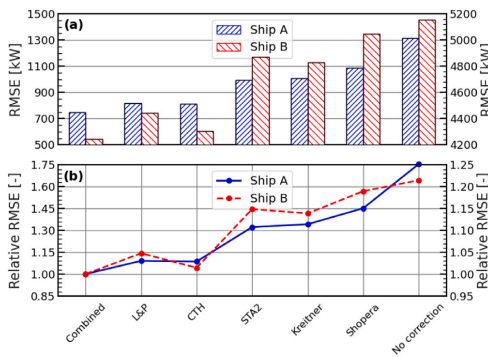


Fig. 34. Error analysis against full-scale measurements for Ship A. Figure (a) and Figure (b) show  $RMSE$  and relative  $RMSE$ .

between the different methods.

$$RMSE \text{ of power prediction} = \sqrt{\frac{1}{n} \sum_{i=1}^n (P_{MEAS,i} - P_{EST,i})^2} \quad (24)$$

$$Relative \text{ } RMSE = \frac{RMSE_{Empirical}}{RMSE_{Combined}} \quad (25)$$

where  $RMSE_{Empirical}$  is the  $RMSE$  of the selected empirical method, and  $RMSE_{Combined}$  is the  $RMSE$  of the Combined method.

It is confirmed that the correction of the propulsion power due to waves is large and strongly varying as function of  $V$ ,  $H_s$ ,  $\alpha$ , and  $T_m$  within the range of the collected data used in the study. Referring

to Fig. 34, Relative  $RMSE$ s on the two ships show a similar trend depending on the overall method, although there is a difference in the value. Compared to the  $RMSE$  of the Combined method, Ship A showed about 30%–45% larger errors for Kreitner, Shopera, and STA2 and about 8%–9% for CTH and L&P, while Ship B had 14%–19% and 1%–5% larger errors. Although we did not list the results here, applying the wave height correction factor also to the L&P method was effective in reducing errors against in-service data that we collected. However, we decided not to include the wave height correction to the L&P method, since it is not part of that method as it is originally published. One should take caution when it is intended to be used in general as it is still a preliminary concept.

In the process of obtaining the added wave resistance of the ship from the in-service data, many uncertainties may be included, such as errors included in the data and estimation of various resistance components. It should be noted that while the Combined method does not include any contribution from steering and yawing to the added resistance, such effects must be expected to be present, to some extent, in the in-service data. However, the following interpretation was obtained in common through the observations of Figs. 32–34. The methods only valid for head waves such as Shopera, Kreitner, and STA2 has the effect of reducing errors in the estimation of the added resistance compared to the case of “no correction”. More complicated methods such as CTH and L&P, which reflect hull shape information and can be used in any wave headings, can significantly reduce errors. The Combined method generally has smaller errors than other semi-empirical methods described here and shows noticeable performance in estimating added wave resistance at high wave height, resonance frequency, arbitrary wave headings, and relatively low ship speeds.

### 5. Conclusions

Estimating the added resistance in arbitrary waves of ships in a proper way has always been a challenging task. In this study, several

**Table A.1**

Experimental study of added resistance in arbitrary waves for tanker.

Model	$L_{pp}$ [m]	B [m]	$F_n$ [-]	Wave heading [deg].	Reference
VLCC	325	53	0.046/0.073/0.091	180	Lee (2015)
VLCC2	323.6	60	0.058	180	Diao et al. (2019)
S-VLCC	323	60	0.137	0/30/60/90/ 120/150/180	Park et al. (2019a)
SR221C	320	58	0.15	180	Kashiwagi et al. (2004)
KVLCC2	320	58	0/0.05/0.055/0.09/ 0.11/0.142/0.18	0/30/60/90/ 120/150/180	Kashiwagi (1992), Guo and Steen (2011); Sadat-Hosseini et al. (2013); Park et al. (2016); Sprenger et al. (2017); Seo et al. (2021)
Tanker2	310	47.2	0	180	Pinkster (1980)
Aframax	245	44	0.0525	180	Diao et al. (2019)
115k Aframax	239	44	0.156	180	Oh et al. (2015)
ULYSSES	187.3	32.3	0.06/0.12/0.168	120/150/180	Papageorgiou and Ptolemaios (2014); Martinsen (2016)
Handy tanker	176	32.2	0.159/0.171/0.183	180	Chen et al. (2019)
16k Product	145.4	23.4	0.177	180	Li et al. (2016)

**Table A.2**

Experimental study of added resistance in arbitrary waves for bulk carrier.

Model	$L_{pp}$ [m]	B [m]	$F_n$ [-]	Wave heading [deg].	Reference
JASNAOE-BC	320	58	0.037/0.074/0.124	30/90/150/180	Wicaksono and Kashiwagi (2018); Wicaksono (2019)
Suezmax BC	285	50	0/0.05/0.1/0.15	0/45/90/135/180	Kadamatsu (1988)
JBC	279	45	0.142	180	Kobayashi et al. (2021)
170k BC	279	45	0.128	0/30/60/90/ 120/150/180	Matsumoto (2000)
82k BC	223.5	32.6	0.017	135	Kumpeng et al. (2021)
Panamax BC1	231	38	0.05	180	Diao et al. (2019)
Panamax BC2	216.7	32.3	0.166/0.188	100/120/140/180	Ichinose (2010); Sogihara et al. (2011)
Handymax BC	192	36	0.17	180	Yu et al. (2017)
K-Supramax	192	36	0.172	120/150/180	Lee et al. (2019); Lee et al. (2020)
S-Cb84	178	32.4	0/0.049/0.099/0.166	30/90/150/180	Yasukawa et al. (2019)
S-Cb87	178	32.4	0.142/0.147	180	Yasukawa and Masaru (2020)
Handysize BC	160.4	27.2	0.15	180	Ichinose et al. (2012)
RIOS	2.4	0.4	0.18	180	Iwashita and Kashiwagi (2018)

**Table A.3**

Experimental study of added resistance in arbitrary waves for liquefied gas carrier.

Model	$L_{pp}$ [m]	B [m]	$F_n$ [-]	Wave heading [deg].	Reference
S-LNGC	290	45	0.13/0.17/0.188	0/30/60/120/150/180	T. Kim et al. (2019), Y. Kim et al. (2019), B.S. Kim et al. (2021)
125k LNG1	273.9	42.3	0.14/0.17/0.2	180	Wichers (1988)
125k LNG2	273	42	0.14/0.17/0.2	90/135/180	Bunnik (1999)
CSSRC LNG	160	26.6	0.036	180	Zheng et al. (2021)

semi-empirical methods were compared using abundant public experimental data with various types, and a new meta-model was proposed combining existing semi-empirical methods. This method is developed for the calculation of added resistance for large fleets of ships, so that robustness, computational efficiency, and applicability to a range of different ship types are priorities.

From the thorough investigation against experimental data, CTH and L&P methods were chosen as a basis for the new model due to high accuracy and the availability against arbitrary wave headings. The two methods have been combined smoothly using a tangent hyperbolic function according to wavelengths and wave headings. The coefficients constituting the combining function were tuned in the direction of minimizing *MSE* between model experiments and provided for each ship type. The Combined method showed improved results without significantly deviating from the prediction range of existing methods. It has been compared with full-scale measurements of a general cargo and a container ship. For the two vessels, the errors of Kreitner, Shopera, and STA2 were larger with about 14%–45%, and CTH and L&P with 1%–9%, compared to the *RMSE* of the Combined method. In particular, it was found that the estimation of added resistance in arbitrary waves was more effective in simulating the environment experienced by ships at sea than the methods considering only head seas. It also

showed good performance in estimating added wave resistance in the range of high wave height, resonance frequency, arbitrary wave headings, and low ship speed. As can be seen from the comparison of models using experimental test data and full-scale measurements, the Combined method showed good overall performance in various environments. The findings suggest that the new method can be widely applied for any purposes requiring the speed-power performance under the influence of waves such as reference at the initial design stage, speed corrections in sea trials, or overall performance evaluation of a fleet, where detailed hull shape information and advanced tools are not available.

Some of the tank tests in regular waves showed that the interval between wave frequencies was too sparse, that the experiment was not sufficiently conducted in some conditions such as short waves, or that collected samples were scattered even within similar frequency ranges. Due to these problems, it was difficult to estimate added resistance in irregular waves using them. If more experimental data in irregular waves are obtained, detailed comparisons between various estimation methods will be possible, and with more experimental data for various conditions, we expect that the reliability of the model can be improved. Furthermore, since the Combined method is combining two existing methods, it is likely that the Combined method has some of the same

**Table A.4**  
Experimental study of added resistance in arbitrary waves for general cargo ship.

Model	$L_{pp}$ [m]	B [m]	$F_n$ [-]	Wave heading [deg].	Reference
S.A. Van Der Stel	152.5	22.8	0.15/0.2/0.25/0.3	180	Gerritsma and Beukelman (1972); Journee (1976)
VWS 2388 (0/2/3)	146.3	24.4	0.2/0.25	180	Kracht (1984); Lee et al. (2018)
Series 60 (4210)	122.0	16.3	0.2/0.266/0.283	180	Sibul (1971); Ström-Tejsten (1973)
Series 60 (4211)	122.0	16.8	0.237/0.254	180	Ström-Tejsten (1973)
Series 60 (4212)	122.0	17.4	0.1/0.15/0.2/ 0.207/0.222/0.25	10/50/90/ 130/170/180	Ström-Tejsten (1973); Barea et al. (2006)
Series 60 (4213)	122.0	18.1	0.177/0.195	180	Ström-Tejsten (1973)
Series 60 (4214)	122.0	18.8	0.147/0.165	180	Ström-Tejsten (1973)

**Table A.5**  
Experimental study of added resistance in arbitrary waves for container ship.

Model	$L_{pp}$ [m]	B [m]	$F_n$ [-]	Wave heading [deg].	Reference
DTC	355	51	0/0.052/0.139	0/30/60/90/ 120/150/180	Moctar et al. (2012); Yokota et al. (2020); Sprenger et al. (2016, 2017)
WILS II	321	48.4	0.183	180	Söding et al. (2014)
HCNTR	315	48.2	0.204	180	Park et al. (2019b)
CON	300	40	0.2/0.247	0/45/90/ 140/160/180	Tsujimoto et al. (2009, 2012)
Panamax con	270	32.2	0.245	180	Bunnik et al. (2010)
KCS	230	32.2	0.054/0.1/0.16/ 0.26/0.33/0.4	0/45/90/135/180	Simonsen et al. (2013); Sadat-Hosseini et al. (2015); Stocker (2016); Yasukawa et al. (2019); Shivachev et al. (2020)
Feeder	191.1	32.3	0.22	90/120/180	Wada (1991)
S175	175	25.4	0.15/0.2/0.25/ 0.275/0.3	0/30/60/90/ 120/150/180	Fujii (1975); Nakamura and Naito (1977); Yamamoto (1986); Yasukawa (2006); Adnan and Yasukawa (2008)

shortcomings as them, as shown in the analysis of speed effect on wave resistance. If improved versions of the two methods we combined become available, where some of the shortcomings are alleviated, our method should be updated.

#### CRedit authorship contribution statement

**Young-Rong Kim:** Conceptualization, Investigation, Methodology, Software, Writing – original draft. **Ehsan Esmailian:** Conceptualization, Software, Writing – review & editing. **Sverre Steen:** Methodology, Writing – review & editing, Supervision.

#### Declaration of competing interest

The authors declare that they have no known competing financial interests or personal relationships that could have appeared to influence the work reported in this paper.

#### Data availability

The authors do not have permission to share data.

#### Acknowledgments

This study is part of the research projects CLIMMS — Climate change mitigation in the maritime sector (Research Council of Norway (RCN) project number 294771).

#### Appendix A. Experimental dataset

See Tables A.1–A.6

#### Appendix B. Detailed comparison of semi-empirical methods

##### Comparison according to the wave heading

As can be seen from the model test results, a peak of head waves was formed near the position where the wavelength and the ship length matched, that is, the radiation force was the largest. As the wave direction went from the head of the ship to the beam, the  $\lambda/L$  of the resonance tended to shorten and the resistance amplitude at the corresponding position tended to decrease.

In Fig. B1(a), the peak position of the STA2 is formed at a shorter  $\lambda/L$  than that of the model test, and this trend also can be seen in other model test cases with a relatively low Froude number on head waves. Since STA2 was mainly developed for the purpose of correction of sea trial results, the evaluation for the low-speed range was perhaps not much considered. According to Holt and Nielsen (2021), a lower Froude number tended to shift the peak value of the transfer function towards  $\lambda/L$  less than 1, which was not in line with the theory. Liu and Papanikolaou (2019) also pointed out that the peak position of STA2 was smaller than the actual value when Froude number was less than 0.15. Moreover, since STA2 was assuming the same response amplitude for 45 degrees off-bow, it did not adequately reflect changes in the resonance frequency position and amplitude of the added resistance according to changes in the encountering angle in head waves (Figs. B1(a)–(f)).

CTH method adjusts the peak position in arbitrary waves by using an encountered frequency correction factor, and the maximum added resistance is calculated by applying the amplitude adjustment factor and compensation factor for the roll motion. As can be seen from the figure, the peak position and the maximum value of the transfer function gradually decreased as the wave direction moved from bow to stern. On the other hand, the L&P method uses wave heading-based trigonometric functions to approximate the location of resonance frequency and maximum added resistance in various headings. As a result, the peak wavelength position was around  $\lambda/L = 1$  at 180 degrees, and as the heading angle decreased, the peak wavelength gradually decreased, and then the peak position was the shortest at 90 degrees. In following waves, the peak position was symmetrically set

**Table A.6**  
Experimental study of added resistance in arbitrary waves for ro-ro/ferry.

Model	$L_{pp}$ [m]	B [m]	$F_n$ [-]	Wave heading [deg].	Reference
Maric cruise	240	32	0.24	180	Liu et al. (2019)
HSVA cruise	220.3	32.2	0.166/0.232	0/30/60/90/120/150/180	Ley et al. (2014); Valanto et al. (2015)
PCC	190	32.3	0.249	140/180	Tsujimoto et al. (2009)
RoPax	90	17.8	0/0.087/0.2424	0/180	Sprengr et al. (2015); Liu and Papanikolaou (2020)

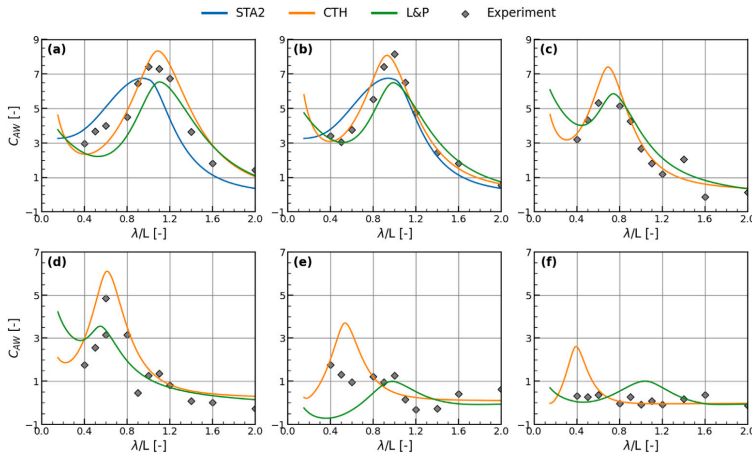


**Fig. B1.** Added resistance of 170k bulk carrier at  $F_n = 0.128$ . (a)  $\alpha = 180$ , (b)  $\alpha = 150$ , (c)  $\alpha = 120$ , (d)  $\alpha = 90$ , (e)  $\alpha = 30$ , (f)  $\alpha = 0$ .

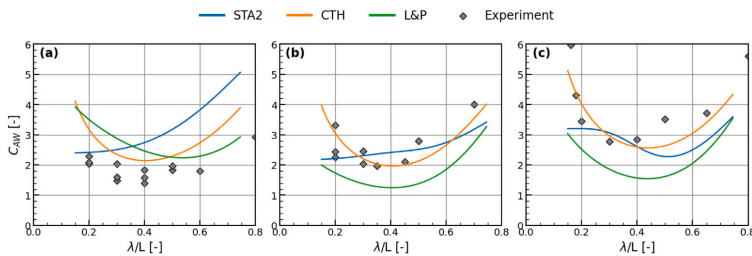


**Fig. B2.** Added resistance in short waves of (a) SR221C,  $F_n = 0.15$ , (b) DTC,  $F_n = 0.139$ , (c) HSVA,  $F_n = 0.232$ . The figure corresponds to the results of head waves.

based on 90 degrees. In both methods, the maximum added resistance decreased as the wave heading decreased, but as explained earlier, the peak position tended to be somewhat different.

**Comparison in short waves**

For added resistance in short waves, wave diffraction due to bow reflection dominates, while the effect by wave radiation is almost insignificant. As can be seen from Fig. B2, STA2 has little curvature in the short waves of wavelength less than 0.3. As Yang et al. (2018) pointed out in their paper, since the reflection coefficient of STA2 becomes unity in the short wave region resulting in constant resistance coefficient, STA2 did not properly estimate an increase of added resistance in the corresponding wavelength range in our case studies. On the other hand, L&P and CTH seems to reasonably estimate the tail shape for short waves., The CTH method was most consistent with experimental results in short waves.

**Comparison at high Froude number**

As illustrated in Fig. B3, STA2 was less accurate in estimating the added wave resistance of a high Froude number than other methods because the maximum resistance at the resonance frequency was underestimated or the positions of the resonance frequency did not match. Meanwhile, in accordance with the bar chart (Fig. 5), the added resistance value estimated from L&P had greater MSE under high-speed operating conditions than that of CTH. As a result of a closer look at the model experiments conducted at Froude number more than 0.25, it generally consisted of datasets of ships that operate in high-speed, such as container ship, general cargo, and Ro-Ro/Ferry. In the case of a container ship at a high Froude number, the two methods provided almost similar results, and even though not described here, there was also no significant difference in the case of other container ships. From such findings, it was determined that this error was not caused by the high Froude number but rather by certain ship types such as general cargo and ro-ro/ferry.

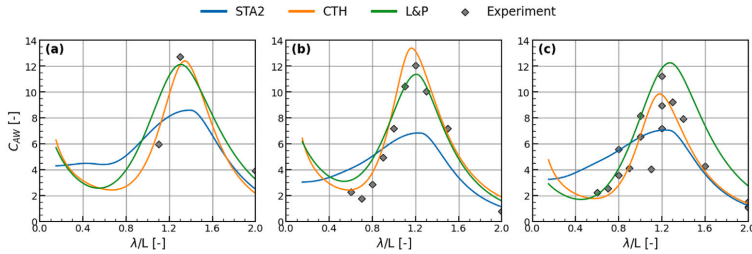


Fig. B3. Added resistance in high Froude number of (a) KCS,  $F_n = 0.4$ , (b) S175,  $F_n = 0.3$ , (c) S60,  $F_n = 0.283$ . The figure corresponds to the results of head waves.

## References

- Anan, F., Yasukawa, H., 2008. Experimental investigation of wave-induced motions of an obliquely moving ship. In: Proceedings of 2nd Regional Conference on Vehicle Engineering and Technology.
- Aufm Keller, W., 1973. Extended diagrams for determining the resistance and required power for single-screw ships. *Int. Shipbuild. Prog.* 20 (225), 133–142.
- Baree, M.S., Islam, M.R., Inoue, Y., 2006. An investigation of added resistance of ships in oblique seas. *HKIE Trans.* 13 (2), 1–8.
- Boese, P., 1970. Eine Einfache Methode Zur Berechnung Der Widerstandserhöhung Eines Schiffes Im Seegang. Technical Report.
- Boom, H., Huisman, H., Mennen, F., 2013. New guidelines for speed/power trials: Level playing field established for IMO EEDI. SWZ Maritime, Schip En Werf de Zee Foundation, Rotterdam.
- Bunnik, T.H., 1999. Seakeeping calculations for ships, taking into account the non-linear steady waves.
- Bunnik, T., Van Daalen, E., Kapsenberg, G., Shin, Y., Huijismans, R., Deng, G., Delhommeau, G., Kashiwagi, M., Beck, B., 2010. A comparative study on state-of-the-art prediction tools for seakeeping. In: *Onr Snh 2010*, Pasadena, California. *Onr*, pp. 1–13.
- Chen, X., Ren, Y., Xiao, H.-s., Cai, X.-g., Zhu, R.-c., 2019. A MDHOBEM energy radiated method to evaluate added wave resistance of ship. In: The 29th International Ocean and Polar Engineering Conference. OnePetro.
- Dalheim, Ø.Ø., Steen, S., 2020. A computationally efficient method for identification of steady state in time series data from ship monitoring. *J. Ocean Eng. Sci.* 5 (4), 333–345.
- Diao, F., Chen, J.-k., Duan, W.-y., Zhou, W.-x., Chen, J., Wei, J.-f., 2019. Prediction of added resistance of a ship in waves at low speed. *J. Hydrodyn.* 31 (6), 1231–1239.
- Faltinsen, O.M., 1980. Prediction of resistance and propulsion of a ship in a seaway. In: Proceedings of the 13th Symposium on Naval Hydrodynamics. Tokyo, 1980.
- Fujii, H., 1975. Experimental study on the resistance increase of a ship in regular oblique waves. In: Proc. of 14th ITTC, 1975, Vol. 4, pp. 351–360.
- Fujiwara, T., 2006. A new estimation method of wind forces and moments acting on ships on the basis of physical components models. *J. Jpn. Soc. Nav. Archit. Ocean Eng.* 2, 243–255.
- Gerritsma, J., Beukelman, W., 1972. Analysis of the resistance increase in waves of a fast cargo ship. *Int. Shipbuild. Prog.* 19 (217), 285–293.
- Guldhammer, H., Harvald, S.A., 1974. SHIP resistance-effect of form and principal dimensions (Revised). Danish Technical Press, Denmark, Danmarks Tekniske Højskole, Kademisk Forlag, St. Kannikestrade 8, DK 1169 Copenhagen.
- Guo, B.-j., Steen, S., 2011. Evaluation of added resistance of KVLCC2 in short waves. *J. Hydrodyn. Ser. B* 23 (6), 709–722.
- Guo, B., Steen, S., Deng, G., 2012. Seakeeping prediction of KVLCC2 in head waves with RANS. *Appl. Ocean Res.* 35, 56–67.
- Gupta, P., Taskar, B., Steen, S., Rasheed, A., 2021. Statistical modeling of ship's hydrodynamic performance indicator. *Appl. Ocean Res.* 111, 102623.
- Haiden, T., Janousek, M., Bidlot, J., Buizza, R., Ferranti, L., Prates, F., Vitart, F., 2018. Evaluation of ECMWF Forecasts, Including the 2018 Upgrade. European Centre for Medium Range Weather Forecasts Reading, UK.
- Havelock, T.H., 1942. XLVII. The drifting force on a ship among waves. *Lond. Edinb. Dub. Philos. Mag. J. Sci.* 33 (221), 467–475.
- Hollenbach, K.U., 1998. Estimating resistance and propulsion for single-screw and twin-screw ships-ship technology research 45 (1998). *Schiffstechnik* 45 (2), 72.
- Holt, P., Nielsen, U.D., 2021. Preliminary assessment of increased main engine load as a consequence of added wave resistance in the light of minimum propulsion power. *Appl. Ocean Res.* 108, 102543.
- Holtrop, J., 1984. A statistical re-analysis of resistance and propulsion data. Published in International Shipbuilding Progress, ISP, Volume 31, Number 363.
- Ichinose, Y., 2010. Estimation of added resistance in waves in a ballast condition. *J. Jpn. Soc. Nav. Archit. Ocean Eng.* 11, 109–116.
- Ichinose, Y., Tsujimoto, M., Shiraishi, K., Sogihara, N., 2012. Decrease of ship speed in actual sea of a bulk carrier in full load and ballast conditions-model test and onboard measurement. *J. Jpn. Soc. Nav. Archit. Ocean Eng.* 15, 37–45.
- IMO, 2016. Supplementary information on the draft revised guidelines for determining minimum propulsion power to maintain the manoeuvrability of ships in adverse conditions, submitted by Denmark, Germany and Japan. MEPC70/INF.30.
- ITTC, 2005. Recommended procedures and guidelines: Full scale measurements speed and power trials analysis of speed.
- ITTC, 2017. Recommended procedures and guidelines: Preparation, conduct and analysis of speed/power trials.
- Iwashita, H., Kashiwagi, M., 2018. An innovative EFD for studying ship seakeeping. In: Proceedings of 33rd IWWWFB (Guidel-Plages, France), pp. 85–88.
- Jinkine, V., Ferdinand, V., 1974. A method for predicting the added resistance of fast cargo ships in head waves. *Int. Shipbuild. Prog.* 21 (238), 149–167.
- Joncquez, S., 2009. Second-Order Forces and Moments Acting on Ships in Waves (Ph. D. Thesis). Technical University of Denmark, Copenhagen, Denmark.
- Joosen, W., 1966. Added resistance of ships in waves. In: Proc. 6th Symp. on Naval Hydrodynamics. Washington, pp. 637–647.
- Journee, J.M., 1976. Motions, Resistance and Propulsion of a Ship in Longitudinal Regular Waves. TUDelft, Faculty of Marine Technology, Ship Hydromechanics Laboratory, Report No. 428.
- Kadomatsu, K., 1988. Study on the Required Minimum Output of Main Propulsion Engine Considering Maneuverability in Rough Sea. Yokohama National University.
- Kashiwagi, M., 1992. Added resistance, wave-induced steady sway force and yaw moment on an advancing ship.
- Kashiwagi, M., Sugimoto, K., Ueda, T., Yamasaki, K., Arihama, K., Kimura, K., Yamashita, R., Itoh, A., Mizokami, S., 2004. An analysis system for propulsive performance in waves. *J.-Kansai Soc. Nav. Archit. Jpn.* 67–82.
- Kim, K.-H., Kim, Y., 2011. Numerical study on added resistance of ships by using a time-domain rankine panel method. *Ocean Eng.* 38 (13), 1357–1367.
- Kim, B.-S., Oh, M.-J., Lee, J.-H., Kim, Y.-h., Roh, M.-I., 2021. Study on hull optimization process considering operational efficiency in waves. *Processes* 9 (5), 898.
- Kim, Y., Park, D.-M., Lee, J.-H., Lee, J., Kim, B.-S., Yang, K.-K., Oh, S., Lee, D.-Y., 2019. Numerical analysis and experimental validation of added resistance on ship in waves. *J. Ship Res.* 63 (04), 268–282.
- Kim, T., Yoo, S., Kim, H.J., 2021. Estimation of added resistance of an LNG carrier in oblique waves. *Ocean Eng.* 231, 109068.
- Kim, T., Yoo, S., Oh, S., Kim, H.J., Lee, D., Kim, B., 2019. Numerical and experimental study on the estimation of added resistance of an LNG carrier in waves. *Int. J. Offshore Polar Eng.* 29 (01), 24–32.
- Kitamura, F., Ueno, M., Fujiwara, T., Sogihara, N., 2017. Estimation of above water structural parameters and wind loads on ships. *Ships Offshore Struct.* 12 (8), 1100–1108.
- Kobayashi, H., Kume, K., Orihara, H., Ikebuchi, T., Aoki, I., Yoshida, R., Yoshida, H., Ryu, T., Arai, Y., Katagiri, K., et al., 2021. Parametric study of added resistance and ship motion in head waves through RANS: Calculation guideline. *Appl. Ocean Res.* 110, 102573.
- Kraich, A., 1984. Einfluss Des Bugwulstes Auf Den Leistungsbedarf Eines Schiffes Im Seegang. *Forschungsbericht des Dt. Schiffbaus.*
- Kreitner, J., 1939. Heave, pitch and resistance of ships in a seaway. *Trans. Royal Inst. Nav. Archit., London* 87.
- Kunpeng, C., Fan, Y., Yunlong, D., 2021. RANS CFD seakeeping simulation for an 82k DWT vessel in head and oblique waves. In: *J. Phys.: Conf. Ser.* 1834, (1), IOP Publishing, 012009.
- Kuroda, M., Tsujimoto, M., Fujiwara, T., Ohmatsu, S., Takagi, K., 2008. Investigation on components of added resistance in short waves. *J. Jpn. Soc. Nav. Archit. Ocean Eng.* 8, 171–176.
- Lang, X., Mao, W., 2020. A semi-empirical model for ship speed loss prediction at head sea and its validation by full-scale measurements. *Ocean Eng.* 209, 107494.
- Lang, X., Mao, W., 2021. A practical speed loss prediction model at arbitrary wave heading for ship voyage optimization. *J. Mar. Sci. Appl.* 20 (3), 410–425.

- Lee, S.-M., 2015. Experimental study on added resistance of VLCC for ship's operating condition in waves. *J. Korean Soc. Mar. Environ. Saf.* 21 (3), 240–245.
- Lee, J.-H., Kim, Y., Kim, B.-S., Gerhardt, F., 2021. Comparative study on analysis methods for added resistance of four ships in head and oblique waves. *Ocean Eng.* 236, 109552.
- Lee, J.-H., Kim, B.-S., Kim, B.-S., Lee, J., Kim, Y., Paik, K.-J., Kim, T., Yang, J.-H., Song, K.-H., Kim, P., et al., 2020. Comparative study on added resistance of a bulk carrier in regular head and oblique waves. In: *The 30th International Ocean and Polar Engineering Conference*. OnePetro.
- Lee, J.-h., Kim, S.-s., Lee, S.-s., Kang, D., Lee, J.-c., 2018. Prediction of added resistance using genetic programming. *Ocean Eng.* 153, 104–111.
- Lee, C.-M., Yu, J.-W., Choi, J.-E., Lee, I., 2019. Effect of bow hull forms on the resistance performance in calm water and waves for 66k DWT bulk carrier. *Int. J. Nav. Archit. Ocean Eng.* 11 (2), 723–735.
- Ley, J., Sigmund, S., el Moctar, O., 2014. Numerical prediction of the added resistance of ships in waves. In: *International Conference on Offshore Mechanics and Arctic Engineering*, Vol. 45400. American Society of Mechanical Engineers, V002T08A069.
- Li, C., Ma, X., Chen, W., Li, J., Dong, G., 2016. Experimental investigation of self propulsion factor for a ship in regular waves. *Shipbuild China* 57 (1), 1–8.
- Liu, S., 2020. Revisiting the influence of a ship's draft on the drift force due to diffraction effect. *Ship Technol. Res.* 67 (3), 175–180.
- Liu, S., Papanikolaou, A., 2016. Fast approach to the estimation of the added resistance of ships in head waves. *Ocean Eng.* 112, 211–225.
- Liu, S., Papanikolaou, A., 2019. Approximation of the added resistance of ships with small draft or in ballast condition by empirical formula. *Proc. Inst. Mech. Eng. M* 233 (1), 27–40.
- Liu, S., Papanikolaou, A., 2020. Regression analysis of experimental data for added resistance in waves of arbitrary heading and development of a semi-empirical formula. *Ocean Eng.* 206, 107357.
- Liu, S., Papanikolaou, A., Feng, P., Fan, S., 2019. A multi-level approach to the prediction of the added resistance and powering of ships in waves. In: *International Conference on Offshore Mechanics and Arctic Engineering*, Vol. 58851. American Society of Mechanical Engineers, V07B706A037.
- Liu, S., Shang, B., Papanikolaou, A., Bolbot, V., 2016. Improved formula for estimating added resistance of ships in engineering applications. *J. Mar. Sci. Appl.* 15 (4), 442–451.
- Martinsen, M., 2016. A Design Tool for Estimating Wave Added Resistance of Container Ships (Master's Thesis). Technical University of Denmark, Copenhagen, Denmark.
- Maruo, H., 1957. The excess resistance of a ship in rough seas. *Int. Shipbuild. Prog.* 4 (35), 337–345.
- Maruo, H., 1960. Wave resistance of a ship in regular head seas. *Bull. Fac. Eng. Yokohama Natl. Univ.* 9, 73–91.
- Maruo, H., 1963. Resistance in waves, research on seakeeping qualities of ships in Japan. *Soc. Nav. Archit. Jpn.* 8, 67–102.
- Matsumoto, K., 2000. Development of energy saving bow shape at sea. In: *Proc. of the 4th Osaka Colloquium on Seakeeping Performance of Ships*, 2000, pp. 479–485.
- Minsas, K., 1982. Grunlag for Fartsprognoser. Technical Report, Marintek (former: Norges Hydrodynamiske Laboratorier).
- Moctar, O.e., Shigunov, V., Zorn, T., 2012. Duisburg test case: Post-panamax container ship for benchmarking. *Ship Technol. Res.* 59 (3), 50–64.
- Mourkogiannis, D., Liu, S., 2021. Investigation of the influence of the main dimensional ratios of a ship on the added resistance and drift force in short waves. In: *The 31st International Ocean and Polar Engineering Conference*. OnePetro.
- Nakamura, S., Naito, S., 1977. Propulsive performance of a container ship in waves. *J. Soc. Nav. Archit. Jpn.* 15.
- Oh, S., Yang, J., Park, S.-H., 2015. Computational and experimental studies on added resistance of afamax-class tankers in head seas. *J. Soc. Nav. Archit. Korea* 52 (6), 471–477.
- Orihara, H., Miyata, H., 2003. Evaluation of added resistance in regular incident waves by computational fluid dynamics motion simulation using an overlapping grid system. *J. Mar. Sci. Technol.* 8 (2), 47–60.
- Papageorgiou, S., Ptolemaios, I., 2014. A comparison of methods for predicting the wave added resistance of slow steaming ships.
- Papanikolaou, A., Zaraphonitis, G., Bitner-Gregersen, E., Shigunov, V., El Moctar, O., Soares, C.G., Reddy, D.N., Sprenger, F., 2015. Energy efficient safe ship operation (SHOPERA). In: *SNAME 5th World Maritime Technology Conference*. OnePetro.
- Park, D.-M., Kim, Y., Seo, M.-G., Lee, J., 2016. Study on added resistance of a tanker in head waves at different drafts. *Ocean Eng.* 111, 569–581.
- Park, D.-M., Lee, J.-H., Jung, Y.-W., Lee, J., Kim, Y., Gerhardt, F., 2019a. Experimental and numerical studies on added resistance of ship in oblique sea conditions. *Ocean Eng.* 186, 106070.
- Park, D.-M., Lee, J.-H., Lee, J., Kim, B.-S., Kim, B.-S., Yang, K.-K., Kim, Y., Lee, Y.-G., Kim, T., Yang, J.-H., et al., 2019b. Comparative study on added resistance of a container ship in waves. In: *The 29th International Ocean and Polar Engineering Conference*. OnePetro.
- Pinkster, J.A., 1980. Low frequency second order wave exciting forces on floating structures.
- Sadat-Hosseini, H., Toxopeus, S., Kim, D.H., Castiglione, T., Sanada, Y., Stocker, M., Simonsen, C., Otzen, J.F., Toda, Y., Stern, F., 2015. Experiments and computations for KCS added resistance for variable heading. In: *SNAME 5th World Maritime Technology Conference*. OnePetro.
- Sadat-Hosseini, H., Wu, P.-C., Carrica, P.M., Kim, H., Toda, Y., Stern, F., 2013. CFD verification and validation of added resistance and motions of KVLC2 with fixed and free surge in short and long head waves. *Ocean Eng.* 59, 240–273.
- Salvesen, N., 1978. Added resistance of ships in waves. *J. Hydraul. Eng.* 104 (1), 24–34.
- Seo, M.G., Ha, Y.J., Nam, B.W., Kim, Y., 2021. Experimental and numerical analysis of wave drift force on KVLC2 moving in oblique waves. *J. Mar. Sci. Eng.* 9 (2), 136.
- Seo, M.-G., Park, D.-M., Yang, K.-K., Kim, Y., 2013. Comparative study on computation of ship added resistance in waves. *Ocean Eng.* 73, 1–15.
- Shaher Sabit, A., 1972. An analysis of the series 60 results. *Int. Shipbuild. Prog.* 19 (211), 81–97.
- Shigunov, V., El Moctar, O., Papanikolaou, A., Potthoff, R., Liu, S., 2018. International benchmark study on numerical simulation methods for prediction of manoeuvrability of ships in waves. *Ocean Eng.* 165, 365–385.
- Ships, I., 2015. Marine technology—Guidelines for the assessment of speed and power performance by analysis of speed trial data. ISO: Geneva, Switzerland.
- Shivachev, E., Khorasanchi, M., Day, S., Turan, O., 2020. Impact of trim on added resistance of KRISO container ship (KCS) in head waves: An experimental and numerical study. *Ocean Eng.* 211, 107594.
- Sibul, O., 1971. Measurements and Calculations of Ship Resistance in Waves. Technical Report, California Univ Berkeley Coll of Engineering.
- Sigmund, S., El Moctar, O., 2018. Numerical and experimental investigation of added resistance of different ship types in short and long waves. *Ocean Eng.* 147, 51–67.
- Simonsen, C.D., Otzen, J.F., Joncquez, S., Stern, F., 2013. EFD and CFD for KCS heaving and pitching in regular head waves. *J. Mar. Sci. Technol.* 18 (4), 435–459.
- Simonsen, C., Otzen, J., Nielsen, C., Stern, F., 2014. CFD prediction of added resistance of the KCS in regular head and oblique waves. In: *30th Symposium on Naval Hydrodynamics*, pp. 2–7.
- Söding, H., Shigunov, V., Schellin, T.E., Moctar, O.e., 2014. A rankine panel method for added resistance of ships in waves. *J. Offshore Mech. Arct. Eng.* 136 (3).
- Sogihara, N., Tsujimoto, M., Ichinose, Y., Minami, Y., Sasaki, N., Ken, T., 2011. Performance prediction of a blunt ship in oblique waves. *J. Jpn. Soc. Nav. Archit. Ocean Eng.* 12, 9–15.
- Sprenger, F., Hassani, V., Maron, A., Delefortrie, G., Van Zwijnsvoorde, T., Cura-Hochbaum, A., Lengwinat, A., 2016. Establishment of a validation and benchmark database for the assessment of ship operation in adverse conditions. In: *International Conference on Offshore Mechanics and Arctic Engineering*, Vol. 49927. American Society of Mechanical Engineers, V001T01A039.
- Sprenger, F., Maron, A., Delefortrie, G., Hochbaum, A., Fathi, D., 2015. Mid-term review of tank test results. SHOPERA Project Deliverable D, 3.
- Sprenger, F., Maron, A., Delefortrie, G., Van Zwijnsvoorde, T., Cura-Hochbaum, A., Lengwinat, A., Papanikolaou, A., 2017. Experimental studies on seakeeping and maneuverability of ships in adverse weather conditions. *J. Ship Res.* 61 (03), 131–152.
- Steen, S., Aarsnes, J.V., 2014. Experimental methods in marine hydrodynamics. In: *Lecture Notes*.
- Stocker, M.R., 2016. Surge Free Added Resistance Tests in Oblique Wave Headings for the KRISO Container Ship Model. The University of Iowa.
- Ström-Tejsten, J., 1973. Added resistance in waves. In: *Paper 3 of the Annual Meeting New York of the Society of Naval Architects and Marine Engineers*, SNAME Transactions 1973, Paper: T1973-1 Transactions. Naval Ship Research and Development Center, Bethesda, Maryland, USA, Research and Development Report, Ship Performance Department.
- Takahashi, T., 1988. A practical prediction method of added resistance of a ship in waves and the direction of its application to hull form design. *Trans. West-Jpn. Soc. Nav. Archit.* 75, 75–95.
- Tsujimoto, M., Kuroda, M., Shibata, K., Sogihara, N., Takagi, K., 2009. On a calculation of decrease of ship speed in actual seas. *J. Jpn. Soc. Nav. Archit. Ocean Eng.* 9, 79–85.
- Tsujimoto, M., Kuroda, M., Shiraiishi, K., Ichinose, Y., Sogihara, N., 2012. Verification on the resistance test in waves using the actual sea model basin. *J. Jpn. Soc. Nav. Archit. Ocean Eng.* 16, 33–39.
- Tsujimoto, M., Shibata, K., Kuroda, M., Takagi, K., 2008. A practical correction method for added resistance in waves. *J. Jpn. Soc. Nav. Archit. Ocean Eng.* 8, 177–184.
- Ursell, F., 1947. The effect of a fixed vertical barrier on surface waves in deep water. In: *Mathematical Proceedings of the Cambridge Philosophical Society*, Vol. 43, no. 3. Cambridge University Press, pp. 374–382.
- Valanto, P., Hong, Y., et al., 2015. Experimental investigation on ship wave added resistance in regular head, oblique, beam, and following waves. In: *The Twenty-Fifth International Ocean and Polar Engineering Conference*. International Society of Offshore and Polar Engineers.
- Wada, Y., 1991. A study on speed drop of a ship in oblique waves. In: *Transactions of the West-Japan Society of Naval Architects*. The Japan Society of Naval Architects and Ocean Engineers, pp. 113–128.
- Wang, J., Bielicki, S., Kluwe, F., Orihara, H., Xin, G., Kume, K., Oh, S., Liu, S., Feng, P., 2021. Validation study on a new semi-empirical method for the prediction of added resistance in waves of arbitrary heading in analyzing ship speed trial results. *Ocean Eng.* 240, 109959.
- Wicaksono, A., 2019. A unified computation method for seakeeping-maneuvering of a ship in waves using slender-ship theory and MMG model.



- Wicaksono, A., Kashiwagi, M., 2018. Wave-induced steady forces and yaw moment of a ship advancing in oblique waves. *J. Mar. Sci. Technol.* 23 (4), 767–781.
- Wichers, J.E.W., 1988. A simulation model for a single point moored tanker.
- Yamamoto, O., 1986. Study on an approximate calculation method of resistance increase in oblique regular waves. *J. Kansai Soc. Nav. Archit.* (201).
- Yang, K.-K., Kim, Y., Jung, Y.-W., 2018. Enhancement of asymptotic formula for added resistance of ships in short waves. *Ocean Eng.* 148, 211–222.
- Yasukawa, H., 2006. Simulations of ship maneuvering in waves (1 st report: Turning motion). *J. Jpn Soc. Nav. Archit. Ocean Eng.* 4, 127–136.
- Yasukawa, H., Hirata, N., Matsumoto, A., Kuroiwa, R., Mizokami, S., 2019. Evaluations of wave-induced steady forces and turning motion of a full hull ship in waves. *J. Mar. Sci. Technol.* 24 (1), 1–15.
- Yasukawa, H., Masaru, T., 2020. Impact of bow shape on added resistance of a full hull ship in head waves. *Ship Technol. Res.* 67 (3), 136–147.
- Yokota, S., Kuroda, M., Fukasawa, R., Ohba, H., Tsujimoto, M., 2020. Detailed study on the behavior of ships in very short waves. In: *International Conference on Offshore Mechanics and Arctic Engineering*, Vol. 84386. American Society of Mechanical Engineers, V06BT06A020.
- Yu, J.-W., Lee, C.-M., Lee, I., Choi, J.-E., 2017. Bow hull-form optimization in waves of a 66,000 DWT bulk carrier. *Int. J. Nav. Archit. Ocean Eng.* 9 (5), 499–508.
- Zheng, M., Ni, Y., Wu, C., Jo, H., 2021. Experimental investigation on effect of sloshing on ship added resistance in head waves. *Ocean Eng.* 235, 109362.

# Article 3

## Application of machine learning algorithms for predicting added resistance in arbitrary wave headings of a ship

Youngrong Kim, Sverre Steen

*Proceedings of the ASME 2022 41st International  
Conference on Ocean, Offshore and Arctic Engineering  
OMAE2022  
June 5-10, 2022, Hamburg, Germany  
DOI: [10.1115/OMAE2022-78433](https://doi.org/10.1115/OMAE2022-78433)*



## APPLICATION OF MACHINE LEARNING ALGORITHMS FOR PREDICTING ADDED RESISTANCE IN ARBITRARY WAVE HEADINGS OF A SHIP

Young-Rong Kim,\* Sverre Steen  
Department of Marine Technology  
Norwegian University of Science and Technology  
7052 Otto Nielsens veg. 10, Trondheim  
Norway

### ABSTRACT

Vessels experience additional resistance by waves during navigation, which becomes a factor that increases energy consumption and exhaust gas emissions. Proper estimation and understanding of this additional resistance is an important task in the marine industry. In this study, we propose a machine-learning model that predicts added resistance in arbitrary wave headings using basic ship parameters. First, extensive model experimental data on added resistance for different ship types and sizes of ships were acquired. To build a proper machine learning model, algorithms such as extreme gradient boosting (XGB), random forest (RF), artificial neural network (ANN),  $k$ -nearest neighbor (ANN), gaussian process regression (GPR), and support vector regression (SVR) were considered. Through nested cross-validation, the evaluation and hyperparameter tuning of algorithms were performed together. As a result, SVR was selected among the candidate models due to high accuracy with robustness to the outliers. In the validation with test data of head waves and all wave headings, the  $R^2$  scores of the selected model were 0.6738-0.7584 and 0.6744-0.7449, respectively, which was better than estimation methods for added resistance in head waves such as STAWAVE-2 and Cepowski (2020), and similar accuracy to those applicable in arbitrary wave headings. Even estimation of added resistance in irregular waves of sea states, the relative deviation with the semi-empirical methods for arbitrary waves was not large, on average 10%.

Keywords: Wave added resistance; machine learning; ship hydrodynamics; model test

### NOMENCLATURE

$\alpha$	Wave heading
$B$	Breadth
$L$	Length between perpendiculars
$T_m$	Mean draft
$T_d$	Design draft
$C_b$	Block coefficient
$\theta$	Trim angle
$F_n$	Froude number
$\lambda$	Wave length
$C_{aw}$	Non-dimensional added wave resistance coefficient
$R_{aw}$	Added resistance in regular waves
$R_{AW}$	Mean wave resistance increase in irregular waves
$\rho$	Water density
$g$	Gravity acceleration
$\omega$	Circular wave frequency
$S$	Modified Pierson-Moskowitz spectrum of ITTC 1978
$H_s$	Significant wave height
$T_1$	Average wave period
$\zeta_a$	Wave amplitude

### 1. INTRODUCTION

During the voyage, the ship is subject to added resistance due to its surrounding wave conditions, which may directly affect

\*Corresponding author: youngrong.kim@ntnu.no

the speed-power performance. For such reason, the estimation of added resistance in waves has been of great interest to many researchers. There are various ways to estimate the added wave resistance of a ship, but especially for purposes such as the initial design stage in which the detailed geometry is not determined, or performance analysis of global fleets for which it is difficult to obtain detailed hull shape, one often relies on semi-empirical methods.

STAWAVE-2 (Boom, 2013) [1], perhaps the most widely known semi-empirical method, uses the ship main dimensions to approximate the transfer function of the mean resistance increase in head waves. It has mainly been applied as a correction method for the sea trial. Liu and Papanicolau (2016) [2] proposed a method of combining Faltinsen (1980) [3] and Jinkine and Ferdinande (1974) [4], and in subsequent studies [5–7], the method was extended to various wave headings by regression analysis based on extensive experimental data. Lang and Mao (2020, 2021) [8, 9] also proposed an estimation method for added resistance in arbitrary waves based on Tsujimoto et al. (2008) [10], and Jinkine and Ferdinande (1974) [4]. However, such semi-empirical methods for arbitrary wave headings required more detailed information related to the hull shape such as length of entrance and length of run. Meanwhile, there have been attempts to apply a machine learning algorithm. Cepowski (2020) [11] proposed a method of predicting added resistance by applying ANN to model experimental data in head waves, which showed very good agreement with the test data set. Martic et al. (2021) [12] presented an ANN model for evaluating added resistance in head waves for a container ship in their study, and the 3D panel method was used to implement the model. Even though the ANN-based methods showed good performance for the prediction of added wave resistance, they were limited to head wave regions, and the consideration of various machine learning algorithms was insufficient.

Based on the results of these preceding studies, this study proposes the application of machine learning models that predict added resistance not only in head waves but also in arbitrary waves using model experimental data including basic information on ships. The following Section 2 introduces the overall procedure for implementing the machine learning model, and descriptions regarding the dataset, input parameters, and candidate machine learning algorithms. Section 3 selects an appropriate model through nested cross-validation and analyzes the model using explainable AI methods. Thereafter, verification of test data with other semi-empirical methods including the selected model in the study is performed, and comparison is also performed on irregular waves. Section 4 includes conclusions.

## 2. MATERIALS AND METHODS

### 2.1 Research procedure

In this study, in order to compare and evaluate the prediction methods for added resistance in waves, the measured values for added wave resistance coefficients of model ships performed in various towing tanks and seakeeping basins were used. The dataset is composed of data from published literature, and consists of a total of 47 ships and 2519 samples, including various wave directions and experimental conditions. Figure 1 shows the added resistance coefficient according to wavelength in various wave headings from the data samples used in the study. As can be seen from the figure, plotted samples show certain trends, and large scatterings of samples are observed, especially in the short wavelength and resonance frequency regions. There may be various causes for such scattering, but factors such as different water tank environments and difficulties in implementing some experimental conditions are believed to have played a major role. This study tried to reduce the effect of some samples with large deviations from the overall trend by using as many samples as possible to implement the model. Moreover, to implement a model predicting added wave resistance coefficient ( $C_{aw}$ ) that may have variability according to different hull shapes and experimental conditions, we introduced a machine learning algorithm represented by  $f(x)$  of Equation 1 such as XGB, RF, KNN, ANN, GPR, and SVR in this study. For generalization and improved performance of the model, the dimensionless parameters  $L/B$ ,  $B/T_m$ ,  $T_m/T_d$ ,  $\theta$ ,  $C_b$ ,  $F_n$ ,  $\alpha$ , and  $\lambda/L$  related to the hull dimension and operating conditions of the ship were used as the inputs to the model. Here, we selected inputs that can be easily obtained without knowing the detailed hull shape among the parameters used in several previous studies [1, 7, 9, 11]. The results of correlation analysis on the input parameters of the model are shown in Figure 2, and the values in the figure represent the Pearson correlation coefficients between parameters. Here,  $\alpha$  and  $F_n$  show the greatest linear correlation with  $C_{aw}$ , which is in line with the fact that the added wave resistance of the ship increases at high speed and head waves. On the other hand, there seems to be a weak or almost no linear correlation with the added wave resistance as other parameters have a correlation coefficient of less than 0.2.

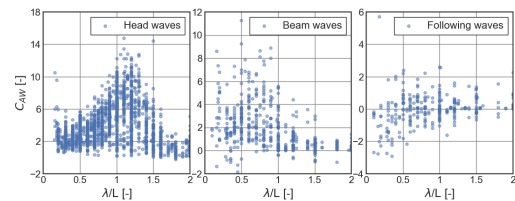


**FIGURE 1.** SCATTER PLOTS OF ADDED WAVE RESISTANCE COEFFICIENT ACCORDING TO THE WAVE HEADINGS.



previous residual to reinforce the weak learner. This process is repeated continuously until the defined criteria are met, and the prediction results for this sample are expressed as in Equation 2. Since XGB aims to prevent overfitting and optimize computational resources, the objective function includes a loss function and a regularization term, as shown in Equation 3.

$$\hat{y}_i = \sum_{k=1}^K f_k(x_i) \quad (2)$$

$$Obj = \sum_{i=1}^n l(y_i, \hat{y}_i) + \sum_{k=1}^K \Omega(f_k) \quad (3)$$

where  $K$  represents the number of decision trees in the ensemble model,  $f_k$  is the  $k$ -th decision tree in the model,  $l$  is the loss function, and  $\Omega$  is a penalization term for the complexity of the model.

**Random forest (RF)** Random forest is an ensemble learning method, which grows multiple decision trees as base learners and averages their predictions to obtain better predictions [16, 17]. Bagging repeatedly selects randomly replaced samples from the training set and fits the regression tree to these samples. In the training process, the predictor variable that provides the best split is used for a binary split on the corresponding node in a tree. Here, the objective function is to minimize impurity criteria such as GINI or entropy. After training, the final prediction can be obtained by averaging the predictions of all individual regression trees for the unseen sample  $x_i$  as in Equation 4.

$$\hat{y}_i = \frac{1}{B} \sum_{b=1}^B f_b(x_i) \quad (4)$$

where  $f_b$  is a regression tree, and  $B$  is the number of bootstrapping.

**K-nearest neighbor regression (KNN)** The  $k$ -nearest neighbor algorithm is a non-parametric method that finds the nearest  $k$  neighbors to the new sample in the training data [18]. Briefly, the algorithm calculates the distance  $d(u, x)$  between the target sample and the given sample as in Equation 5 (Euclidean distance is used in this study), and the average value of  $k$ -nearest neighbors are used as its predicted value, as shown in Equation 6.

$$d(u, x) = \sqrt{\sum_{j=1}^p (u_j - x_j)^2} \quad (5)$$

$$\hat{y}_i = \frac{1}{K} \sum_{k=1}^K y_{ik} \quad (6)$$

where  $u$  is the unseen sample,  $d(u, x)$  is the Euclidean distance between the unseen sample and a given sample,  $p$  is the dimension of the input vector,  $K$  is the defined number of nearest neighbors, and  $y_k$  is the output of the nearest neighbor.

**Artificial Neural Network (ANN)** The artificial neural network (ANN) has been one of the most popular machine learning algorithms, and a multilayer perceptron algorithm is used to train a neural network by backpropagation. It consists of an input layer, hidden layer, and output layer, and can be expressed as in Equation 7. In this study, Rectified Linear Unit (ReLU) function [19] is used for the transfer function for the hidden layer ( $g$ ), and the squared error with a L2 regularization is used for the objective function as in Equation 8 [20]. In addition, a multilayer perceptron algorithm updates the weight of the neural network through backpropagation.

$$\hat{y}_i = g \left( \omega_{i0} + \sum_{j=1}^p x_{ij} \omega_j \right) \quad (7)$$

$$Obj = \frac{1}{2} \sum_{i=1}^n (y_i - \hat{y}_i)^2 + \frac{\lambda}{2} \sum_{j=1}^p \|\omega_j\|^2 \quad (8)$$

where  $g$  is relu function,  $w_0$  is bias,  $x$  is input to neuron,  $\omega$  represents weights,  $p$  is the number of inputs from the previous layer, and  $\lambda$  is weight penalty parameter.

**Gaussian Process Regression (GPR)** A Gaussian process is a nonparametric, Bayesian approach to a regression problem, which calculates the probability distribution over all possible functions that fit the data [21]. In GPR, prior knowledge of the function space can be specified as a Gaussian process prior using the mean function  $m(x)$  and the covariance function  $k(x, x')$ , known as the kernel function. After that, it uses the training data to calculate the posterior distribution and the predicted posterior distribution for the invisible sample. It can be described as follows:

$$m(x) = E[f(x)] \quad (9)$$

$$k(x, x') = E[(f(x) - m(x))(f(x') - m(x')))] \quad (10)$$

$$f(x) \sim GP(m(x), k(x, x')) \quad (11)$$

**Support Vector Regression (SVR)** Support vector machine (SVM) uses kernel functions for mapping nonlinear problems in input space to linear problems in new feature space with higher dimensions, and they are created so that the decision boundary has a maximum margin [22, 23]. In addition, the number of hyperparameters to be adjusted is not as many as other machine learning algorithms, so it has the advantage of being able to identify factors that affect learning relatively simply. The Support Vector Regression (SVR) uses the same principles as SVM, of which the approximated function and the objective function can be expressed as in Equations 12-13. To solve the complex nonlinear regression problems through kernels, radial basis function (RBF) is considered in this study as in Equation 14.

$$\hat{y}_i = \omega^T \phi(x_i) + b \quad (12)$$

$$Obj = \frac{1}{2} \|\omega\|^2 + C \sum_{i=1}^n |\xi_i| \quad (13)$$

$$\begin{aligned} & \text{subject to } |\hat{y}_i - y_i| \leq \epsilon + |\xi_i| \\ & k(x_i, x_j) = \exp\left(-\frac{\|x_i - x_j\|^2}{2\sigma^2}\right) \end{aligned} \quad (14)$$

where  $\phi(x)$  is the higher dimension space converted from the input vector, and  $\omega$  is weight vector, and  $b$  represents a threshold.  $C$  is the regularization parameter,  $\epsilon$  is the margin of error, and  $\xi$  is the deviation from the margin, and  $\sigma$  is the length scale of the kernel.

### 2.3 Evaluation metrics

In this paper, the coefficient of determination ( $R^2$ ), root mean squared error ( $RMSE$ ), and mean absolute error ( $MAE$ ) are used as a metric for evaluating the accuracy of models, and the formulas are as shown in Equations 15-17.

$$R^2 = 1 - \frac{\sum_{i=1}^n (y_i - \hat{y}_i)^2}{\sum_{i=1}^n (y_i - \bar{y}_i)^2} \quad (15)$$

$$RMSE = \sqrt{\frac{1}{n} \sum_{i=1}^n (y_i - \hat{y}_i)^2} \quad (16)$$

$$MAE = \frac{1}{n} \sum_{i=1}^n |y_i - \hat{y}_i| \quad (17)$$

## 3. RESULTS

### 3.1 Model selection

Ideally, if there is a lot of data, it is best to divide the entire dataset into a training set, validation set, and test set independently. However, due to the nature of ship model experiments, it is time-consuming and expensive, and the number of

publicly available data is limited. In addition, since this study aims to compare the performance of various machine learning algorithms, nested cross-validation, which is suitable for efficient use of dataset even in relatively small amounts of data sets is introduced in the study. Unlike model selection using typical cross-validation, nested cross-validation can prevent leakage of information and overfitting of data because the dataset is divided into multiple folds, and model evaluation and hyperparameter tuning are performed simultaneously [24].

As shown in Figure 4, the inner fold is used for selecting the best model within the range of hyperparameters, while the outer fold is used for evaluating the trained model from the inner loop with the test set. In this study, 10 outer cross-validations were applied and 5 inner cross-validations were applied and the 6 candidate models XGB, RF, KNN, ANN, GPR, and SVR were compared. As listed in Table 2, grid search was performed on the range of hyperparameters for each algorithm, and hyperparameters of the model with the best performance were finally used for model training.

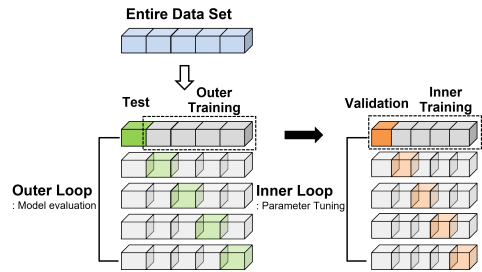


**FIGURE 4.** DIAGRAM SHOWING THE NESTED CROSS-VALIDATION WITH FIVE OUTER AND FIVE INNER LOOPS.

Figure 5 shows the verification results of the candidate models for the test data of the outer loop in the nested cross-validation. The average  $R^2$  values of XGB, SVR, and RF were 0.8939, 0.8792, and 0.8748, respectively, which were remarkably higher among candidate algorithms, while SVR, GPR, and ANN showed the lowest errors in  $RMSE$  and  $MAE$  metrics at 0.34, 0.36, and 0.39. Overall, SVR showed excellent generalization capability with high prediction accuracy for all metrics used.

Figure 6 shows one of the ship cases used for training (S175 Container,  $F_n=0.25$ ) as an example to visualize the prediction trends of each method. The blue dot represents a case where the observed value is larger than the predicted value, and the red dot represents a case where the observed value is smaller than the



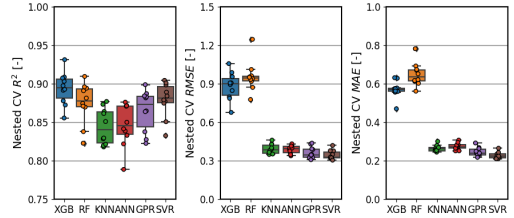
**TABLE 2.** THE RANGES AND SELECTED VALUES OF HYPERPARAMETERS FOR THE MACHINE LEARNING ALGORITHMS.

ML algorithm	Parameter name	Search range	Optimal value
XGB	n_estimators	[500, 2000]	2000
	learning_rate	[0.01, 0.1]	0.01
	max_depth	[4, 8]	8
	min_child_weight	[1, 5]	3
	subsample	[0.5, 0.9]	0.5
	colsample_bytree	[0.5, 0.9]	0.9
	alpha	[0.001, 0.1]	0.01
	gamma	[0.2, 0.4]	0.2
	RF	n_estimators	[500, 2000]
max_depth		[10, 50]	50
max_features		[auto,sqrt,log2]	log2
min_samples_leaf		[3, 11]	3
min_samples_split		[3, 11]	3
bootstrap		[True, False]	False
KNN		n_neighbors	[1, 20]
	leaf_size	[5, 30]	10
	p	[1, 5]	2
ANN	hidden_neurons	[4, 14]	14
	hidden_layers	[1, 2]	2
	batch_size	[8, 64]	16
	epochs	[10, 1000]	1000
	learning_rate	[0.0001, 0.1]	0.01
	optimizer	[SGD, RMSprop, Adagrad, Adam]	Adam
	dropout_rate	[0, 0.8]	0
weight_constraint	[1, 5]	3	
	GPR	n_restarts_optimizer	[0, 64]
alpha		[0.0001, 1]	0.01
SVR	kernel	[rbf, sigmoid]	rbf
	c	[0.1, 100]	10
	gamma	[0.01, 10]	1

predicted value. In other words, it can be said that a model with a small distance between the predicted surface and the observed sample and has evenly distributed blue and red samples across all prediction ranges, is well-trained without bias. XGB showed the highest  $R^2$  as a powerful algorithm that repeatedly combines the predictions of multiple weak learners, but the predicted surface for the additional wave resistance coefficient due to wavelength and wave was not smooth. Such a trend of decision tree-based models can also be seen in RF. On the other hand, SVR has a smooth surface and evenly distributed sample colors, so it can be seen that it is robust to outliers and seems to better simulate the added resistance of ships by waves.

Since the data collected in the study may include uncertainty from experiments in different water tank environments and short-wavelength regions, it was judged that a model robust to outliers

and noise would be best for the aim of the study. Therefore, SVR was selected as the final model among candidate algorithms based on the model evaluation results by nested cross-validation and the analysis of the predictive surface.

**FIGURE 5.** EVALUATION OF MACHINE LEARNING MODELS THROUGH NESTED CROSS-VALIDATION.

### 3.2 Interpretation of model using SHAP method

Recently, there have been studies dealing with how to interpret predictions obtained from machine learning models [25–27]. Here, SHapley Additive exPlanations (SHAP) method [28] based on cooperative game theory was introduced to analyze the global and local relationship between input parameters and added wave resistance coefficient. The Shapley value means the average expected marginal contribution of one feature after all possible combinations have been considered, which can be expressed as in Equation 18.

$$\phi_i = \sum_{S \subseteq M \setminus \{i\}} \frac{|S|!(M-|S|-1)!}{M!} (v(S \cup \{i\}) - v(S)), \quad i = 1, \dots, M. \quad (18)$$

where  $\phi_i$  is Shapley value of the  $i$ th input parameter,  $S \subseteq M = \{1, \dots, M\}$  is a subset consisting of  $M$  parameters, and  $v(x)$  is the contribution of  $S$  calculated based on the marginal contribution of the input values.

The left side of Figure 7 represents the global importance of parameters used in SVR model. Since the parameters with high importance are indicated from top to bottom,  $\lambda/L$  (0.37),  $\alpha$  (0.33), and  $F_n$  (0.25) have the highest average impact on model output among the input parameters, while the influence of  $T_m/T_d$  (0.03) and  $\theta$  (0.02) was relatively small compared to other input parameters. The results of Shapley value had the advantage of being able to grasp the importance of variables with non-linear relationships, such as  $\lambda/L$ , slightly different from the results of the correlation analysis in Figure 2.

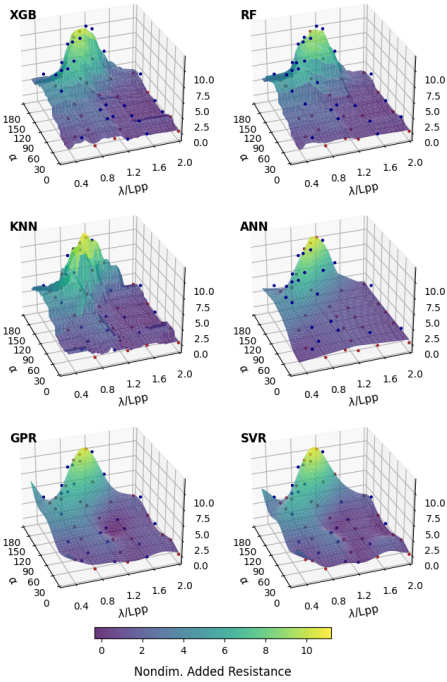


**FIGURE 6.** AN EXAMPLE OF THE ADDED WAVE RESISTANCE COEFFICIENT PREDICTION (S175 CONTAINER,  $FN=0.25$ ).

The right side of Figure 7 shows the SHAP’s summary plot describing the relation between the input and Shapley values. The x-axis is determined by the Shapley value, and each sample point is a Shapley value for the corresponding feature with the y-axis showing the distribution of the feature values. The color denotes the value of the parameter, where the red-colored point means the higher values, and the blue one represents the lower values. That is, if the Shapley value increases as the value of the parameter increases, the corresponding parameter has a positive impact on the added wave resistance, and vice versa. Similarly, the SHAP dependency plot (Figure 8) shows the Shapley value in more detail according to the change in the input value. As can be seen in the Shap summary plot and the dependence plot, the  $F_n$  and  $\alpha$  have a clearly positive correlation relationship with the Shapley value, which is consistent with generally known results.  $L/B$  also seems to have a positive correlation with added wave resistance overall but tends to have the most negative impact at  $L/B = 6$ .  $\lambda/L$  has a clear negative effect on the high value, but

has a relatively high Shapley value near the region of the resonance frequency ( $\lambda/L \approx 1$ ). This showed that the wavelength and added wave resistance are in a complicated and nonlinear relationship, as can be seen in the dependence plot. There is no obvious pattern observed in Shapley values of  $T_m/T_d$  and  $\theta$ , which may be due to the influence of lacking the collected dataset according to changes in  $T_m/T_d$  and  $\theta$ .

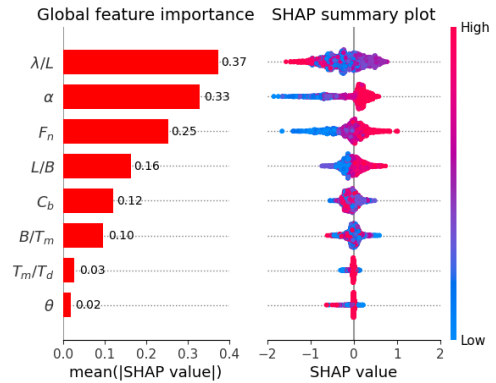


**FIGURE 7.** SHAP FEATURE IMPORTANCE AND SUMMARY PLOTS OF ADDED WAVE RESISTANCE COEFFICIENT.

### 3.3 Validation by test data set

Validation of the SVR model and other previous methods (STAWAVE-2 [1], Cepowski (2020) [11], Lang&Mao (2021) [9], SNNM [7]) is performed on the ship experiment cases that are not used for the model training. Details of a container ship [29, 30], bulk carrier [31], and an oil tanker ship [32] used for the test data are shown in Table 3. The predicted values of each method for the experimental cases of ships A, B, and C and their accuracy are shown in Figures 9-10 and Tables 4 and 5. Considering the scope of application of each method, the prediction results are divided into head waves and all directions of waves, respectively. Since the STAWAVE-2 and Cepowski (2020) models can only predict in head waves, the identical values of the added resistance according to the wavelength were applied from 135 degrees to 180 degrees. For the rest of the wave heading regions (0 degrees to 135 degrees), the prediction values are set to 0, which also can be identified in Figure 10.

Overall, SNNM predicted the added resistance at all ships’ head waves well with  $R^2$  between 0.7704 and 0.7871, and RMSE and MAE were also relatively low. In addition, SVR showed

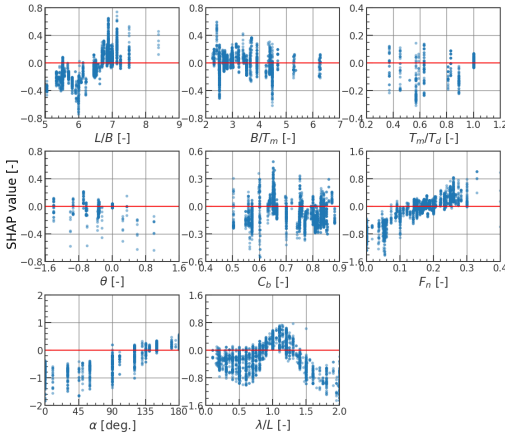


**FIGURE 8.** SHAP FEATURE DEPENDENCE PLOTS FOR THE MAIN PARAMETERS.

fairly good performance with  $R^2$  between 0.5738 and 0.7584 although its accuracy was slightly lower than SNNM. Since Cepowski's ANN model was trained only with 180 degrees experimental data of 14 ships, which was a smaller dataset than the other methods, it tended to be less accurate in some vessels. The prediction accuracy of STAWAVE-2 and Lang&Mao (2021) was also good enough, but in a specific case (Ship C) among the ships compared in this study, the prediction power was significantly reduced (In Tables 3-4,  $R^2$  denoted by '\*\*\*' means a negative value and corresponds to a case where using the regression line is worse than using the average of the samples [33]).

Meanwhile, looking at the accuracy in all wave directions, the predictive power in arbitrary waves was excellent for SNNM, SVR, and Lang&Mao (2021). There was a large error gap between the method only for head waves and the method for arbitrary waves. This is because the added resistance in the beam and following waves corresponding to 135 degrees to 0 degrees was not considered.

### 3.4 Comparison of added resistance in irregular waves

To compare the added resistance of the ship in irregular waves by  $C_{aw}$  predictions from different methods,  $R_{AW}$  was calculated by assuming the wave spectrum at specific sea states. A modified Pierson-Moskowitz wave spectrum, which is widely used in well-developed seas, was applied to the  $C_{aw}$ , as shown in Equations 19-21, and  $R_{AW}$  was estimated as shown in Equations 22-23. Here, wave spectrums corresponding to sea state 3 to 7 (See Figure 12) were applied to the comparison cases. In addition, prediction results of the added wave resistance coefficient

**TABLE 3.** MAIN PARTICULARS AND EXPERIMENTAL CONDITIONS FOR SUBJECT SHIPS.

Particulars	Ship A	Ship B	Ship C
Ship type	Container	Bulk carrier	Oil tanker
Length, $L$ [m]	300	279	323
Breadth, $B$ [m]	40	45	60
Mean draft, $T_m$ [m]	14	16.5	21
Block coefficient, $C_b$ [-]	0.65	0.86	0.81
Froude no., $F_n$ [-]	0.2	0.128	0.137

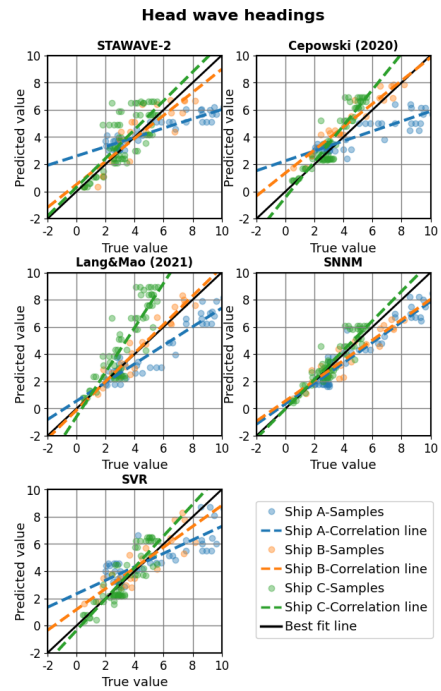


**FIGURE 9.** PLOTS OF THE TRUE VERSUS PREDICTED VALUES OF ADDED RESISTANCE COEFFICIENTS IN HEAD WAVES.

of Ship B (See Figure 11, in which the overall prediction error for all methods was smallest in the previous section, were used.

$$S(\omega) = \frac{A}{\omega^5} e^{-B/\omega^4} \quad (19)$$

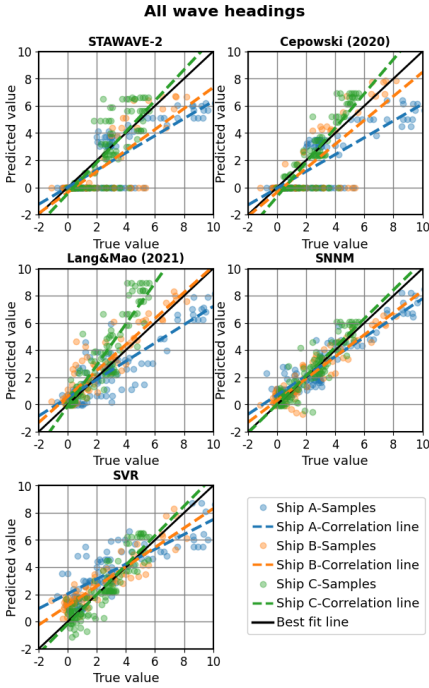


**FIGURE 10.** PLOTS OF THE TRUE VERSUS PREDICTED VALUES OF ADDED RESISTANCE COEFFICIENTS IN ALL WAVE HEADINGS.

$$A = 173 \frac{H_s^2}{T_1^4} \quad (20)$$

$$B = \frac{691}{T_1^4} \quad (21)$$

$$R_{aw}(\omega) = \rho g \zeta_a^2 B^2 / LC_{aw} \quad (22)$$

$$R_{AW} = 2 \int_0^\infty \frac{R_{aw}(\omega) S(\omega)}{\zeta_a^2} d\omega \quad (23)$$

In the current study, since sea trial or in-service data was not used for the validation, it was not possible to accurately evaluate the prediction error of the models in irregular waves. However, the relative deviation between each method was calculated based

**TABLE 4.** VALIDATION RESULTS BY TEST DATA SET IN HEAD WAVES.

Test case	Model	$R^2$	RMSE	MAE
Ship A	STAWAVE-2	0.4085	2.40	1.82
	Cepowski (2020)	0.3641	2.49	1.87
	Lang&Mao (2021)	0.6885	1.74	1.39
	SNNM	0.7704	1.50	1.23
	SVR	0.6382	1.88	1.53
Ship B	STAWAVE-2	0.7438	1.10	0.95
	Cepowski (2020)	0.8149	0.94	0.77
	Lang&Mao (2021)	0.9040	0.67	0.56
	SNNM	0.8711	1.00	0.83
	SVR	0.7584	1.07	0.89
Ship C	STAWAVE-2	0.0514	1.40	1.06
	Cepowski (2020)	0.4300	1.09	0.85
	Lang&Mao (2021)	**	2.18	1.71
	SNNM	0.7720	0.69	0.52
	SVR	0.5738	0.94	0.77

**TABLE 5.** VALIDATION RESULTS BY TEST DATA SET IN ALL WAVE HEADINGS.

Test case	Model	$R^2$	RMSE	MAE
Ship A	STAWAVE-2	0.5177	2.23	1.70
	Cepowski (2020)	0.4962	2.28	1.73
	Lang&Mao (2021)	0.7272	1.68	1.33
	SNNM	0.8378	1.29	1.01
	SVR	0.6744	1.83	1.47
Ship B	STAWAVE-2	0.4560	1.69	1.14
	Cepowski (2020)	0.4743	1.66	1.09
	Lang&Mao (2021)	0.7782	1.08	0.74
	SNNM	0.8597	0.86	0.68
	SVR	0.7449	1.15	0.99
Ship C	STAWAVE-2	0.3297	1.42	1.02
	Cepowski (2020)	0.4768	1.25	0.90
	Lang&Mao (2021)	**	1.80	1.28
	SNNM	0.7880	0.80	0.57
	SVR	0.7261	0.91	0.73

on the predicted value of the SVR model as shown in Equation 24, and through this, the prediction trends of resistance in irregular waves could be compared. That is, if the relative deviation is 0%, it means that the prediction value of the compared model accurately matches the predicted value of the SVR. Figure 13 shows the results of summing all the added wave resistance in head waves (within  $\pm 45$  degrees off the bow), and Figure 14 shows the results in all wave directions (0-360 degrees). The value shown above the bar chart of each sea state is the predicted added resistance in irregular waves by the SVR method.

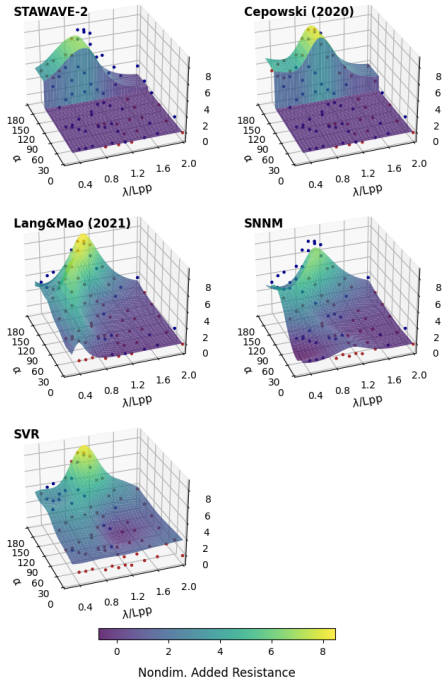


**FIGURE 11.** THE RESULTS OF THE ADDED WAVE RESISTANCE COEFFICIENT PREDICTION FOR SHIP B.

$$Relative\ deviation[\%] = \frac{|R_{AW,MODEL} - R_{AW,SVR}|}{R_{AW,SVR}} \times 100 \quad (24)$$

As shown in Figure 13, as a result of comparing the relative deviations for sea states 3 to 7 in head waves, the relative difference with SNNM was the smallest at about 2-20%, and other methods differed by an average of 20% and up to 38%. However, in the case of all wave directions in Figure 14, Lang&Mao (2021) and SNNM, which are applicable to arbitrary waves, differed by less than about 10% and up to 20% on average, while STAWAVE-2 and Cepowski (2020) differed by 50-80%. The reliability of the SVR model in irregular waves could be verified to some extent because the relative deviation of SNNM, which showed the most accurate prediction for  $C_{aw}$ , was not large.

Indeed, the added resistance of head waves is considerably greater than that of the beam or following waves. However, as-

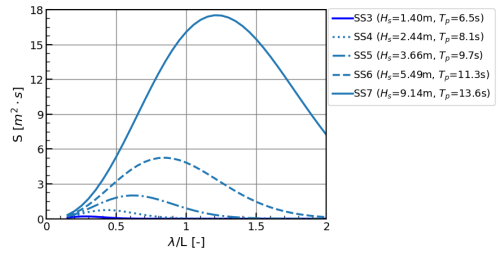


**FIGURE 12.** ITTC WAVE SPECTRUM ACCORDING TO THE SEA STATES.

suming that the ship encounters random waves in all directions, the prediction results of additional wave resistance in irregular waves showed a significant difference between methods for arbitrary waves and head waves as can be seen in Figure 14. In other words, considering the realistic environment that ships experience at sea, this fact supports the need for resistance prediction methods at arbitrary waves.

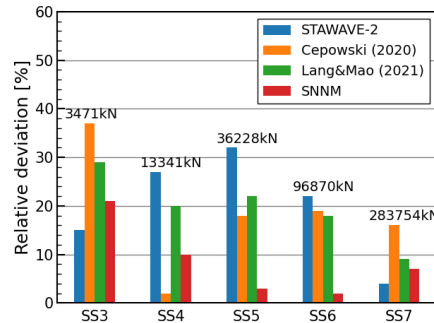


**FIGURE 13.** THE SUM OF ADDED RESISTANCE IN IRREGULAR HEAD WAVES.

#### 4. CONCLUSIONS & FUTURE WORK

In this study, we proposed a method of predicting added wave resistance in arbitrary waves by applying machine learning algorithms to basic ship parameter data. Various machine learning algorithms were considered, and SVR, which showed the most stable and best performance, was selected as the final model through nested cross-validation. In addition, the predictive effect of each parameter on the output of the model was

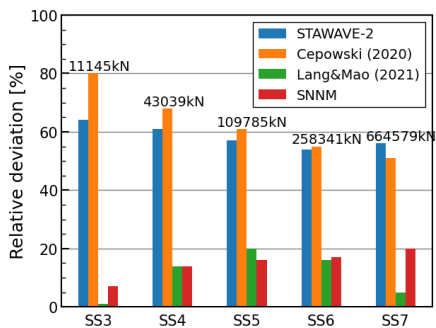


**FIGURE 14.** THE SUM OF ADDED RESISTANCE IN IRREGULAR ARBITRARY WAVES.

further interpreted through Shapley value, which had a global influence on the prediction of added wave resistance in the order of  $\lambda/L$ ,  $\alpha$ , and  $F_n$ . Validation of the selected model was performed on 3 model ship cases not used in the training process, and SVR showed excellent overall predictive performance with  $R^2$  0.6744-0.7449,  $RMSE$  0.91-1.83, and  $MAE$  0.73-1.47 in various wave headings compared to other existing methods. As a result of estimating the added resistance in irregular arbitrary waves according to sea state 3 to 7, the relative deviation of SVR with semi-empirical methods for arbitrary waves was approximately 10% on average.

Therefore, the model proposed in this study had the advantage of being able to estimate added resistance in all wave headings fairly accurately using simple ship information without advanced tools. It is thought that this can be applied practically throughout the marine industry, including initial ship design without detailed hull information and speed-power performance evaluation in sea trials. If more experimental data can be used for the training of the machine learning model, it will be possible to further improve the accuracy and coverage of the model. Even in this case, retraining the currently proposed method is relatively easier than, for example, SNNM method. In addition, it is expected that there is room for the application of methods such as physics-guided neural networks [34], which combine scientific knowledge of physics-based models with machine learning structures as well as semi-empirical methods and data-driven machine learning algorithms covered in this study, to predict added wave resistance.

#### ACKNOWLEDGMENT

This study is part of the research projects CLIMMS – Climate change mitigation in the maritime sector (Research Council of Norway (RCN) project number 294771) and SFI Smart Mar-

itime - Norwegian Centre for improved energy-efficiency and reduced emissions from the maritime sector (RCN project number 237917).

#### REFERENCES

- [1] Boom, H., Huisman, H., and Mennen, F., 2013. “New guidelines for speed/power trials: Level playing field established for imo eedi”. *SWZ Maritime, Schip en Werf de Zee Foundation, Rotterdam*.
- [2] Liu, S., and Papanikolaou, A., 2016. “Fast approach to the estimation of the added resistance of ships in head waves”. *Ocean Engineering*, **112**, pp. 211–225.
- [3] Faltinsen, O. M., 1980. “Prediction of resistance and propulsion of a ship in a seaway”. In Proceedings of the 13th symposium on naval hydrodynamics, Tokyo, 1980.
- [4] Jinkine, V., and Ferdinande, V., 1974. “A method for predicting the added resistance of fast cargo ships in head waves”. *International Shipbuilding Progress*, **21**(238), pp. 149–167.
- [5] Liu, S., and Papanikolaou, A., 2019. “Approximation of the added resistance of ships with small draft or in ballast condition by empirical formula”. *Proceedings of the Institution of Mechanical Engineers, Part M: Journal of Engineering for the Maritime Environment*, **233**(1), pp. 27–40.
- [6] Liu, S., and Papanikolaou, A., 2020. “Regression analysis of experimental data for added resistance in waves of arbitrary heading and development of a semi-empirical formula”. *Ocean Engineering*, **206**, p. 107357.
- [7] Wang, J., Bielicki, S., Kluwe, F., Orihara, H., Xin, G., Kume, K., Oh, S., Liu, S., and Feng, P., 2021. “Validation study on a new semi-empirical method for the prediction of added resistance in waves of arbitrary heading in analyzing ship speed trial results”. *Ocean Engineering*, **240**, p. 109959.
- [8] Lang, X., and Mao, W., 2020. “A semi-empirical model for ship speed loss prediction at head sea and its validation by full-scale measurements”. *Ocean Engineering*, **209**, p. 107494.
- [9] Lang, X., and Mao, W., 2021. “A practical speed loss prediction model at arbitrary wave heading for ship voyage optimization”. *Journal of Marine Science and Application*, **20**(3), pp. 410–425.
- [10] Tsujimoto, M., Shibata, K., Kuroda, M., and Takagi, K., 2008. “A practical correction method for added resistance in waves”. *Journal of the Japan Society of Naval Architects and Ocean Engineers*, **8**, pp. 177–184.
- [11] Cepowski, T., 2020. “The prediction of ship added resistance at the preliminary design stage by the use of an artificial neural network”. *Ocean Engineering*, **195**, p. 106657.
- [12] Martić, I., Degiuli, N., Majetić, D., and Farkas, A., 2021. “Artificial neural network model for the evaluation of added

- resistance of container ships in head waves”. *Journal of Marine Science and Engineering*, **9**(8), p. 826.
- [13] Pedregosa, F., Varoquaux, G., Gramfort, A., Michel, V., Thirion, B., Grisel, O., Blondel, M., Prettenhofer, P., Weiss, R., Dubourg, V., et al., 2011. “Scikit-learn: Machine learning in python”. *the Journal of machine Learning research*, **12**, pp. 2825–2830.
- [14] Friedman, J., Hastie, T., and Tibshirani, R., 2000. “Additive logistic regression: a statistical view of boosting (with discussion and a rejoinder by the authors)”. *The annals of statistics*, **28**(2), pp. 337–407.
- [15] Chen, T., and Guestrin, C., 2016. “Xgboost: A scalable tree boosting system”. In Proceedings of the 22nd acm sigkdd international conference on knowledge discovery and data mining, pp. 785–794.
- [16] Ho, T. K., 1995. “Random decision forests”. In Proceedings of 3rd international conference on document analysis and recognition, Vol. 1, IEEE, pp. 278–282.
- [17] Breiman, L., 2001. “Random forests”. *Machine learning*, **45**(1), pp. 5–32.
- [18] Altman, N. S., 1992. “An introduction to kernel and nearest-neighbor nonparametric regression”. *The American Statistician*, **46**(3), pp. 175–185.
- [19] Nair, V., and Hinton, G. E., 2010. “Rectified linear units improve restricted boltzmann machines”. In Icm1.
- [20] Caponnetto, A., and De Vito, E., 2007. “Optimal rates for the regularized least-squares algorithm”. *Foundations of Computational Mathematics*, **7**(3), pp. 331–368.
- [21] Rasmussen, C. E., 2003. “Gaussian processes in machine learning”. In Summer school on machine learning, Springer, pp. 63–71.
- [22] Vapnik, V., 1999. *The nature of statistical learning theory*. Springer science & business media.
- [23] Platt, J., et al., 1999. “Probabilistic outputs for support vector machines and comparisons to regularized likelihood methods”. *Advances in large margin classifiers*, **10**(3), pp. 61–74.
- [24] Cawley, G. C., and Talbot, N. L., 2010. “On over-fitting in model selection and subsequent selection bias in performance evaluation”. *The Journal of Machine Learning Research*, **11**, pp. 2079–2107.
- [25] Molnar, C., 2020. *Interpretable machine learning*. Lulu.com.
- [26] Goldstein, A., Kapelner, A., Bleich, J., and Pitkin, E., 2015. “Peeking inside the black box: Visualizing statistical learning with plots of individual conditional expectation”. *journal of Computational and Graphical Statistics*, **24**(1), pp. 44–65.
- [27] Ribeiro, M. T., Singh, S., and Guestrin, C., 2016. “‘‘ why should i trust you?’’ explaining the predictions of any classifier”. In Proceedings of the 22nd ACM SIGKDD international conference on knowledge discovery and data mining, pp. 1135–1144.
- [28] Lundberg, S. M., and Lee, S.-I., 2017. “A unified approach to interpreting model predictions”. In *Advances in Neural Information Processing Systems 30*, I. Guyon, U. V. Luxburg, S. Bengio, H. Wallach, R. Fergus, S. Vishwanathan, and R. Garnett, eds. Curran Associates, Inc., pp. 4765–4774.
- [29] Tsujimoto, M., Kuroda, M., Shibata, K., Sogihara, N., and Takagi, K., 2009. “On a calculation of decrease of ship speed in actual seas”. *Journal of the Japan Society of Naval Architects and Ocean Engineers*, **9**, pp. 79–85.
- [30] Tsujimoto, M., Kuroda, M., Shiraishi, K., Ichinose, Y., and Sogihara, N., 2012. “Verification on the resistance test in waves using the actual sea model basin”. *Journal of the Japan Society of Naval Architects and Ocean Engineers*, **16**, pp. 33–39.
- [31] Matsumoto, K., 2000. “Development of energy saving bow shape at sea”. In Proc. of the 4th Osaka Colloquium on Seakeeping Performance of Ships, 2000, pp. 479–485.
- [32] Park, D.-M., Lee, J.-H., Jung, Y.-W., Lee, J., Kim, Y., and Gerhardt, F., 2019. “Experimental and numerical studies on added resistance of ship in oblique sea conditions”. *Ocean Engineering*, **186**, p. 106070.
- [33] Scikit-learn. *sklearn.metrics.r2\_score*. Available at [https://scikit-learn.org/stable/modules/generated/sklearn.metrics.r2\\_score.html](https://scikit-learn.org/stable/modules/generated/sklearn.metrics.r2_score.html) (accessed: 2021-11-21).
- [34] Karpatne, A., Watkins, W., Read, J., and Kumar, V., 2017. “Physics-guided neural networks (pgnn): An application in lake temperature modeling”. *arXiv preprint arXiv:1710.11431*.

# Article 4

## Modeling of ship resistance and power consumption for the global fleet: The MariTEAM model

Youngrong Kim, Sverre Steen, Diogo Kramel, Helene Muri, Anders  
Hammer Strømman

*Submitted to Ocean Engineering*





# Modeling of ship resistance and power consumption for the global fleet: The MariTEAM model

Young-Rong Kim<sup>a,\*</sup>, Sverre Steen<sup>a</sup>, Diogo Kramel<sup>b</sup>, Helene Muri<sup>b</sup> and Anders Hammer Strømman<sup>b</sup>

<sup>a</sup>Department of Marine Technology, Norwegian University of Science and Technology (NTNU), Trondheim, 7050, Norway

<sup>b</sup>Industrial Ecology Programme, Norwegian University of Science and Technology (NTNU), Trondheim, 7034, Norway

---

## ARTICLE INFO

### Keywords:

Ship resistance  
Propulsion power prediction  
Emission assessment  
Bottom-up approach  
Fleet-level analysis  
AIS data

## ABSTRACT

A system that can reliably estimate power consumption based on operational profiles and weather conditions is needed to evaluate global shipping emissions and alternative reduction scenarios. Due to a lack of detailed ship information, uncertainties in collected data, and computing complexity, many prior bottom-up investigations used simplified calculations and empirical equations. Some methodologies offered only approximate estimates that were not enough to capture power consumption trends based on the global fleet's geographical, seasonal, and operational features. This work intends to develop and implement a power prediction method that can be applied in a bottom-up approach based on fleet composition and trading patterns. We present a comprehensive approach for powering prediction, encompassing data pre-processing, ship resistance estimation, and propulsion efficiency, based on the Maritime Transport Environmental Assessment Model. As a result of comparison with the full-scale measurements of three operating ships and 2018 EU-MRV data from the fleet segments, the predictions from the model are shown to be fairly well-matched. Thus, the proposed model can be used to simulate the power performance and energy consumption of worldwide shipping.

---

## 1. Introduction


The maritime industry is facing the challenge of reducing its emission to achieve carbon neutrality. The International Maritime Organization (IMO) has announced an initial strategy to phase out greenhouse gas emissions (GHG) by at least 50% by 2050 as of 2018, and strategies to mitigate emissions such as NO<sub>x</sub>, SO<sub>x</sub>, and black carbon are also being adopted (IMO, 2018, 2021). Many measures are being considered to reduce GHG emissions, such as the use of alternative fuels with low carbon intensity, the development of ship technology to increase energy efficiency, and the promotion of new policies (Bouman et al., 2017; Balcombe et al., 2019). It is crucial to have a clear grasp of the actual climate impact of the current global fleet operations along with assessment of different mitigation strategies. Furthermore, estimating GHG emissions at sea and evaluating their effects on the climate will be helpful in developing international regulations, identifying the most effective emission mitigation strategies, and making future decisions for emissions reduction.

The emission evaluation models used in the maritime industry can be divided into two types: a top-down approach and a bottom-up approach, where the former collects total fuel consumption based on bunker sales data and models emissions from it, while the latter is modeled to evaluate energy consumed by individual ship and the resulting emissions (Corbett and Koehler, 2003; Psaraftis and Kontovas, 2009). The bottom-up method has recently become more widely used due to the advantage that it can produce more accurate results along with the use of ship automatic identification system (AIS) data and can be combined with various scenarios (Johansson et al., 2017).

There have been several studies using AIS data along with ship-specific information to apply a spatial distribution bottom-up approach to the emissions from the marine sector (Smith et al., 2013, 2014; Olmer et al., 2017; Jalkanen et al., 2009, 2012; Johansson et al., 2017; Faber et al., 2020). The developed models enabled predictions of emissions in marine transport, helping to provide insights into technical and operational energy efficiency to achieve IMO goals. However, due to constraints of fleet-level analysis including a lack of detailed information about ships, the uncertainty of the collected data, and the calculation complexity, their methods for predicting power or energy consumption relied

---

\*Corresponding author

 youngrong.kim@ntnu.no (Y. Kim)  
ORCID(s): 0000-0002-5859-0854 (Y. Kim)

on very simple calculations or empirical methods. For instance, the ship's power in calm water was calculated using the cubic rule or admiralty formula, and the weather effect was corrected using a particular percentage of sea margin. Additionally, the identical fouling penalty was applied to all ships, taking into account the increase in resistance due to hull roughness changes. These methods are only somewhat rough estimates, and obtaining more accurate estimates of the entire fleet and its subsegments requires an approach that can accurately capture power consumption trends according to various operating profiles. Although more complex methods have recently been used in some studies, it is necessary to develop a comprehensive powering prediction method that can be used for a bottom-up approach by supplementing existing studies.

Therefore, this work aims to provide an improved power performance prediction model suitable for the bottom-up approach of analyzing energy consumption and emissions from global shipping. This model mainly uses AIS data, ship technical information, and weather hindcast data, which are commonly available in fleet-level analysis, and it is developed based on the ship resistance and power prediction module of the Maritime Transport Environmental Assessment Model (MariTEAM) presented in Bouman et al. (2016), Muri et al. (2019a,b), and Kramel et al. (2021). The established power prediction model can be used to evaluate fuel consumption, emission, and energy efficiency for the different fleet segments, as well as to find appropriate solutions for reducing GHG emissions in combination with different fuels, energy-saving devices, and ship segment scenarios.

Section 2 explains the background of the analysis of the global fleet level and introduces previous studies on the complete powering prediction methods. Section 3 describes the data pre-processing method for the ship dataset and the estimation of each ship resistance component and propulsive efficiency for the power prediction. Section 4 verifies the established power prediction model using the full-scale measurements of several ships, and shows the comparison results of the fuel consumption between the 2018 EU-MRV (European Union-The Monitoring, Reporting, and Verification) data and the predicted results. Section 5 covers the conclusion.

Abbreviations	
AHR	Average Hull Roughness
AIS	Automatic Identification System
DWT	DeadWeight Tonnage
ECMWF	European Centre for Medium-Range Weather Forecasts
EEOI	Energy Efficiency Operational Indicator
EU-MRV	European Union-The Monitoring, Reporting, and Verification
ICCT	International Council on Clean Transportation
IMO	International Maritime Organization
ITTC	International Towing Tank Conference
LDT	LightDisplacement Tonnage
MariTEAM	Maritime Transport Environmental Assessment Model
MCR	Maximum Continuous Rating
NRMSE	Normalized Root-Mean-Squared Error
SFOC	Specific Fuel Oil Consumption
SLCF	Short-Lived Climate Forcer
STA-JIP	Sea Trial Analysis Joint Industry Project
<b>Nomenclature</b>	
$\beta$	Wave heading. The wave angle relative to the ship's heading (180 degrees: head waves)
$\Delta C_F$	Roughness allowance
$\eta_H$	Hull efficiency
$\eta_O$	Open water efficiency
$\eta_R$	Relative rotative efficiency
$\eta_S$	Shaft efficiency
$\eta_T$	Total propulsive efficiency
$\nabla$	Volume displacement
$\nabla_{Td}$	Volume displacement at design draught
$\omega$	Circular frequency of regular waves
$\psi$	Heading of the ship
$\psi_{WRref}$	Relative wind direction at reference height (0 degrees: head wind)
$\psi_{WT}$	True wind direction
$\rho_a$	Air density
$\rho_w$	Sea water density
$\zeta_a$	Wave amplitude
$A_{XV}$	Area of maximum transverse section exposed to the wind
$B$	Breadth
$C_A$	Correlation allowance coefficient
$C_B$	Block coefficient
$C_M$	Midship section coefficient
$C_P$	Prismatic coefficient
$C_R$	Residual resistance coefficient
$C_X$	Wind resistance coefficient
$C_{AA}$	Air resistance coefficient
$C_{aw}$	Non-dimensional added wave resistance coefficient
$C_{calm}$	Calm water resistance coefficient
$C_F$	Frictional resistance coefficient
$C_{Th}$	Thrust loading coefficient
$C_{WP}$	Waterplane coefficient
$D_p$	Propeller diameter
$E$	Directional wave spectrum
$E_L$	Engine load for MCR in design condition
$F_n$	Froude's number
$H_s$	Significant wave height
$I_{AHR}$	Annual change in AHR over the dry dock cycle
$k$	Form factor
$k_{yy}$	Pitch gyration
$L_{bufl}$	Length of the bow on the waterline to 95% of maximum beam
$L_d$	Displacement length
$L_E$	Length of entrance
$L_{fn}$	Computational Froude length
$L_F$	Engine load adjustment factor
$L_{os}$	Length overall submerged
$L_{pp}$	Length between perpendiculars
$L_R$	Length of run
$L_{wl}$	Length on waterline
$N$	Ship age
$P_B$	Engine brake power
$r$	Pearson correlation coefficient
$R^2$	Coefficient of determination
$R_{AHR}$	Hull roughness reduction in drydocking
$R_{awl}$	Mean resistance in long crested irregular waves
$R_{aw}$	Added resistance in regular waves
$R_{calm}$	Calm water resistance
$R_T$	Total resistance
$R_{wave}$	Added resistance due to waves
$R_{wind}$	Added resistance due to wind
$S$	Wetted surface area
$S_{AHR}$	Initial AHR
$S_{Tc}$	Wetted surface area at current draught
$S_{Td}$	Wetted surface area at design draught
$T$	Mean draught
$t$	Thrust deduction factor
$T_A$	After draught
$T_c$	Current draught
$T_d$	Design draught
$T_{sc}$	Scantling draught
$V_S$	Ship's speed
$V_{WRref}$	Relative wind speed at reference height
$V_{WTref}$	True wind speed at the reference height
$w$	Wake fraction

## 2. Background

For the evaluation of ship fuel consumption and emissions, the calculation of the energy efficiency operation index (EEOI), and the optimization of navigation, numerous studies have proposed complete power prediction methods, and various approaches are being used depending on the available data and the objective of the research. Table 1 contains a list of previous papers that utilized the comprehensive power prediction approach, as well as the calculation methods of each ship resistance component and propulsive efficiency used to estimate power.

Jalkanen et al. (2009) proposed the Ship Traffic Emission Assessment Model (STEAM) for estimating GHG emissions and short-lived climate forcers (SLCFs) using AIS data, where a cubic rule for the required power at calm water conditions and speed penalties due to weather effects was used, and this model applied to evaluate the emissions in Baltic Sea. Jalkanen et al. (2012) and Johansson et al. (2017) further improved the early STEAM model and expanded its application range from the Baltic Sea and Danish Straits to the worldwide oceans. The IMO GHG (Smith et al., 2014; Faber et al., 2020) study and International Council on Clean Transportation (ICCT) study (Olmer et al., 2017), which are representative of bottom-up approaches, analyzed global shipping emissions based on AIS data, and in their studies, a very simplified calculation method such as the admiralty formula and constant sea margin was adopted to calculate ship power. However, this does not represent current ships particularly well, with exponent three of the velocity and two-thirds of the displacement, which is typically employed in admiralty coefficients, and the discrepancy is even greater at higher speeds. Moreover, the sea margin cannot properly capture the weather effects of geographical and seasonal changes in the areas where the ship operates.

Meanwhile, there have been some studies using more complex methods recently. On the basis of the ship basin database, well-established empirical methods such as Holtrop and Mennen (1982), Hollenbach (1998), Gulddammer and Harvald (1974), and Kristensen and Lützen (2012) were used to estimate calm water resistance. In order to improve accuracy, the weather effect is subdivided into wind and waves, and methods for estimating added resistance due to wind such as Blendermann (1996), ITTC (2017b), and Fujiwara (2006), and waves such as ITTC (2017b), Liu and Papanikolaou (2016), and Liu et al. (2016) were employed. Tillig et al. (2017) introduced ShipCLEAN, a generic ship energy system model that combines the outputs of numerous existing empirical equations for resistance estimations to compute ship power performance and predict fuel consumption under operating conditions with little input. The VERDE model, developed by Tveten et al. (2020) and Guo et al. (2022), can assess the fuel consumption of ships mainly based on Holtrop and Mennen (1982). In their study, a machine learning algorithm was applied to speed up calculations and obtain added resistance due to the weather.

Although various methods have been used in many of these studies, it was necessary to develop a comprehensive powering prediction method that can be used for a bottom-up approach by supplementing the shortcomings identified in previous studies and finding appropriate methods. For this reason, Bouman et al. (2016) and Muri et al. (2019a,b) presented a Maritime Transport Environmental Assessment Model (MariTEAM), which adopted a resistance-based approach to calculate the instantaneous power demand of a ship. This study covers the powering prediction method that can be used in the bottom-up approach of the global fleet, including the improvements in conjunction with subsequent studies of the MariTEAM, such as Dale (2020) and Kramel et al. (2021).

Table 1: The methods employed in earlier studies to calculate the ship resistance components and propeller efficiency. For subsequent studies conducted in the same research group, only the methods used in the most recent study are shown in the table.

Related work	Calm water resistance & Fouling penalty	Weather effect correction	Total propulsive efficiency
STEAM 1, 2, 3; Jalkanen et al. (2009, 2012), Johansson et al. (2017)	HB method	Townsin-Kwon	Emmerson's formula
Smith et al. (2013)	Power scaling based on HM method	Sea margin 10-15%	-
3 <sup>rd</sup> /4 <sup>th</sup> IMO GHG study; Smith et al. (2014), Faber et al. (2020)	Admiralty formula + 9% fouling penalty	Sea margin 10-15%	-
Lu et al. (2015)	HM method	Kwon	Sea-trial report
Rakke (2016)	HM method	Sea margin 15%	Values from similar ships
ICCT; Oliwer et al. (2017)	Admiralty formula + Fouling factor according to ship age	Sea margin 10-15%	-
ShipCLEAN; Tilling et al. (2017), Tilling and Ringsberg (2019), Tilling et al. (2020)	HM method, GH method	Wind: Blendemann; Waves: STA2, NTUA-SDL, NTUA-SDL2	OpenProp, HM method
Kim et al. (2020)	HM method	Wind: Blendemann; Waves: STA1, STA2	Barnittas, HM method
VERDE; Tveite et al. (2020), Guo et al. (2022)	HM method + 10% fouling penalty	Wind: Blendemann, Fujiwara; Waves: SNNM	Kristensen and Lutzen, HM method
MariTEAM; Bouman et al. (2016), Muri et al. (2019a,b), Dale (2020), Kramel et al. (2021)	HM method, HB method GH <sup>1</sup> method, OM <sup>1</sup> method + Fouling factor according to ship age	Wind: Fujiwara, Datasets (STA-JIP, Blendemann); Waves: Combined method	Kristensen and Lutzen, HM/HB/GH method

\* HB: Hollenbach (1998), HM: Holtrop and Mennen (1982), GH: Gulhammer and Harvald (1974), OM: Orrtneressen (1971), GH<sup>1</sup>: Kristensen and Lutzen (2012), OM<sup>1</sup>: Helmore (2008), Townsin-Kwon: Townsin and Kwon (1993), Kwon: Kwon (2008), Blendemann: Blendemann (1996), STA-JIP: ITTC (2017b), Fujiwara: Fujiwara (2006), STA/STA2: Boom et al. (2013), NTUA-SDL: Liu and Papanikolaou (2016), NTUA-SDL2: Liu et al. (2016), SNNM: Liu and Papanikolaou (2020), Combined: Kim et al. (2022a) Emerson: Watson (1998), Barnittas: Barnittas et al. (1981)

### 3. Materials & Methods

#### 3.1. Data pre-processing

##### 3.1.1. Data sources

This section provides an overview of the databases available for the global fleet, for power prediction, as well as the pre-processing of the data and estimation of the required parameters. For the power prediction of the operating ship, ship dynamic data, technical information, and environmental data are generally required. Ship dynamic data, or operational profile, refers to information on a ship that may change as the ship operates, such as the location, speed, heading, and draught of the ship, and is usually obtained from AIS data in the bottom-up approach. Ship technical data consists of main dimensions and engine specifications, and in this study, the IHS Sea-web database is used to obtain data on 76,937 ships, with a total tonnage of 100 tons or more (IHS, 2019). Weather-related data includes wind and wave conditions at the time and location the ship is sailing, and it is obtained from the ERA-Interim (ECMWF reanalysis) dataset provided by the European Center for Mid-Range Weather Forecasting (ECMWF) (Hersbach et al., 2020).

Before the raw data is used for ship resistance and power estimation, it is necessary to quality check the data. As incorrect information can lead to erroneous results and analysis, data should be prepared in an appropriate manner (Gupta et al., 2022). Additionally, the collected data should be transformed into the input format required by each module to conduct the calculation. Therefore, in this study, the collected data is handled with several typical procedures as outlined below.

##### 3.1.2. Voyage trajectory completion

Data are often missing in AIS ship trajectory data due to heavy traffic or irregular reception of AIS data (Liu et al., 2019). Also, since AIS data is acquired in different ways (satellite, shore-based reception), the AIS data for a single voyage of a single ship might be found in different sources. This lack of ship tracks may impede the precise evaluation of the ship's fuel consumption and emissions, as it tends to underestimate the ship's power consumption during operation. To complete the trajectory in an area where AIS data is missing, Kramel et al. (2021) proposed a method to restore the ship's trajectory at  $0.1^\circ$  latitude-longitude resolution intervals using a combined A\* algorithm (Hart et al., 1968) and Dijkstra algorithm (Dijkstra, 2022) with reference to information on port callings by each ship. In this study, this approach is used to complete the missing trajectory of the vessel, which accounts for around 37% of the total AIS messages.

##### 3.1.3. Ship draught correction

Among the parameters obtainable from AIS data, ship location, heading, and speed are relatively accurate because they are automatically received from the onboard system. However, because draught in AIS data is entered manually by the ship operator, it is frequently not updated in a timely manner or is entered incorrectly (Jia et al., 2019; Zhou et al., 2019). Due to these characteristics, it is almost impossible to grasp the immediate change in draught according to the actual operation of the ship from the draught data collected from the AIS data. Instead, this study checks whether the collected draught data is placed within a reasonable range, and if necessary, correction for the draught is performed. If the collected draught is less than the minimum allowable draught defined by the ship's classification rule or greater than the scantling or design draught of a ship, it is considered an abnormal value (refer to Table A1) and replaced with the average operating draught of the corresponding ship type (refer to Table A2). Since only design draught could be acquired in this study, design draught was used instead of scantling draught.

##### 3.1.4. Missing data handling

The ship's technical information is very important because it is to be used as a basic input of empirical methods for further calculations. However, for some ships, some parameter values in the data might be missing. If there are a few missing values, deleting some ship cases may not have a significant impact on the results. However, if such proportions are not small, the number of ship cases for analysis will reduce, the statistical performance of the model will decrease, and the ability to perform a comprehensive and reliable bottom-up analysis of the global fleet will have a negative impact. Many studies have proposed curve-fitting equations or regression equations related to the main parameters of the ship, which ensures fairly high accuracy. However, it is not suitable for all ship cases because it is not applicable if the required parameters used in the formula are missing. In this work, the missing data handling algorithm for ship principal data proposed by Kim et al. (2022b) is used here. The algorithm consists of three processes: initial computation, final imputation, and minor adjustment, and missing values for various ship cases can be estimated based

on multiple nonlinear regression analysis, regardless of missing parameters. In this study, this method is applied to replace the missing values of the parameters included in about 46.6% of all 76,937 ships.

### 3.1.5. Weather hindcast data correction

To estimate the added resistance that the ship experiences due to the external environment, weather information in the surrounding sea area where the ship is sailing is required. Although weather-related information is sometimes measured on board with equipment such as anemometers and wave radars, open sources such as weather hindcast data provided by ECMWF are typically used for fleet-level analyses. It is possible to estimate the wind and wave conditions, such as wind speed, wind direction, significant wave height, mean wave period, and mean wave direction, that corresponds to the specific time stamp and coordinates of each ship by performing interpolation over a time and space grid using the hindcast data (Gupta et al., 2022). However, the hindcast data related to waves is often zero or masked in some regions and times, mainly on the coast adjacent to the land. The resolution of the land-sea mask may cause us some trouble with the values needed along the coast. In this case, it is recommended to replace the value by referring to the average wave characteristics of the sea state proportional to the wind speed at the corresponding time and location.

### 3.1.6. Ship hydrostatic parameter estimation

The AIS data and technical information used in this study do not include detailed information on the hull shape of the ship, and in general, such information is impractical to be obtained from the data sources available in the bottom-up study of the global fleet. In order to calculate the ship resistance components and propulsive efficiency, parameters such as propeller diameter, wetted surface, and displacement, which are used as input values for empirical equations, are essential. Thus, in this section, we list well-known empirical formulas and regression equations that can be used to estimate relevant parameters that are useful for these purposes as shown in Tables B1-B4. If one can obtain accurate information about the ship, this parameter estimation step can be omitted.

## 3.2. Estimation of ship resistance components

According to ITTC (2018), the total resistance of a ship operating at sea can be generally calculated as the sum of the resistance components such as calm water resistance and the added resistance due to wind and waves as in Eq. (1). Here, the influence of steering and maneuvering on power consumption is neglected for the sake of simplicity. The method of estimating each resistance component is introduced in the following section.

$$R_T = R_{calm} + R_{wind} + R_{wave} \quad (1)$$

where  $R_T$  is the ship's total resistance,  $R_{calm}$  is the resistance in calm water condition,  $R_{wind}$  is added resistance due to wind, and  $R_{wave}$  is added resistance in waves.

### 3.2.1. Calm water resistance

Several bottom-up studies for the fleet segment used the cubic rule (Jalkanen et al., 2009) and the admiralty formula (Smith et al., 2014; Olmer et al., 2017; Faber et al., 2020) to estimate the calm water resistance due to their simple and easy calculations. However, these approaches are a very approximation that does not fit well with modern ships and may produce significantly higher power consumption than other modern empirical formulas (Brown and Aldridge, 2019; Gupta et al., 2021). In contrast, there were also empirical methods for estimating calm water resistance such as the systematic series and the regression-based method, which comprehensively covers more hydrodynamic details of ships. However, methods such as Ayre (Schneekluth and Bertram, 1998), Taylor-Gertler (Gertler, 1954), Series-60 (Todd, 1957), and Lap-keller (Lap, 1954; Auf'm Keller, 1973), are not suitable for modern hull forms and are outdated (Bertram, 2011). There were other methods, Holtrop and Mennen (1982), Hollenbach (1998), and Guldhammer and Harvald (1974), which were established based on relatively recent hull-shaped model test results and found to be applicable to a variety of ships. However, since the coverage range and input requirements are different, and the accuracy may vary depending on the ship profiles, it is necessary to carefully consider the estimation methods for calm water resistance.

According to Dale (2020), the estimation of calm water resistance based on the HM, HB, and GH methods of 7 ships was analyzed against model tests, sea tests, and full measurement data. Due to the relatively limited number of ships, it was difficult to conclude the superiority among the methods, but it is noteworthy that considering various



methods for the ship's calm water resistance would broaden the applicable range of the ship and lower the deviation of the prediction error.

This study focuses on establishing a model with good prediction accuracy while being applicable to a wide range of ships with only limited input values. Consequently, HM (Holtrop and Mennen, 1982), HB (Hollenbach, 1998), and GH (Guldhammer and Harvald, 1974; Kristensen and Lützen, 2012) methods, which are known to provide adequate accuracy for estimating the calm water resistance of modern ships while being applicable to a variety of ship types, are considered candidate methods. Here, an updated version of Oortmerson's method (OM method) is also added to cover relatively small vessels (Oortmerssen, 1971; Helmore, 2008). For each ship case, an appropriate method from these available options is selected by a determination algorithm. The determination algorithm will be described in the later sections. A brief introduction to the empirical methods of estimating the calm water resistance of the ship used in this study is given in Table 2.

**Table 2**

Comparison of the estimation methods for ship calm water resistance.

	HM method	HB method	GH method	OM method
Applicable area	Universal, wide range	Universal, modern ship, single/twin screw vessel	Universal, tankers, single/twin screw vessel	Small ship
Range	$0.55 < C_p < 0.85$ $3.9 < L_{pp}/B < 9.5$ $F_n < 0.45$	$0.49 < C_B < 0.83$ $4.71 < L_{pp}/B < 7.11$ $1.99 < B/T < 4.00$ $0.43 < D_p/T_A < 0.84$ $4.49 < L_{pp}/\sqrt[3]{V} < 6.01$	$0.55 < C_B < 0.85$ $5 < L_{pp}/B < 8$ $4 < L/\sqrt[3]{V} < 6$ $F_n < 0.33$	$0.5 < C_p < 0.725$ $0.73 < C_M < 0.97$ $3 < L_{pp}/B < 6.2$ $1.9 < B/T < 4.0$ $F_n < 0.5$ $16 < L_{pp} < 72$
Reference	Holtrop and Mennen (1982)	Hollenbach (1998)	Guldhammer and Harvald (1974) Kristensen and Lützen (2012)	Oortmerssen (1971) Helmore (2008)

Under the main assumption that the resistance of the ship can be largely divided into viscous resistance and residual resistance, this study takes the empirical form of resistance composition proposed by MARINTEK (Minsaas, 1982; Steen and Aarsnes, 2014) as shown in Eqs. (2)-(3). It applies a modified form of the ITTC'78 procedure (ITTC, 2017a), including the roughness correction in the viscous resistance term. The calculation of each resistance coefficient term that makes up the calm water resistance coefficient is applied slightly differently for each empirical method. Here, since the detailed hull design characteristic such as the transom and appendage of the ship are not specified, added resistance due to them is not considered separately.

$$R_{calm} = \frac{1}{2} \rho_w S V_S^2 C_{calm} \quad (2)$$

$$C_{calm} = (1 + k)(C_F + \Delta C_F) + C_R + C_A + C_{AA} \quad (3)$$

where  $\rho_w$  is water density,  $S$  is wetted surface area,  $V_S$  is the ship's speed,  $C_{calm}$  is calm water resistance coefficient,  $C_F$  is frictional resistance coefficient, which is obtained from ITTC friction line (ITTC, 2017b).  $\Delta C_F$  is the roughness allowance, which is obtained from Marintek (2022) (refer to section 3.2.2).  $k$  is the form factor, which can be obtained from HM and Marintek.  $C_R$ , and  $C_A$  are residual resistance and correlation allowance, which are estimated from each empirical method.  $C_{AA}$  is air resistance coefficient.

### 3.2.2. Added resistance due to hull roughness & fouling

The hull roughness of the ship is increased by the degree of biofouling and aging of the hull surface, which can lead to an increase in frictional resistance. Biofouling on the hull surface may result in an average increase in the total resistance of 2-11% on global fleet segments (Olmer et al., 2017). Despite these effects, many preceding studies of the bottom-up approach just applied the typical hull roughness of a newly built ship or applied 9-10% of the same fouling penalty for all the ships (Faber et al., 2020; Guo et al., 2022). As such hull fouling causes a significant difference in the energy consumption of ships, it is necessary to properly consider it in fleet-level analysis. The following Table 3 shows the typical average hull roughness (*AHR*) according to the age of the ship as indicated in several studies.

**Table 3**

Average hull roughness according to the ship age.

Age of ship (year)	Bowden and Davison (1974)	Townsin (2003a,b); Willsher (2007)	Stenson (2015)	Approximation method of Stenson (2015)
0-5	120-240	120-150	Varies according	120-160
6-10	120-240	200	to coating and	135-175
11-15	120-240	300	blasting type	150-190
16-20	120-240	400	(refer to Figs. 1-2)	165-205
20≤	120-240	500		180-

Townsin et al. (1986) presented an increase in average hull roughness according to ship age based on 86 sample surveys conducted in 1984-1985. Based on these findings, Olmer et al. (2017)'s GHG study estimated the average hull roughness according to the age of the ship by assuming dry docking at 5-year intervals, and the resulting added resistance was determined. However, according to Stenson (2015), 845 ship samples collected from 2003 to 2014 in drydock showed that the average hull roughness increased by  $10\mu\text{m}$  on average annually after drydock, and even if the age is more than 25 years, hull roughness can be maintained at a relatively low level of  $200\mu\text{m}$  or less (refer to Fig. 1 (a)). Although the deviation of the collected samples is observed somewhat large even on the same year basis, this may be due to differences in hull condition management, such as anti-fouling coating type, blasting type, and cleaning interval for each ship. The difference in trends in the two studies seems to be quite significant, which might be explained by the fact that the development of hull coating technology, environmental changes and regulations, and ship design and operational trends have changed considerably (Yeginbayeva and Atlar, 2018).

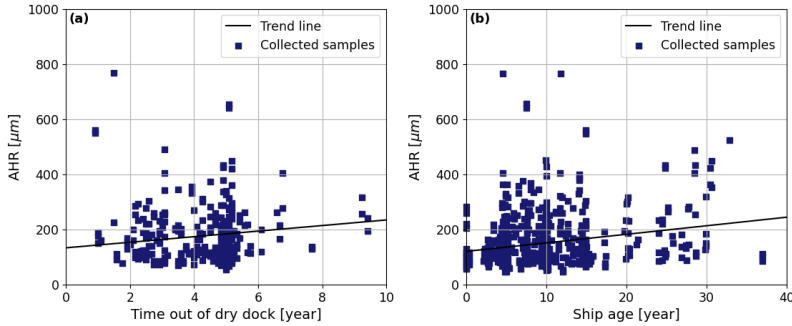


**Figure 1:** (a)  $AHR$  change over time out of dry dock, (b)  $AHR$  change according to ship age. It is based on 845 ships' data collected in drydock from 2003 to 2014. The figures are adapted from Stenson (2015) with minor modifications.

As shown in Fig. 2, the trend of  $AHR$  increase after drydock over time is different according to coating technology and substrate preparation at dry dock, and Stenson (2015) proposed an  $AHR$  estimation equation considering these parameters in his study. Since it is not possible to specify coating type, cleaning type, and drying docking period in a fleet-level analysis, this study replaced detailed values with averaged values from Figs 1-3 and simplified the formula by assuming a dry-docking interval of 5 years as shown in Eq. (4). In addition, the resistance increase due to hull roughness is calculated from Marintek's equation, which is a correction of the frictional resistance coefficient due to average hull roughness (refer to Eq. (5)). Fig. 3 shows the typical  $AHR$  change according to the age of the ship estimated by this simplified equation. It should be noted that various factors were assumed approximately in this approach to estimate  $AHR$  for the global fleet application, but exact information on hull cleaning and coating type is required when examining a specific ship case.

$$AHR = S_{AHR} + I_{AHR} \cdot N - R_{AHR} \left[ \frac{n}{5} \right] \quad (4)$$

$$\Delta C_F = [110 \cdot (AHR \cdot V_S)^{0.21} - 403] \cdot C_F^2 \quad (5)$$

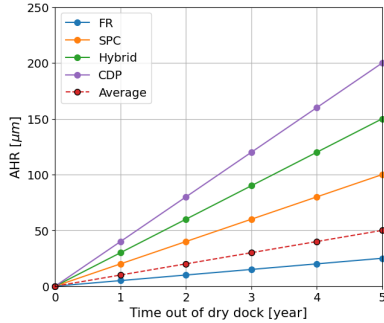


**Figure 2:**  $AHR$  change over time out of dry dock according to anti-fouling coating type. FR is foul release, SPC is self-polishing co-polymer, CDP is controlled depletion polymer, and Hybrid is a mixture of SPC and CDP. The 'Average' shown in the figure is the average  $AHR$  increase of the ships collected in Fig. 1 (b). The figure is adapted from Stenson (2015) with minor modifications.

where,  $AHR$  is current hull roughness in  $\mu m$ ,  $S_{AHR}$  is initial  $AHR$ ;  $120\mu m$  (Bowden and Davison, 1974; Townsin, 2003a),  $I_{AHR}$  is the annual change in  $AHR$  over the dry dock cycle;  $10\mu m$  (refer to Fig. 1),  $R_{AHR}$  is hull roughness reduction in drydocking;  $35\mu m$  (refer to Fig. 1),  $N$  is ship age, and  $\Delta C_F$  is roughness allowance.

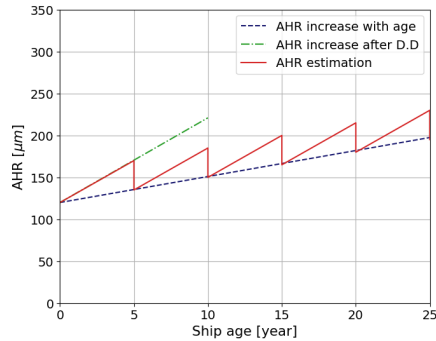


**Figure 3:** Estimated  $AHR$  according to the age of the vessel considering hull cleaning and re-coating in dry docking. It assumes a regular drydocking interval of five-year. The trends shown in the figure are approximations based on the data in Figs. 1 and 2.

### 3.2.3. Added resistance due to wind

According to ITTC (2017b), if there is no available wind tunnel test result of the target ship during the speed/power trial, wind resistance coefficients data sets (Boom et al., 2013; Kaiser, 2016) or regression equations (Fujiwara, 2006) can be used for calculating resistance increase due to wind. ITTC (2018) also included the wind tunnel test results of Blendermann (1996) to consider the speed reduction by the wind. Table 4 shows the ship types and loading conditions applicable to each estimation method of the wind resistance coefficient, and the details and wind resistance coefficients of the corresponding vessels are shown in Appendix C. Depending on the method, the ship type, loading type, and dimensions of the wind resistance coefficient that can be estimated are different. It is necessary to consider as many wind tunnel test results as possible to more accurately estimate the added resistance due to wind of the global fleet, which includes various ship types and a wide range of sizes.

Therefore, in this study, the wind tunnel test results of ITTC (2017b) and Blendermann (1996) and the regression equation of Fujiwara (2006) are mainly used to expand the applicable range and increase accuracy. If there is a wind

**Table 4**

Applicable ship type of wind resistance coefficient estimation methods. 'O' contains both the laden and ballast voyages, and 'O (avg.)' represents only average voyage.

Ship type	Blendermann (1996)	ITTC (2017b)	Fujiwara (2006)
Container	O	O	O
Oil tanker	O	O	O
Bulk carrier	X	O	O
Liquefied gas	O	O (Avg.)	O
General cargo	O	O	X
Ro-Ro	O	O (Avg.)	X
Passenger	O (Avg.)	O (Avg.)	O
Offshore	O (Avg.)	X	X

tunnel test result of the ship type and size consistent with the target ship, the average value between the wind tunnel tests and the estimated value by Fujiwara (2006) is used, otherwise, only Fujiwara (2006) is used. The parameters related to the superstructure of the ship used as the input of the regression equation are estimated using Kitamura et al. (2017). As a result, added resistance due to wind is calculated by substituting the estimated wind resistance coefficient of the ship into the following equations.

$$R_{wind} = \frac{1}{2}\rho_a C_X(0) A_{XV} V_S^2 - \frac{1}{2}\rho_a C_X(\psi_{WRef}) A_{XV} V_{WRef}^2 \quad (6)$$

$$V_{WRef} = \sqrt{V_{WTref}^2 + V_S^2 + 2V_{WTref} V_S \cos(\psi_{WT} - \psi)} \quad (7)$$

where  $C_X$  is wind resistance coefficient, which can be obtained from Blendermann (1996), ITTC (2017b), and Fujiwara (2006).  $A_{XV}$  is area of maximum transverse section exposed to the wind estimated from Kitamura et al. (2017),  $V_S$  is ship's speed over ground,  $V_{WRef}$  is relative wind speed at reference height,  $\rho_a$  is mass density of air,  $\psi_{WRef}$  is relative wind direction at reference height; 0 means heading wind.

### 3.2.4. Added resistance in waves

Added wave resistance of a ship can be estimated through various methods as shown in Table 5, and each method differs in the scope of application, input parameters, and features. Among the estimation methods for the added wave resistance of ITTC (2017b), STAwave-1 (STA1) and STAwave-2 (STA2) methods have been applied in several complete power prediction methods because they can provide good results with only a few inputs (Tillig et al., 2020; Kim et al., 2020; Kramel et al., 2021). However, they are limited to the added resistance at head waves from the bow to 45 degrees, implicitly assuming zero added wave resistance in other headings. Meanwhile, recently, methods such as Lang and Mao (2021), Liu and Papanikolaou (2020), and Kim et al. (2022a) have been proposed that can predict added wave resistance in all wave headings.

As the added resistance in head waves is much more dominant than in beam and following waves, some previous studies have considered only the added resistance in head waves. However, since the ship experiences waves in all directions while actually operating at sea, the approach capable of estimating the added wave resistance in all wave headings can greatly reduce the error compared to that of only taking into account head waves (Kim and Steen, 2022). Therefore, this study uses a Combined method, presented in Kim et al. (2022a), tuned for model test data of various ship types while being able to calculate added resistance in all wave directions. According to Eq. (8), the directional wave spectrum and the transfer function of the mean resistance increase in regular waves are superimposed linearly to estimate the resistance increase in short-crested irregular waves. Here, the added wave resistance coefficient is estimated from the combined method, and an example of the added wave resistance coefficients in arbitrary waves according to the speed of the ship is shown in Fig. 4.

$$R_{wave} = 2 \int_0^{2\pi} \int_0^\infty \frac{R_{aw}(\omega, \beta; V_S)}{\zeta_a^2} E(\omega, \beta) d\omega d\beta \quad (8)$$

**Table 5**

Comparison of semi-empirical methods for the ship added wave resistance.

	STA1	STA2	CTH	SNNM	Combined
Range	Head waves (180-135)	Head waves (180-135)	Arbitrary waves (180-0)	Arbitrary waves (180-0)	Arbitrary waves (180-0)
Input	$L_{bul}, B, H_s$	$L_{pp}, B, T, V_S,$ $V_S, C_B, k_{yy}$	$L_{pp}, B, T, V_S,$ $L_e, C_B, k_{yy}, \beta$	$L_{pp}, B, T, V_S,$ $L_e, L_r, C_B, k_{yy}, \beta$	$L_{pp}, B, T, V_S,$ $C_B, k_{yy}, \beta$ ( $L_e, L_r$ estimated)
Output	$R_{awl}$	$R_{aw}$	$R_{aw}$	$R_{aw}$	$R_{aw}$
Feature	Radiation effect is neglected; Heave and pitch irregular waves; are assumed to be small	Applicable to long crested Low Fn. test cases are not included	Applicable to short crested irregular waves	Developed based on 1477 cases	Tuned according to various ship types; Applicable with limited inputs
Reference	ITTC (2017b)	ITTC (2017b)	Lang and Mao (2021)	Liu and Papanikolaou (2020)	Kim et al. (2022a)

$$C_{aw} = \frac{R_{aw}}{\rho_w g \zeta_a^2 B^2 / L_{pp}} \quad (9)$$

where  $R_{aw}$  is the transfer function of mean resistance increase in regular waves,  $C_{aw}$  is the added resistance coefficient in regular waves, which can be obtained from Kim et al. (2022a),  $E$  is directional spectrum, which can be obtained from ITTC (2017b),  $\zeta_a$  is wave amplitude.

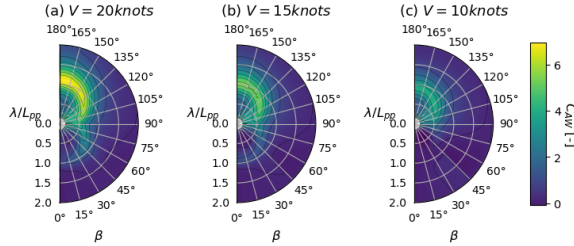


**Figure 4:** An example case of the added resistance coefficients in regular waves estimated from the Combined method. 173k LNG carrier at (a) 20knots, (b) 15knots, (c) 10knots.

### 3.3. Estimation of total propulsive efficiency

The total propulsive efficiency can be estimated approximately by applying a straightforward empirical formula, or by calculating each efficiency coefficient that makes up the total propulsive efficiency, such as open water efficiency, hull efficiency, relative rotational efficiency, etc., separately. In the former case, there exist approaches like Emerson's formula (Watson, 1998), the method of Danckwardt (1969), and the method of Auf'm Keller (1973). Emerson's formula covers contemporary propeller designs but applies only to low propeller RPMs, and Danckwardt (1969) and Auf'm Keller (1973) are only relevant to specific ship types (Birk, 2019). In this study, we, therefore, chose to estimate the total propulsive efficiency for a ship by estimating the sub-components related to the hull and propeller, and engine and shaft connections, and then, multiplying them together as shown in Eq. (10).

$$\eta_T = \eta_O \eta_H \eta_R \eta_S \quad (10)$$

where  $\eta_T$  is total propulsive efficiency,  $\eta_O$  is open water efficiency,  $\eta_H$  is hull efficiency,  $\eta_R$  is relative rotational efficiency, and  $\eta_S$  is shaft efficiency.

There are simple approaches to estimate open water efficiency, such as Gawn (1957), Newton (1961), and Oosterveld (1970), but they may not be suitable for modern propeller designs and have a limited range of ships for which they are applicable. For the estimation of open water efficiency, the Wageningen B series, a wide range of open water diagrams according to various propeller design combinations of blade count, expansion area ratio, and pitch ratio is widely used. However, without a detailed propeller design, they require many assumptions and estimations for the propeller specs. In this study, the approximation of the Wageningen B-series (Breslin and Andersen, 1996; Kristensen and Lützen, 2012), which enables the calculation of open water efficiency with only limited input such as propeller diameter, is applied as following Eqs. (11)-(13).

$$\eta_O = \frac{2}{1 + \sqrt{C_{Th} + 1}} f(C_{Th}) \quad (11)$$

$$f(C_{Th}) = 0.81 - 0.014C_{Th} \quad (12)$$

$$C_{Th} = \frac{8}{\pi} \frac{R_T}{\rho_w(1-t)((1-w)V_S D_p)^2} \quad (13)$$

where  $C_{Th}$  is thrust loading coefficient,  $f(C_{Th})$  should not be lower than 0.69,  $t$  is thrust deduction factor and  $w$  is the wake fraction, and  $D_p$  is the propeller diameter.

Hull efficiency can be calculated as in Eq. (14), where thrust deduction ( $t$ ) and wake fraction ( $w$ ) are determined by empirical methods provided as parts of the empirical methods for prediction of calm water resistance. Moreover, Alte and Baur (1986) suggested an average value of 1.0 for a single screw for relative rotational efficiency, which often ranges from 0.95 to 1.05. Here, constant values of  $\eta_R = 1.0$  and  $\eta_S = 0.98$  are assumed respectively (Kristensen and Lützen, 2012).

$$\eta_H = \frac{1-t}{1-w} \quad (14)$$

### 3.4. Estimation of engine power

After taking into consideration the ship's total propulsive efficiency, an estimate of the main engine's brake power can be derived by combining it with the ship's total resistance as shown in Eq. (15).

$$P_B = \frac{R_T V_S}{\eta_T} \quad (15)$$

Kramel et al. (2021) presented a load adjustment factor based on the fact that the ship's power at the design condition is generally within about 80 to 95% of the installed engine maximum continuous rating (MCR). If the engine power estimated from the empirical methods at the design condition is out of the range, it is considered an irrational value, and a load adjustment factor that scales it within the range is applied. Assuming that ships operate most frequently close to design conditions, this method is considered to be plausible if there is no other information for the validation.

Meanwhile, according to 4<sup>th</sup> IMO GHG study (Faber et al., 2020), power consumption was calculated based on the service speed of ships registered in IHS data set, but it was observed that fuel consumption was greatly overestimated than the real case in some passenger ships and large container ships. This is due to the fact that some large ships are outfitted with engines larger than those required for service speed, allowing them to have enough performance to operate at a significantly higher speed than the stated service speed. In particular, since cruise ships tend to be equipped with advanced propulsion systems such as diesel-electric, the power predictions are also often overestimated.

Therefore, based on these findings, this study proposes an algorithm that can determine an appropriate empirical method to estimate calm water resistance for each ship case, and calculate the final brake power of the ship as shown in Fig. 5. When the initial brake power at design condition is within 80–95% of the MCR, i.e. the estimated value is within the normal range, it is then determined whether the ship profile is within the applicable range of the empirical method. If there is a method that satisfies both, the brake power under the given condition of the ship is finally calculated using the corresponding method. If multiple methods are selected, the average of the predicted values is used.

This algorithm is further subdivided into cases where the engine load is less than 80% and more than 95% than previously proposed methods in Kramel et al. (2021). If the engine load at design condition is less than 80%, an engine load of less than 80% could be obtained regardless of the accuracy of the candidate methods due to the various reasons mentioned above. In this case, since it is difficult to identify a clear cause only with limited information, the average of brake powers predicted from the candidate methods is used for the final brake power. On the other hand, since it is clear that the engine load under the design conditions cannot exceed 95% of the installed engines, the estimated engine power is scaled down by applying the load adjustment factor, which is obtained based on the design condition. This determination algorithm applies only to the contribution of calm water resistance to brake power. The validity of the algorithm needs to be thoroughly investigated for detailed ship cases through more data in the future.

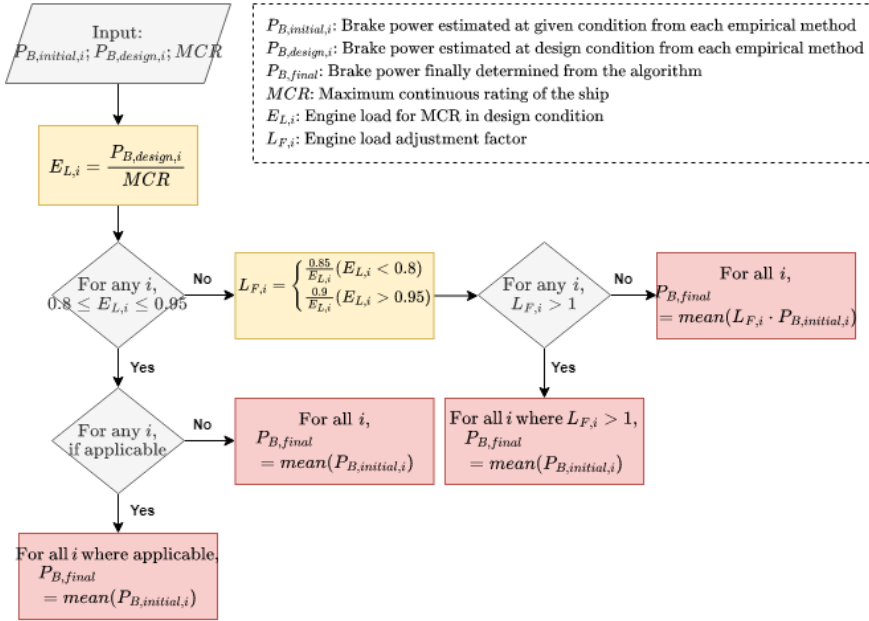


**Figure 5:** Determination algorithm for the estimation methods of ship resistance in calm water. This algorithm checks whether the corresponding ship case is within the applicable range of the candidate method and whether the estimated power at the ship's design condition is within the permissible range.

### 3.5. Power prediction model for the global fleet: The MariTEAM model

As previously described in section 3.1-3.4, Fig. 6 shows a flowchart for estimating the propulsion power of the ship in the MariTEAM model, and Fig. 7 shows an overview of the MariTEAM model, a bottom-up approach for evaluating fuel consumption and emissions in global shipping. Here, ship technical information from the Sea-web database, ship dynamic information from the AIS data, and weather hindcast data from ECMWF are used as initial inputs for the model, and they undergo the data correction and parameter estimation process outlined above. The processed data is entered into the resistance component modules of calm water, roughness, wind, and waves, respectively, from which the total resistance of the ship is calculated. The total resistance and total propulsive efficiency of the ship are used to compute its initial brake power. Through a determination algorithm presented in Section 3.4, the initial brake power is converted into the final brake power for a given ship.

Several simplifications and assumptions have been made in the power prediction module of the MariTEAM model to reasonably estimate the power consumption of the worldwide fleet in the absence of exact information on hull shape, propeller, and specific operating conditions.

In relation to the propeller efficiency of the ship, relative rotative efficiency and shaft efficiency are roughly applied with a constant value, and the approximation of the Wageningen B-series, which relies heavily on the propeller diameters of the ship, is used for open water efficiency. Also, any effect of waves on the thrust deduction and wake fraction is disregarded. Since the real-time status of the ship's draught and trim changes is not available from AIS data, their instantaneous impact is not expected to be captured. It is assumed that every five years, the ship is regularly cleaned and re-coated in a dry dock when determining the average hull roughness based on the age of the vessel. For simplicity, there is no submerged transom and appendages of the vessel, and the effect of steering and maneuvering on power consumption is ignored. Therefore, it may include uncertainty due to these factors for a specific ship case.

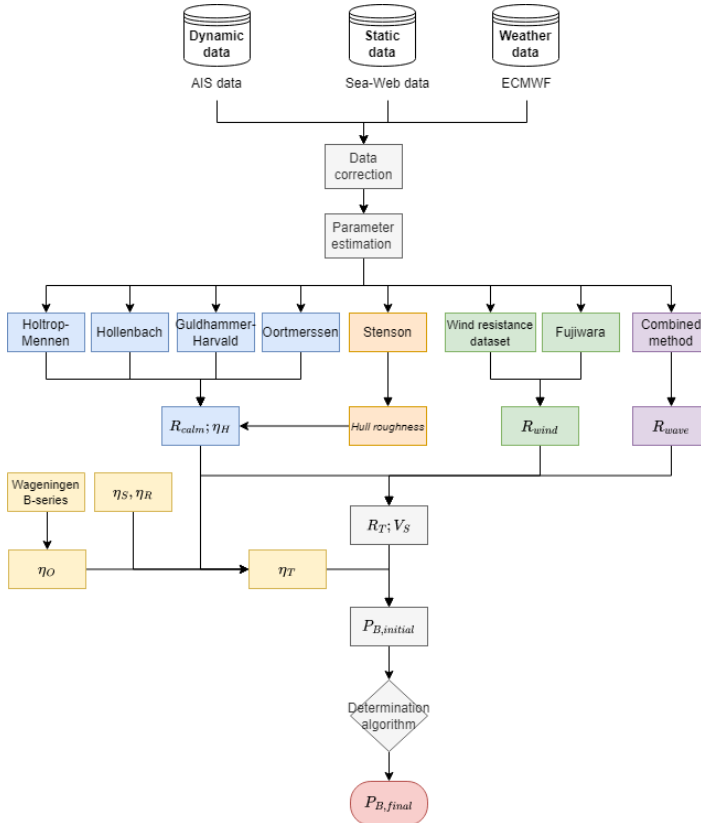
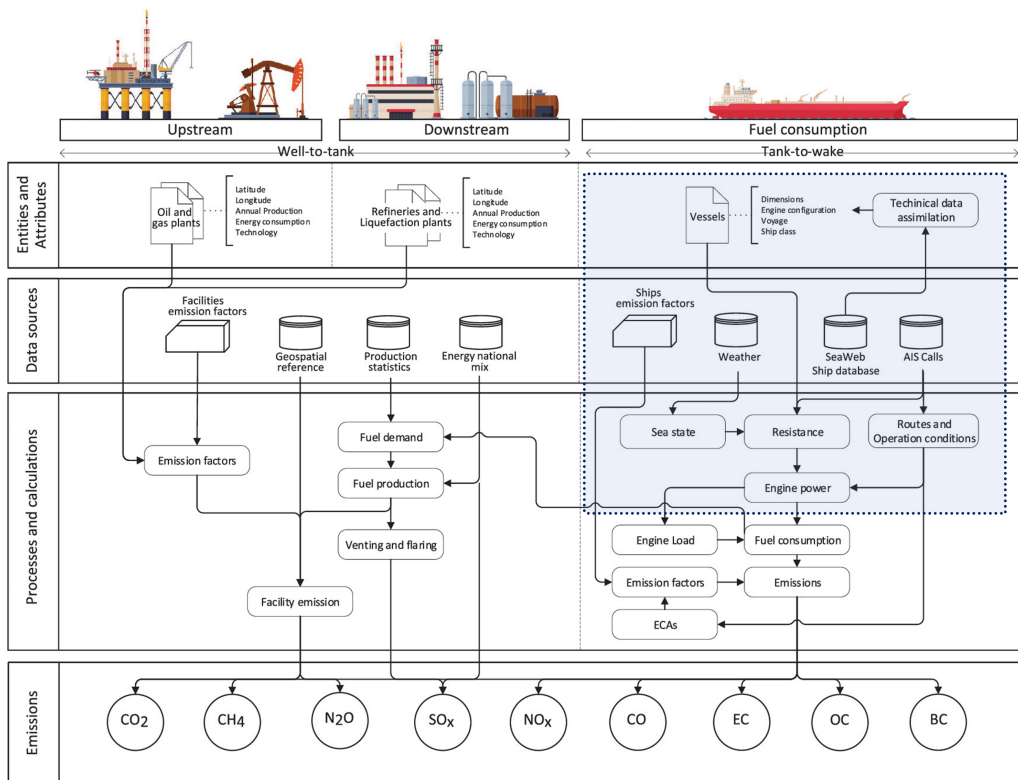


Figure 6: Schematic diagram of ship power prediction module of the MariTEAM model.



Modeling of ship resistance and power consumption for the global fleet: The MariTEAM model



**Figure 7:** MariTEAM modeling framework for global well-to-wake emissions. The blue-shaded part is the ship power prediction module outlined in Fig. 6. The figure is adapted from Kramel et al. (2021) with minor modifications.

## 4. Results & Discussion

This section verifies the performance of the developed power prediction method in the MariTEAM model using full-scale measurements and MRV data and presents a case study of the application of the model to the evaluation of the resistance components and  $CO_2$  emissions from the global fleet. Additionally, the analysis results using the model are provided together.

### 4.1. Comparison with the full-scale measurements

The full-scale measurement acquired from the ships for a certain period of time is used to evaluate the performance of the power prediction suggested in this study. Here, as shown in Table 6, three ships; a LNG, general cargo, and container are used, each consisting of different data collection periods and sampling intervals. Only the ship's position, speed, and draft information from the in-service data are used as inputs for the model, and other parameter estimation and power prediction followed by the method described in section 3. Fig. 8 shows the main engine power obtained from the in-service data of ships according to the time series and the predicted values obtained from the model. Fig. 9 shows the scatter plot of the actual value and the predicted value. Here, error metrics such as  $r$ ,  $R^2$ , and  $NRMSE$  are presented together, which represent the Pearson correlation coefficient, the coefficient of determination, and the normalized root-mean-squared error, respectively, as shown in Eqs. (16)-(18).

$$r = \frac{\sum_{i=1}^n (x_i - \bar{x})(y_i - \bar{y})}{\sqrt{\sum_{i=1}^n (x_i - \bar{x})^2} \sqrt{\sum_{i=1}^n (y_i - \bar{y})^2}} \quad (16)$$

$$R^2 = 1 - \frac{\sum_{i=1}^n (x_i - y_i)^2}{\sum_{i=1}^n (x_i - \bar{y}_i)^2} \quad (17)$$

$$NRMSE = \frac{\sqrt{\frac{1}{n} \sum_{i=1}^n (x_i - y_i)^2}}{MCR} \quad (18)$$

where  $x_i$  is the true value measured from the ship,  $\bar{x}$  is the mean of  $x$  samples,  $y_i$  is the predicted value from the model,  $\bar{y}$  is the mean of  $y$  samples,  $n$  is the number of samples, and  $MCR$  is the maximum continuous rating of main engine.

For a more accurate comparison between the predicted values in the model and the in-service data, the steady-state detection algorithm presented in Gupta et al. (2022), which can be used to filter out the parts of the time series in which the ship's propulsion state changes, is applied here. It may be erroneous to use data in this condition for analysis because the speed may suddenly descend or recover having time gaps with the ship's power when the propulsion state of the ship changes, such as during acceleration, deceleration, and maneuvering.

**Table 6**  
Details of main characteristics and full-scale measurement data.

Description	Ship A	Ship B	Ship C
Ship type	LNG carrier	General cargo	Container
Length [m]	283	194	350
Breadth [m]	46	32	48
Design draught [m]	12.5	12.6	14.5
Block coefficient [-]	0.78	0.80	0.66
Deadweight tonnage [ton]	95800	50700	141000
Maximum continuous rating [kW]	21500	10780	68600
Sailing area	Europe-Africa	Worldwide	East Asia-Europe
Data collection period	2 month	2.9 years	1.2 years
Data sampling interval	4 seconds	15 minutes	1minute

As shown in Fig. 8, it is observed that Ships A and C tend to underestimate the engine power of the actual ship, and Ship B tends to overestimate compared to the full-scale measurements. However, it seems that the predictions are generally within an acceptable range, and appear to consistently predict power changes in different operational profiles.

Referring to the error metrics between the predicted and actual values in Fig. 9, the  $R^2$  values of Ships A and B are 0.77, 0.68, making a good prediction for the actual power consumption of the ship, while the  $R^2$  value of Ship C shows a relatively low accuracy of 0.34.  $NRMSE$  ranges from about 8.7 to 12.2%. These errors may be caused by the uncertainty of the collected data, the process of estimating ship-specific parameters and applying empirical methods. Nevertheless, it is noteworthy that there is a strong positive correlation between the actual value and the predicted value of all three ships, with a correlation coefficient of 0.88 to 0.95. As a result, the estimated results of the MariTEAM model can result in some errors in comparison with specific ship cases due to various constraints, but it is expected to simulate the overall power performance trends of various ships well.

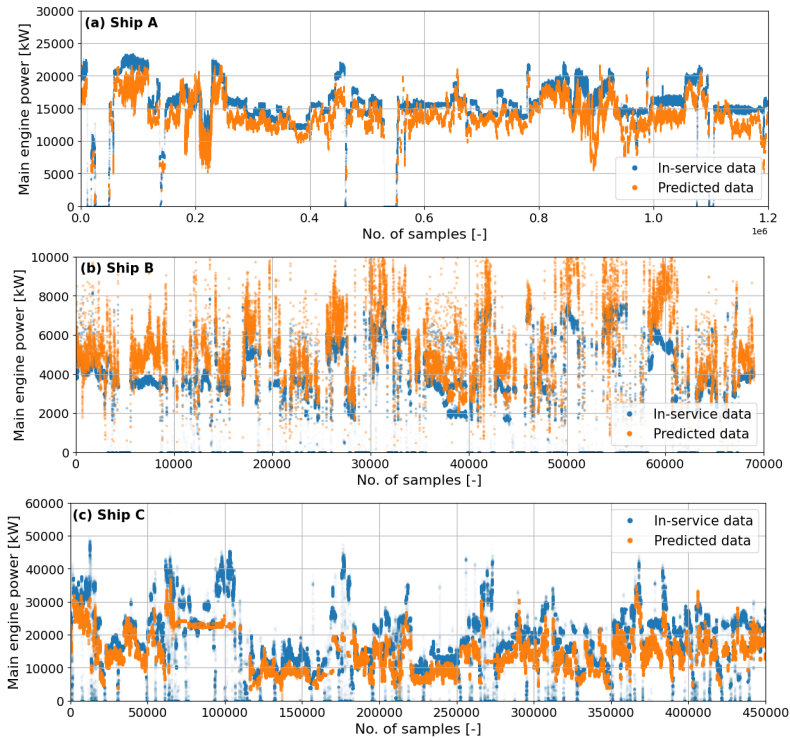


**Figure 8:** Comparison of the onboard measurement and predicted values of (a) Ship A, (b) Ship B, and (c) Ship C.

#### 4.2. Comparison with EU-MRV data

In the previous section, the model has been validated in individual ship cases, and here, how the model's prediction performs at a wider fleet across different segments is presented. Thus, the performance of the developed model is evaluated by benchmarking the fuel consumption reported in the EU-MRV data for 2018 (EMSA, 2018). The EU-MRV data contains information on annual fuel consumption and emissions for approximately 12,000 ships with European origin or destination. To compare the results of the model and MRV, the AIS data of the vessel matching the MRV data is identified, and the annual energy consumption of the corresponding vessel is tracked based on it. In this analysis, we compare 10,425 vessels that are found in both MRV and AIS data. Here, the AIS messages from the global fleet

## Modeling of ship resistance and power consumption for the global fleet: The MariTEAM model

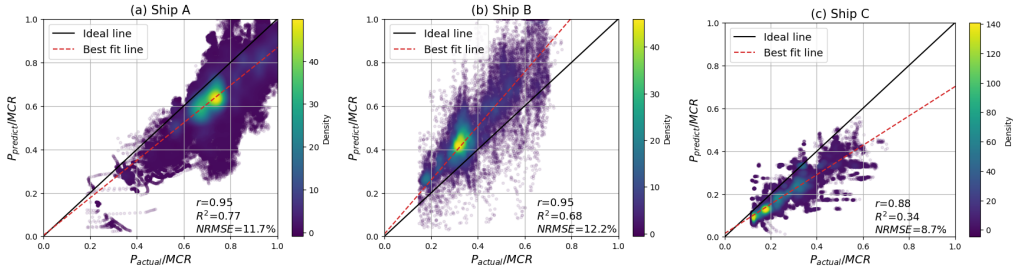


**Figure 9:** The goodness of fit plots showing onboard measured versus predicted engine powers for (a) Ship A, (b) Ship B, and (c) Ship C. A solid line represents an ideal line where  $x$  and  $y$  match, a dotted line represents a linear line of the best fit between  $x$  and  $y$ , and a color bar on the right shows the density of the samples.

obtained from NorSat-satellites of the Norwegian Space Center cooperation with Kystverket of Norwegian Coastal Administration are used (Eriksen et al., 2020).

The fuel consumption of a ship is calculated based on the instantaneous power and the specific fuel oil consumption (SFOC) according to the load conditions of the engine. Here, the main engine power is estimated by the developed model from the previous section. Since information on the auxiliary engine is often unavailable from ship databases, different auxiliary engine models are developed in accordance with the IMO guidelines for the estimation of installed power in auxiliary engines (IMO, 2014). Auxiliary power demanded is calculated as 2.5% of the main engine MCR + 250 kW if MCR is higher than 10 MW, or as 5% of MCR if not, regardless of operational conditions. SFOC depends on the type of fuel oil and the type of engine, and its value is calculated assuming a low calorific value of 40.2 MJ/kg for HFO and 42.7 MJ/kg for MGO-fueled engines, with a thermal engine efficiency of 50% in both cases.

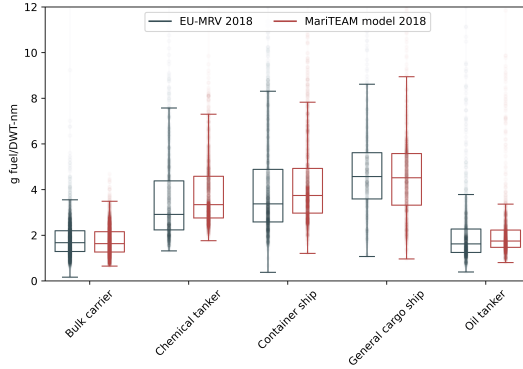
Fig. 10 displays as box plots MRV data and model estimates for the annual average fuel consumption per transport work ( $g/dwt - nm$ ) for the various fleet segments. Both ends of the box are in the 25-75% interquartile range, the solid line in the middle represents the median value, both ends of the whisker mean the minimum and maximum values, and the outliers are shown in transparent. The distribution of fuel consumption across all ship segments at the aggregation level appears to be quite accurately reproduced by the MariTEAM model, from the fact that the 25-75% and median values of the box plot are almost identical and the whiskers of the two datasets are also very similar.

Fig. 11 shows the detailed comparison results for the sub-segments based on the size of each ship type following the same distribution used in the 4<sup>th</sup> IMO GHG study. The left side of each subplot shows the aggregated density distribution for the fuel consumption of the corresponding ship type, and the right side shows boxplots based on the sub-segment.

The fuel consumption distributions of bulk carriers, container ships, general cargo ships, and oil tankers, seem to be well-matched overall. In the case of chemical ships, the fuel consumption distribution is generally similar to the predicted distribution, but the predicted results are slightly shifted toward higher fuel consumption. The MariTEAM model can also similarly catch the shape of the distribution, such as hump and hollow curved shown in the distribution of container ships and general cargo ships.

Looking at the box plot on the right side, some sub-segments of small bin sizes, such as bulk carriers, chemical ships, general cargo ships, and oil tankers, tend to show a relatively large difference between model predictions and MRV reported values. However, since the number of ship samples included in these sub-segments is very small, the accuracy of the reporting results may be questionable. Additionally, differences in the distribution of MRV and the developed model may stem from assumptions on auxiliary engines and boilers. Overall, the model shows good performance for most of the sub-segments compared to the 25% and 75% quartile ranges and 1.5\*IQR. Based on the comparison results of Sections 4.1 and 4.2, the MariTEAM model can simulate the overall trends of the estimation of energy consumption and emissions from global shipping adequately.

Modeling of ship resistance and power consumption for the global fleet: The MariTEAM model



**Figure 10:** Box plot comparing annual average fuel consumption per transport work ( $g/dwt - nm$ ) of fleet segments in 2018 between EU-MRV data and the MariTEAM model.

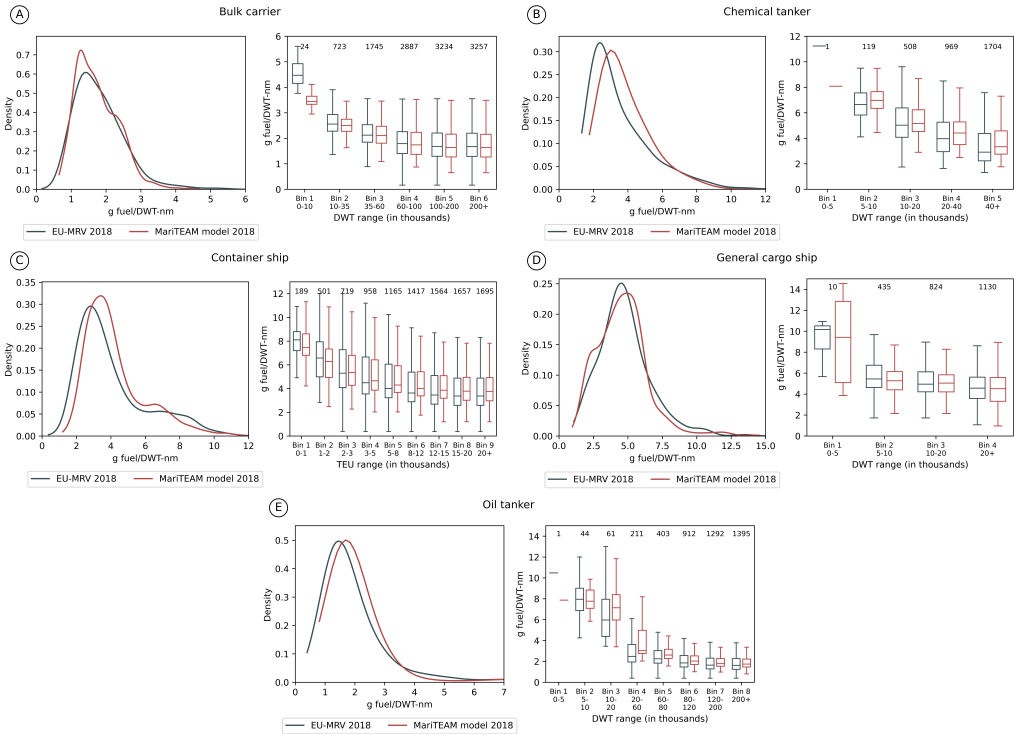


**Figure 11:** Comparison of annual average fuel consumption per transport work ( $g/dwt - nm$ ) by sub-segment of (a) bulk carriers, (b) chemical tankers, (c) container ships, (d) general cargo ships, and (e) oil tankers. The left side of each subfigure represents the density distribution for the fuel consumption of the corresponding ship type, and the right side represents the box plot of the fuel consumption for each bin size. The number above the x-axis to the right subfigure indicates the sample size of each bin category.

### 4.3. Global assessment of ship resistance components and CO<sub>2</sub> emissions

In this section, the power prediction and energy consumption of the worldwide fleet based on the proposed model are analyzed, and the findings are shown according to the ship's resistance components. The 2018 AIS data for 45,891 vessels in the Sea-web database are examined. The upper part of Fig. 12 shows the average annual power increase due to the added wind resistance of the entire fleet, and the lower part shows the case of added wave resistance estimated from the MariTEAM model.

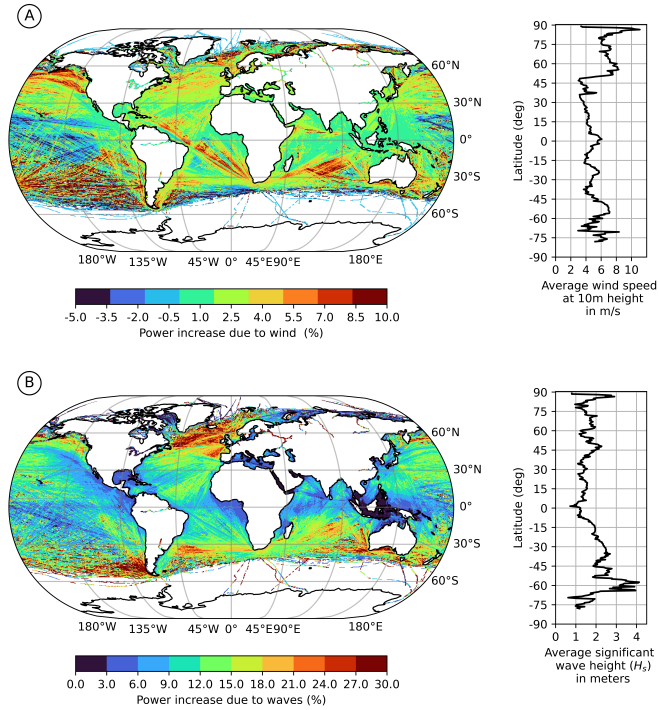


**Figure 12:** Geographical distribution of power increase due to added resistance in (a) wind and (b) waves. Here, the power increase is calculated by power increased by added resistance due to wind and waves compared to the required power in calm water resistance of a ship.

In high-latitude waters over 45 degrees with strong winds and waves, particularly in the North Sea, the North Atlantic, South Africa, and the southern coast of Australia, it can be observed that ships experience noticeably more resistance due to the weather. On the other hand, in coastal and inland seas, the power increase due to added resistance due to wind and waves is relatively insignificant. Depending on the global wind pattern at the oceans and the actual operational profile of ships, the average power consumption trends vary mostly between -5 and 10%, with an average of 2 to 3%. In the case of wind, a negative value for the power increase can be indicated when a ship is experiencing a tailwind or a direction that is advantageous for the ship's operation. The increase in power due to the added wave resistance of the ship can reach 0 to 30% depending on the sea area, and 8 to 9% on average globally.

Examining the distribution of the added wind resistance reveals that the power increase on the ship's main path is noteworthy due to the influence of global wind patterns. For example, in the case of a route between the Cape of Good Hope in Africa and North America or a route across the Indian Ocean, it is evident that ships sail this route because it is the shortest distance, even though the ship encounters a considerable amount of added resistance due to trade winds.

The estimation results from this model illustrate the energy consumption trends of ships worldwide according to the global climate distribution. Through this analysis, it is found that the weather effect can significantly increase the ship’s power consumption to an average of about 10-12%, which is almost similar to the sea margins applied in many bottom-up studies. However, if the same sea margin is applied to the entire sea and fleet, added resistance due to wind and waves in some areas may differ from reality on an annual average of about -30 to +20%, which can lead to significant inaccuracies in fuel consumption and emissions predictions.

Fig. 13 shows the percentage of each resistance component to the total resistance according to the ship type. Among the resistance components, the calm water resistance accounts for the largest proportion of total resistance, which on average is about 83% of the total resistance on average. Referring to the share of the added resistance due to hull fouling, the power increase ranges from 7 to 12% depending on the ship type. On average, it can increase ship required power by about 10%, which is slightly larger than the fouling coefficients of 7 and 9%, applied in IMO (Faber et al., 2020) and ICCT GHG studies (Olmer et al., 2017). These results can vary depending on various factors such as the characteristics, operation profiles, and main trading routes of the corresponding fleet. For instance, in Fig. 13, ship types with more surface area above the waterline (such as containers and general cargo ships) have a bigger share of added resistance due to wind. Similarly, segments operating at higher speeds (i.e. container ships between 12 and 17 knots) have a higher calm water resistance if compared to segments at lower speeds (i.e. bulk carriers between 9 and 12 knots) thus having a lower share of added resistance due to waves.

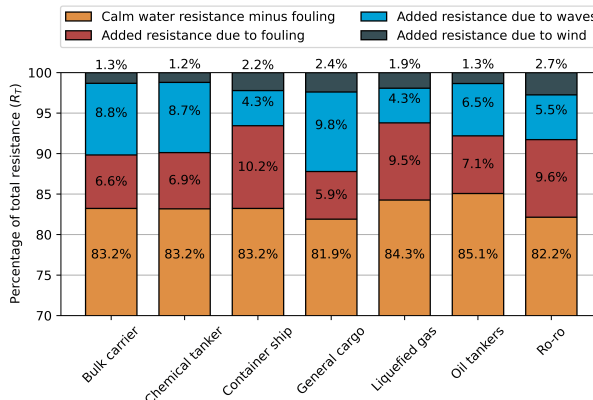


Figure 13: Share of ship resistance components to the total resistance according to ship segments.

Fig. 14 depicts the geographical distribution of annual  $CO_2$  emissions ( $kg \cdot km^{-2}$ ) derived from AIS data for global ships in 2018.  $CO_2$  emissions are determined geographically based on the location of the global ship’s trajectory, and the yearly accumulated emissions for each square meter are used.  $CO_2$  emissions per square meter are depicted according to color, highlighting the regions with the highest emissions: the Mediterranean, the Red Sea, the European coast, Southeast Asia, and the East and South China Seas. These locations are generally identified as the most dense trade routes in the world. The global sum of  $CO_2$  emissions from the ships was 961 million tons.

As a result, it is found that the power prediction model presented in this study, which is capable of predicting the resistance components of ships under varied ship characteristics, operational profiles, and weather conditions, can be useful for evaluating emissions from global shipping.

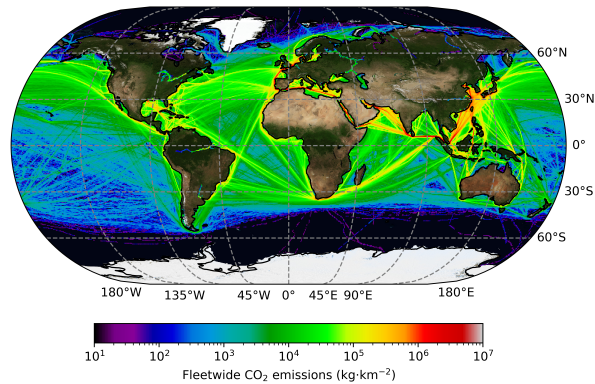


Figure 14: Geographical distribution of annual  $CO_2$  emissions ( $kg \cdot km^{-2}$ ) from global shipping.

## 5. Conclusions

To successfully achieve GHG reduction in global shipping, it is critical to properly evaluate and understand the impact of the combination of operational scenarios and various mitigation measures, which requires a system that can accurately predict the required power for the global fleet under the actual operating profile and the weather condition.

Thus, in this study, we proposed an improved method for power prediction of ships, suitable for bottom-up analysis of the global fleet based on the MariTEAM model. To achieve this, a strategy is taken in this study to either find the method or combination of methods among those used in prior studies that are most appropriate or to modify and improve them. A comprehensive calculation procedure for the powering performance of the global fleet, encompassing data pre-processing, ship resistance estimation, and propulsive efficiency, is presented throughout the paper.

Through the comparison results with the three ships' full-scale measurements and 2018 EU-MRV data, it is demonstrated that the developed model provides fairly accurate power prediction according to the various operational profiles and captures the trend of energy consumption well of the global fleet. Based on the developed complete power prediction model, follow-up research will be conducted on fuel consumption and emissions assessment and strategy derivation according to various trade patterns. It can also be combined with various energy reduction scenarios to identify suitable pathways to reduce GHG emissions. Future advancements in data collection and pre-processing technology for the fleet level are expected to further help improve the accuracy and reliability of these results.

## CRedit authorship contribution statement

**Young-Rong Kim:** Conceptualization, Investigation, Methodology, Software, Writing - Original Draft. **Sverre Steen:** Conceptualization, Methodology, Writing - Review & Editing, Supervision. **Diogo Kramel:** Conceptualization, Methodology, Software, Writing - Review & Editing. **Helene Muri:** Conceptualization, Methodology, Writing - Review & Editing, Supervision. **Anders Hammer Strømman:** Conceptualization, Methodology, Writing - Review & Editing, Supervision.

## Acknowledgements

This study is part of the research projects CLIMMS – Climate change mitigation in the maritime sector (RCN project number 294771) and SFI Smart Maritime – Norwegian Centre for Improved Energy-Efficiency and Reduced Emissions from the Maritime Sector (RCN project number 237917). We further acknowledge our partners involved in these projects. The AIS data were provided by Kystverket (Norwegian Coastal Administration). Part of the computations and data storage were performed on resources provided by Sigma2 - the National Infrastructure for High Performance Computing and Data Storage in Norway, Projects NN9576k and NS9576K, and NTNU IDUN computing



cluster. We acknowledge technical support including data management from Radek Lonka and the Industrial Ecology Digital Laboratory.

## References

- Alte, R., Baur, M., 1986. Propulsion. handbuch der werften. Hansa 18, 132.
- Auf'm Keller, W., 1973. Extended diagrams for determining the resistance and required power for single-screw ships. *International Shipbuilding Progress* 20, 133–142.
- Balcombe, P., Brierley, J., Lewis, C., Skatvedt, L., Speirs, J., Hawkes, A., Staffell, I., 2019. How to decarbonise international shipping: Options for fuels, technologies and policies. *Energy conversion and management* 182, 72–88.
- Barnitsas, M.M., Ray, D., Kinley, P., 1981. KT, KQ and efficiency curves for the Wageningen B-series propellers. Technical Report. University of Michigan.
- Bertram, V., 2011. Practical ship hydrodynamics. Elsevier.
- Bertram, V., Wobig, M., 1999. Simple empirical formulae to estimate main form parameter. *Schiff Hafen* 11, 118–121.
- Birk, L., 2019. Fundamentals of ship hydrodynamics: Fluid mechanics, ship resistance and propulsion. John Wiley & Sons.
- Blendermann, W., 1996. Wind loading of ships collected data from wind tests tunnel in uniform flow. Institut für Schiffbau der Universität Hamburg.
- Boom, H., Huisman, H., Mennen, F., 2013. New guidelines for speed/power trials. Level playing field established for IMO EEDI. SWZ Maritime, 1–11.
- Bouman, E.A., Lindstad, E., Rialland, A.I., Strømman, A.H., 2017. State-of-the-art technologies, measures, and potential for reducing ghg emissions from shipping—a review. *Transportation Research Part D: Transport and Environment* 52, 408–421.
- Bouman, E.A., Lindstad, H.E., Stromman, A.H., 2016. Life-cycle approaches for bottom-up assessment of environmental impacts of shipping, in: SNAME Maritime Convention, OnePetro.
- Bowden, B., Davison, N., 1974. Resistance increments due to hull roughness associated with form factor extrapolation methods. NPL.
- Breslin, J.P., Andersen, P., 1996. Hydrodynamics of ship propellers. 3, Cambridge university press.
- Brown, I.N., Aldridge, M.F., 2019. Power models and average ship parameter effects on marine emissions inventories. *Journal of the Air & Waste Management Association* 69, 752–763.
- Corbett, J.J., Koehler, H.W., 2003. Updated emissions from ocean shipping. *Journal of Geophysical Research: Atmospheres* 108.
- Dale, T., 2020. Development of Simplified Methods for Ship Powering Performance Calculations. Master's thesis. NTNU.
- Danckwardt, E., 1969. Ermittlung des widerstandes von frachtschiffen und hecktrawlern beim entwurf.
- Dijkstra, E.W., 2022. A note on two problems in connexion with graphs, in: Edsger Wybe Dijkstra: His Life, Work, and Legacy, pp. 287–290.
- DNVGL, 2018. Rules for classification: Ships. part 3 hull. chapter 1 general principles. Høvik, Norway: DNVGL-RU-SHIP Pt.3 Ch.1.
- EMSA, 2018. Emsa/thetis-mrv database. URL. <https://mrv.emsa.europa.eu>.
- Eriksen, T., Hellenen, Ø., Skauen, A.N., Storesund, F.A., Bjørnevik, A., Åsheim, H., Blindheim, E.V., Harr, J., 2020. In-orbit ais performance of the norwegian microsatellites norsat-1 and norsat-2. *CEAS Space Journal* 12, 503–513.
- Faber, J., Hanayama, S., Zhang, S., Pereda, P., Comer, B., Hauerhof, E., Schim van der Loeff, W., Smith, T., Zhang, Y., Kosaka, H., et al., 2020. Fourth imo ghg study. London, UK.
- Fujiwara, T., 2006. A new estimation method of wind forces and moments acting on ships on the basis of physical components models. *Journal of the Japan society of naval architects and ocean engineers* 2, 243–255.
- Gawn, R., 1957. Effect of cavitation on the performance of a series of 16 in. model propellers, in: Meeting of the Institution of Naval Architects, TINA, London, 1954, Published in: RINA Transactions: 1957-32, Paper 3.
- Gertler, M., 1954. A reanalysis of the original test data for the Taylor Standard Series. Technical Report. DAVID TAYLOR MODEL BASIN WASHINGTON DC.
- Guldhammer, H., Harvald, S.A., 1974. Ship resistance-effect of form and principal dimensions.(revised). Danish Technical Press, Danmark, Danmarks Tekniske Højskole, kademisk Forlag, St. kannikestrade 8, DK 1169 Copenhagen.
- Guo, B., Liang, Q., Tvete, H.A., Brinks, H., Vanem, E., 2022. Combined machine learning and physics-based models for estimating fuel consumption of cargo ships. *Ocean Engineering* 255, 111435.
- Gupta, P., Kim, Y.R., Steen, S., Rasheed, A., 2022. Data processing framework for ship performance analysis. arXiv preprint arXiv:2202.01000.
- Gupta, P., Taskar, B., Steen, S., Rasheed, A., 2021. Statistical modeling of ship's hydrodynamic performance indicator. *Applied Ocean Research* 111, 102623.
- Hart, P.E., Nilsson, N.J., Raphael, B., 1968. A formal basis for the heuristic determination of minimum cost paths. *IEEE transactions on Systems Science and Cybernetics* 4, 100–107.
- Helmores, P., 2008. Update on oantmeressen's resistance prediction, in: Pacific 2008 International Maritime Conference.
- Hersbach, H., Bell, B., Berrisford, P., Hirahara, S., Horányi, A., Muñoz-Sabater, J., Nicolas, J., Peubey, C., Radu, R., Schepers, D., et al., 2020. The era5 global reanalysis. *Quarterly Journal of the Royal Meteorological Society* 146, 1999–2049.
- Hollenbach, K.U., 1998. Estimating resistance and propulsion for single-screw and twin-screw ships-ship technology research 45 (1998). *Schiffstechnik* 45, 72.
- Holtrop, J., Mennen, G., 1982. An approximate power prediction method. *International Shipbuilding Progress* 29, 166–170.
- IHS, 2019. Sea-web ships. URL. <https://maritime.ihs.com>.
- IMO, 2014. Report of the marine environment protection committee on its sixty-sixth session. MEPC 66/21.
- IMO, 2018. Strategy on reduction of ghg emissions from ships. MEPC 304, 72.
- IMO, 2021. Guidelines on the method of calculation of the attained energy efficiency existing ship index (eexi). MEPC 76/15/Add.2/Annex 7.
- ITTC, 2017a. 1978 ittc performance prediction method.

- ITTC, 2017b. Recommended procedures and guidelines, preparation, conduct and analysis of speed/power trials.
- ITTC, 2018. Recommended procedures and guidelines, calculation of the weather factor  $f_w$  for decrease of ship speed in wind and waves.
- Jalkanen, J.P., Brink, A., Kalli, J., Pettersson, H., Kukkonen, J., Stipa, T., 2009. A modelling system for the exhaust emissions of marine traffic and its application in the baltic sea area. *Atmospheric Chemistry and Physics* 9, 9209–9223.
- Jalkanen, J.P., Johansson, L., Kukkonen, J., Brink, A., Kalli, J., Stipa, T., 2012. Extension of an assessment model of ship traffic exhaust emissions for particulate matter and carbon monoxide. *Atmospheric Chemistry and Physics* 12, 2641–2659.
- Jia, H., Prakash, V., Smith, T., 2019. Estimating vessel payloads in bulk shipping using ais data. *International Journal of Shipping and Transport Logistics* 11, 25–40.
- Johansson, L., Jalkanen, J.P., Kukkonen, J., 2017. Global assessment of shipping emissions in 2015 on a high spatial and temporal resolution. *Atmospheric Environment* 167, 403–415.
- Kaiser, M., 2016. Results of aerodynamic model tests for HSBC. Technical Report. Technical Report No. RH-2016/T-104E, CTO S.A., Gdansk, Poland.
- Kim, S.H., Roh, M.I., Oh, M.J., Park, S.W., Kim, I.I., 2020. Estimation of ship operational efficiency from ais data using big data technology. *International Journal of Naval Architecture and Ocean Engineering* 12, 440–454.
- Kim, Y., Esmailian, E., Steen, S., 2022a. A meta-model for added resistance in waves. *Ocean Engineering* 266, 112749.
- Kim, Y., Steen, S., Muri, H., 2022b. A novel method for estimating missing values in ship principal data. *Ocean Engineering* 251, 110979.
- Kim, Y.R., Steen, S., 2022. Application of machine learning algorithms for predicting added resistance in arbitrary wave headings of a ship, in: *International Conference on Offshore Mechanics and Arctic Engineering*, American Society of Mechanical Engineers. p. V05BT06A026.
- Kitamura, F., Ueno, M., Fujiwara, T., Sogihara, N., 2017. Estimation of above water structural parameters and wind loads on ships. *Ships and Offshore Structures* 12, 1100–1108.
- Kramel, D., Muri, H., Kim, Y., Lonka, R., Nielsen, J.B., Ringvold, A.L., Bouman, E.A., Steen, S., Strømman, A.H., 2021. Global shipping emissions from a well-to-wake perspective: the mariteam model. *Environmental science & technology* 55, 15040–15050.
- Kristensen, H.O., Lützen, M., 2012. Prediction of resistance and propulsion power of ships. *Clean Shipping Currents* 1, 1–52.
- Kwon, Y., 2008. Speed loss due to added resistance in wind and waves. *Nav Archit* 3, 14–16.
- Lang, X., Mao, W., 2021. A practical speed loss prediction model at arbitrary wave heading for ship voyage optimization. *Journal of Marine Science and Application* 20, 410–425.
- Lap, A., 1954. Diagrams for determining the resistance of single-screw ships. *International Shipbuilding Progress* 1, 179–193.
- Liu, J., Shi, G., Zhu, K., 2019. Vessel trajectory prediction model based on ais sensor data and adaptive chaos differential evolution support vector regression (acde-svr). *Applied Sciences* 9, 2983.
- Liu, S., Papanikolaou, A., 2016. Fast approach to the estimation of the added resistance of ships in head waves. *Ocean Engineering* 112, 211–225.
- Liu, S., Papanikolaou, A., 2020. Regression analysis of experimental data for added resistance in waves of arbitrary heading and development of a semi-empirical formula. *Ocean Engineering* 206, 107357.
- Liu, S., Shang, B., Papanikolaou, A., Bolbot, V., 2016. Improved formula for estimating added resistance of ships in engineering applications. *Journal of Marine Science and Application* 15, 442–451.
- Lu, R., Turan, O., Boulougouris, E., Banks, C., Incecik, A., 2015. A semi-empirical ship operational performance prediction model for voyage optimization towards energy efficient shipping. *Ocean Engineering* 110, 18–28.
- Minsaas, K., 1982. Grunnlag for fartsprognoser. Technical Report. Technical report, Marintek (former: Norges Hydrodynamiske Laboratorier . . . .
- Muri, H., Strømman, A.H., Ringvold, A.L., Lonka, R., Bouman, E., 2019a. Influence of weather on emissions from the global shipping fleet., in: *Geophysical Research Abstracts*.
- Muri, H., Strømman, A.H., Ringvold, A.L., Lonka, R., Lindstad, E., Bouman, E.A., 2019b. A new emission inventory of the global maritime fleet; the effect of weather, in: *AGU Fall Meeting Abstracts*, pp. A21W–2637.
- Newton, R., 1961. Performance data of propellers for high speed craft. Admiralty Experiment Works, Haslar, UK. Published by: The Royal Institution of Naval Architects, RINA Transactions 1961-07, Volume 103, No. 2, Quarterly Transactions, pp. 93-129 .
- Olmer, N., Comer, B., Roy, B., Mao, X., Rutherford, D., 2017. Greenhouse gas emissions from global shipping, 2013–2015 detailed methodology. *International Council on Clean Transportation: Washington, DC, USA* , 1–38.
- Oortmersen, G.v., 1971. A power prediction method and its application to small ships. *ISP* 18.
- Oosterveld, M.W.C., 1970. Wake adapted ducted propellers. Technical Report.
- Papanikolaou, A., 2014. Ship design: methodologies of preliminary design. Springer.
- Psarafitis, H.N., Kontovas, C.A., 2009. Co2 emission statistics for the world commercial fleet. *WMU Journal of Maritime Affairs* 8, 1–25.
- Rakke, S., 2016. Ship emissions calculation from AIS-annotated. Ph.D. thesis. M. Sc. Thesis. Norwegian University of Science and Technology, Norway.
- Schneekloth, H., Bertram, V., 1998. Ship design for efficiency and economy. volume 218. Butterworth-Heinemann Oxford.
- Smith, T., O’Keeffe, E., Aldous, L., Agnolucci, P., 2013. Assessment of shipping’s efficiency using satellite ais data .
- Smith, T.W., Jalkanen, J.P., Anderson, B., Corbett, J.J., Faber, J., Hanayama, S., O’Keeffe, E., Parker, S., Johansson, L., Aldous, L., et al., 2014. Third imo ggh study 2014. International maritime organization (IMO), London, UK , 2014.
- Steen, S., Aarsnes, J.V., 2014. Experimental methods in marine hydrodynamics. Lecture notes .
- Stenson, P., 2015. Predicting the rough and the smooth. *The Naval Architect* February, 36–38.
- Tillig, F., Ringsberg, J., Mao, W., Ramne, B., 2017. A generic energy systems model for efficient ship design and operation. *Proceedings of the Institution of Mechanical Engineers, Part M: Journal of Engineering for the Maritime Environment* 231, 649–666.
- Tillig, F., Ringsberg, J.W., 2019. A 4 dof simulation model developed for fuel consumption prediction of ships at sea. *Ships and Offshore Structures* 14, 112–120.
- Tillig, F., Ringsberg, J.W., Psarafitis, H.N., Zis, T., 2020. Reduced environmental impact of marine transport through speed reduction and wind assisted propulsion. *Transportation Research Part D: Transport and Environment* 83, 102380.

- Todd, F., 1957. Series 60-the effect upon resistance and power of variation in ship proportions. Trans. SNAME 65, 445–589.
- Townsin, R., 2003a. Calculating the cost of marine surface roughness on ship performance. Akzo Nobel .
- Townsin, R., 2003b. The ship hull fouling penalty. Biofouling 19, 9–15.
- Townsin, R., Byrne, D., Svendsen, T., Milne, A., 1986. Fuel economy due to improvements in ship hull surface condition 1976–1986. International shipbuilding progress 33, 127–130.
- Townsin, R., Kwon, Y., 1993. Estimating the influence of weather on ship performance .
- Tvete, H.A., Guo, B., Liang, Q., Brinks, H., 2020. A modelling system for power consumption of marine traffic, in: International Conference on Offshore Mechanics and Arctic Engineering, American Society of Mechanical Engineers. p. V06AT06A029.
- Watson, D.G., 1998. Practical ship design. volume 1. Elsevier.
- Willsher, J., 2007. The effect of biocide free foul release systems on vessel performance. International Paint Ltd., London/UK 6.
- Yeginbayeva, I., Atlar, M., 2018. An experimental investigation into the surface and hydrodynamic characteristics of marine coatings with mimicked hull roughness ranges. Biofouling 34, 1001–1019.
- Zhou, Y., Daamen, W., Vellinga, T., Hoogendoorn, S.P., 2019. Ship classification based on ship behavior clustering from ais data. Ocean Engineering 175, 176–187.

## Appendix A Draught correction

**Table A1**

Minimum design ballast draught (DNVGL, 2018).  $T_{sc}$  in the table refers to the scantling draught of a ship.

Ship type	Minimum design ballast draught
Cargo	$0.35T_{sc}$
Oil	$2+0.02L_{pp}(L_{pp} \geq 150)$
Passenger	$0.75T_{sc}$
Ro-Ro	$0.5T_{sc}$

**Table A2**

Average annual draught ratio in 2015 (Olmer et al., 2017). Draught ratio ( $T_c/T_d$ ) refers to the ratio between current draught ( $T_c$ ) and design draught ( $T_d$ ).

Ship type	Ballast	Laden	Average
Bulk dry	0.57	0.91	0.80
Chemical	0.65	0.89	0.85
General cargo	0.65	0.89	0.84
Liquefied gas	0.67	0.88	0.87
Oil	0.60	0.89	0.82
Container	-	-	0.87
Passenger	-	-	0.93
Ro-Ro	-	-	0.91

## Appendix B Parameter estimation

**Table B1**  
Estimation of length parameters.

Estimation equation	Applied to	Reference
$L_{wl} = 1.01L_{pp}$	Container, Ro-Ro	Kristensen and Lützen (2012)
$L_{wl} = 1.02L_{pp}$	Other	
$L_{os} = 1.04L_{wl}$		Hollenbach (1998)
$L_{fn} = L_{os}$	$L_{os}/L_{pp} < 1$	Hollenbach (1998)
$L_{fn} = L_{pp} + 2/3(L_{os} - L_{pp})$	$1 \leq L_{os}/L_{pp} < 1.1$	
$L_{fn} = 1.0667L_{pp}$	$1.1 \leq L_{os}/L_{pp}$	
$L_d = (L_{wl} + L_{pp})/2$		Oortmersen (1971)

**Table B2**  
Estimation of propeller diameter.

Estimation equation	Applied to	Reference
$D_p = 0.395T_d + 1.3$	Bulk carrier ( $5 \leq T_d \leq 25$ )	Kristensen and Lützen (2012)
$D_p = 0.623T_d - 0.16$	Container ( $4 \leq T_d \leq 16$ )	
$D_p = 0.713T_d - 0.08$	Ro-Ro ( $1 \leq T_d \leq 11$ )	
$D_p = 0.46T_d$	Bulk carrier	Jalkanen et al. (2012)
$D_p = 0.5T_d$	Chemical	
$D_p = 0.48T_d$	Oil	
$D_p = 0.53T_d$	Liquefied gas	
$D_p = 0.62T_d$	Container	
$D_p = 0.52T_d$	General	
$D_p = 0.65T_d$	Passenger	
$D_p = 0.63T_d$	Other	

**Table B3**  
Estimation of volume displacement and wetted surface area.

Estimation equation	Applied to	Reference
$\nabla_{T_d} = (LDT + DWT) \cdot 10^3 / \rho_w$	General	
$S_{T_d} = 0.995(\nabla_{T_d}/T_d + 1.9L_{wl}T_d)$	Container	Kristensen and Lützen (2012)
$S_{T_c} = S_{T_d} - 2.4(T_d - T_c)$		
$S_{T_d} = 0.99(\nabla_{T_d}/T_d + 1.9L_{wl}T_d)$	Bulk, Tanker	
$S_{T_c} = S_{T_d} - 2(T_d - T_c)$		
$S_{T_d} = 0.87(\nabla_{T_d}/T_d + 2.7L_{wl}T_d)$	Ro-Ro	
$S_{T_c} = S_{T_d} - 3(T_d - T_c)$		
$S_{T_d} = 1.11(\nabla_{T_d}/T_d + 1.7L_{wl}T_d)$	Passenger	
$S_{T_c} = S_{T_d} - 2.4(T_d - T_c)$		

**Table B4**  
Estimation of ship hydrodynamic coefficients.

Estimation equation	Applied to	Reference
$C_B = \nabla_{T_c} / (L_{pp} \cdot B \cdot T_c)$		
$C_M = 0.93 + 0.08C_B$		Schneekluth and Bertram (1998)
$C_P = C_B / C_M$		
$C_{WP} = 0.763(C_P + 0.34)$	Tanker, Bulk, Cargo ship	Bertram and Wobig (1999)
$C_{WP} = 3.226(C_P - 0.36)$	Container	Bertram and Wobig (1999)
$C_{WP} = (1 + 2C_B)/3$	Other (general)	Papanikolaou (2014)

## Appendix C Wind resistance coefficient

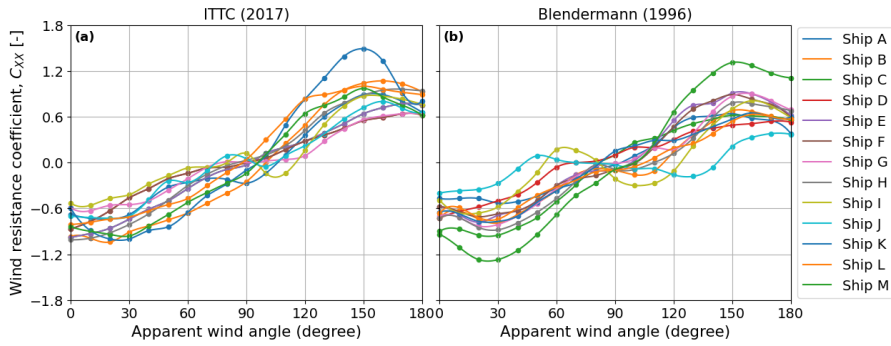


Figure C1: Wind resistance coefficients.

Table C1

Information of ships listed in Tables.

	ITTC (2017b)	Blendermann (1996)
Ship A	container ship (laden, 6800TEU)	container ship (laden, 2500TEU)
Ship B	container ship (ballast, 6800TEU)	container ship (ballast, 2500TEU)
Ship C	oil tanker (laden, 280kDWT)	oil tanker (laden, 300kDWT)
Ship D	oil tanker (ballast, 280kDWT)	oil tanker (ballast, 300kDWT)
Ship E	dry bulk (laden, 280kDWT)	liquefied gas (laden, moss)
Ship F	dry bulk (ballast, 280kDWT)	liquefied gas (ballast, moss)
Ship G	dry bulk (ballast, 50kDWT)	ro-ro (laden)
Ship H	liquefied gas (average, 125km3)	ro-ro (ballast)
Ship I	ro-ro (average)	ro-ro (average)
Ship J	passenger (average)	passenger (average)
Ship K	general cargo (average)	general cargo (laden)
Ship L	general cargo (ballast, 19000DWT)	general cargo (ballast)
Ship M	general cargo (laden, 19000DWT)	other offshore (average)

**Table C2**

Wind resistance coefficient according to angle of attack from ITTC (2017b).

Angle of attack	Ship A	Ship B	Ship C	Ship D	Ship E	Ship F	Ship G	Ship H	Ship I	Ship J	Ship K	Ship L	Ship M
0	-0.68	-0.97	-0.98	-0.87	-0.98	-0.87	-0.59	-1.01	-0.53	-0.7	-0.6	-0.81	-0.84
10	-0.73	-0.99	-0.93	-0.77	-0.93	-0.77	-0.63	-0.99	-0.56	-0.72	-0.89	-0.78	-0.9
20	-0.74	-1.04	-0.86	-0.63	-0.86	-0.63	-0.56	-0.92	-0.47	-0.73	-1	-0.74	-0.94
30	-0.68	-0.91	-0.74	-0.46	-0.74	-0.46	-0.55	-0.81	-0.42	-0.7	-1	-0.71	-0.96
40	-0.49	-0.83	-0.61	-0.34	-0.61	-0.34	-0.5	-0.67	-0.28	-0.48	-0.89	-0.63	-0.83
50	-0.32	-0.75	-0.5	-0.21	-0.5	-0.21	-0.36	-0.49	-0.17	-0.24	-0.84	-0.55	-0.68
60	-0.26	-0.66	-0.34	-0.14	-0.34	-0.14	-0.21	-0.3	-0.07	-0.26	-0.65	-0.47	-0.52
70	-0.21	-0.53	-0.19	-0.07	-0.19	-0.07	-0.06	-0.15	-0.06	-0.1	-0.43	-0.3	-0.39
80	-0.22	-0.4	-0.09	-0.06	-0.09	-0.06	0.01	-0.04	0	0.09	-0.28	-0.13	-0.27
90	-0.27	-0.25	-0.03	0	-0.03	0	0	0.03	0.12	0.05	-0.1	0.04	-0.14
100	-0.14	0	0.12	0.06	0.12	0.06	0.02	0.1	-0.14	-0.05	0.09	0.3	0.11
110	0.1	0.25	0.2	0.17	0.2	0.17	0.04	0.22	-0.14	0.09	0.49	0.57	0.37
120	0.36	0.49	0.28	0.28	0.28	0.28	0.09	0.42	0.16	0.22	0.83	0.83	0.64
130	0.6	0.76	0.39	0.36	0.39	0.36	0.28	0.65	0.5	0.38	1.11	0.89	0.75
140	0.77	0.95	0.51	0.45	0.51	0.45	0.44	0.78	0.74	0.57	1.39	0.95	0.86
150	0.89	1.04	0.64	0.55	0.64	0.55	0.56	0.88	0.87	0.72	1.49	1	0.97
160	0.89	1.07	0.72	0.59	0.72	0.59	0.61	0.95	0.87	0.8	1.33	0.96	0.86
170	0.8	1.03	0.77	0.64	0.77	0.64	0.64	0.96	0.83	0.71	0.91	0.92	0.75
180	0.66	0.93	0.75	0.62	0.75	0.62	0.64	0.94	0.76	0.66	0.81	0.89	0.62

**Table C3**

Wind resistance coefficient according to angle of attack from Blendermann (1996).

Angle of attack	Ship A	Ship B	Ship C	Ship D	Ship E	Ship F	Ship G	Ship H	Ship I	Ship J	Ship K	Ship L	Ship M
0	-0.47	-0.73	-0.9	-0.73	-0.58	-0.58	-0.7	-0.73	-0.49	-0.4	-0.65	-0.66	-0.94
10	-0.47	-0.63	-0.87	-0.64	-0.68	-0.64	-0.72	-0.72	-0.66	-0.37	-0.67	-0.59	-1.11
20	-0.47	-0.74	-0.95	-0.58	-0.78	-0.71	-0.83	-0.85	-0.66	-0.35	-0.77	-0.72	-1.27
30	-0.53	-0.79	-0.95	-0.5	-0.69	-0.67	-0.81	-0.88	-0.58	-0.27	-0.77	-0.74	-1.27
40	-0.51	-0.68	-0.85	-0.42	-0.63	-0.63	-0.7	-0.79	-0.38	-0.08	-0.7	-0.59	-1.15
50	-0.44	-0.53	-0.72	-0.26	-0.5	-0.5	-0.54	-0.65	-0.13	0.09	-0.52	-0.43	-0.94
60	-0.34	-0.36	-0.51	-0.06	-0.3	-0.3	-0.34	-0.47	0.17	0.04	-0.37	-0.32	-0.68
70	-0.26	-0.16	-0.29	0	-0.16	-0.21	-0.18	-0.24	0.16	0	-0.21	-0.23	-0.43
80	-0.1	-0.08	-0.03	0.02	-0.11	-0.17	-0.05	-0.03	0.03	-0.01	-0.05	-0.12	-0.27
90	-0.03	-0.1	0.1	0.1	-0.1	-0.09	-0.01	-0.09	-0.21	-0.03	0.15	-0.1	-0.09
100	0.09	-0.16	0.26	0.2	0.03	-0.01	0.05	-0.09	-0.3	-0.08	0.22	-0.05	0
110	0.23	-0.11	0.32	0.2	0.25	0.2	0.19	0	-0.27	-0.08	0.29	0.06	0.25
120	0.46	0.14	0.42	0.3	0.55	0.47	0.17	0.12	-0.11	-0.16	0.29	0.19	0.66
130	0.59	0.36	0.51	0.41	0.75	0.7	0.38	0.32	0.22	-0.18	0.37	0.25	0.95
140	0.61	0.54	0.57	0.45	0.78	0.81	0.67	0.59	0.49	-0.06	0.47	0.38	1.17
150	0.64	0.68	0.62	0.49	0.91	0.89	0.87	0.78	0.7	0.21	0.57	0.54	1.31
160	0.58	0.67	0.61	0.51	0.9	0.83	0.9	0.77	0.81	0.33	0.65	0.63	1.27
170	0.55	0.61	0.6	0.54	0.79	0.76	0.81	0.73	0.74	0.38	0.59	0.6	1.17
180	0.38	0.56	0.55	0.53	0.62	0.59	0.69	0.68	0.59	0.37	0.6	0.57	1.11



# Article 5

## Potential Energy Savings of Air Lubrication Technology on Merchant Ships

Youngrong Kim, Sverre Steen

*Submitted to International Journal of Naval Architecture and Ocean  
Engineering*





# Potential energy savings of air lubrication technology on merchant ships

Young-Rong Kim<sup>a,\*</sup>, Sverre Steen<sup>a</sup>

<sup>a</sup>Department of Marine Technology, Norwegian University of Science and Technology (NTNU), Trondheim, 7050, Norway

---

## ARTICLE INFO

### Keywords:

Air lubrication system  
Drag reduction  
Energy saving  
Fleet-level analysis  
Ship transportation

## ABSTRACT

As the reduction of greenhouse gas emissions has become an important issue, measures and devices to reduce energy consumption are in increasing demand. In this study, the potential energy saving due to the application of air lubrication technology in merchant ships is analyzed. We propose a simplified empirical model, covering three different air lubrication technologies, based on the experimental results and assumptions taken in the existing studies. The bottom surface area covered with air is important for the efficiency of the air lubrication system, according to the sensitivity analysis. From the global fleet analysis, net-percentage power saving varies according to the operational profile as well as the technology. Net-percentage power savings of 2-5% from air bubble, 8-14% from air layer, and 16-22% from air cavity technology were obtained assuming calm-water conditions. The methodology can be adopted in early design stage and fleet-wide analyses of various energy-saving measures.

---

## 1. Introduction

Along with the acceleration of global warming, the international community is paying keen attention to greenhouse gas emissions. The International Maritime Organization (IMO) released an initial strategy, which aims to reduce greenhouse gas emissions by at least 50% in shipping by 2050 compared to 2008 levels and reduces emissions in stages as soon as possible, at Marine Environment Protection Committee (MEPC 72) in 2018 (IMO, 2018). In addition, IMO adopted EEXI (Energy Efficiency eXisting Ship Index) and CII (Carbon Intensity Indicator) as direct and short-term measures for this (IMO, 2021). In response to this international trend, various types of energy-saving devices and measures have been studied and applied to ships (Bouman et al., 2017; Zhang et al., 2021).

The total resistance encountered by a ship moving in water is largely composed of frictional resistance, viscous pressure resistance, and wave resistance. Of these, frictional resistance generally accounts for the largest proportion of the total resistance, especially on slow-moving ships, which can account for more than 80% of the total. Frictional resistance is determined by properties such as wetted surface area, operating speed, and viscosity of the fluid, and the wetted surface area can be effectively reduced through air lubrication of the bottom of the hull. Therefore, air lubrication system (ALS) is anticipated that one of the promising energy-saving technologies that can successfully lower fuel consumption and greenhouse gas emissions from ships.

Mitsubishi Heavy Industry first installed its air lubrication system (MALS) on a newly built ship and showed up to 12% net energy savings in a sea trial of a module carrier (Mizokami et al., 2010). As the thickness of the air layer that forms on the bottom of the hull increases, it has also been confirmed that net energy savings increase as well. In a subsequent study, Kawabuchi et al. (2011) analyzed the distribution of air bubbles on the hull surface and its effect on propeller performance using CFD. Silverstream developed an air carpet technology that covers the entire bottom of the ship by injecting micro bubbles from air release units, and it was confirmed that a net energy reduction of about 4% could be achieved from actual operations of 40k DWT tanker (Silberschmidt et al., 2016). In Lee et al. (2017), they observed results from model tests, sea trials, and in-service data from two ships fitted with air-lubrication systems (SAVER) made by Samsung Heavy Industry (SHI). As a result, in the case of a heavy cargo carrier, power savings of 8.8% were estimated in the sea trial results, and on the basis of long-term trip data, power savings of roughly 4-5% were recorded for a LNG carrier. In the meantime, Damen group unveiled the Air Chamber Energy Saving (ACES) system, which uses a chamber-shaped design on the bottom of the hull to create a cavity where air is supplied to prevent water from coming into contact with the lower hull surface (Pavlov et al., 2020). According to several investigations (ABS,

---

\*Corresponding author

✉ [youngrong.kim@ntnu.no](mailto:youngrong.kim@ntnu.no) (Y. Kim)  
ORCID(s): 0000-0002-5859-0854 (Y. Kim)

2019; Gebraad et al., 2021), there have been about 50 ships with air lubrication systems installed by 2021, including some test cases, and interest in the technology continues to increase considering recent orders.

Many previous studies have looked at the applicability and performance of air-lubrication systems for certain ship cases based on model tests, sea trials, or CFD. On the other hand, some studies have suggested a simplified method for estimating energy savings in the air lubrication system. Mäkiharju and Ceccio (2011), and Mäkiharju et al. (2012) established a method of calculating the energy economy of the air lubrication system using experimental data and presented the energy-saving results based on the assumption of various situations for the U.S. Great Lakes vessel. Comer et al. (2019) applied a similar method to perform an analysis on route-based fuel and emission reduction of the three ships installed with ALS.

In this study, a simplified model, capable of applying different types of ALS considering various ship types and profiles, is presented. Through the suggested model, this study aims to assess the impact of ALS on different ship types and obtain knowledge to help reduce maritime emissions. The suggested model is intended for early-design estimations, fleet-wide studies, and similar applications where quick calculations requiring limited input are desired. The underlying idea for the simplified method is that the layer of air produced by the air lubrication system reduces frictional resistance by covering a portion of the hull's surface area with air, or air bubbles. In order to enable the evaluation of the effectiveness of air lubrication technology for ships with different design characteristics and operating profiles, the aforementioned simplified empirical approach is adopted. The model has been established based on previously published experimental results and various information found in open literature, and throughout this paper, the calculation process and basic assumptions are explained. It includes three types of air lubrication: air bubble, air layer, and air cavity.

In Chapter 2, the general concepts and different types of air lubrication systems are presented, and relevant studies used to develop the simplified method are also introduced. In the following chapter, the background of the various formulas employed in the model to calculate the potential savings of an air lubricating system is discussed. Additionally, by comparing the results of the model with those of other studies, the overall properties and performance are demonstrated. Chapter 4 presents the research outcomes based on the model that has been established. Here, parametric studies are performed on the main factors of an air lubrication system, and potential power savings for the global fleet in calm water and a specific vessel in the real sea are evaluated. The last chapter presents the conclusions obtained from the study and proposes future works.

## 2. Background

Frictional resistance often predominates among the resistance components that a ship encounters when moving through water, and it is heavily influenced by the wetted surface area, operating speed, and viscosity of the fluid. Basically, the main principle of air lubrication technology is to reduce frictional resistance by reducing direct contact with water, that is to reduce the wetted surface area by releasing air bubbles and covering some part of the bottom surface area of the hull. Air lubrication can be classified into three different techniques; the air bubble concept that injects micro air bubbles at the bottom of the hull, the air film concept covers the bottom surface with a continuous air layer through increased air flux, and the air cavity concept fills the recessed area beneath the hull with air (Foeth et al., 2009; ABS, 2019). In the rest of the text, air bubble concept will be referred to as BDR (Bubble drag reduction), air film as ALDR (Air layer drag reduction), and air cavity as PCDR (Partial cavity drag reduction).

BDR reduces the local density by injecting numerous microbubbles into the boundary layer, thereby reducing the Reynolds stress. At the same time, the effective viscosity is reduced due to an increase in void fraction, which consequently serves to suppress the turbulence of the flow and reduce skin friction (Park and Lee, 2018; ABS, 2019). As the injected air flux increases from this state, a transition occurs in which the air bubbles and the air layer coalesce with each other in the gas-liquid mixture. When sufficient air is injected into the near wall region of the turbulent boundary layer, the air is aggregated with each other to form a continuous air layer separating the hull surface from the water flow. It was found that such a developed air layer, so-called ALDR can significantly reduce frictional resistance compared to bubbly flow (Ceccio, 2010; Elbing et al., 2013). PCDR reduces frictional resistance by injecting air into a recess or cavity at the bottom of the hull to separate the lower part of the hull from water (Lay et al., 2010). A typical hull design for PCDR consists of a slightly downward sloping closure downstream from the starting wall of the cavity into which air is injected, which forms a partial cavity to trap the air. This drag reduction effect by the cavity air layer is associated with the design of the bottom cavity and the continuous injection of air to maintain a stable air layer (Wu and Ou, 2019).

To analyze the impact of an air lubrication system on the speed-power performance of a ship and to get insight into the optimal hull design and arrangement of the air lubrication system, several methods such as a model test, full-scale measurements, and CFD computation are typically used. Fig. 1 presents the net-percentage power savings of each air lubrication system collected from these studies as a horizontal box plot, along with a scatter plot of the collected data. Several studies have used various metrics such as fuel consumption, gas emission, drag reduction, and power saving, but since net-percentage power savings defined in Eq. (1) will be used as a performance metric of ALS throughout this study, only the results that can estimate such value are presented here, and the detailed sources are presented in Table A.1 in appendix A. Although each experiment was classified and listed by ALS type, some experiments may correspond to a transitional region depending on the injected airflow. According to the 25%-75% quartile ranges corresponding to both ends of the box, BDR indicates a net-percentage power saving of about 3 to 6%, ALDR of 4 to 12%, and PCDR of 16 to 22%. It is clear that there are scatters in any type of air lubrication because the effectiveness of power savings is highly dependent on the operational profiles of the ship, the details of the air lubrication arrangement, and the experimental setup.

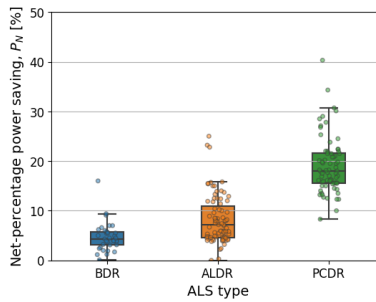


Figure 1: Potential net-percentage power savings achieved from previous studies.

### 3. Methodology

#### 3.1. Modelling of air lubrication technology

The purpose of the method developed in this study is to evaluate the potential energy saving of air lubrication systems on merchant ships and to obtain practical knowledge through the obtained results. It is anticipated that the applicability of air lubrication technology will vary because ships operating globally have diverse design characteristics and operating profiles. Since it is an analysis of a wide variety of general-purpose levels, it is necessary to develop a model that can simulate the overall trend in energy savings using the fundamental ship information. Therefore, the energy economic calculation approach used in Mäkiharju et al. (2012) was adopted in this study as the performance evaluation method of ALS, and required volumetric fluxes of gas for the air-lubrication were estimated based on experimental data obtained from large cavitation tunnel in Elbing et al. (2008) and Mäkiharju et al. (2010). In addition, a number of assumptions and simplifications were made regarding the application and composition of the air lubrication system based on the findings of earlier studies that were published.

##### 3.1.1. Energy saving by air lubrication system

The energy savings by the air lubrication system are determined by the reduction of the power required to overcome the frictional drag on the lubricated surface and the power consumed to inject gas into the bottom surface. Here, the performance index of the air lubrication system uses the percentage of net power saving to total brake power, that is, net-percentage power saving, as stated in Eq. (1).

$$P_N [\%] = \frac{P_{save} - P_{cons}}{P_B} \times 100 = \frac{P_{net}}{P_B} \times 100 \quad (1)$$

where  $P_N$  is net-percentage power saving,  $P_{save}$  is power saved by air lubrication system; it can be replaced by  $P_{save,wc}$  if there is an influence of weather,  $P_{cons}$  is power consumed by air compressor,  $P_{net}$  is net power saving by air lubrication system, and  $P_B$  is total brake power.

It is possible to estimate each of the resistance components that make up the ship's total resistance using established empirical methods, and the methods used in this study are listed in Table 1. The total resistance and overall efficiency can be used to estimate the total brake power, as shown in Eq. (2). Here, the total resistance in real sea conditions can be simply expressed as Eq. (3), and it is considered as the sum of the calm water resistance and the additional resistance caused by wind and waves. For the estimation of the calm water resistance of a ship, it can be estimated from various methods listed in Table 1 to suit the dimensions and operating range of each ship. To use wind resistance coefficients taking into account different ship types and windage area above the waterline, wind tunnel test results from Blendermann (1996), Fujiwara (2006), and ISO (2015) were gathered. Moreover, the Combined Method, by Kim et al. (2022b) is used in the model to compute the added resistance in arbitrary wave headings using a few basic inputs. In order to obtain the propulsive efficiency for various ships, this study uses the simplified method (Kristensen and Lützen, 2012), which can obtain a quick estimate from Wageningen B-series (Oosterveld and van Oossanen, 1975) using a limited input value, and the methods found in Birk (2019). In Nagamatsu et al. (2002)'s full-scale experiment, a bubble injector was dedicatedly designed to prevent the decrease in propeller efficiency due to the inflow of air bubbles into the propeller. However, according to later studies (Kawakita et al., 2011; Kawabuchi et al., 2011; Jang et al., 2014), the loss of propulsive efficiency before and after starting the air lubrication system was less than about 1%, demonstrating that air bubbles may not have much of an impact on a propeller. Based on this fact and for the simplicity of the model, this study neglect to include any change in propulsive efficiency caused by air bubbles.

In Section 5, the resistance of different commercial ships in the global fleet is estimated. The resistance is calculated using the well-established empirical methods listed in Table 1. A method for selection of the best empirical methods for each ship has been established (Kramel et al., 2021). In the fleetwide calculation in this work, an updated version is applied, where some additional empirical methods are included, as listed in Table 1. The main feature of this resistance calculation method is that it requires few input parameters. If more detailed information is available, more advanced resistance prediction methods can be applied.

$$P_B = \frac{R_T \times V}{\eta_T} \quad (2)$$

$$R_T = R_{Calm} + R_{Wind} + R_{Wave} \quad (3)$$

where  $R_T$  is total resistance in real sea conditions,  $R_{Calm}$  is total resistance in calm water conditions,  $R_{Wind}$  is added resistance due to wind,  $R_{Wave}$  is added resistance in waves,  $\eta_T$  is overall efficiency, and  $V$  is ship speed.

**Table 1**

Estimation of resistance components using empirical methods used in the study.

Component	Method
$R_{Calm}$	Holtrop-Mennen (Holtrop and Mennen, 1982), Hollenbach (Hollenbach, 1998), Guldhammer (Guldhammer and Harvald
$R_{wind}$	Blendermann (Blendermann, 1996), Fujiwara (Fujiwara, 2006), STAJIP (ISO, 2015)
$R_{wave}$	Combined Method (Kim et al., 2022b)
$\eta_T$	Kristensen (Oosterveld and van Oossanen, 1975; Kristensen and Lützen, 2012), Birk (Birk, 2019)

### 3.1.2. Power saving by the air lubrication

The air lubricating device serves to reduce the resistance of the area covered with air on the bottom surface among the frictional resistance generated from the fluid surrounding the hull during ship operation. Therefore, the power that can be saved from the air lubrication can be calculated by simply taking into account the power due to the frictional resistance generated by the wetted surface area, the proportion of the air covered area to the total wetted surface, and the drag reduction achieved by the air covered area, as shown in Eq. (4).

$$P_{save} = P_F D_R \frac{A_a}{A_w} \quad (4)$$

where  $P_F$  is the power required to overcome the frictional drag,  $D_R$  is frictional drag reduction fraction due to air lubrication,  $A_a$  is air covered area at the bottom surface, and  $A_w$  is wetted surface area.

As in Eq. (5), the power needed to overcome the frictional drag can be obtained by multiplying the total brake power by the proportion of frictional drag to total drag. Here, the frictional drag coefficient of the flat plate can be calculated using the ITTC 1957 friction line (ITTC, 1978) from Eq. (7), and accordingly, the frictional resistance is obtained from Eq. (6). As indicated in Eq. (3), the total resistance can be determined from empirical methods.

$$P_F = P_B \times \frac{R_F}{R_T} \quad (5)$$

$$R_F = \frac{1}{2} \rho_w A_w C_F V^2 \quad (6)$$

$$C_F = \frac{0.075}{(\log_{10} R_n - 2)^2} \quad (7)$$

where  $\rho_w$  is water density,  $R_F$  is frictional resistance,  $C_F$  is frictional coefficient, and  $R_n$  is Reynolds number

According to Silberschmidt et al. (2016), the estimated appendage drag of the air release units attached to the bottom surface of LNG carriers or cruise ships was less than 0.5% of the total. In this study, the influence of appendages for all ALS types is ignored for simplicity, and in the case of PCDR, it is assumed that there is a newly built ship with proper design alterations for the cavity form. By ignoring appendage drag for the ALS, it is in fact assumed that great care has been taken to design the ALS in a careful way.

Among the wetted surface areas under the waterline of a ship, the air covered area, which can be expected to reduce frictional resistance by the air lubrication system, is expressed in the form of  $A_a/A_w$  as shown in the following Eq. (8) to facilitate calculation in this study. Here, wetted surface area, bottom area, and air covered area are defined as shown in Fig. 2. The area that can be covered with air bubbles or layers increases as the flat bottom surface of the hull increases. This implies that the potential energy saving from the air lubrication grows.

The bottom area of a ship can be estimated from the particular hull shape of the ship, but as it is nearly impossible to get comprehensive hull shape data for ships at the fleet level, this study proposed regression equations to estimate the bottom area of a ship (refer to Eq. (9)). They have been developed based on 22 ships with various hull shapes (refer to Table A.2 in appendix A), and presented the ratio of bottom surface area to wetted surface area ( $A_b/A_w$ ) according to draught ratio ( $T/T_d$ ) and block coefficient ( $C_b$ ) as illustrated in Fig. 3. Here,  $C_b$  is based on the design draught of the ship. It is obvious that the  $A_b/A_w$  rises as  $C_b$  increases, and the  $A_b/A_w$  of the ballast condition is higher than that of the laden condition. For bulk carrier and tankers with normally blunt hull shapes, the flat bottom area tends to be bigger, whereas, for container ships and ferries with typically slender hull shapes, it tends to be smaller.

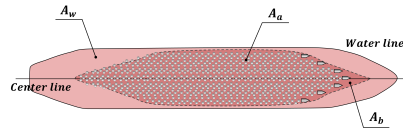


Figure 2: Bottom-up view showing air covered area, bottom area, and wetted surface area of a ship.

$$\frac{A_a}{A_w} = \frac{A_b}{A_w} \frac{A_a}{A_b} \quad (8)$$

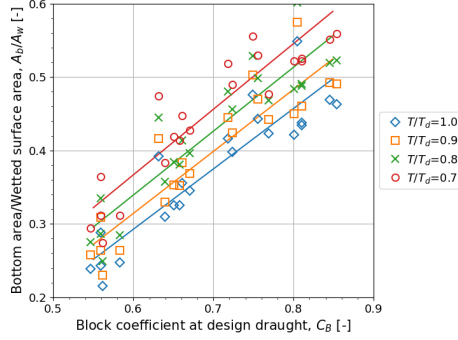


Figure 3: The ratio of bottom area to wetted surface area according to  $C_b$  of a ship at various draught.

$$\frac{A_b}{A_w} = \begin{cases} 0.8227C_b - 0.201 & T/T_d = 1.0 \\ 0.8449C_b - 0.1927 & T/T_d = 0.9 \\ 0.871C_b - 0.1834 & T/T_d = 0.8 \\ 0.8942C_b - 0.1698 & T/T_d = 0.7 \end{cases} \quad (9)$$

where  $A_b$  is bottom surface area of a ship,  $C_b$  is block coefficient,  $T$  is sailing draught, and  $T_d$  is design draught.

Meanwhile, the arrangement of the air release device and the hull bottom design of the specific ship may affect the air covered area. Kim et al. (2021) found that the reduction rate of frictional resistance gradually increased as the air injection holes were placed wider in the width direction, and Park and Lee (2018) reported that it was more effective to inject air distributedly in multiple locations than in a single injection location. In this regard, it is important to appropriately arrange the injectors to increase the covering area of air at the bottom of the hull as much as possible. Based on the result in Wu and Ou (2019), 0.84 was used as a ratio of air covered area to the bottom area ( $A_a/A_b$ ) in this study. However, this value can be changed as needed depending on each ship's ALS configurations.

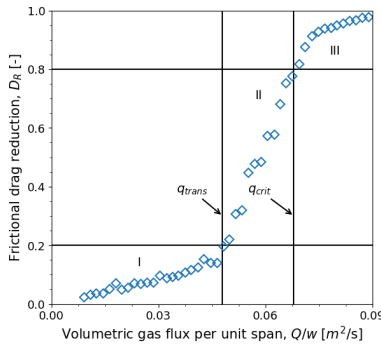


Figure 4: Drag reduction of three regions according to the gas injection rate measured from the model tests on the flat-plate. I, II, and III represent BDR region, transition region between BDR and ALDR, and ALDR region, respectively. The figure is adapted from Elbing et al. (2008) with minor modifications.

Fig. 4 depicts the boundaries for three drag reduction regions based on flow rate in the air bubble injection experiment on the flat plate as given in Elbing et al. (2008). According to the flow rate, I represents the BDR region, II the transitional region between the BDR and ALDR, and III the ALDR region. The transitional gas injection rate for BDR ( $q_{trans}$ ) and the critical gas injection rate for ALDR ( $q_{crit}$ ) are indicated by the vertical lines in the figure. In region I, when air is injected into the bottom surface of the hull, the flow of air-liquid mixture predominates at the turbulent boundary. As the air flux gradually increases, some air bubbles are combined to form a partial air layer, and a transition in which the mixed flow and the air layer coexist occurs ( $q_{trans}$ ). Here, in region II, as the air flux increases, the frictional drag reduction starts to rapidly increase from 20% to 80%. When the air flux exceeds the critical value ( $q_{crit}$ ), a continuous air layer is completely developed, and the drag reduction is 80% or more.

The drag reduction values shown in Fig. 4 were measured at a location of 6.05 m in the streamwise direction from the air injector at the bottom of the plate, which is approximately half the length of the entire plate. In fact, as the bubbles move toward the downstream direction, the sizes of the bubbles change due to the coalescences and splits or the bubbles escape from the near wall boundary layer, thereby reducing the drag reduction effect (Kodama et al., 2005; Elbing et al., 2008; Verschoof et al., 2016). In some studies, endplates were installed along the entire length to trap the air bubble in the bottom to achieve an effect (Kawashima et al., 2007; Hoang et al., 2009). As such, it is very important to maintain the continuity of air bubbles at the bottom of the hull. It is assumed that the generated air layer persists along the bottom of the hull with the bubbles evenly distributed and maintaining the level of drag reduction at the certain air flux measured in the experiment. These experimental results were used as a criterion for designing the ALS model in this study, and thus a drag reduction of 20% in the transition region of BDR and 80% in the critical region of ALDR were assumed. Since the cavity closure has a drag reduction of more than 95% once it has been completed, as per Lay et al. (2010)'s analysis, a conservative 95% is used for the PCDR here. In other words, the relevant fixed drag reduction value and the air flux necessary under specified circumstances for each type of ALS are employed as indicated in Fig. 4. However, in model tests or real ships injected with different air flow rates, it is anticipated that a slightly varying drag reduction may be attained.

### 3.1.3. Power consumption by air compressor

An air compressor or blower must be used to send air to the outlet nozzles at the bottom of the hull in order to form and maintain an air bubble layer beneath the ship's surface. The power used by the compressor varies according to the pressure and volume of air transferred, which has a significant impact on the real gain of an air lubrication system. According to Buckingham and Pearson (2019), using compressor manufacturer data may be more accurate in estimating compressor power consumption, but in this paper, keeping simplicity and versatility prioritized, the power needed to compress the gas at a specified mass flow rate is determined using the polytropic process (Mäkiharju et al., 2012), as shown in Eqs. (10)-(11). The expansion or compression process including heat transfer is approximately described by the polytropic process equation (Nag, 2013).

$$P_{cons} = \frac{P_{comp}}{\eta_e} \quad (10)$$

$$P_{comp} = \frac{\dot{m}_g}{\eta_c \rho_1} P_1 \frac{n}{n-1} \left( \left[ \frac{P_2}{P_1} \right]^{\frac{n-1}{n}} - 1 \right) \quad (11)$$

where  $P_{comp}$  is the power needed to compress a specified quantity of gas,  $\eta_e$  is the efficiency of electrical motor ( $\eta_e=0.9$ ),  $\eta_c$  is efficiency of an air compressor ( $\eta_c=0.6$ ),  $\dot{m}_g$  is the mass flow rate of air necessary to maintain the given volume flow rate of air on the bottom surface,  $\rho_1$  is the initial density of the air where it is compressed,  $P_1$  is the atmospheric pressure,  $P_2$  is the air delivery pressure from the compressor, and  $n$  is the polytropic index, chosen as the value valid for adiabatic processes ( $n=1.4$ ).

The pressure ( $P_2$ ) required by the compressor to deliver air to the bottom of the hull to achieve air lubrication, consisting of static pressure and dynamic pressure of the bottom air inlet of the hull, and pressure loss due to the piping as shown in Eqs. (13)-(14). In general, since the hull is deeply submerged in water, the influence of static pressure contributes the most to the compressor power. The amount of pressure loss caused by piping losses varies on a number of factors, including the piping length, roughness, and the relevant design of the air lubrication system. Some of the



existing articles calculated frictional pressure loss and minor loss from a moody chart assuming a certain pipe surface roughness (Mäkiharju et al., 2012; Comer et al., 2019), while others (Ceccio and Mäkiharju, 2012; Jang et al., 2014; Gallardo Martínez et al., 2016) used a range of 1-1.5 atm for the pressure drop due to piping losses. As a cautious estimate for the pressure drop caused by pipe, 1.5 atm was used in this study.

$$\dot{m}_g = qw \frac{\rho_1 P_3}{P_1} \quad (12)$$

$$P_2 = P_3 + \Delta P_{loss} \quad (13)$$

$$P_3 = \rho_w g T + \frac{1}{2} \rho_w V^2 \quad (14)$$

where  $q$  is the volumetric gas flux per unit span,  $w$  is the width of air covered area,  $P_3$  is the pressure under the hull,  $\Delta P_{loss}$  is pressure drop due to piping losses, and  $g$  is gravitational acceleration.

For the estimation of the volume flux of gas required to achieve a given air lubrication type beneath the hull, the experimental data of Elbing et al. (2008) and Makiharju et al. (2010) conducted in the large cavitation tank was used. Fig. 5 shows volumetric air flux per span ( $q$ ) for each air lubrication type according to the flow rate measured from the experiments. In Elbing et al. (2008), air flux was converted to an air layer thickness, and drag reduction according to thickness was used in their studies. In this model, as shown in Fig. 5 gas flux according to flow speed was used as reference data for calculating compressor power for each ALS type. In addition, the gas fluxes of the air lubrication system estimated from the sea trials of the bulk carrier and module carrier are also displayed (Hoang et al., 2009; Mizokami et al., 2010). According to Mäkiharju et al. (2012), these investigations hypothesize that an air layer or transitional region formed on the hull's bottom because the reduction in friction drag was lowered by 20 to 40%, which is partly compatible with the outcomes of Elbing et al. (2008), and Makiharju et al. (2010).

The air flux required to achieve the air layer or air cavity grows proportionally as the flow rate rises. In this study, BDR used  $q_{trans}$  in the transition region between BDR and ALDR with 20% drag reduction as in Fig. 4. The required air flux in the corresponding state is much less than the air flux for maintaining the ALDR at the smooth and rough plates. In the case of ALDR, the result was obtained in a state in which the  $q_{crit}$ , that is, the continuous air layer is fully developed. It can be confirmed that the rough surface requires additional gas flux to achieve the same extent of frictional drag reduction as on the smooth surface. In the case of partial cavity drag reduction, it is separated into the gas flow necessary to establish or maintain the cavity, and the required airflow of them is significantly different. Since the gas flux needed to maintain the cavity is less than half that needed to generate it and is almost identical to the gas flux needed for the BDR, hence the power used by the compressor for the PCDR is actually very little.

According to Makiharju et al. (2010), in the flat plate experiment, the air cavity did not easily reach the beach (end of the closure) at a lower flow speed, and the flow in the cavitation tunnel fluctuated with overshooting the beach at a higher speed. Therefore, the corresponding study used a range of flow speeds showing a stable flow rate change while the closure area can be completely filled with air, and this limited range is also applied in this study as shown in Fig. 5. Similar experimental results can be found in other studies. More power was required to maintain the air cavity than not lubricating in some low-speed conditions, and if the flow is too low, the water might re-attach too close to the cavity step (Pavlov et al., 2020). In addition, according to Butterworth et al. (2015), the efficiency of the air cavity decreases as the speed increases. If it is too high, the bubbles may escape from the side of the cavity, resulting in negative net savings. However, the effect of reducing drag on the air layer and the leakage of air from the bottom hull is greatly influenced by the design characteristics of the bottom cavity (Slyozkin et al., 2014; Butterworth et al., 2015). In fact, many studies have been conducted for the air cavity in high-speed planning ships, and if the air flow rate is optimized and the hull is properly designed for the ship's operating characteristics, it might be utilized several speed ranges (Pavlov et al., 2020). From the review of previous work summarized in the preceding discussion, it might be concluded that air cavity is an immature type of ALS, requiring further research. However, we still chose to include it in this study.

To determine the amount of air required for each ALS, the model uses regression equations based on experimental data on the flat plate as shown in Eqs. (15)-(17). At sufficiently high Reynolds numbers, the dependence of gas flux on Reynolds number can be weakened (Lay et al., 2010), and in experiments with different size scales of comparable

Potential energy savings of air lubrication technology on merchant ships

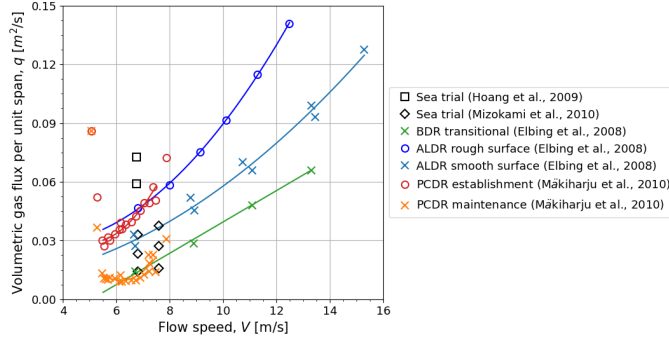


**Figure 5:** The volumetric air flux per unit span required for different air lubrication techniques according to the flow speed. The figure is adapted from Mäkiharju et al. (2012) with minor modifications.

shape, the normalized gas flux for air lubrication may be in the same range (Mäkiharju et al., 2010; Mäkiharju et al., 2012). Thus, this study used the results of these model scales to estimate the actual gas flow rate on a full-scale ship. A curve fitting equation was developed based on the experimental results at the transition gas injection rate of BDR, and the gas flux necessary to accomplish ALDR and PCDR was then applied as demonstrated in the study of Mäkiharju et al. (2012). Here, the gas flux of ALDR was selected using the regression equation of the rough plate assuming that the surface of the hull would be somewhat rough rather than completely smooth. Instead of using the establishment gas flux of PCDR, maintenance was employed since it was assumed that keeping a cavity using an air lubricating system during the voyage would be more common. In this model, it is assumed that the air lubrication system is automatically controlled, such as the volume gas flux according to the flow speed shown in Fig. 5, and that the system automatically shuts off if the compressor consumes more power than the saving power or if it is outside the operating speed range.

The curve fits for volumetric air flux per unit span ( $q$ ) for BDR at the transitional gas injection rate are as follows:

$$q_{BDR} = 0.008V - 0.0405 \quad 5.5 < V < 12.5 \quad (15)$$

The curve fits for volumetric air flux per unit span for ALDR on a rough surface, and the curve fits for maintaining PCDR are expressed:

$$q_{ALDR} = 0.00126V^2 - 0.00755V + 0.0391 \quad 5.5 < V < 12.5 \quad (16)$$

$$q_{PCDR} = 0.00701V^2 - 0.0866V + 0.277 \quad 5.5 < V < 7.5 \quad (17)$$

Table 2 shows the specifications and power of the compressor used for air lubrication systems reported in several studies. Here, main dimensions without accurate information from the references are obtained through a similar ship or simple estimation method (Kim et al., 2022a). By substituting the given information into Eqs. (10)-(13), the compressor powers of the various ships listed in the table are estimated, and they are compared in Fig. 6. As the operating conditions and information of the vessel and ALS compressor shown in the table do not exactly match the setting used in this model, it may be a rather rough estimate. However, as shown in the figure, estimates are quite well correlated with the reported data.

### 3.1.4. Weather correction for the efficiency of air lubrication system

Depending on the environment the vessel is operating in, the ALS performance may change. According to the sea-trial results for a cruise ship from Foreship (Pavlov et al., 2020), a relatively small tendency of net power saving due to air bubbles according to ALS on-off was seen for Beaufort scale 6 and above compared to less than Beaufort scale 4. According to the model test of a tanker by Borusevich et al. (2017), as the sea-state (ss) increased, cavity

**Table 2**

Compressor specifications for air lubrication of ships from reported data. The asterisk symbol in the table represents the estimated value.

Ship type	L [m] × B [m] × T [m]	Speed [knots]	Air flow [m <sup>3</sup> /min]	Compressor power [kW]	References
Bulk carrier	230 × 43 × 6.6-12.8	14	150-250	500-840	(Mizokami et al., 2013)
Module carrier	153 × 38 × 4.5	13.25	40.5-94.5	72-211	(Mizokami et al., 2010)
Tanker	168 × 32 × 10.6	11-14	-	150-230	(Silberschmidt et al., 2016)
Container	350 × 51* × 15.5*	24	200-550	680-1900	(Mizokami et al., 2013)
Container	321* × 45.6 × 14.75	19	133	600	(Borusevich et al., 2017)
Ferry	105 × 17.9 × 6.3	14	26-110	13-60	(Nagamatsu et al., 2002)
Passenger ship	240 × 32.2* × 7.8*	17	100-200	230-460	(Mizokami et al., 2013)

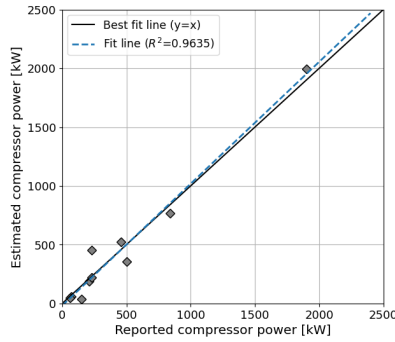


**Figure 6:** Comparison of estimated compressor power from the model and the reported compressor power in Table 2.

instability due to waves occurred in PCDR. As a result, the power saving efficiency of the air cavity system dropped by 20% in ss5, 40% in ss6, and 90% in ss7, and was hardly functional above. The extreme pitch motion of the ship in the rough sea is found to have the potential to seriously disturb the air layer on the bottom of the hull. As a result, the drag reduction from the air layer system is reduced, and more air is needed to keep the air lubrication at its calm water level.

It has been challenging to evaluate the effect of waves on the air lubrication system because the majority of ALS research has used model experiments in towing tanks or sea trials in relatively calm water conditions. As a result, this study used the findings of Borusevich et al. (2016) to roughly represent the effects of weather in the model. As indicated in Eq. (18), in order to estimate the power saving reflecting the weather effect, the power savings estimated by Eq. (4) is multiplied by the correction factor as shown in Table 3. Although it is cautiously expected that the air cavity system will have a greater loss due to ship motion than air bubble or air layer on the bottom surface, the coefficient is identically given to all ALS kinds and ship types. Nevertheless, further tests and full-scale observations are required to fully understand how weather affects ALS performance in relation to the sea state and ship design. A comparison of ALS performance according to the application of actual sea conditions and weather correction factors is further discussed in Section 4.4.

$$P_{save,wc} = P_{save} \times C_{wc} \tag{18}$$

where  $P_{save,wc}$  is saved power by air lubrication system after weather effect correction,  $C_{wc}$  is weather correction factor.

**Table 3**

Weather correction factor for the efficiency of air lubrication system according to the sea-state.

Sea-state	Max sig.wave height [m]	Correction factor [-]
1	0.1	1
2	0.5	1
3	1.25	1
4	2.5	1
5	4	0.8
6	6	0.6
7	9	0.1
8	-	0

### 3.2. Comparison with previous studies

This section examines the validity of the model by comparing the results obtained from several experiments such as model tests, CFD, and full-scale measurements with the estimates of the model proposed in Section 3.1. Fig. 7 (a) shows the results of CFD analysis for the 320m cruise ship from Foreship (Pavlov et al., 2020). Here, the ship's speed changed from 14 knots to 22 knots, and net-percentage power savings for four different air flow rates were shown. According to CFD calculations, the power saved by air bubbles tends to drop constantly as ship speed increases at relatively low flow rates of 2.3 to 7.3 kg/s, however, at 10 kg/s, the saving rises until 19 knots and then declines. BDR estimations from the proposed model reflect a trend where savings gradually decrease as speed increases, while the ALDR estimates gradually grow with speed and then gradually fall beyond 18 knots. Although the figures do not exactly match, it seems to capture the saving trend of ALS according to the speed and flow rate of the ship. Compared to the CFD results, the volatility of net-percentage power saving with speed seems small, but comparing the model tests and full-scale measurements in Fig. 7 (b), it can be seen that the volatility may not be so large.

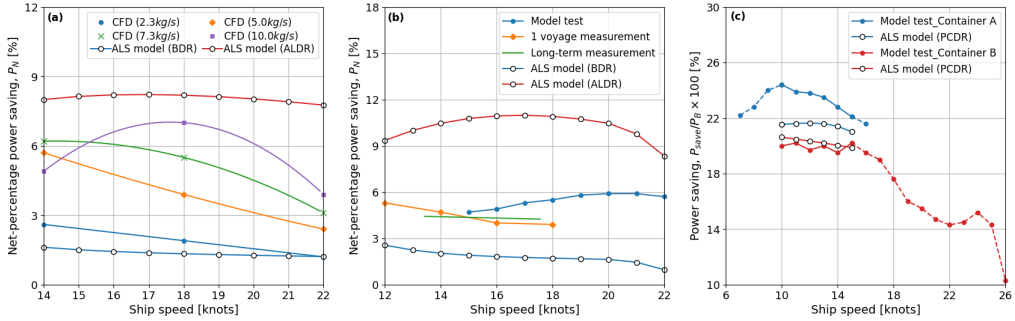
The net-percentage power savings achieved by the air lubrication system during the laden voyage of a LNG ship are shown in Fig. 7 (b). In the Model test, about 5-6% saving is attainable, and the optimal performance can be achieved near the ship's service speed, which is similar to the trend of ALDR predictions from the proposed model. In this experiment, two rows of air injectors in the forward and one in the aft were arranged at the bottom of the ship model, and the thickness of the air layer was formed 2, 3, and 5 mm, respectively, which is presumed to correspond to transitional air layer drag reduction. The results show net-percentage power savings of roughly 4-5% from the ship's real operations, and they tend to decline slightly as speed increases, which is similar to the BDR predictions made by our model.

Fig. 7 (c) shows the results of PCDR analysis of two container ships. As shown in the figure, it was not possible to collect the power consumption of the compressor according to speed from the relevant research (Borusevich et al., 2017; Pavlov et al., 2020), they were compared in terms of power saving by ALS, without correcting for compressor power. Looking at the predicted results, it can be seen that it is in quite good agreement with the results of two ships within the computable area.

The BDR estimates in this model tended to be somewhat smaller than the results of other studies, apparently because the BDR was calculated based on the transitional gas injection rate. Some of the studies related to the air bubble system may have progressed beyond the area where only air bubbles exist to the transitional region where air bubbles and air layers coexist through the adjustment of air flux. Overall, the ALDR has a tendency to overestimate, which is probably because this model assumes that a completely continuous air layer has been formed. In the case of PCDR, it tends to be almost similar to the experimental results within the application range. Fig. 7 shows that the prediction method presented in Section 3.1 gives fairly good estimates, seen in the light of the simplicity of the model and the complexity of the physics it attempts to represent. The comparison in Fig. 7 is also a reminder that our model is not intended to be an accurate representation and not a replacement for model tests or detailed numerical studies.

Due to the various assumptions and the settings of ALS in the model, these comparison results were not accurately matched. This model assumes that the air lubrication system is automatically controlled to maintain the drag reduction level at a specific air flow rate measured in the experiment. Moreover, an air layer is generated and maintained along the bottom of the hull without loss of bubbles, and the reduction in propulsive efficiency due to bubbles is ignored. In particular, during the actual operation of the ship, the drag reduction effect of the air layer may have been influenced by

several uncertain factors such as the ship’s motion, environments, and ship-specific conditions. As a result, it is difficult to replicate the precise conditions of tests undertaken in prior studies, hence this can only provide an approximation of the model’s validity.



**Figure 7:** Comparison of estimates of the proposed model with previous experimental results (a) Cruise ship (Pavlov et al., 2020), (b) LNG carrier (Lee et al., 2017), (c) Container ship A (Borusevich et al., 2017) and Container ship B (Pavlov et al., 2020). The figures are adapted from the referenced papers with minor modifications.

## 4. Results

### 4.1. Parametric study

The energy saving trend of the air lubrication technology was investigated using a parametric study on changes in ship speed, air covered area, loading condition, and block coefficients in accordance with various ship operating and design conditions. Here, a supramax-class general cargo ship was selected for the case study and had the dimensions shown in Table 4. The settings for each simulation case were specified as shown in Table 5, and the findings thereof are depicted in Fig. 8; the upper graph displays the net-percentage power saving, while the lower graph displays the net power saving. To investigate the influence of block coefficient in Case 4, it is assumed that the hull shape design has been modified, i.e., that the air lubrication system has been installed on different ships (85-100%  $C_b$ ).

**Table 4**  
Ship basic information.

	General cargo
Length [m]	194
Breadth [m]	32
Design draught [m]	12.6
Block coefficient [-]	0.79
Wetted surface area at design draught [m <sup>2</sup> ]	9370
Deadweight tonnage [ton]	50700
Maximum continuous rating [kW]	10780
Service speed [knots]	15.5

In Fig. 8 (a), the net power saving increases for all ALS types as ship speed rises. While, the net-percentage power saving gradually declines in BDR, and for ALDR and PCDR, it is gradually increased to a certain speed and then decreased. In principle, it is advantageous for ships to operate at a low service speed because the frictional resistance is predominant at low speeds, while at high speeds, the wave-making resistance contributes more to the total resistance. However, since the air flux required by the compressor varies for each ALS type as illustrated in Fig. 5, the speed conditions at which the maximum saving could be achieved from the ALS could be slightly different.

**Table 5**

Parametric study of the air lubrication systems for the target ship. Sea-states are assumed to be calm water condition.

Case	$V_s$ [knots]	$T$ [m]	$C_b$ [-]	$A_a/A_b$ [-]
1	10.5-15.5 (0.7-1.0 $V_s$ )	12.6	0.79	0.84
2	10.5-15.5 (0.7-1.0 $V_s$ )	12.6	0.79	0.6-1.0
3	15.5	8.8-12.6 (0.7-1.0 $T_d$ )	0.79	0.84
4	15.5	12.6	0.68-0.79 (0.85-1.0 $C_b$ )	0.84

The lower and upper limits of the net-percentage power saving are depicted in Fig. 8 (b), which only changes the ratio of the air covered area from 60% to 100% under the same conditions as in Case 1. Due to the hull structure and arrangement of air release units, it is practically impossible to completely cover the bottom region with air; nonetheless, the range is assumed to be 60-100% to examine the effect of the air covered area. Depending on the ALS type, this difference in the air covered area may lead to a significant difference in savings of 3 to 10%. In other words, it is clear that the configurations of the ALS installation, which decide how much air can cover the bottom region, can have a significant impact on performance in addition to the ship's flat bottom area.

Case 3 demonstrates that the net saving of the air lubrication decreases as the draught increases. This is because the energy consumed by the compressor to supply air to the bottom of the ship is increasing with increasing draught. Additionally, the underwater area increases along with the draught, increasing the hydrodynamic drag forces, which has the effect of increasing the overall required power.

Fig. 8 (d) shows the parametric study results of the block coefficients. The bottom area of the ship generally tends to widen as the block coefficient increases, thus even if it is assumed that the same percentage of air is covering the hull bottom, it can be seen that the amount of frictional resistance can be decreased. That is, the efficiency of air lubrication system is high at a high block coefficient as can be observed from the figure.

#### 4.2. Global sensitivity analysis

The Sobol method, a global sensitivity analysis method, was used to determine how each parameter affected the model's output. The Sobol sensitivity index can be used to quantify each parameter's contribution to the variance of the model output. A low Sobol index indicates that the variation of the output caused by a change in the corresponding parameter is relatively small (Homma and Saltelli, 1996; Saltelli and Annoni, 2010). The first-order index is measuring the direct effect of each parameter on the variance of the model. It can be expressed as Eq. (19), and it means an expected decrease in the variance of the model when  $X_i$  is fixed. The total index, which includes both the first-order index, as well as the sensitivity due to the interaction between that parameter and all other parameters, can be expressed as Eq. (20). The larger the difference between the first and total index, the greater the effect of sensitivity on variance due to the interaction.

$$S_i = \frac{Var[E(Y|X_i)]}{Var(Y)} \quad (19)$$

$$S_i^T = \frac{Var[E(Y|X_{-i})]}{Var(Y)} \quad (20)$$

where,  $E(Y|X_i)$  stands for the predicted output value when  $X_i$  is fixed, and  $X_{-i}$  denotes all uncertain parameters except  $X_i$ .

Here, as shown in Fig. 9, global sensitivity was examined within the range ( $V_s$ : 10.5-15.5,  $T$ : 8.9-12.6,  $A_a/A_b$ : 0.6-1.0) that was taken into account in the previous section. Within this range, it was assumed that the parameters were distributed uniformly. For each sensitivity analysis group, different block coefficients were used of 0.68, 0.74, and 0.79 to support the assumption that the air lubrication system was installed on the different ships, respectively. As a result of the preliminary analysis, the interaction between speed, draught, and the ratio of air covered area to the bottom surface area was not significant, there was little difference between the total index and the first index. Thus, only the first-order Sobol indices are displayed in the figure. Within the parameter range defined in this research, the ratio of air covered

Potential energy savings of air lubrication technology on merchant ships

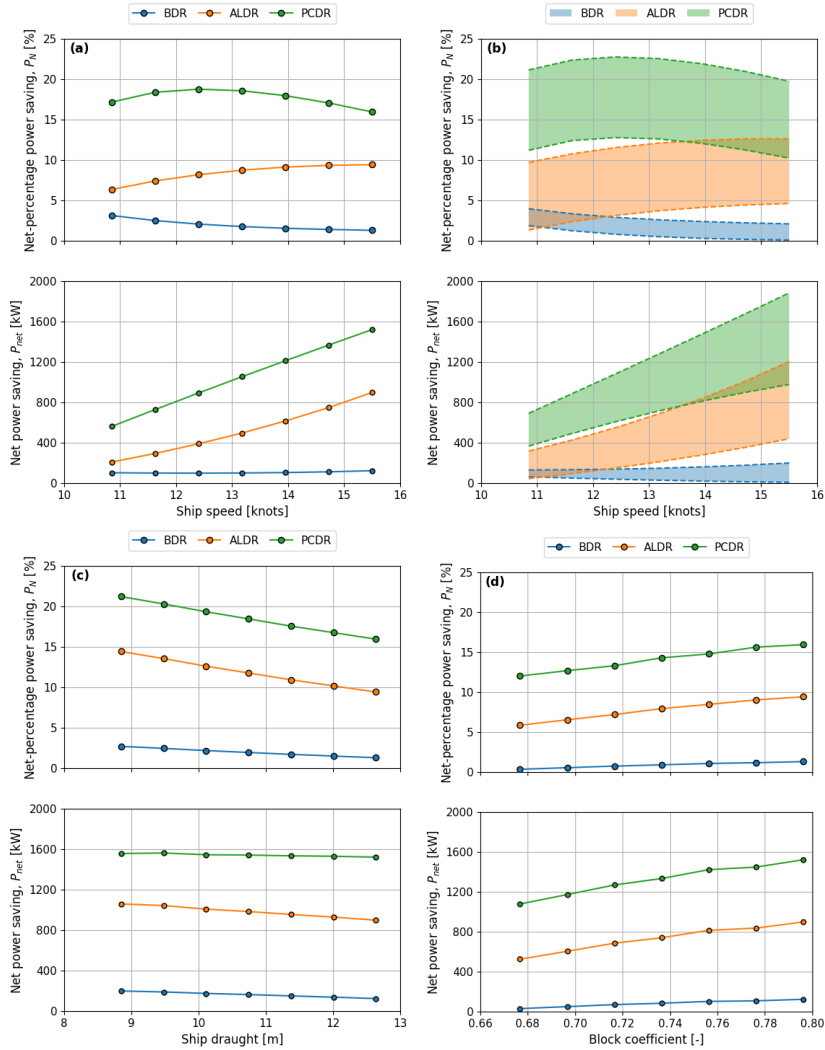


**Figure 8:** Results of parametric study for the air lubrication systems: (a) speed, (b) ratio of air covered area to the bottom surface area, (c) draught, (d) block coefficient.

area to the bottom surface area is the most influential as it accounts for about 46 to 85% of the total variance. In BDR, speed is a relatively more important parameter than ALDR and PCDR, which is about 35-42% of the total. The change in the Sobol index of various parameters according to block coefficient is not significant, but the influence of draught is relatively greater in ships with a large block coefficient.

### 4.3. Case study of global fleet in calm water condition

On about 48,710 global fleet registered in the Seaweb database, performance analysis in calm sea conditions according to the installation of the air lubrication system was carried out. Here, five ship categories of bulk carrier,

Potential energy savings of air lubrication technology on merchant ships

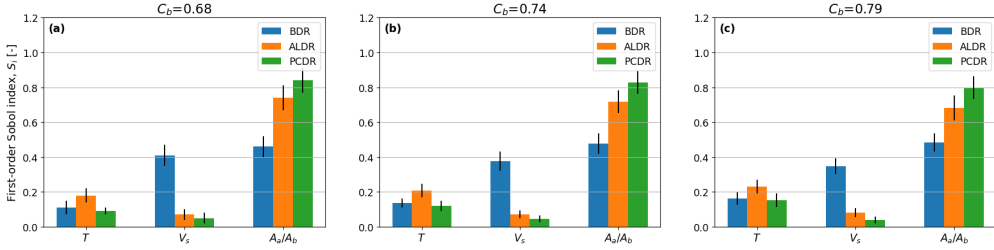


**Figure 9:** Sensitivity analysis with Sobol's indices for each parameter according to different block coefficient. The bars in the figure represent the first order Sobol index using 10,000 random samples from the Monte Carlo method.

chemical tanker, general cargo, container ship, and oil tanker were examined, and ship type and size were categorized in accordance with the IMO's fourth greenhouse gas study (IMO, 2020), as indicated in Table 6. The draught ratio for each ship type was used as given in Table 7 in order to assume the laden and ballast voyage of the ship operation (Olmer et al., 2017). Here, ballast-only voyages are uncommon for container ships unlike other ship types, thus the average draught ratio is applied for all voyage types. According to the study's specified bin size, Fig. 10 depicts the composition of each type of ship, and the distributions of ship parameters employed in this case study are shown in Fig. 11.

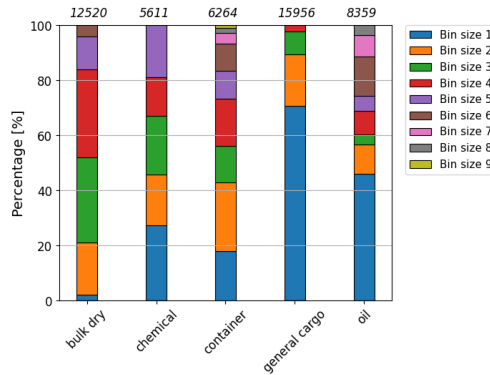


**Figure 10:** Percentage of vessels by bin size obtained from the sea-web database.

Fig. 12 displays the comparison of the global fleet's potential net-percentage power savings by type of air lubrication. The blue and red boxes represent the case study assuming that there is no environmental force when navigating at service speed under ballast and laden conditions.

The saving of the air lubrication system during a ballast voyage is higher than that of a laden voyage, as can be demonstrated in this plot. Container ships deliver the same results because their draught is assumed to be the same. Inspecting the overall results for each ship type, bulk carriers and tankers with flat bottom shapes that can hold more air bubbles in the hull bottom, i.e., generally associated with high block coefficients, are advantageous. Referring to Fig. 11, it can be seen that a ship with a relatively low operating speed compared to the size of the ship, that is, the Froude number, rather than the operating speed, has a more direct effect on power saving. The potential net-percentage power savings of BDR, ALDR, and PCDR are 2 to 5%, 8 to 14%, and 16 to 22%, respectively, when the results of the entire fleet of 25 to 75% quantile in ballast and laden voyages are taken into account.

A more detailed comparison according to the bin size for each ship type is displayed in the following Fig. 13. The PCDR results of some container ships are not provided here, which were not calculated because the service speeds



Potential energy savings of air lubrication technology on merchant ships

**Table 6**  
Vessel type and categories.

Ship type	Bin size	Capacity	Unit
Bulk carrier	1	0-9,999	DWT
	2	10,000-34,999	
	3	35,000-59,999	
	4	60,000-99,999	
	5	100,000-199,999	
	6	200,000-	
Chemical tanker	1	0-4,999	DWT
	2	5,000-9,999	
	3	10,000-19,999	
	4	20,000-39,999	
	5	40,000-	
Container ship	1	0-999	TEU
	2	1,000-1,999	
	3	2,000-2,999	
	4	3,000-4,999	
	5	5,000-7,999	
	6	8,000-11,999	
	7	12,000-14,999	
	8	14,500-19,999	
	9	20,000-	
General cargo	1	0-4,999	DWT
	2	5,000-9,999	
	3	10,000-19,999	
	4	20,000-30,000	
Oil tanker	1	0-4,999	DWT
	2	5,000-9,999	
	3	10,000-19,999	
	4	20,000-59,999	
	5	60,000-79,999	
	6	80,000-119,999	
	7	120,000-199,999	
	8	200,000-	

**Table 7**  
Average draught ratio according to the voyage type of different ship types. Draught ratio is defined as the ratio of actual draught to design draught.

Ship type	Ballast voyage	Laden voyage
Bulk carrier	0.58	0.91
Chemical tanker	0.66	0.88
General cargo	0.65	0.89
Oil tanker	0.60	0.89
Container ship	0.82	

of the vessels belonging to the corresponding bin sizes were outside the operating range of the PCDR. It is clear that even within the same ship type, performance can vary significantly depending on the operation profile and hull characteristics. Additionally, it can be shown that overall savings tend to rise as bin size grows. This is thought to be the case since the proportion of frictional resistance in total resistance increases with ship size. On the other hand, the net-percentage power savings tend to no longer increase but rather slightly decrease in the case of a large tanker such as bins 7 and 8 because the air compressor's power consumption rises due to the hull design with deep draught. Based

Potential energy savings of air lubrication technology on merchant ships

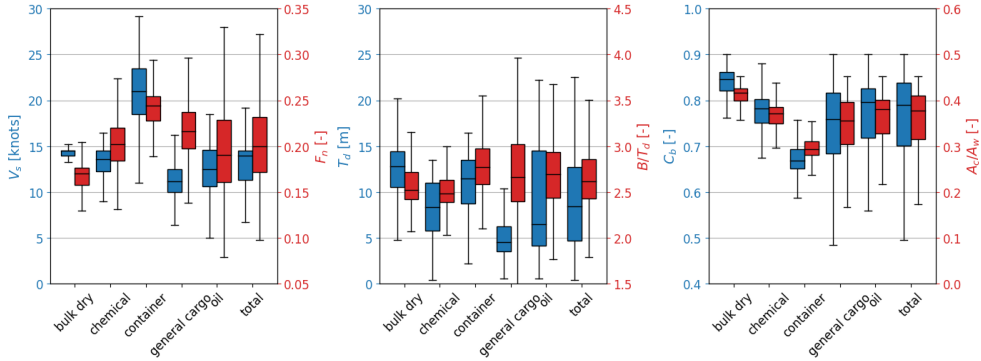


Figure 11: Distribution of ship parameters relevant to ALS according to the ship type used in the study.

on these results, coastal barges with flat bottom hull shapes that typically operate at low draught and low speeds are believed to be an ideal ship type, although not investigated in this study.

The results shown here are obtained under the assumption of calm water conditions and can be somewhat optimistic due to the various assumptions and simplifications. In order to obtain the corresponding amount of drag reduction on an actual ship, an appropriate design must follow. However, the estimated results in Fig. 12 are fairly consistent and are distributed in a similar range to the previous research as in Fig. 1, despite the fact that a ship-to-ship comparison between them cannot be done due to different experimental setups, such as ship speed, loading conditions, and air lubrication system.

Considering the actual use of air lubrication technology, the following characteristics can be considered from the above analysis results. For ships that are already in operation, the retrofit is comparatively easy with BDR and ALDR and a certain degree of drag reduction can be expected. Furthermore, it is investigated that the impact on the ship’s maneuvering and sea-keeping capabilities is not significant (Thill et al., 2005; Foeth et al., 2009; Gallardo Martínez et al., 2016). However, according to the hull shape and operating profile, it is required to assess the actual gain between savings by air lubrication and consumption by the air compressor. Meanwhile, PCDR is expected to be effective when the ship maintains an air lubrication system throughout actual operations due to the relatively small air flux required to keep the air cavity. However, the system can be functional in a limited range, and there is still some ambiguity regarding air cavity loss caused by ship motion. Additionally, it is appropriate mostly for newly constructed ships because it necessitates a hull design that is specifically devoted to PCDR, which can lead to an increase in initial capital expenses. As a result, it would be most suited for ships with sailing tactics that take place in environments where maintaining the air cavity is relatively easy and the speed profile falls within the PCDR’s operational range.

Potential energy savings of air lubrication technology on merchant ships

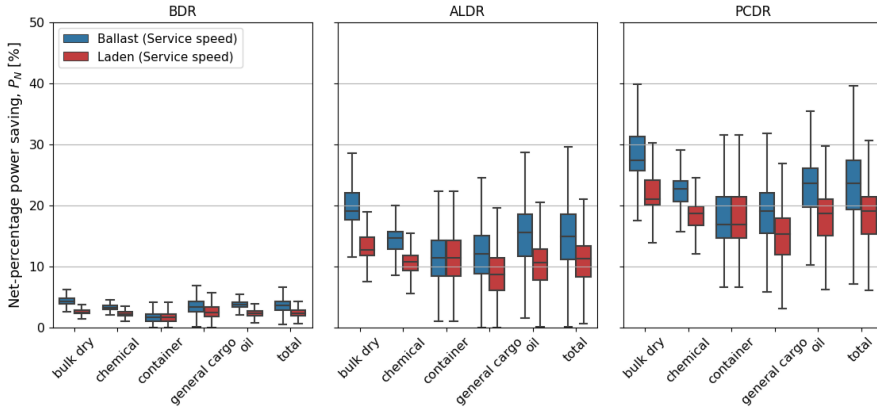


Figure 12: Comparison of potential net power saving of global fleet by air lubrication type.

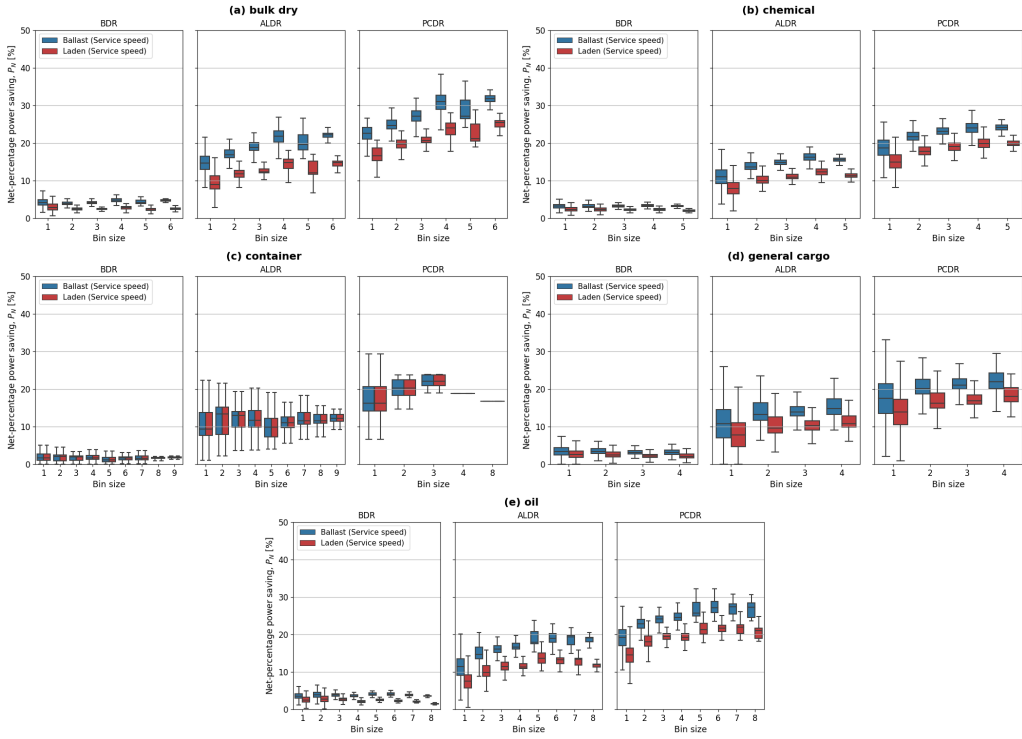
4.4. Case study of a target ship in real sea condition

In the previous section, due to a large amount of calculation of the global fleets, results were obtained by assuming calm water conditions, i.e., external environmental factors are ignored, but in this section, the performance of ALS according to the weather effect is analyzed. For ease of calculation, it is assumed that a ship operates a fixed trade pattern at service speed annually, and three different scenarios are compared: a calm sea condition, a real sea condition, and the real sea condition where weather adjustment factors are applied.

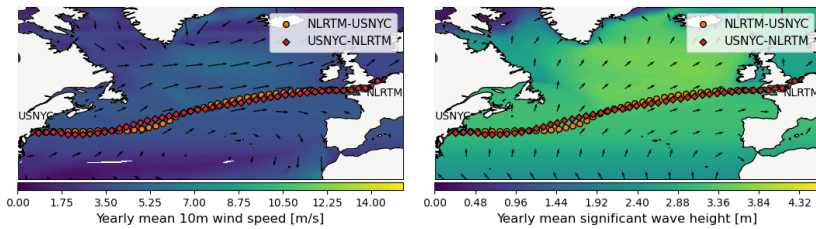
The general cargo ship in Table 4 was used, and a scenario was assumed in which the ship sailed the route between Rotterdam, Netherlands (NLRM), and New York, USA (USNYC), at a constant service speed of 15.5 knots, as indicated in Fig. 14. NLRM-USNYC is assumed as a laden voyage and in the opposite direction is ballast voyage, and 50 waypoints were uniformly defined throughout the route. The histograms of the apparent wind speed, apparent wind angle, significant wave height, and relative wave angle that the ship may experience while operating are presented in Fig. 15, which was created using meteorological data from the appropriate route from the ECMWF reanalysis weather hindcast data for 2020 (In the figure, 0 degrees represents headwind and head wave). On average, the ship encounters more headwinds from NLRM to USNYC and following winds from USNYC to NLRM during the voyage.

Fig. 16 represents an example of ALDR in the ship’s laden voyage among the results of annual energy-saving simulations, and Fig. 16 (a) and Fig. 16 (b) show seasonal changes and three different scenarios, respectively. The ship typically experiences headwinds at the start of the voyage outside the Strait of Gibraltar, and in the North Atlantic Ocean, net-percentage power savings tend to decline dramatically as a result of rather strong external environments, since the total resistance increases significantly, while the frictional resistance reduction by ALS is not influenced. In addition, seasonal variations show that from June to August, there is an average saving of about 8%, while from December to February, the average saving in some areas drops to less than 4%. It is evident that there is a significant variation in the performance efficiency of air lubrication depending on the region and season. In Fig. 16 (b), the difference in net-percentage power saving according to the actual weather conditions at sea can be confirmed. In calm sea conditions, the savings of the ship is constant annually at all waypoints, but when considering the weather profiles of the real sea, the net-percentage power saving changes geographically and seasonally, and there is a difference of about 30% on average. When the weather adjustment factor proposed in this study is additionally applied, it tends to decrease by about 5% more than that. Thus, the weather correction factor itself is of minor importance compared to the increase of resistance and related power consumption due to wind and waves. Fig. 17 shows the results of three scenarios for all ALS types and voyage types at once. It can be seen that the overall energy-saving effect decreases by roughly 15 to 35% compared to the calm water conditions, taking into account the actual weather environment and weather correction effect. The difference in efficiency between the ballast voyage and the laden voyage is also shown in Fig. 17, which is expected to be largely due to the meteorological characteristics of such a specified route, where the annual weather condition is much more severe in the laden voyage, as shown Fig. 15.

Potential energy savings of air lubrication technology on merchant ships



**Figure 13:** Comparison of potential net power saving of global fleet in bin categories according to ship type: (a) bulk dry, (b): chemical, (c): container, (d): general cargo, (e) oil.



**Figure 14:** (a) Yearly mean wind speed (b) Yearly mean significant wave height at North Atlantic Ocean 2020. Arrows in the figures represent the mean direction of the wind and waves. Orange circle is route from NLRTM to USNYC and red diamond is from USNYC to NLRTM.

Potential energy savings of air lubrication technology on merchant ships

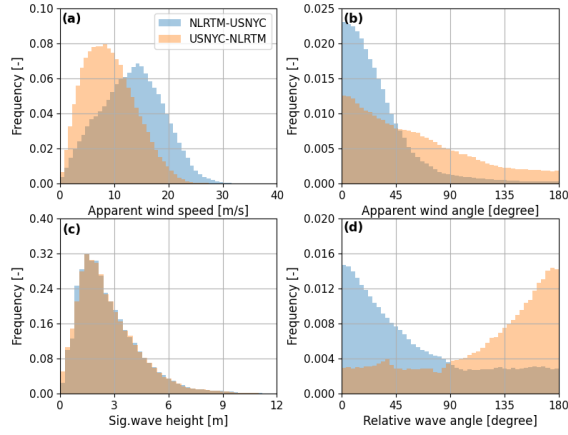


**Figure 15:** Histograms of the actual weather conditions that ship encounters: (a) apparent wind speed, (b) apparent wind angle, (c) significant wave height, (d) relative wave angle.

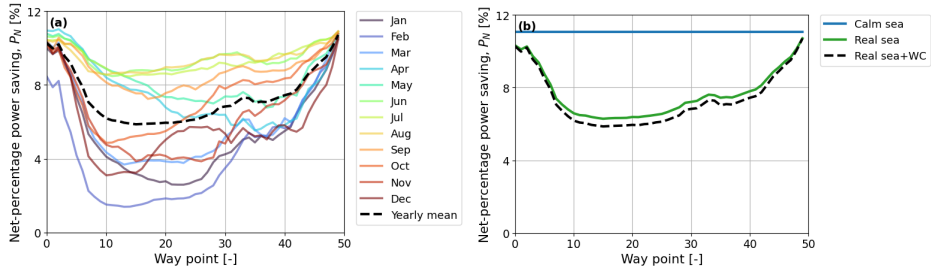


**Figure 16:** Net power savings of a ship using ALDR at laden voyage (NLRTM-USNYC): (a) seasonal changes, (b) weather influences.

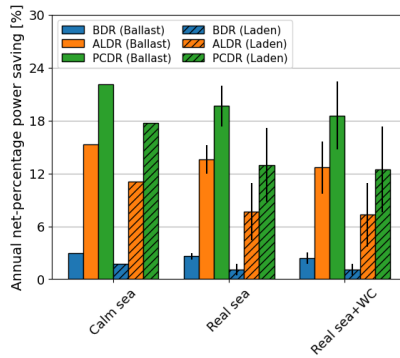


**Figure 17:** Comparison of average annual net power saving of ALS according to the application of weather effects.

## 5. Conclusions

Most of the existing studies related to ALS have introduced ship-specific approaches such as model tests, CFD, and full-scale measurements, and few simplified models can be applied to various vessels with different operating profiles and evaluate energy-saving trends. This study presents an easy-to-use tool that can be applied at the global fleet level in order to assess the energy saving potential of air lubrication systems of different configurations. The tool might also be useful for early-design considerations of installation of air lubrication systems. The overall theoretical background underpinning the modeling, the estimation methods of several factors, and the assumptions were addressed. On the basis of the established model, parametric and sensitivity analyses were carried out, and insights on the variables influencing ALS performance were provided. Additionally, potential energy reduction trends for each ship type were examined, and changes in performance according to the location and seasonal effects were discovered for specific waters.

Through the parametric study, despite air lubrication systems being more efficient for ships operating at low speeds, the parametric study indicates that the ideal operating conditions may vary slightly depending on the type of air lubrication. The efficiency of ALS increases as the block coefficient rises because high block usually comes with large flat bottom area. Not only this, but it is also important how much air can cover the bottom area of the ship in relation to the configuration of ALS. The ratio of air covered area to the bottom surface area could explain 46 to 85% of the total variation of net-percentage power savings within the given parameter range in this study, according to a sensitivity analysis utilizing the Sobol index. As higher draught increases the energy needed to overcome hydrodynamic drag forces and increases the energy of the compressor used to supply air, the savings are larger in ballast than in laden conditions.

According to the case study conducted under the assumption that the entire global fleet would be equipped with ALS, the possible net-percentage power savings would be BDRs of 2-5%, ALDRs of 8-14%, and PCDRs of 16-22%. The level of savings identified in the fleet-wide study agrees fairly well with the level of savings of the various studies of individual ships found in the literature. Overall, bulk carriers and tanker with blunt hulls and moderate running speeds showed larger savings than container ships with slender hulls and high operating speeds. The operation profile and hull features, however, can significantly affect performance even within the same ship class. Considering the actual weather environment and weather correction effect, it can be observed that the effect decreases by about 15 to 35% compared to the calm water conditions.

The approach taken in this study can be applied to provide preliminary performance estimates when considering the installation of an air lubricating system during the ship's initial design phase, and an evaluation of the anticipated performance of the global fleet can also be taken into consideration. In the area of international shipping, this will help to emphasize the potential of air lubrication technology to reduce emissions. Nonetheless, it should be noted that some of the assumptions and simplifications of the model might lead to somewhat optimistic results. In fact, careful hull and system design suited to those systems will be needed to achieve the same level of power reduction as the results achieved from this work. The model would benefit from an improved model of the effect of waves and ship motions on the ALS, as well as the effect of ALS on the propulsive efficiency. Further study of airflow at large scales and high Reynolds numbers, as well as closer examination using full-scale measurements from ALS-equipped ships, are necessary in order to close the gap between model-scale and full-scale results and to more accurately capture the impact of the air layer below the hull. In a future study, it is planned to analyze the energy saving and related emission reduction potential from use of air lubrication, taking into account the real operational pattern and environment, including the wave correction on the air lubrication effectiveness.

## CRedit authorship contribution statement

**Young-Rong Kim:** Conceptualization, Investigation, Methodology, Software, Writing - Original Draft. **Sverre Steen:** Conceptualization, Methodology, Writing - Review & Editing, Supervision.

## Acknowledgements

This study is part of the research projects CLIMMS – Climate change mitigation in the maritime sector (Research Council of Norway (RCN) project number 294771).

## References

- ABS, 2019. Air lubrication technology. American Bureau of Shipping: Spring, TX, USA .
- Alamsyah, M.A., Hakim, M.L., Utama, I., 2018. Study of shear and pressure flow on the variation of ship hull shapes as one of the biofouling growth factors, in: Proceedings of the 3rd International Conference on Marine Technology. SCITEPRESS-Science and Technology Publications, pp. 97–105.
- Aronietis, R., Crozet, Y., Ferrari, C., Frouws, K., Grootbod, H., Guihery, L., Kapros, S., Laroche, F., Lloyd, M., Roubountsos, A., et al., 2011. Innosutra project deliverable d4 and d5-topical assessment of innovative successes and not-yet-successes .
- Birk, L., 2019. Fundamentals of ship hydrodynamics: Fluid mechanics, ship resistance and propulsion. John Wiley & Sons.
- Blendermann, W., 1996. Wind loading of ships collected data from wind tests tunnel in uniform flow. Institut für Schiffbau der Universität Hamburg .
- Borusevich, V., Poustoshny, A., Sverchkov, A., Trincas, G., 2017. Future outlook of artificial cavity application for reducing hydrodynamic resistance of containerships .
- Borusevich, V., Poustoshny, A., Sverchkov, A., Trincas, G., 2016. Impact of air cavity technology on ship drag reduction: experience from research studies, in: 10th Symposium on High-Performance Marine Vehicles-HIPER 16, TUHH, pp. 94–107.
- Bouman, E.A., Lindstad, E., Riialand, A.I., Strømman, A.H., 2017. State-of-the-art technologies, measures, and potential for reducing ghg emissions from shipping—a review. Transportation Research Part D: Transport and Environment 52, 408–421.
- Buckingham, J., Pearson, D., 2019. Modelling alternative propulsion technologies for merchant vessels. RINA, Power & Propulsion Alternatives for Ships, 23rd January .
- Bunnik, T.H., 1999. Seakeeping calculations for ships, taking into account the non-linear steady waves .
- Butterworth, J., Atlar, M., Shi, W., 2015. Experimental analysis of an air cavity concept applied on a ship hull to improve the hull resistance. Ocean Engineering 110, 2–10.
- Ceccio, S.L., 2010. Friction drag reduction of external flows with bubble and gas injection. Annual Review of Fluid Mechanics 42, 183–203.
- Ceccio, S.L., Mäkiharju, S., 2012. Air lubrication drag reduction on great lakes ships. Great Lakes Maritime Research Institute .
- Comer, B., Chen, C., Stolz, D., Rutherford, D., 2019. Rotors and bubbles: Route-based assessment of innovative technologies to reduce ship fuel consumption and emissions. J. ICCT working paper 11, 6.
- Elbing, B.R., Mäkiharju, S., Wiggins, A., Perlin, M., Dowling, D.R., Ceccio, S.L., 2013. On the scaling of air layer drag reduction. Journal of fluid mechanics 717, 484–513.
- Elbing, B.R., Winkel, E.S., Lay, K.A., Ceccio, S.L., Dowling, D.R., Perlin, M., 2008. Bubble-induced skin-friction drag reduction and the abrupt transition to air-layer drag reduction. Journal of Fluid Mechanics 612, 201–236.
- Foeth, E., Eggers, R., van der Hout, I., Quadvlieg, F., 2009. Reduction of frictional resistance by air bubble lubrication, in: SNAME Maritime Convention, OnePetro.
- Fotopoulos, A.G., Margaris, D.P., 2020. Computational analysis of air lubrication system for commercial shipping and impacts on fuel consumption. Computation 8, 38.
- Fujiwara, T., 2006. A new estimation method of wind forces and moments acting on ships on the basis of physical components models. Journal of the Japan society of naval architects and ocean engineers 2, 243–255.
- Gallardo Martínez, A., et al., 2016. Investigation of the air-lubrication effect on friction resistance .
- Gebraad, J., Quispel, M., Karaarslan, S., Lehne, M., Rafael, R., Eppich, M., Janssens, G., Smidt, H., Barcanescu, M., 2021. Structuring towards zero emission waterborne transport, d2.1. state-of-play of decarbonisation of waterborne transport “technology application atlas. URL: <https://www.waterborne.eu/projects/coordination-projects/steerer/results>.
- Gerritsma, J., Beukelman, W., 1972. Analysis of the resistance increase in waves of a fast cargo ship. International shipbuilding progress 19, 285–293.
- Guldhammer, H., Harvald, S.A., 1974. Ship resistance-effect of form and principal dimensions.(revised). Danish Technical Press, Denmark, Danmarks Tekniske Højskole, kademisk Forlag, St. kannikestrade 8, DK 1169 Copenhagen .
- Gupta, P., Steen, S., Rasheed, A., 2019. Big data analytics as a tool to monitor hydrodynamic performance of a ship, in: International Conference on Offshore Mechanics and Arctic Engineering, American Society of Mechanical Engineers. p. V07AT06A059.
- Helmre, P., 2008. Update on oortmerssen’s resistance prediction, in: Pacific 2008 International Maritime Conference.
- Hinostraza, M., Xu, H., Soares, C.G., 2019. Manoeuvring test for a self-running ship model in various water depth conditions, in: Sustainable Development and Innovations in Marine Technologies. CRC Press, pp. 187–196.
- Hoang, C., Toda, Y., Sanada, Y., 2009. Full scale experiment for frictional resistance reduction using air lubrication method, in: The Nineteenth International Offshore and Polar Engineering Conference, OnePetro.
- Hollenbach, K.U., 1998. Estimating resistance and propulsion for single-screw and twin-screw ships-ship technology research 45 (1998). Schiffstechnik 45, 72.
- Holtrop, J., Mennen, G., 1982. An approximate power prediction method. International Shipbuilding Progress 29, 166–170.
- Homma, T., Saltelli, A., 1996. Importance measures in global sensitivity analysis of nonlinear models. Reliability Engineering & System Safety 52, 1–17.
- IMO, 2018. Strategy on reduction of ghg emissions from ships. MEPC 304, 72.
- IMO, 2020. Fourth imo ghg study: Reduction of ghg emissions from ships. MEPC 75/7/15 .
- IMO, 2021. Guidelines on the method of calculation of the attained energy efficiency existing ship index (ceci). MEPC 76/15/Add.2/Annex 7 .
- ISO, E., 2015. 9001: 2015. Sistema de Gestão da Qualidade .
- ITTC, 1978. Report of performance committee. Proceedings 15th ITTC , 389–392.
- Jang, J., Choi, S.H., Ahn, S.M., Kim, B., Seo, J.S., 2014. Experimental investigation of frictional resistance reduction with air layer on the hull bottom of a ship. International Journal of Naval Architecture and Ocean Engineering 6, 363–379.

- Kawabuchi, M., Kawakita, C., Mizokami, S., Higasa, S., Kodan, Y., Takano, S., 2011. Cfd predictions of bubbly flow around an energy-saving ship with mitsubishi air lubrication system. *Mitsubishi Heavy Industries Technical Review* 48, 53–57.
- Kawakita, C., Takano, S., Kodan, Y., Mizokami, S., 2011. Experimental investigation of the behavior of injected air on the ship bottom and its influence on propeller. *Journal of the Japan Society of Naval Architects and Ocean Engineers* 12, 43–50.
- Kawashima, H., Kodama, Y., Hinatsu, M., Hori, T., Makino, M., Ohnawa, M., Takeshi, H., Sakoda, M., Kawashima, H., Matsuno, F., 2007. A research project on application of air bubble injection to a full scale ship for drag reduction, in: *Fluids Engineering Division Summer Meeting*, pp. 265–274.
- Kim, H.T., Kim, H.T., Kim, H.J., Kim, J.J., 2021. Study on the evaluation of frictional drag reduction by air lubrication and the arrangement of air injection parts for a liquefied natural gas carrier. *Journal of the Society of Naval Architects of Korea* 58, 144–157.
- Kim, T., Yoo, S., Oh, S., Kim, H.J., Lee, D., Kim, B., 2019. Numerical and experimental study on the estimation of added resistance of an lng carrier in waves. *International Journal of Offshore and Polar Engineering* 29, 24–32.
- Kim, Y., Steen, S., Muri, H., 2022a. A novel method for estimating missing values in ship principal data. *Ocean Engineering* 251, 110979.
- Kim, Y.R., Esmailian, E., Steen, S., 2022b. A meta-model for added resistance in waves. *Ocean Engineering* 266, 112749.
- Kodama, Y., Takahashi, T., Makino, M., Hori, T., Ueda, T., Kawamura, N., Shibata, M., Kato, H., Inoue, T., Suzuki, T., et al., 2005. Practical application of microbubbles to ships—large scale model experiments and a new full scale experiment, in: *Proceedings of the 6th International Symposium on Smart Control of Turbulence*.
- Kodama, Y.e., Hinatsu, M., Hori, T., Kawashima, H., Takeshi, H., Makino, M., Ohnawa, M., Sanada, Y., Murai, Y., Ohta, S., 2008. A full-scale air lubrication experiment using a large cement carrier for energy saving (result and analysis), in: *Proc. Japan Soc. Naval Architects and Ocean Engineers Conference*, pp. 163–166.
- Kracht, A., 1984. Einfluss des Bugwulstes auf den Leistungsbedarf eines Schiffes im Seegang. *Forschungszentrum des Dt. Schiffbaus*.
- Kramel, D., Muri, H., Kim, Y., Lonka, R., Nielsen, J.B., Ringvold, A.L., Bouman, E.A., Steen, S., Strømman, A.H., 2021. Global shipping emissions from a well-to-wake perspective: the maritane model. *Environmental science & technology* 55, 15040–15050.
- Kristensen, H.O., Lützen, M., 2012. Prediction of resistance and propulsion power of ships. *Clean Shipping Currents* 1, 1–52.
- Kumagai, I., Takahashi, Y., Murai, Y., 2015. Power-saving device for air bubble generation using a hydrofoil to reduce ship drag: Theory, experiments, and application to ships. *Ocean Engineering* 95, 183–194.
- Larsson, L., Stern, F., Visonneau, M., 2013. Cfd in ship hydrodynamics—results of the gothenburg 2010 workshop, in: *MARINE 2011, IV International Conference on Computational Methods in Marine Engineering*, Springer, pp. 237–259.
- Latorre, R., Miller, A., Philips, R., 2002. Microbubble resistance reduction for high-speed craft. *SNAME Transactions* 110, 259–277.
- Lay, K.A., Yakushiji, R., Makiharju, S., Perlin, M., Ceccio, S.L., 2010. Partial cavity drag reduction at high reynolds numbers. *Journal of Ship Research* 54, 109–119.
- Lee, C.M., Yu, J.W., Choi, J.E., Lee, I., 2019. Effect of bow hull forms on the resistance performance in calm water and waves for 66k dwt bulk carrier. *International Journal of Naval Architecture and Ocean Engineering* 11, 723–735.
- Lee, J., Kim, J., Jang, J., McStay, P., Raptakis, G., Fitzpatrick, P., 2017. Full scale applications of air lubrication for reduction of ship frictional resistance, in: *SNAME Maritime Convention, OnePetro*.
- Liu, W., Suzuki, K., Shibanuma, K., 2015. Nonlinear dynamic response and structural evaluation of container ship in large freak waves. *Journal of Offshore Mechanics and Arctic Engineering* 137.
- Mäkiharju, S., Ceccio, S.L., 2011. Air lubrication drag reduction on great lakes ships. *University of Michigan*.
- Makiharju, S., Elbing, B., Wiggins, A., Dowling, D., Perlin, M., Ceccio, S., 2010. Perturbed partial cavity drag reduction at high reynolds numbers, in: *Proc. 28th Symp. on Naval Hydrodynamics*.
- Mäkiharju, S.A., Perlin, M., Ceccio, S.L., 2012. On the energy economics of air lubrication drag reduction. *International Journal of Naval Architecture and Ocean Engineering* 4, 412–422.
- Mizokami, S., Kawakado, M., Kawano, M., Hasegawa, T., Hirakawa, I., 2013. Implementation of ship energy-saving operations with mitsubishi air lubrication system. *Mitsubishi Heavy Industries Technical Review* 50, 44–49.
- Mizokami, S., Kawakita, C., Kodan, Y., Takano, S., Higasa, S., Shigenaga, R., 2010. Experimental study of air lubrication method and verification of effects on actual hull by means of sea trial. *Mitsubishi Heavy Industries Technical Review* 47, 41–47.
- Mizokami, S., Kuroiwa, R., 2019. Installation of air lubrication system for ro-pax ferry and verification of its effect in actual seas based on onboard measurement data. *Japan Society of Naval Architects and Ocean Engineers* 29, 1–9.
- Moctar, O.e., Shigunov, V., Zorn, T., 2012. Duisburg test case: Post-panamax container ship for benchmarking. *Ship Technology Research* 59, 50–64.
- Nag, P., 2013. *Engineering thermodynamics*. Tata McGraw-Hill Education.
- Nagamatsu, T., Kodama, Y., Kakugawa, A., Takai, M., Murakami, K., Ishikawa, S., Kamiirisa, H., Ogiwara, S., Yoshida, Y., Suzuki, T., et al., 2002. A full-scale experiment on microbubbles for skin friction reduction using "seiuin maru" part 2: The full-scale experiment. *Journal of the Society of Naval Architects of Japan* 2002, 15–28.
- Olmer, N., Comer, B., Roy, B., Mao, X., Rutherford, D., 2017. Greenhouse gas emissions from global shipping, 2013–2015 detailed methodology. *International Council on Clean Transportation: Washington, DC, USA*, 1–38.
- Oortmerssen, G.v., 1971. A power prediction method and its application to small ships. *ISP* 18.
- Oosterveld, M.W.C., van Oossanen, P., 1975. Further computer-analyzed data of the wageningen b-screw series. *International shipbuilding progress* 22, 251–262.
- Park, D.M., Lee, J.H., Jung, Y.W., Lee, J., Kim, Y., Gerhardt, F., 2019a. Experimental and numerical studies on added resistance of ship in oblique sea conditions. *Ocean Engineering* 186, 106070.
- Park, D.M., Lee, J.H., Lee, J., Kim, B.S., Kim, B.S., Yang, K.K., Kim, Y., Lee, Y.G., Kim, T., Yang, J.H., et al., 2019b. Comparative study on added resistance of a container ship in waves, in: *The 29th International Ocean and Polar Engineering Conference, OnePetro*.



## Potential energy savings of air lubrication technology on merchant ships

- Park, S.H., Lee, I., 2018. Optimization of drag reduction effect of air lubrication for a tanker model. *International Journal of Naval Architecture and Ocean Engineering* 10, 427–438.
- Pavlov, G.A., Yun, L., Bliault, A., He, S.L., 2020. *Air lubricated and air cavity ships*. Springer.
- Pinkster, J.A., 1980. Low frequency second order wave exciting forces on floating structures.
- Reguram, B.R., Surendran, S., Lee, S.K., 2016. Application of fin system to reduce pitch motion. *International Journal of Naval Architecture and Ocean Engineering* 8, 409–421.
- Saltelli, A., Annoni, P., 2010. How to avoid a perfunctory sensitivity analysis. *Environmental Modelling & Software* 25, 1508–1517.
- Silberschmidt, N., Tasker, D., Pappas, T., Johannesson, J., 2016. Silverstream system-air lubrication performance verification and design development, in: *Conference of Shipping in Changing Climate*, Newcastle, UK, pp. 10–11.
- Silverstream, 2022. Silverstream® system performance. URL: <https://www.silverstream-tech.com/what-is-air-lubrication/>.
- Simonsen, C.D., Otzen, J.F., Joncquez, S., Stern, F., 2013. Efd and cfd for kcs heaving and pitching in regular head waves. *Journal of Marine Science and Technology* 18, 435–459.
- Sindagi, S., Vijayakumar, R., Saxena, B.K., 2022. Experimental investigation on ship's model in carrying out energy economics of bdr/als methodology. *Ships and Offshore Structures* 17, 1437–1446.
- Slyozkin, A., Atlar, M., Sampson, R., Seo, K.C., 2014. An experimental investigation into the hydrodynamic drag reduction of a flat plate using air-fed cavities. *Ocean engineering* 76, 105–120.
- Surendran, S., Lee, S., Reddy, J.V.R., Lee, G., 2005. Non-linear roll dynamics of a ro-ro ship in waves. *Ocean Engineering* 32, 1818–1828.
- Thill, C., Toxopeus, S., van Walree, F., 2005. Project energy-saving air-lubricated ships (pels), in: *Proceedings of the 2nd International Symposium on Seawater Drag Reduction*, pp. 1–16.
- Tsujimoto, M., Kuroda, M., Shibata, K., Sogihara, N., Takagi, K., 2009. On a calculation of decrease of ship speed in actual seas. *Journal of the Japan Society of Naval Architects and Ocean Engineers* 9, 79–85.
- Van, S., 1997. Measurement of flows around a 3600teu container ship model, in: *Annual Autumn Meeting, SNAK*, Seoul, Korea, 1997.
- Verschoof, R.A., Van Der Veen, R.C., Sun, C., Lohse, D., 2016. Bubble drag reduction requires large bubbles. *Physical review letters* 117, 104502.
- Wu, H., Ou, Y.p., 2019. Experimental study of air layer drag reduction with bottom cavity for a bulk carrier ship model. *China Ocean Engineering* 33, 554–562.
- Zhang, X., Bao, Z., Ge, Y.E., 2021. Investigating the determinants of shipowners' emission abatement solutions for newbuilding vessels. *Transportation Research Part D: Transport and Environment* 99, 102989.

## Appendix A

**Table A.1**

Relevant studies on the energy saving of air lubrication systems used in Fig. 1.

Type of ALS	Method	References
BDR	Model test	Kodama et al. (2005); Lee et al. (2017)
	Sea-trial	Latorre et al. (2002); Nagamatsu et al. (2002); Hoang et al. (2009); Kumagai et al. (2015); Silberschmidt et al. (2016); Lee et al. (2017); Mizokami and Kuroiwa (2019); Pavlov et al. (2020); Silverstream (2022)
ALDR	CFD	Pavlov et al. (2020)
	Model test	Jang et al. (2014); Lee et al. (2017); Sindagi et al. (2022)
	Sea-trial	Kodama et al. (2008); Hoang et al. (2009); Mizokami et al. (2010); Lee et al. (2017); Pavlov et al. (2020)
PCDR	CFD	Fotopoulos and Margaritis (2020)
	Model test	Butterworth et al. (2015); Borusevich et al. (2016); Borusevich et al. (2017); Pavlov et al. (2020)
	Sea-trial	Aronietis et al. (2011); Borusevich et al. (2016); Pavlov et al. (2020)

**Table A.2**  
Dimension of ships used for the regression equations in Eq. (9)

Ship type	$L_{pp}$ [m]	B [m]	$T_d$ [m]	$C_b$ [-]	References
Tanker	161-323	28-60	9-21	0.72-0.85	Pinkster (1980);Bunnik (1999);Larsson et al. (2013); Park et al. (2019a);Hinostroza et al. (2019);Kim et al. (2019)
General cargo	60-194	15-32	3.2-12.6	0.56-0.80	Gupta et al. (2019);Gerritsma and Beukelman (1972); Kracht (1984);Alamsyah et al. (2018)
Bulk carrier	192	36	11.2	0.85	Lee et al. (2019)
Container	119-355	19-51	6-14.5	0.58-0.76	Moctar et al. (2012);Van (1997);Simonsen et al. (2013); Park et al. (2019b);Reguram et al. (2016);Liu et al. (2015)
Ro-Ro/Ferry	158-178	21-32	6.1-8.2	0.54-0.56	Tsujimoto et al. (2009); Surendran et al. (2005)
Total	60-355	15-60	3.2-21	0.55-0.85	



Previous PhD theses published at the Department  
of Marine Technology

Norwegian University of Science and Technology



**Previous PhD theses published at the Department of Marine Technology  
(earlier: Faculty of Marine Technology)  
NORWEGIAN UNIVERSITY OF SCIENCE AND TECHNOLOGY**

<b>Report No.</b>	<b>Author</b>	<b>Title</b>
	Kavlie, Dag	Optimization of Plane Elastic Grillages, 1967
	Hansen, Hans R.	Man-Machine Communication and Data-Storage Methods in Ship Structural Design, 1971
	Gisvold, Kaare M.	A Method for non-linear mixed -integer programming and its Application to Design Problems, 1971
	Lund, Sverre	Tanker Frame Optimalization by means of SUMT-Transformation and Behaviour Models, 1971
	Vinje, Tor	On Vibration of Spherical Shells Interacting with Fluid, 1972
	Lorentz, Jan D.	Tank Arrangement for Crude Oil Carriers in Accordance with the new Anti-Pollution Regulations, 1975
	Carlsen, Carl A.	Computer-Aided Design of Tanker Structures, 1975
	Larsen, Carl M.	Static and Dynamic Analysis of Offshore Pipelines during Installation, 1976
UR-79-01	Brigt Hatlestad, MK	The finite element method used in a fatigue evaluation of fixed offshore platforms. (Dr.Ing. Thesis)
UR-79-02	Erik Pettersen, MK	Analysis and design of cellular structures. (Dr.Ing. Thesis)
UR-79-03	Sverre Valsgård, MK	Finite difference and finite element methods applied to nonlinear analysis of plated structures. (Dr.Ing. Thesis)
UR-79-04	Nils T. Nordsve, MK	Finite element collapse analysis of structural members considering imperfections and stresses due to fabrication. (Dr.Ing. Thesis)
UR-79-05	Ivar J. Fylling, MK	Analysis of towline forces in ocean towing systems. (Dr.Ing. Thesis)
UR-79- x	Finn Gunnar Nielsen, MH	Hydrodynamic problems related to oil barriers for offshore application
UR-80-06	Nils Sandsmark, MM	Analysis of Stationary and Transient Heat Conduction by the Use of the Finite Element Method. (Dr.Ing. Thesis)
UR-80-09	Sverre Haver, MK	Analysis of uncertainties related to the stochastic modeling of ocean waves. (Dr.Ing. Thesis)

UR-81-15	Odland, Jonas	On the Strength of welded Ring stiffened cylindrical Shells primarily subjected to axial Compression
UR-82-17	Engesvik, Knut	Analysis of Uncertainties in the fatigue Capacity of Welded Joints
UR-82-18	Rye, Henrik	Ocean wave groups
UR-83-30	Eide, Oddvar Inge	On Cumulative Fatigue Damage in Steel Welded Joints
UR-83-33	Mo, Olav	Stochastic Time Domain Analysis of Slender Offshore Structures
UR-83-34	Amdahl, Jørgen	Energy absorption in Ship-platform impacts
UR-84-37	Mørch, Morten	Motions and mooring forces of semi submersibles as determined by full-scale measurements and theoretical analysis
UR-84-38	Soares, C. Guedes	Probabilistic models for load effects in ship structures
UR-84-39	Aarsnes, Jan V.	Current forces on ships
UR-84-40	Czujko, Jerzy	Collapse Analysis of Plates subjected to Biaxial Compression and Lateral Load
UR-85-46	Alf G. Engseth, MK	Finite element collapse analysis of tubular steel offshore structures. (Dr.Ing. Thesis)
UR-86-47	Dengody Sheshappa, MP	A Computer Design Model for Optimizing Fishing Vessel Designs Based on Techno-Economic Analysis. (Dr.Ing. Thesis)
UR-86-48	Vidar Aanesland, MH	A Theoretical and Numerical Study of Ship Wave Resistance. (Dr.Ing. Thesis)
UR-86-49	Heinz-Joachim Wessel, MK	Fracture Mechanics Analysis of Crack Growth in Plate Girders. (Dr.Ing. Thesis)
UR-86-50	Jon Taby, MK	Ultimate and Post-ultimate Strength of Dented Tubular Members. (Dr.Ing. Thesis)
UR-86-51	Walter Lian, MH	A Numerical Study of Two-Dimensional Separated Flow Past Bluff Bodies at Moderate KC-Numbers. (Dr.Ing. Thesis)
UR-86-52	Bjørn Sortland, MH	Force Measurements in Oscillating Flow on Ship Sections and Circular Cylinders in a U-Tube Water Tank. (Dr.Ing. Thesis)
UR-86-53	Kurt Strand, MM	A System Dynamic Approach to One-dimensional Fluid Flow. (Dr.Ing. Thesis)
UR-86-54	Arne Edvin Løken, MH	Three Dimensional Second Order Hydrodynamic Effects on Ocean Structures in Waves. (Dr.Ing. Thesis)
UR-86-55	Sigurd Falch, MH	A Numerical Study of Slamming of Two-

Dimensional Bodies. (Dr.Ing. Thesis)

UR-87-56	Arne Braathen, MH	Application of a Vortex Tracking Method to the Prediction of Roll Damping of a Two-Dimension Floating Body. (Dr.Ing. Thesis)
UR-87-57	Bernt Leira, MK	Gaussian Vector Processes for Reliability Analysis involving Wave-Induced Load Effects. (Dr.Ing. Thesis)
UR-87-58	Magnus Småvik, MM	Thermal Load and Process Characteristics in a Two-Stroke Diesel Engine with Thermal Barriers (in Norwegian). (Dr.Ing. Thesis)
MTA-88-59	Bernt Arild Bremdal, MP	An Investigation of Marine Installation Processes – A Knowledge - Based Planning Approach. (Dr.Ing. Thesis)
MTA-88-60	Xu Jun, MK	Non-linear Dynamic Analysis of Space-framed Offshore Structures. (Dr.Ing. Thesis)
MTA-89-61	Gang Miao, MH	Hydrodynamic Forces and Dynamic Responses of Circular Cylinders in Wave Zones. (Dr.Ing. Thesis)
MTA-89-62	Martin Greenhow, MH	Linear and Non-Linear Studies of Waves and Floating Bodies. Part I and Part II. (Dr.Techn. Thesis)
MTA-89-63	Chang Li, MH	Force Coefficients of Spheres and Cubes in Oscillatory Flow with and without Current. (Dr.Ing. Thesis)
MTA-89-64	Hu Ying, MP	A Study of Marketing and Design in Development of Marine Transport Systems. (Dr.Ing. Thesis)
MTA-89-65	Arild Jæger, MH	Seakeeping, Dynamic Stability and Performance of a Wedge Shaped Planing Hull. (Dr.Ing. Thesis)
MTA-89-66	Chan Siu Hung, MM	The dynamic characteristics of tilting-pad bearings
MTA-89-67	Kim Wikstrøm, MP	Analysis av projekteringen for ett offshore projekt. (Licenciat-avhandling)
MTA-89-68	Jiao Guoyang, MK	Reliability Analysis of Crack Growth under Random Loading, considering Model Updating. (Dr.Ing. Thesis)
MTA-89-69	Arnt Olufsen, MK	Uncertainty and Reliability Analysis of Fixed Offshore Structures. (Dr.Ing. Thesis)
MTA-89-70	Wu Yu-Lin, MR	System Reliability Analyses of Offshore Structures using improved Truss and Beam Models. (Dr.Ing. Thesis)
MTA-90-71	Jan Roger Hoff, MH	Three-dimensional Green function of a vessel with forward speed in waves. (Dr.Ing. Thesis)
MTA-90-72	Rong Zhao, MH	Slow-Drift Motions of a Moored Two-Dimensional Body in Irregular Waves. (Dr.Ing. Thesis)
MTA-90-73	Atle Minsaas, MP	Economical Risk Analysis. (Dr.Ing. Thesis)



MTA-90-74	Knut-Aril Farnes, MK	Long-term Statistics of Response in Non-linear Marine Structures. (Dr.Ing. Thesis)
MTA-90-75	Torbjørn Sotberg, MK	Application of Reliability Methods for Safety Assessment of Submarine Pipelines. (Dr.Ing. Thesis)
MTA-90-76	Zeuthen, Steffen, MP	SEAMAID. A computational model of the design process in a constraint-based logic programming environment. An example from the offshore domain. (Dr.Ing. Thesis)
MTA-91-77	Haagensen, Sven, MM	Fuel Dependant Cyclic Variability in a Spark Ignition Engine - An Optical Approach. (Dr.Ing. Thesis)
MTA-91-78	Løland, Geir, MH	Current forces on and flow through fish farms. (Dr.Ing. Thesis)
MTA-91-79	Hoen, Christopher, MK	System Identification of Structures Excited by Stochastic Load Processes. (Dr.Ing. Thesis)
MTA-91-80	Haugen, Stein, MK	Probabilistic Evaluation of Frequency of Collision between Ships and Offshore Platforms. (Dr.Ing. Thesis)
MTA-91-81	Sødahl, Nils, MK	Methods for Design and Analysis of Flexible Risers. (Dr.Ing. Thesis)
MTA-91-82	Ornberg, Harald, MK	Non-linear Response Analysis of Floating Fish Farm Systems. (Dr.Ing. Thesis)
MTA-91-83	Marley, Mark J., MK	Time Variant Reliability under Fatigue Degradation. (Dr.Ing. Thesis)
MTA-91-84	Krokstad, Jørgen R., MH	Second-order Loads in Multidirectional Seas. (Dr.Ing. Thesis)
MTA-91-85	Molteberg, Gunnar A., MM	The Application of System Identification Techniques to Performance Monitoring of Four Stroke Turbocharged Diesel Engines. (Dr.Ing. Thesis)
MTA-92-86	Mørch, Hans Jørgen Bjelke, MH	Aspects of Hydrofoil Design: with Emphasis on Hydrofoil Interaction in Calm Water. (Dr.Ing. Thesis)
MTA-92-87	Chan Siu Hung, MM	Nonlinear Analysis of Rotordynamic Instabilities in Highspeed Turbomachinery. (Dr.Ing. Thesis)
MTA-92-88	Bessason, Bjarni, MK	Assessment of Earthquake Loading and Response of Seismically Isolated Bridges. (Dr.Ing. Thesis)
MTA-92-89	Langli, Geir, MP	Improving Operational Safety through exploitation of Design Knowledge - an investigation of offshore platform safety. (Dr.Ing. Thesis)
MTA-92-90	Sævik, Svein, MK	On Stresses and Fatigue in Flexible Pipes. (Dr.Ing. Thesis)
MTA-92-91	Ask, Tor Ø., MM	Ignition and Flame Growth in Lean Gas-Air Mixtures. An Experimental Study with a Schlieren

		System. (Dr.Ing. Thesis)
MTA-86-92	Hessen, Gunnar, MK	Fracture Mechanics Analysis of Stiffened Tubular Members. (Dr.Ing. Thesis)
MTA-93-93	Steinebach, Christian, MM	Knowledge Based Systems for Diagnosis of Rotating Machinery. (Dr.Ing. Thesis)
MTA-93-94	Dalane, Jan Inge, MK	System Reliability in Design and Maintenance of Fixed Offshore Structures. (Dr.Ing. Thesis)
MTA-93-95	Steen, Sverre, MH	Cobblestone Effect on SES. (Dr.Ing. Thesis)
MTA-93-96	Karunakaran, Daniel, MK	Nonlinear Dynamic Response and Reliability Analysis of Drag-dominated Offshore Platforms. (Dr.Ing. Thesis)
MTA-93-97	Hagen, Arnulf, MP	The Framework of a Design Process Language. (Dr.Ing. Thesis)
MTA-93-98	Nordrik, Rune, MM	Investigation of Spark Ignition and Autoignition in Methane and Air Using Computational Fluid Dynamics and Chemical Reaction Kinetics. A Numerical Study of Ignition Processes in Internal Combustion Engines. (Dr.Ing. Thesis)
MTA-94-99	Passano, Elizabeth, MK	Efficient Analysis of Nonlinear Slender Marine Structures. (Dr.Ing. Thesis)
MTA-94-100	Kvålsvold, Jan, MH	Hydroelastic Modelling of Wetdeck Slamming on Multihull Vessels. (Dr.Ing. Thesis)
MTA-94-102	Bech, Sidsel M., MK	Experimental and Numerical Determination of Stiffness and Strength of GRP/PVC Sandwich Structures. (Dr.Ing. Thesis)
MTA-95-103	Paulsen, Hallvard, MM	A Study of Transient Jet and Spray using a Schlieren Method and Digital Image Processing. (Dr.Ing. Thesis)
MTA-95-104	Hovde, Geir Olav, MK	Fatigue and Overload Reliability of Offshore Structural Systems, Considering the Effect of Inspection and Repair. (Dr.Ing. Thesis)
MTA-95-105	Wang, Xiaozhi, MK	Reliability Analysis of Production Ships with Emphasis on Load Combination and Ultimate Strength. (Dr.Ing. Thesis)
MTA-95-106	Ulstein, Tore, MH	Nonlinear Effects of a Flexible Stern Seal Bag on Cobblestone Oscillations of an SES. (Dr.Ing. Thesis)
MTA-95-107	Solaas, Frøydis, MH	Analytical and Numerical Studies of Sloshing in Tanks. (Dr.Ing. Thesis)
MTA-95-108	Hellan, Øyvind, MK	Nonlinear Pushover and Cyclic Analyses in Ultimate Limit State Design and Reassessment of Tubular Steel Offshore Structures. (Dr.Ing. Thesis)
MTA-95-109	Hermundstad, Ole A., MK	Theoretical and Experimental Hydroelastic Analysis of High Speed Vessels. (Dr.Ing. Thesis)

MTA-96-110	Bratland, Anne K., MH	Wave-Current Interaction Effects on Large-Volume Bodies in Water of Finite Depth. (Dr.Ing. Thesis)
MTA-96-111	Herfjord, Kjell, MH	A Study of Two-dimensional Separated Flow by a Combination of the Finite Element Method and Navier-Stokes Equations. (Dr.Ing. Thesis)
MTA-96-112	Æsøy, Vilmar, MM	Hot Surface Assisted Compression Ignition in a Direct Injection Natural Gas Engine. (Dr.Ing. Thesis)
MTA-96-113	Eknes, Monika L., MK	Escalation Scenarios Initiated by Gas Explosions on Offshore Installations. (Dr.Ing. Thesis)
MTA-96-114	Erikstad, Stein O., MP	A Decision Support Model for Preliminary Ship Design. (Dr.Ing. Thesis)
MTA-96-115	Pedersen, Egil, MH	A Nautical Study of Towed Marine Seismic Streamer Cable Configurations. (Dr.Ing. Thesis)
MTA-97-116	Moksnes, Paul O., MM	Modelling Two-Phase Thermo-Fluid Systems Using Bond Graphs. (Dr.Ing. Thesis)
MTA-97-117	Halse, Karl H., MK	On Vortex Shedding and Prediction of Vortex-Induced Vibrations of Circular Cylinders. (Dr.Ing. Thesis)
MTA-97-118	Igland, Ragnar T., MK	Reliability Analysis of Pipelines during Laying, considering Ultimate Strength under Combined Loads. (Dr.Ing. Thesis)
MTA-97-119	Pedersen, Hans-P., MP	Levendefiskteknologi for fiskefartøy. (Dr.Ing. Thesis)
MTA-98-120	Vikestad, Kyrre, MK	Multi-Frequency Response of a Cylinder Subjected to Vortex Shedding and Support Motions. (Dr.Ing. Thesis)
MTA-98-121	Azadi, Mohammad R. E., MK	Analysis of Static and Dynamic Pile-Soil-Jacket Behaviour. (Dr.Ing. Thesis)
MTA-98-122	Ulltang, Terje, MP	A Communication Model for Product Information. (Dr.Ing. Thesis)
MTA-98-123	Torbergsen, Erik, MM	Impeller/Diffuser Interaction Forces in Centrifugal Pumps. (Dr.Ing. Thesis)
MTA-98-124	Hansen, Edmond, MH	A Discrete Element Model to Study Marginal Ice Zone Dynamics and the Behaviour of Vessels Moored in Broken Ice. (Dr.Ing. Thesis)
MTA-98-125	Videiro, Paulo M., MK	Reliability Based Design of Marine Structures. (Dr.Ing. Thesis)
MTA-99-126	Mainçon, Philippe, MK	Fatigue Reliability of Long Welds Application to Titanium Risers. (Dr.Ing. Thesis)
MTA-99-127	Haugen, Elin M., MH	Hydroelastic Analysis of Slamming on Stiffened Plates with Application to Catamaran Wetdecks. (Dr.Ing. Thesis)
MTA-99-	Langhelle, Nina K., MK	Experimental Validation and Calibration of

128		Nonlinear Finite Element Models for Use in Design of Aluminium Structures Exposed to Fire. (Dr.Ing. Thesis)
MTA-99-129	Berstad, Are J., MK	Calculation of Fatigue Damage in Ship Structures. (Dr.Ing. Thesis)
MTA-99-130	Andersen, Trond M., MM	Short Term Maintenance Planning. (Dr.Ing. Thesis)
MTA-99-131	Tveiten, Bård Wathne, MK	Fatigue Assessment of Welded Aluminium Ship Details. (Dr.Ing. Thesis)
MTA-99-132	Søreide, Fredrik, MP	Applications of underwater technology in deep water archaeology. Principles and practice. (Dr.Ing. Thesis)
MTA-99-133	Tønnessen, Rune, MH	A Finite Element Method Applied to Unsteady Viscous Flow Around 2D Blunt Bodies With Sharp Corners. (Dr.Ing. Thesis)
MTA-99-134	Elvekrok, Dag R., MP	Engineering Integration in Field Development Projects in the Norwegian Oil and Gas Industry. The Supplier Management of Norne. (Dr.Ing. Thesis)
MTA-99-135	Fagerholt, Kjetil, MP	Optimeringsbaserte Metoder for Ruteplanlegging innen skipsfart. (Dr.Ing. Thesis)
MTA-99-136	Bysveen, Marie, MM	Visualization in Two Directions on a Dynamic Combustion Rig for Studies of Fuel Quality. (Dr.Ing. Thesis)
MTA-2000-137	Storteig, Eskild, MM	Dynamic characteristics and leakage performance of liquid annular seals in centrifugal pumps. (Dr.Ing. Thesis)
MTA-2000-138	Sagli, Gro, MK	Model uncertainty and simplified estimates of long term extremes of hull girder loads in ships. (Dr.Ing. Thesis)
MTA-2000-139	Tronstad, Harald, MK	Nonlinear analysis and design of cable net structures like fishing gear based on the finite element method. (Dr.Ing. Thesis)
MTA-2000-140	Kroneberg, André, MP	Innovation in shipping by using scenarios. (Dr.Ing. Thesis)
MTA-2000-141	Haslum, Herbjørn Alf, MH	Simplified methods applied to nonlinear motion of spar platforms. (Dr.Ing. Thesis)
MTA-2001-142	Samdal, Ole Johan, MM	Modelling of Degradation Mechanisms and Stressor Interaction on Static Mechanical Equipment Residual Lifetime. (Dr.Ing. Thesis)
MTA-2001-143	Baarholm, Rolf Jarle, MH	Theoretical and experimental studies of wave impact underneath decks of offshore platforms. (Dr.Ing. Thesis)
MTA-2001-144	Wang, Lihua, MK	Probabilistic Analysis of Nonlinear Wave-induced Loads on Ships. (Dr.Ing. Thesis)
MTA-2001-145	Kristensen, Odd H. Holt, MK	Ultimate Capacity of Aluminium Plates under Multiple Loads, Considering HAZ Properties.

(Dr.Ing. Thesis)

MTA-2001-146	Greco, Marilena, MH	A Two-Dimensional Study of Green-Water Loading. (Dr.Ing. Thesis)
MTA-2001-147	Heggelund, Svein E., MK	Calculation of Global Design Loads and Load Effects in Large High Speed Catamarans. (Dr.Ing. Thesis)
MTA-2001-148	Babalola, Olusegun T., MK	Fatigue Strength of Titanium Risers – Defect Sensitivity. (Dr.Ing. Thesis)
MTA-2001-149	Mohammed, Abuu K., MK	Nonlinear Shell Finite Elements for Ultimate Strength and Collapse Analysis of Ship Structures. (Dr.Ing. Thesis)
MTA-2002-150	Holmedal, Lars E., MH	Wave-current interactions in the vicinity of the sea bed. (Dr.Ing. Thesis)
MTA-2002-151	Rognebakke, Olav F., MH	Sloshing in rectangular tanks and interaction with ship motions. (Dr.Ing. Thesis)
MTA-2002-152	Lader, Pål Furset, MH	Geometry and Kinematics of Breaking Waves. (Dr.Ing. Thesis)
MTA-2002-153	Yang, Qinzhen, MH	Wash and wave resistance of ships in finite water depth. (Dr.Ing. Thesis)
MTA-2002-154	Melhus, Øyvind, MM	Utilization of VOC in Diesel Engines. Ignition and combustion of VOC released by crude oil tankers. (Dr.Ing. Thesis)
MTA-2002-155	Ronæss, Marit, MH	Wave Induced Motions of Two Ships Advancing on Parallel Course. (Dr.Ing. Thesis)
MTA-2002-156	Økland, Ole D., MK	Numerical and experimental investigation of whipping in twin hull vessels exposed to severe wet deck slamming. (Dr.Ing. Thesis)
MTA-2002-157	Ge, Chunhua, MK	Global Hydroelastic Response of Catamarans due to Wet Deck Slamming. (Dr.Ing. Thesis)
MTA-2002-158	Byklum, Eirik, MK	Nonlinear Shell Finite Elements for Ultimate Strength and Collapse Analysis of Ship Structures. (Dr.Ing. Thesis)
IMT-2003-1	Chen, Haibo, MK	Probabilistic Evaluation of FPSO-Tanker Collision in Tandem Offloading Operation. (Dr.Ing. Thesis)
IMT-2003-2	Skaugset, Kjetil Bjørn, MK	On the Suppression of Vortex Induced Vibrations of Circular Cylinders by Radial Water Jets. (Dr.Ing. Thesis)
IMT-2003-3	Chezian, Muthu	Three-Dimensional Analysis of Slamming. (Dr.Ing. Thesis)
IMT-2003-4	Buhaug, Øyvind	Deposit Formation on Cylinder Liner Surfaces in Medium Speed Engines. (Dr.Ing. Thesis)
IMT-2003-5	Tregde, Vidar	Aspects of Ship Design: Optimization of Aft Hull with Inverse Geometry Design. (Dr.Ing. Thesis)

IMT-2003-6	Wist, Hanne Therese	Statistical Properties of Successive Ocean Wave Parameters. (Dr.Ing. Thesis)
IMT-2004-7	Ransau, Samuel	Numerical Methods for Flows with Evolving Interfaces. (Dr.Ing. Thesis)
IMT-2004-8	Soma, Torkel	Blue-Chip or Sub-Standard. A data interrogation approach of identity safety characteristics of shipping organization. (Dr.Ing. Thesis)
IMT-2004-9	Ersdal, Svein	An experimental study of hydrodynamic forces on cylinders and cables in near axial flow. (Dr.Ing. Thesis)
IMT-2005-10	Brodtkorb, Per Andreas	The Probability of Occurrence of Dangerous Wave Situations at Sea. (Dr.Ing. Thesis)
IMT-2005-11	Yttervik, Rune	Ocean current variability in relation to offshore engineering. (Dr.Ing. Thesis)
IMT-2005-12	Fredheim, Arne	Current Forces on Net-Structures. (Dr.Ing. Thesis)
IMT-2005-13	Heggemes, Kjetil	Flow around marine structures. (Dr.Ing. Thesis)
IMT-2005-14	Fouques, Sebastien	Lagrangian Modelling of Ocean Surface Waves and Synthetic Aperture Radar Wave Measurements. (Dr.Ing. Thesis)
IMT-2006-15	Holm, Håvard	Numerical calculation of viscous free surface flow around marine structures. (Dr.Ing. Thesis)
IMT-2006-16	Bjørheim, Lars G.	Failure Assessment of Long Through Thickness Fatigue Cracks in Ship Hulls. (Dr.Ing. Thesis)
IMT-2006-17	Hansson, Lisbeth	Safety Management for Prevention of Occupational Accidents. (Dr.Ing. Thesis)
IMT-2006-18	Zhu, Xinying	Application of the CIP Method to Strongly Nonlinear Wave-Body Interaction Problems. (Dr.Ing. Thesis)
IMT-2006-19	Reite, Karl Johan	Modelling and Control of Trawl Systems. (Dr.Ing. Thesis)
IMT-2006-20	Smogeli, Øyvind Notland	Control of Marine Propellers. From Normal to Extreme Conditions. (Dr.Ing. Thesis)
IMT-2007-21	Storhaug, Gaute	Experimental Investigation of Wave Induced Vibrations and Their Effect on the Fatigue Loading of Ships. (Dr.Ing. Thesis)
IMT-2007-22	Sun, Hui	A Boundary Element Method Applied to Strongly Nonlinear Wave-Body Interaction Problems. (PhD Thesis, CeSOS)
IMT-2007-23	Rustad, Anne Marthine	Modelling and Control of Top Tensioned Risers. (PhD Thesis, CeSOS)
IMT-2007-24	Johansen, Vegar	Modelling flexible slender system for real-time

simulations and control applications

IMT-2007-25	Wroldsen, Anders Sunde	Modelling and control of tensegrity structures. (PhD Thesis, CeSOS)
IMT-2007-26	Aronsen, Kristoffer Høy	An experimental investigation of in-line and combined inline and cross flow vortex induced vibrations. (Dr. avhandling, IMT)
IMT-2007-27	Gao, Zhen	Stochastic Response Analysis of Mooring Systems with Emphasis on Frequency-domain Analysis of Fatigue due to Wide-band Response Processes (PhD Thesis, CeSOS)
IMT-2007-28	Thorstensen, Tom Anders	Lifetime Profit Modelling of Ageing Systems Utilizing Information about Technical Condition. (Dr.ing. thesis, IMT)
IMT-2008-29	Refsnes, Jon Erling Gorset	Nonlinear Model-Based Control of Slender Body AUVs (PhD Thesis, IMT)
IMT-2008-30	Berntsen, Per Ivar B.	Structural Reliability Based Position Mooring. (PhD-Thesis, IMT)
IMT-2008-31	Ye, Naiquan	Fatigue Assessment of Aluminium Welded Box-stiffener Joints in Ships (Dr.ing. thesis, IMT)
IMT-2008-32	Radan, Damir	Integrated Control of Marine Electrical Power Systems. (PhD-Thesis, IMT)
IMT-2008-33	Thomassen, Paul	Methods for Dynamic Response Analysis and Fatigue Life Estimation of Floating Fish Cages. (Dr.ing. thesis, IMT)
IMT-2008-34	Pákozdi, Csaba	A Smoothed Particle Hydrodynamics Study of Two-dimensional Nonlinear Sloshing in Rectangular Tanks. (Dr.ing.thesis, IMT/ CeSOS)
IMT-2007-35	Grytøy, Guttorm	A Higher-Order Boundary Element Method and Applications to Marine Hydrodynamics. (Dr.ing.thesis, IMT)
IMT-2008-36	Drummen, Ingo	Experimental and Numerical Investigation of Nonlinear Wave-Induced Load Effects in Containerships considering Hydroelasticity. (PhD thesis, CeSOS)
IMT-2008-37	Skejic, Renato	Maneuvering and Seakeeping of a Singel Ship and of Two Ships in Interaction. (PhD-Thesis, CeSOS)
IMT-2008-38	Harlem, Alf	An Age-Based Replacement Model for Repairable Systems with Attention to High-Speed Marine Diesel Engines. (PhD-Thesis, IMT)
IMT-2008-39	Alsos, Hagbart S.	Ship Grounding. Analysis of Ductile Fracture, Bottom Damage and Hull Girder Response. (PhD-thesis, IMT)
IMT-2008-40	Graczyk, Mateusz	Experimental Investigation of Sloshing Loading and Load Effects in Membrane LNG Tanks Subjected to Random Excitation. (PhD-thesis, CeSOS)

IMT-2008-41	Taghipour, Reza	Efficient Prediction of Dynamic Response for Flexible and Multi-body Marine Structures. (PhD-thesis, CeSOS)
IMT-2008-42	Ruth, Eivind	Propulsion control and thrust allocation on marine vessels. (PhD thesis, CeSOS)
IMT-2008-43	Nystad, Bent Helge	Technical Condition Indexes and Remaining Useful Life of Aggregated Systems. PhD thesis, IMT
IMT-2008-44	Soni, Prashant Kumar	Hydrodynamic Coefficients for Vortex Induced Vibrations of Flexible Beams, PhD thesis, CeSOS
IMT-2009-45	Amlashi, Hadi K.K.	Ultimate Strength and Reliability-based Design of Ship Hulls with Emphasis on Combined Global and Local Loads. PhD Thesis, IMT
IMT-2009-46	Pedersen, Tom Arne	Bond Graph Modelling of Marine Power Systems. PhD Thesis, IMT
IMT-2009-47	Kristiansen, Trygve	Two-Dimensional Numerical and Experimental Studies of Piston-Mode Resonance. PhD-Thesis, CeSOS
IMT-2009-48	Ong, Muk Chen	Applications of a Standard High Reynolds Number Model and a Stochastic Scour Prediction Model for Marine Structures. PhD-thesis, IMT
IMT-2009-49	Hong, Lin	Simplified Analysis and Design of Ships subjected to Collision and Grounding. PhD-thesis, IMT
IMT-2009-50	Koushan, Kamran	Vortex Induced Vibrations of Free Span Pipelines, PhD thesis, IMT
IMT-2009-51	Korsvik, Jarl Eirik	Heuristic Methods for Ship Routing and Scheduling. PhD-thesis, IMT
IMT-2009-52	Lee, Jihoon	Experimental Investigation and Numerical in Analyzing the Ocean Current Displacement of Longlines. Ph.d.-Thesis, IMT.
IMT-2009-53	Vestbøstad, Tone Gran	A Numerical Study of Wave-in-Deck Impact using a Two-Dimensional Constrained Interpolation Profile Method, Ph.d.thesis, CeSOS.
IMT-2009-54	Bruun, Kristine	Bond Graph Modelling of Fuel Cells for Marine Power Plants. Ph.d.-thesis, IMT
IMT-2009-55	Holstad, Anders	Numerical Investigation of Turbulence in a Skewed Three-Dimensional Channel Flow, Ph.d.-thesis, IMT.
IMT-2009-56	Ayala-Uraga, Efrén	Reliability-Based Assessment of Deteriorating Ship-shaped Offshore Structures, Ph.d.-thesis, IMT
IMT-2009-57	Kong, Xiangjun	A Numerical Study of a Damaged Ship in Beam Sea Waves. Ph.d.-thesis, IMT/CeSOS.
IMT-2010-58	Kristiansen, David	Wave Induced Effects on Floaters of Aquaculture Plants, Ph.d.-thesis, CeSOS.



IMT 2010-59	Ludvigsen, Martin	An ROV-Toolbox for Optical and Acoustic Scientific Seabed Investigation. Ph.d.-thesis IMT.
IMT 2010-60	Hals, Jørgen	Modelling and Phase Control of Wave-Energy Converters. Ph.d.thesis, CeSOS.
IMT 2010- 61	Shu, Zhi	Uncertainty Assessment of Wave Loads and Ultimate Strength of Tankers and Bulk Carriers in a Reliability Framework. Ph.d. Thesis, IMT/ CeSOS
IMT 2010-62	Shao, Yanlin	Numerical Potential-Flow Studies on Weakly-Nonlinear Wave-Body Interactions with/without Small Forward Speed, Ph.d.thesis,CeSOS.
IMT 2010-63	Califano, Andrea	Dynamic Loads on Marine Propellers due to Intermittent Ventilation. Ph.d.thesis, IMT.
IMT 2010-64	El Khoury, George	Numerical Simulations of Massively Separated Turbulent Flows, Ph.d.-thesis, IMT
IMT 2010-65	Seim, Knut Sponheim	Mixing Process in Dense Overflows with Emphasis on the Faroe Bank Channel Overflow. Ph.d.thesis, IMT
IMT 2010-66	Jia, Huirong	Structural Analysis of Intact and Damaged Ships in a Collision Risk Analysis Perspective. Ph.d.thesis CeSoS.
IMT 2010-67	Jiao, Linlin	Wave-Induced Effects on a Pontoon-type Very Large Floating Structures (VLFS). Ph.D.-thesis, CeSOS.
IMT 2010-68	Abrahamsen, Bjørn Christian	Sloshing Induced Tank Roof with Entrapped Air Pocket. Ph.d.thesis, CeSOS.
IMT 2011-69	Karimirad, Madjid	Stochastic Dynamic Response Analysis of Spar-Type Wind Turbines with Catenary or Taut Mooring Systems. Ph.d.-thesis, CeSOS.
IMT - 2011-70	Erlend Meland	Condition Monitoring of Safety Critical Valves. Ph.d.-thesis, IMT.
IMT – 2011-71	Yang, Limin	Stochastic Dynamic System Analysis of Wave Energy Converter with Hydraulic Power Take-Off, with Particular Reference to Wear Damage Analysis, Ph.d. Thesis, CeSOS.
IMT – 2011-72	Visscher, Jan	Application of Particle Image Velocimetry on Turbulent Marine Flows, Ph.d.Thesis, IMT.
IMT – 2011-73	Su, Biao	Numerical Predictions of Global and Local Ice Loads on Ships. Ph.d.Thesis, CeSOS.
IMT – 2011-74	Liu, Zhenhui	Analytical and Numerical Analysis of Iceberg Collision with Ship Structures. Ph.d.Thesis, IMT.
IMT – 2011-75	Aarsæther, Karl Gunnar	Modeling and Analysis of Ship Traffic by Observation and Numerical Simulation. Ph.d.Thesis, IMT.

Imt – 2011-76	Wu, Jie	Hydrodynamic Force Identification from Stochastic Vortex Induced Vibration Experiments with Slender Beams. Ph.d.Thesis, IMT.
Imt – 2011-77	Amini, Hamid	Azimuth Propulsors in Off-design Conditions. Ph.d.Thesis, IMT.
IMT – 2011-78	Nguyen, Tan-Hoi	Toward a System of Real-Time Prediction and Monitoring of Bottom Damage Conditions During Ship Grounding. Ph.d.thesis, IMT.
IMT- 2011-79	Tavakoli, Mohammad T.	Assessment of Oil Spill in Ship Collision and Grounding, Ph.d.thesis, IMT.
IMT- 2011-80	Guo, Bingjie	Numerical and Experimental Investigation of Added Resistance in Waves. Ph.d.Thesis, IMT.
IMT- 2011-81	Chen, Qiaofeng	Ultimate Strength of Aluminium Panels, considering HAZ Effects, IMT
IMT- 2012-82	Kota, Ravikiran S.	Wave Loads on Decks of Offshore Structures in Random Seas, CeSOS.
IMT- 2012-83	Sten, Ronny	Dynamic Simulation of Deep Water Drilling Risers with Heave Compensating System, IMT.
IMT- 2012-84	Berle, Øyvind	Risk and resilience in global maritime supply chains, IMT.
IMT- 2012-85	Fang, Shaoji	Fault Tolerant Position Mooring Control Based on Structural Reliability, CeSOS.
IMT- 2012-86	You, Jikun	Numerical studies on wave forces and moored ship motions in intermediate and shallow water, CeSOS.
IMT- 2012-87	Xiang ,Xu	Maneuvering of two interacting ships in waves, CeSOS
IMT- 2012-88	Dong, Wenbin	Time-domain fatigue response and reliability analysis of offshore wind turbines with emphasis on welded tubular joints and gear components, CeSOS
IMT- 2012-89	Zhu, Suji	Investigation of Wave-Induced Nonlinear Load Effects in Open Ships considering Hull Girder Vibrations in Bending and Torsion, CeSOS
IMT- 2012-90	Zhou, Li	Numerical and Experimental Investigation of Station-keeping in Level Ice, CeSOS
IMT- 2012-91	Ushakov, Sergey	Particulate matter emission characteristics from diesel engines operating on conventional and alternative marine fuels, IMT
IMT- 2013-1	Yin, Decao	Experimental and Numerical Analysis of Combined In-line and Cross-flow Vortex Induced Vibrations, CeSOS

IMT-2013-2	Kurniawan, Adi	Modelling and geometry optimisation of wave energy converters, CeSOS
IMT-2013-3	Al Ryati, Nabil	Technical condition indexes doe auxiliary marine diesel engines, IMT
IMT-2013-4	Firoozkoohi, Reza	Experimental, numerical and analytical investigation of the effect of screens on sloshing, CeSOS
IMT-2013-5	Ommani, Babak	Potential-Flow Predictions of a Semi-Displacement Vessel Including Applications to Calm Water Broaching, CeSOS
IMT-2013-6	Xing, Yihan	Modelling and analysis of the gearbox in a floating spar-type wind turbine, CeSOS
IMT-7-2013	Balland, Océane	Optimization models for reducing air emissions from ships, IMT
IMT-8-2013	Yang, Dan	Transitional wake flow behind an inclined flat plate----Computation and analysis, IMT
IMT-9-2013	Abdillah, Suyuthi	Prediction of Extreme Loads and Fatigue Damage for a Ship Hull due to Ice Action, IMT
IMT-10-2013	Ramirez, Pedro Agustin Pérez	Ageing management and life extension of technical systems- Concepts and methods applied to oil and gas facilities, IMT
IMT-11-2013	Chuang, Zhenju	Experimental and Numerical Investigation of Speed Loss due to Seakeeping and Maneuvering. IMT
IMT-12-2013	Etemaddar, Mahmoud	Load and Response Analysis of Wind Turbines under Atmospheric Icing and Controller System Faults with Emphasis on Spar Type Floating Wind Turbines, IMT
IMT-13-2013	Lindstad, Haakon	Strategies and measures for reducing maritime CO2 emissons, IMT
IMT-14-2013	Haris, Sabril	Damage interaction analysis of ship collisions, IMT
IMT-15-2013	Shainee, Mohamed	Conceptual Design, Numerical and Experimental Investigation of a SPM Cage Concept for Offshore Mariculture, IMT
IMT-16-2013	Gansel, Lars	Flow past porous cylinders and effects of biofouling and fish behavior on the flow in and around Atlantic salmon net cages, IMT
IMT-17-2013	Gaspar, Henrique	Handling Aspects of Complexity in Conceptual Ship Design, IMT
IMT-18-2013	Thys, Maxime	Theoretical and Experimental Investigation of a Free Running Fishing Vessel at Small Frequency of Encounter, CeSOS
IMT-19-2013	Aglen, Ida	VIV in Free Spanning Pipelines, CeSOS

IMT-1-2014	Song, An	Theoretical and experimental studies of wave diffraction and radiation loads on a horizontally submerged perforated plate, CeSOS
IMT-2-2014	Rogne, Øyvind Ygre	Numerical and Experimental Investigation of a Hinged 5-body Wave Energy Converter, CeSOS
IMT-3-2014	Dai, Lijuan	Safe and efficient operation and maintenance of offshore wind farms ,IMT
IMT-4-2014	Bachynski, Erin Elizabeth	Design and Dynamic Analysis of Tension Leg Platform Wind Turbines, CeSOS
IMT-5-2014	Wang, Jingbo	Water Entry of Freefall Wedged – Wedge motions and Cavity Dynamics, CeSOS
IMT-6-2014	Kim, Ekaterina	Experimental and numerical studies related to the coupled behavior of ice mass and steel structures during accidental collisions, IMT
IMT-7-2014	Tan, Xiang	Numerical investigation of ship's continuous- mode icebreaking in level ice, CeSOS
IMT-8-2014	Muliawan, Made Jaya	Design and Analysis of Combined Floating Wave and Wind Power Facilities, with Emphasis on Extreme Load Effects of the Mooring System, CeSOS
IMT-9-2014	Jiang, Zhiyu	Long-term response analysis of wind turbines with an emphasis on fault and shutdown conditions, IMT
IMT-10-2014	Dukan, Fredrik	ROV Motion Control Systems, IMT
IMT-11-2014	Grimsmo, Nils I.	Dynamic simulations of hydraulic cylinder for heave compensation of deep water drilling risers, IMT
IMT-12-2014	Kvittem, Marit I.	Modelling and response analysis for fatigue design of a semisubmersible wind turbine, CeSOS
IMT-13-2014	Akhtar, Juned	The Effects of Human Fatigue on Risk at Sea, IMT
IMT-14-2014	Syahroni, Nur	Fatigue Assessment of Welded Joints Taking into Account Effects of Residual Stress, IMT
IMT-1-2015	Böckmann, Eirik	Wave Propulsion of ships, IMT
IMT-2-2015	Wang, Kai	Modelling and dynamic analysis of a semi-submersible floating vertical axis wind turbine, CeSOS
IMT-3-2015	Fredriksen, Arnt Gunvald	A numerical and experimental study of a two-dimensional body with moonpool in waves and current, CeSOS
IMT-4-2015	Jose Patricio Gallardo Canabes	Numerical studies of viscous flow around bluff bodies, IMT

IMT-5-2015	Vegard Longva	Formulation and application of finite element techniques for slender marine structures subjected to contact interactions, IMT
IMT-6-2015	Jacobus De Vaal	Aerodynamic modelling of floating wind turbines, CeSOS
IMT-7-2015	Fachri Nasution	Fatigue Performance of Copper Power Conductors, IMT
IMT-8-2015	Oleh I Karpa	Development of bivariate extreme value distributions for applications in marine technology, CeSOS
IMT-9-2015	Daniel de Almeida Fernandes	An output feedback motion control system for ROVs, AMOS
IMT-10-2015	Bo Zhao	Particle Filter for Fault Diagnosis: Application to Dynamic Positioning Vessel and Underwater Robotics, CeSOS
IMT-11-2015	Wenting Zhu	Impact of emission allocation in maritime transportation, IMT
IMT-12-2015	Amir Rasekhi Nejad	Dynamic Analysis and Design of Gearboxes in Offshore Wind Turbines in a Structural Reliability Perspective, CeSOS
IMT-13-2015	Arturo Jesús Ortega Malca	Dynamic Response of Flexibles Risers due to Unsteady Slug Flow, CeSOS
IMT-14-2015	Dagfinn Husjord	Guidance and decision-support system for safe navigation of ships operating in close proximity, IMT
IMT-15-2015	Anirban Bhattacharyya	Ducted Propellers: Behaviour in Waves and Scale Effects, IMT
IMT-16-2015	Qin Zhang	Image Processing for Ice Parameter Identification in Ice Management, IMT
IMT-1-2016	Vincentius Rumawas	Human Factors in Ship Design and Operation: An Experiential Learning, IMT
IMT-2-2016	Martin Storheim	Structural response in ship-platform and ship-ice collisions, IMT
IMT-3-2016	Mia Abrahamsen Prsic	Numerical Simulations of the Flow around single and Tandem Circular Cylinders Close to a Plane Wall, IMT
IMT-4-2016	Tufan Arslan	Large-eddy simulations of cross-flow around ship sections, IMT

IMT-5-2016	Pierre Yves-Henry	Parametrisation of aquatic vegetation in hydraulic and coastal research,IMT
IMT-6-2016	Lin Li	Dynamic Analysis of the Instalation of Monopiles for Offshore Wind Turbines, CeSOS
IMT-7-2016	Øivind Kåre Kjerstad	Dynamic Positioning of Marine Vessels in Ice, IMT
IMT-8-2016	Xiaopeng Wu	Numerical Analysis of Anchor Handling and Fish Trawling Operations in a Safety Perspective, CeSOS
IMT-9-2016	Zhengshun Cheng	Integrated Dynamic Analysis of Floating Vertical Axis Wind Turbines, CeSOS
IMT-10-2016	Ling Wan	Experimental and Numerical Study of a Combined Offshore Wind and Wave Energy Converter Concept
IMT-11-2016	Wei Chai	Stochastic dynamic analysis and reliability evaluation of the roll motion for ships in random seas, CeSOS
IMT-12-2016	Øyvind Selnes Patricksson	Decision support for conceptual ship design with focus on a changing life cycle and future uncertainty, IMT
IMT-13-2016	Mats Jørgen Thorsen	Time domain analysis of vortex-induced vibrations, IMT
IMT-14-2016	Edgar McGuinness	Safety in the Norwegian Fishing Fleet – Analysis and measures for improvement, IMT
IMT-15-2016	Sepideh Jafarzadeh	Energy efficiency and emission abatement in the fishing fleet, IMT
IMT-16-2016	Wilson Ivan Guachamin Acero	Assessment of marine operations for offshore wind turbine installation with emphasis on response-based operational limits, IMT
IMT-17-2016	Mauro Candeloro	Tools and Methods for Autonomous Operations on Seabed and Water Coumn using Underwater Vehicles, IMT
IMT-18-2016	Valentin Chabaud	Real-Time Hybrid Model Testing of Floating Wind Tubines, IMT
IMT-1-2017	Mohammad Saud Afzal	Three-dimensional streaming in a sea bed boundary layer
IMT-2-2017	Peng Li	A Theoretical and Experimental Study of Wave-induced Hydroelastic Response of a Circular Floating Collar
IMT-3-2017	Martin Bergström	A simulation-based design method for arctic maritime transport systems

IMT-4-2017	Bhushan Taskar	The effect of waves on marine propellers and propulsion
IMT-5-2017	Mohsen Bardestani	A two-dimensional numerical and experimental study of a floater with net and sinker tube in waves and current
IMT-6-2017	Fatemeh Hoseini Dadmarzi	Direct Numerical Simulation of turbulent wakes behind different plate configurations
IMT-7-2017	Michel R. Miyazaki	Modeling and control of hybrid marine power plants
IMT-8-2017	Giri Rajasekhar Gunnu	Safety and efficiency enhancement of anchor handling operations with particular emphasis on the stability of anchor handling vessels
IMT-9-2017	Kevin Koosup Yum	Transient Performance and Emissions of a Turbocharged Diesel Engine for Marine Power Plants
IMT-10-2017	Zhaolong Yu	Hydrodynamic and structural aspects of ship collisions
IMT-11-2017	Martin Hassel	Risk Analysis and Modelling of Allisions between Passing Vessels and Offshore Installations
IMT-12-2017	Astrid H. Brodtkorb	Hybrid Control of Marine Vessels – Dynamic Positioning in Varying Conditions
IMT-13-2017	Kjersti Bruserud	Simultaneous stochastic model of waves and current for prediction of structural design loads
IMT-14-2017	Finn-Idar Grøtta Giske	Long-Term Extreme Response Analysis of Marine Structures Using Inverse Reliability Methods
IMT-15-2017	Stian Skjong	Modeling and Simulation of Maritime Systems and Operations for Virtual Prototyping using co-Simulations
IMT-1-2018	Yingguang Chu	Virtual Prototyping for Marine Crane Design and Operations
IMT-2-2018	Sergey Gavrilin	Validation of ship manoeuvring simulation models
IMT-3-2018	Jeevith Hegde	Tools and methods to manage risk in autonomous subsea inspection, maintenance and repair operations
IMT-4-2018	Ida M. Strand	Sea Loads on Closed Flexible Fish Cages
IMT-5-2018	Erlend Kvinge Jørgensen	Navigation and Control of Underwater Robotic Vehicles

IMT-6-2018	Bård Stovner	Aided Inertial Navigation of Underwater Vehicles
IMT-7-2018	Erlend Liavåg Grotle	Thermodynamic Response Enhanced by Sloshing in Marine LNG Fuel Tanks
IMT-8-2018	Børge Rokseth	Safety and Verification of Advanced Maritime Vessels
IMT-9-2018	Jan Vidar Ulveseter	Advances in Semi-Empirical Time Domain Modelling of Vortex-Induced Vibrations
IMT-10-2018	Chenyu Luan	Design and analysis for a steel braceless semi-submersible hull for supporting a 5-MW horizontal axis wind turbine
IMT-11-2018	Carl Fredrik Rehn	Ship Design under Uncertainty
IMT-12-2018	Øyvind Ødegård	Towards Autonomous Operations and Systems in Marine Archaeology
IMT-13-2018	Stein Melvær Nornes	Guidance and Control of Marine Robotics for Ocean Mapping and Monitoring
IMT-14-2018	Petter Norgren	Autonomous Underwater Vehicles in Arctic Marine Operations: Arctic marine research and ice monitoring
IMT-15-2018	Minjoo Choi	Modular Adaptable Ship Design for Handling Uncertainty in the Future Operating Context
MT-16-2018	Ole Alexander Eidsvik	Dynamics of Remotely Operated Underwater Vehicle Systems
IMT-17-2018	Mahdi Ghane	Fault Diagnosis of Floating Wind Turbine Drivetrain- Methodologies and Applications
IMT-18-2018	Christoph Alexander Thieme	Risk Analysis and Modelling of Autonomous Marine Systems
IMT-19-2018	Yugao Shen	Operational limits for floating-collar fish farms in waves and current, without and with well-boat presence
IMT-20-2018	Tianjiao Dai	Investigations of Shear Interaction and Stresses in Flexible Pipes and Umbilicals
IMT-21-2018	Sigurd Solheim Pettersen	Resilience by Latent Capabilities in Marine Systems
IMT-22-2018	Thomas Sauder	Fidelity of Cyber-physical Empirical Methods. Application to the Active Truncation of Slender Marine Structures
IMT-23-2018	Jan-Tore Horn	Statistical and Modelling Uncertainties in the Design of Offshore Wind Turbines



IMT-24-2018	Anna Swider	Data Mining Methods for the Analysis of Power Systems of Vessels
IMT-1-2019	Zhao He	Hydrodynamic study of a moored fish farming cage with fish influence
IMT-2-2019	Isar Ghamari	Numerical and Experimental Study on the Ship Parametric Roll Resonance and the Effect of Anti-Roll Tank
IMT-3-2019	Håkon Strandenes	Turbulent Flow Simulations at Higher Reynolds Numbers
IMT-4-2019	Siri Mariane Holen	Safety in Norwegian Fish Farming – Concepts and Methods for Improvement
IMT-5-2019	Ping Fu	Reliability Analysis of Wake-Induced Riser Collision
IMT-6-2019	Vladimir Krivopolianskii	Experimental Investigation of Injection and Combustion Processes in Marine Gas Engines using Constant Volume Rig
IMT-7-2019	Anna Maria Kozłowska	Hydrodynamic Loads on Marine Propellers Subject to Ventilation and out of Water Condition.
IMT-8-2019	Hans-Martin Heyn	Motion Sensing on Vessels Operating in Sea Ice: A Local Ice Monitoring System for Transit and Stationkeeping Operations under the Influence of Sea Ice
IMT-9-2019	Stefan Vilsen	Method for Real-Time Hybrid Model Testing of Ocean Structures – Case on Slender Marine Systems
IMT-10-2019	Finn-Christian W. Hanssen	Non-Linear Wave-Body Interaction in Severe Waves
IMT-11-2019	Trygve Olav Fossum	Adaptive Sampling for Marine Robotics
IMT-12-2019	Jørgen Bremnes Nielsen	Modeling and Simulation for Design Evaluation
IMT-13-2019	Yuna Zhao	Numerical modelling and dynamic analysis of offshore wind turbine blade installation
IMT-14-2019	Daniela Myland	Experimental and Theoretical Investigations on the Ship Resistance in Level Ice
IMT-15-2019	Zhengru Ren	Advanced control algorithms to support automated offshore wind turbine installation
IMT-16-2019	Drazen Polic	Ice-propeller impact analysis using an inverse propulsion machinery simulation approach
IMT-17-2019	Endre Sandvik	Sea passage scenario simulation for ship system performance evaluation

IMT-18-2019	Loup Suja-Thauvin	Response of Monopile Wind Turbines to Higher Order Wave Loads
IMT-19-2019	Emil Smilden	Structural control of offshore wind turbines – Increasing the role of control design in offshore wind farm development
IMT-20-2019	Aleksandar-Sasa Milakovic	On equivalent ice thickness and machine learning in ship ice transit simulations
IMT-1-2020	Amrit Shankar Verma	Modelling, Analysis and Response-based Operability Assessment of Offshore Wind Turbine Blade Installation with Emphasis on Impact Damages
IMT-2-2020	Bent Oddvar Arnesen Haugalokken	Autonomous Technology for Inspection, Maintenance and Repair Operations in the Norwegian Aquaculture
IMT-3-2020	Seongpil Cho	Model-based fault detection and diagnosis of a blade pitch system in floating wind turbines
IMT-4-2020	Jose Jorge Garcia Agis	Effectiveness in Decision-Making in Ship Design under Uncertainty
IMT-5-2020	Thomas H. Viuff	Uncertainty Assessment of Wave-and Current-induced Global Response of Floating Bridges
IMT-6-2020	Fredrik Mentzoni	Hydrodynamic Loads on Complex Structures in the Wave Zone
IMT-7-2020	Senthuran Ravinthrakumar	Numerical and Experimental Studies of Resonant Flow in Moonpools in Operational Conditions
IMT-8-2020	Stian Skaalvik Sandøy	Acoustic-based Probabilistic Localization and Mapping using Unmanned Underwater Vehicles for Aquaculture Operations
IMT-9-2020	Kun Xu	Design and Analysis of Mooring System for Semi-submersible Floating Wind Turbine in Shallow Water
IMT-10-2020	Jianxun Zhu	Cavity Flows and Wake Behind an Elliptic Cylinder Translating Above the Wall
IMT-11-2020	Sandra Hogenboom	Decision-making within Dynamic Positioning Operations in the Offshore Industry – A Human Factors based Approach
IMT-12-2020	Woongshik Nam	Structural Resistance of Ship and Offshore Structures Exposed to the Risk of Brittle Failure
IMT-13-2020	Svenn Are Tutturen Værnø	Transient Performance in Dynamic Positioning of Ships: Investigation of Residual Load Models and Control Methods for Effective Compensation
IMT-14-2020	Mohd Atif Siddiqui	Experimental and Numerical Hydrodynamic Analysis of a Damaged Ship in Waves
IMT-15-2020	John Marius Hegseth	Efficient Modelling and Design Optimization of Large Floating Wind Turbines

IMT-16-2020	Asle Natskår	Reliability-based Assessment of Marine Operations with Emphasis on Sea Transport on Barges
IMT-17-2020	Shi Deng	Experimental and Numerical Study of Hydrodynamic Responses of a Twin-Tube Submerged Floating Tunnel Considering Vortex-Induced Vibration
IMT-18-2020	Jone Torsvik	Dynamic Analysis in Design and Operation of Large Floating Offshore Wind Turbine Drivetrains
IMT-1-2021	Ali Ebrahimi	Handling Complexity to Improve Ship Design Competitiveness
IMT-2-2021	Davide Proserpio	Isogeometric Phase-Field Methods for Modeling Fracture in Shell Structures
IMT-3-2021	Cai Tian	Numerical Studies of Viscous Flow Around Step Cylinders
IMT-4-2021	Farid Khazaeli Moghadam	Vibration-based Condition Monitoring of Large Offshore Wind Turbines in a Digital Twin Perspective
IMT-5-2021	Shuaishuai Wang	Design and Dynamic Analysis of a 10-MW Medium-Speed Drivetrain in Offshore Wind Turbines
IMT-6-2021	Sadi Tavakoli	Ship Propulsion Dynamics and Emissions
IMT-7-2021	Haoran Li	Nonlinear wave loads, and resulting global response statistics of a semi-submersible wind turbine platform with heave plates
IMT-8-2021	Einar Skiftestad Ueland	Load Control for Real-Time Hybrid Model Testing using Cable-Driven Parallel Robots
IMT-9-2021	Mengning Wu	Uncertainty of machine learning-based methods for wave forecast and its effect on installation of offshore wind turbines
IMT-10-2021	Xu Han	Onboard Tuning and Uncertainty Estimation of Vessel Seakeeping Model Parameters
IMT-01-2022	Ingunn Marie Holmen	Safety in Exposed Aquaculture Operations
IMT-02-2022	Prateek Gupta	Ship Performance Monitoring using In-service Measurements and Big Data Analysis Methods
IMT-03-2022	Sangwoo Kim	Non-linear time domain analysis of deepwater riser vortex-induced vibrations
IMT-04-2022	Jarle Vinje Kramer	Hydrodynamic Aspects of Sail-Assisted Merchant Vessels
IMT-05-2022	Øyvind Rabliås	Numerical and Experimental Studies of Maneuvering in Regular and Irregular Waves

IMT-06-2022	Pramod Ghimire	Simulation-Based Ship Hybrid Power System Conspect Studies and Performance Analyses
IMT-07-2022	Carlos Eduardo Silva de Souza	Structural modelling, coupled dynamics, and design of large floating wind turbines
IMT-08-2022	Lorenzo Balestra	Design of hybrid fuel cell & battery systems for maritime vessels
IMT-09-2022	Sharmin Sultana	Process safety and risk management using system perspectives – A contribution to the chemical process and petroleum industry
IMT-10-2022	Øystein Sture	Autonomous Exploration for Marine Minerals
IMT-11-2022	Tiantian Zhu	Information and Decision-making for Major Accident Prevention – A concept of information-based strategies for accident prevention
IMT-12-2022	Siamak Karimi	Shore-to-Ship Charging Systems for Battery-Electric Ships
IMT-01-2023	Huili Xu	Fish-inspired Propulsion Study: Numerical Hydrodynamics of Rigid/Flexible/Morphing Foils and Observations on Real Fish
IMT-02-2023	Chana Sinsabvarodom	Probabilistic Modelling of Ice-drift and Ice Loading on Fixed and Floating Offshore Structures
IMT-03-2023	Martin Skaldebo	Intelligent low-cost solutions for underwater intervention using computer vision and machine learning
IMT-04-2023	Hans Tobias Slette	Vessel operations in exposed aquaculture – Achieving safe and efficient operation of vessel fleets in fish farm systems experiencing challenging metocean conditions
IMT-05-2023	Ruochen Yang	Methods and models for analyzing and controlling the safety in operations of autonomous marine systems
IMT-06-2023	Tobias Rye Torben	Formal Approaches to Design and Verification of Safe Control Systems for Autonomous Vessels
IMT-07-2023	Youngrong Kim	Modeling Operational Performance for the Global Fleet & Application of an Energy Saving Measure